Universität Siegen

fwu

Mitteilungen des Forschungsinstituts Wasser und Umwelt der Universität Siegen

Leon Jänicke

Assessing changes of tidal dynamics in the North Sea

An investigation of the temporal and spatial developments between 1958 and 2014

Heft 14

2022

ISSN 1868-6613

Leon Jänicke

Assessing changes of tidal dynamics in the North Sea
An investigation of the temporal and spatial developments between 1958 and 2014

Erscheinungsort: Siegen
Erscheinungsjahr: 2022
D 467

Mitteilungen des Forschungsinstituts Wasser und Umwelt der Universität Siegen
Heft 14 | 2022

Herausgeber:
Forschungsinstitut Wasser und Umwelt (fwu)
der Universität Siegen
Paul-Bonatz-Str. 9-11
57076 Siegen

Druck:
UniPrint, Universität Siegen

ISSN 1868-6613

Vorwort

Mit der ersten Promotion am Forschungsinstitut Wasser und Umwelt (fwu) im Jahr 2009 wurde eine eigene fwu-Schriftenreihe etabliert. Neben Promotionen werden in dieser Schriftenreihe Forschungsergebnisse und Berichte zu Institutsveranstaltungen im Kontext des fwu veröffentlicht.

In dem vorliegenden Heft 14 (2022) wird die Promotion von Herrn Leon Jänicke mit dem Titel „Assessing changes of tidal dynamics in the North Sea - An investigation of the temporal and spatial developments between 1958 and 2014“ in Papierform veröffentlicht; die digitale Veröffentlichung erfolgte im April 2022 über die Universitätsbibliothek Siegen. Herr Jänicke hat die Dissertation als Monografie in englischer Sprache verfasst. Inhalte der Dissertationsschrift wurden parallel auch in begutachteten Beiträgen in internationalen Fachzeitschriften veröffentlicht, bspw. im Journal of Geophysical Research: Oceans.

An der Deutschen Nordseeküste wurde die Ausprägung der Gezeiten und insbesondere des Tidehubs bis vor wenigen Jahrzehnten als nahezu konstant angesehen, allenfalls beeinflusst durch den postglazialen Meeresspiegelanstieg (MSL). Die Tideparameter wurden bei nahezu konstanten Beckengeometrien als konstant bzw. nur um den MSL parallel verschoben, angenommen. Auf Basis von Pegeldatenanalysen weist der Unterzeichner 1984 erstmals großräumige Änderungen der Tideparameter für die Nordseeküste in der zweiten Hälfte des 20. Jahrhunderts nach. Die räumliche Ausdehnung dieser Änderungen sowie deren Ursachen konnten bislang nicht eindeutig identifiziert und quantitativ zugeordnet werden. Die bisherigen Arbeiten dazu zeigen, dass die offensichtliche Überlagerung von kleinräumigen und großräumigen Einflüssen die Ursachenforschung und die Identifizierung der physikalischen Ursachen und deren Zuordnung zu beobachteten Gezeitenänderungen erschwert. Die bisherigen Forschungen haben astronomische, großräumige morphologische oder tektonische Ursachen als treibende Faktoren ausgeschlossen und einen Anstieg des MSL weiterhin als wahrscheinliche Ursache angegeben.

Da die Ursachen der beobachteten Entwicklung bis heute nicht eindeutig beantwortet werden konnten, war das Ziel der Promotion von Herrn Jänicke, die Veränderungen der Gezeiten im Untersuchungsgebiet der Nordsee zu untersuchen und mögliche physikalische Ursachen zu identifizieren. Die im Rahmen der Dissertation von Herrn Jänicke erarbeiteten Ergebnisse liefern einen wichtigen Beitrag zum Prozessverständnis der Änderungen der Tidedynamik und in den Tideparametern in der Nordsee. Herrn Jänicke ist es gelungen, großräumige Gezeitenänderungen in der Nordsee zu detektieren und zu beschreiben, sowie zugrundeliegende Effekte zu identifizieren, zu separieren und zu quantifizieren.

Für die Mitwirkung im Promotionsverfahren möchte ich mich bei Herrn J.-Prof. Dr.-Ing. Arne Arns, Professur für Küstenschutz und Küstendynamik der Universität Rostock und Frau Univ.-Prof. Dr.-Ing. habil. Kerstin Lesny vom fwu, Lehrstuhl für Geotechnik der Universität Siegen sowie bei Herrn Univ.-Prof. Dr. phil. habil. Jorge Leandro vom fwu, Lehrstuhl für Hydromechanik und Wasserbau der Universität herzlich bedanken.

Siegen im April 2022

Univ.-Prof. Dr.-Ing. Jürgen Jensen

Assessing changes of tidal dynamics in the North Sea

-An investigation of the temporal and spatial developments between 1958 and 2014-

Vom Department Bauingenieurwesen der Naturwissenschaftlich-Technischen Fakultät der Universität Siegen angenommene

Dissertation

zur Erlangung des akademischen Grades eines
Doktor der Ingenieurwissenschaften (Dr.-Ing.)
von

Leon Jänicke, M.Sc.

Referent:	**Univ.-Prof. Dr.-Ing. Jürgen Jensen** Universität Siegen
Korreferent:	**J.-Prof. Dr.-Ing. Arne Arns** Universität Rostock
Prüfer:	**Univ.-Prof. Dr.-Ing. habil. Kerstin Lesny** Universität Siegen
Vorsitzender:	**Univ.-Prof. Dr. phil. habil. Jorge Leandro** Universität Siegen

Tag der Einreichung: 31.08.2021
Tag der mündlichen Prüfung: 07.12.2021

gedruckt auf alterungsbeständigem holz- und säurefreien Papier

About the cover image:

The cover image represents an artistic interpretation of the North Sea area and parts of the adjacent North Atlantic and the Baltic Sea. Image source: Anton Balazh / Shutterstock.com

Contact: Leon Jänicke | Email: Leon.Jaenicke@gmx.de

Danksagung

Diese Dissertationsschrift wurde zwischen 2018 und 2021 am Forschungsinstitut Wasser und Umwelt (fwu) im Department Bauingenieurwesen der Naturwissenschaftlich-Technischen Fakultät der Universität Siegen unter Leitung von Herrn Univ.-Prof. Dr.-Ing. Jürgen Jensen verfasst. Ich möchte mich in diesem Vorwort bei einigen Personen bedanken, ohne deren Unterstützung das Verfassen dieser Arbeit nicht möglich gewesen wäre.

Zunächst möchte ich an dieser Stelle meinem Doktorvater Herrn Prof. Dr.-Ing. Jürgen Jensen danken, der mir nicht nur das Verfassen dieser Arbeit ermöglich hat, sondern auch meinen bisherigen wissenschaftlichen Werdegang seit meiner Einstellung als studentische Hilfskraft am fwu im Jahr 2012 begleitet und unterstützt hat. Seine hohen Ansprüche, seine Anregungen, seine Offenheit gegenüber Neuem aber auch seine Kritik waren stets ein hervorragender Anreiz, die bestmögliche Leistung zu erbringen. Weiterhin danke ich Herrn J.-Prof. Dr.-Ing. Arne Arns von der Universität Rostock für die unzähligen wissenschaftlichen Diskussionen und Anregungen sowie für seine Bereitschaft zur Übernahme des Korreferats. Dank gebührt darüber hinaus Univ.-Prof. Dr. phil. habil. Jorge Leandro als Vorsitzender der Promotionskommission sowie Univ.-Prof. Dr.-Ing. habil. Kerstin Lesny, die sich bereit erklärt hat, die Prüfungskommission zu vervollständigen.

Außerdem gilt mein besonderer Dank Sönke Dangendorf, Andra Ebener, Ivan Haigh, Sebastian Niehüser, Michael Schindelegger sowie Philip Woodworth ohne deren fachliche Hinweise und Diskussionen diese Arbeit in dieser Form nicht möglich gewesen wäre. Ebenso möchte ich mich bei dem gesamten fwu-Team dieser Jahre herzlich bedanken, insbesondere bei: Jens Bender, Kristina Fehler, Sebastian Gürke, Mai Habib, Matthias Hirt, Jessica Kelln, Jens Metzger, Felix Soltau, Volker Spieß, Andre Stettner-Davis, Sandra Sziburies, Daniela Vollmer und Jörg Wieland.

Neben anderen im Verlauf dieser Arbeit entsprechend gekennzeichneten Software-Tools wurde von DHI das Softwarepacket MIKE21® für die Analysen im Rahmen dieser Dissertation zur Verfügung gestellt, vielen Dank dafür!

Ich danke außerdem meiner Familie und meinen Freunden für die moralische Unterstützung während des Verfassens dieser Arbeit. Insbesondere möchte ich meiner Frau Elina danken, ohne deren Geduld und Unterstützung diese Arbeit niemals hätte entstehen können. Danke für alles!

Abstract

Perhaps because of the close connection between the periodic and predictable nature of astronomical variations and the corresponding tidal water levels, the tidal parameters of tidal low water, tidal high water and tidal range were generally assumed to be constant on time scales over which basin geometry undergoes only minor changes (i.e. decades to centuries, Jänicke et al., 2020). Jensen (1984) and Führböter & Jensen (1985) were the first to discuss large-scale, potentially basin-wide changes in tidal parameters for the North Sea in the second half of the 20th century. Nevertheless, the spatial extend of these changes as well as their forcing factors remain uncertain, considering the stationarity of astronomical forcing over the period of tide gauge observations. The superposition of small-scale and large-scale effects on water level has proven to be particularly problematic in causal research and been identified by many studies in the past as the most important unsolved obstacle in identifying physical causes and attributing them to observed tidal changes (Woodworth, 2010; Haigh et al., 2020; Talke & Jay, 2020).

To examine the spatial extent of tidal changes in the North Sea, in this thesis the long-term trends of the three tidal parameters were considered first and significant changes were detected. A median basin-wide increase of both tidal low and high water was detected, forming a dipole-like pattern with tidal low water trends exceeding tidal high water trends in the United Kingdom (UK) and vice versa in the German Bight. As a result, negative trends of tidal range occur in the UK whereas positive trends can be detected in the German Bight. A Principal Component Analysis was then performed to separate large-scale signals appearing coherently over multiple stations from rather localized, small-scale changes. Two leading principal components (PCs) were identified for each of the three tidal parameters, representing large-scale effects, which explain a major part of the changes and resemble the dipole pattern of the trends. In a last step, physical causes were assigned to these signals and large-scale changes in both tidal low and high water could be assigned mainly to changes in Mean Sea Level. Furthermore, changes in tidal range were attributed to a baroclinic (PC1) and a barotropic large-scale signal (PC2) by applying numerical and statistical analyses. PC2 is caused by an external and basin-wide forcing mechanism from the adjacent North Atlantic, while PC1 dominates in the southern North Sea and originates, at least in part, from stratification changes in nearby shallow waters.

Therefore, it was possible to not only detect and describe large-scale tidal changes, but to identify, separate, and quantify the underlying large-scale effects for the first time. These analyses not only significantly improve the fundamental understanding of the underlying processes, but could also form the basis for future forecasting of tidal changes and their consequences, e.g. in coastal protection or the navigability of North Sea ports.

Kurzfassung

Die drei Tideparameter Tideniedrigwasser, Tidehochwasser und Tidehub wurden für lange Zeit im Allgemeinen als konstant angenommen. Nur auf Zeitskalen von vielen hundert Jahren und länger waren großräumige Tideveränderungen durch Variationen der Beckengeometrie bekannt (Jänicke et al., 2020). Erst in den 1980er Jahren wurden von Jensen (1984) bzw. Führböter & Jensen (1985) großräumige, potenziell beckenweite Veränderungen der Tideparameter anhand von Pegelmessungen in der Nordsee für die zweite Hälfte des 20. Jahrhunderts diskutiert. Da von einer Stationarität der astronomischen Einflüsse auf die Tide über die Zeitspanne der Pegelbeobachtungen ausgegangen werden kann, verbleiben sowohl die physikalischen Ursachen als auch die räumliche Ausdehnung der Veränderungen unbekannt. Die bisherigen Erkenntnisse auf diesem Gebiet zeigen weiterhin, dass die Überlagerung von klein- und großräumigen Einflüssen die Ursachenforschung grundsätzlich erschwert und damit als maßgebliches Hindernis bei der Identifizierung physikalischer Ursachen sowie deren Zuordnung zu beobachteten Tideänderungen gilt (Woodworth, 2010; Haigh et al., 2020; Talke & Jay, 2020).

Um die räumliche Ausdehnung der Tideänderungen in der Nordsee zu untersuchen, wurden in dieser Dissertation die langfristigen Trends der drei genannten Tideparameter untersucht und signifikante Veränderungen detektiert. Es konnte jeweils ein mittlerer, beckenweiter Anstieg des Tideniedrig- und des Tidenhochwassers nachgewiesen werden. Hierbei übersteigen die Trends des Tideniedrigwassers die des Tidehochwassers in Großbritannien während in der Deutschen Bucht die Trends des Tidehochwassers größer ausfallen als die des Tideniedrigwassers. Es resultiert ein dipolartiges Muster in den Trends des Tidehubs mit negativen Trends in Großbritannien sowie positiven Trends in der Deutschen Bucht. Anschließend wurde eine Hauptkomponentenanalyse durchgeführt, um großräumige Signale, die kohärent über mehrere Tidepegel auftreten, von eher lokalen, kleinräumigen Veränderungen zu separieren. Für jeden der drei Tideparameter konnten großräumige Signale (PCs) detektiert werden, die einen Großteil der Veränderungen erklären. In einem weiteren Schritt wurden diesen PCs physikalische Ursachen zugeordnet. Die Veränderungen der Tidewasserstände konnten größtenteils auf Veränderungen des mittleren Meeresspiegels zurückgeführt werden. Die Veränderungen im Tidehub basieren dagegen auf einem baroklinen (PC1) und einem barotropen Effekt (PC2). PC2 wirkt vornehmlich an der britischen Nordseeküste und scheint durch einen externen, beckenweiten Antriebsmechanismus aus dem Nordatlantik verursacht zu werden. PC1 dagegen dominiert die südliche und östliche Nordsee und wird größtenteils durch Schichtungsänderungen in den Flachwasserbereichen erzeugt.

Es ist damit erstmals gelungen, großräumige Gezeitenänderungen der Nordsee zu detektieren und zu beschreiben sowie die zugrundeliegenden großräumigen, physikalischen Effekte zu identifizieren, zu separieren und zu quantifizieren. Diese Analysen verbessern nicht nur das fundamentale Verständnis der zugrundeliegenden Prozesse erheblich, sondern könnten auch die Grundlage für künftige Vorhersagen von Gezeitenänderungen und deren Folgen, z. B. für den Küstenschutz oder die Schiffbarkeit von Nordseehäfen, bilden.

Table of contents

List of figures

List of tables

List of equations

List of abbreviations

Abbreviation	Full name
AMOC	Atlantic Meridional Overturning Circulation
EAP	East Atlantic Pattern
GB	German Bight
HAT	Highest Astronomical Tide
IC	Irminger Current
LAT	Lowest Astronomical Tide
MSL	Mean Sea Level
NAC	North Atlantic Current
NAO	North Atlantic Oscillation
NC	Norwegian Current
NOAA	National Oceanic and Atmospheric Administration
PC	Principal Component
PCA	Principal Component Analysis
RMSE	Root Mean Square Error
RT	Rockall Trough
SPG	Sub Polar Gyre
STG	Sub Tropical Gyre
THW	Tidal High Water
TLW	Tidal Low Water
TR	Tidal Range
UK	United Kingdom

List of symbols

Symbol	Units (SI)	Description
d	m	Distance
δH	m	Depth over which density is averaged
h	M	Water depth
F	N	Gravitational force
f_i	$°\cdot h^{-1}$	Fundamental tidal frequencies
Fn	-	Form number
fu	-	Mathematical function of Principal Component
G	$N\cdot m^2\cdot kg^{-2}$	Gravitational constant
g	$m\cdot s^{-2}$	Gravitational acceleration of the Earth
g_n	$°\cdot h^{-1}$	Tidal phase
h	m	Water depth
i	-	Index
L	M	Wave length
LB	Variable	Lower Bound
$m_{1/2}$	kg	Mass
n	-	Index
n_i	-	Doodson numbers
p	h	Period
π	°	Mathematical constant of approx. 3.14
r	-	Coefficient of correlation
RMSE	Variable	Root Mean Square Error
ρ_{bed}	$kg\cdot m^{-3}$	Mean density across 25, 30 and 35 m
ρ_{top}	$kg\cdot m^{-3}$	Averaged density over depths 0, 2 and 4 m
S	Variable	Standard deviation

σ_n	°	Angular frequency
S_X	Variable	Standard error
t	s	Time
TV	m	Tidal variation
UB	Variable	Upper Bound
v	$m \cdot s^{-1}$	Velocity
ve	Variable	Exemplary randomized vector
w	-	Weighting parameter of Kriging algorithm
x	Variable	Exemplary data series
y	Variable	Exemplary data series
yr	a	Year
z	-	Specific value of the t-distribution
$\hat{Z}$	Variable	Result of Kriging algorithm
Z_i	Variable	Original observations in the context of Kriging

Symbols whose units vary depending on the context are marked as "Variable"

1 Introduction

1.1 Background and research questions

For thousands of years and all over the world, tides have had a great influence on coastal areas and their residents. Then as now, they have influenced economic decisions such as the use of landing stages or fishing and have formed the shape of coastlines as well as the human settlement areas. Tidal levels have defined many boundaries and geodetic systems. For example, the baseline determining the seaward border of a coastal nation's jurisdiction is defined as the mean low water in most cases (Shalowitz, 1962; Shalowitz, 1964). The vertical datum used in Germany and large parts of Western Europe from 1879 to 1992 is also based on tidal levels, in this case the Amsterdam Ordnance Datum, which represents the historical mean high water in Amsterdam between September 1, 1683 and September 1, 1684 (Liebsch, 2009). In today's world, there are additional topics added like increasing considerations of renewable energy schemes, assessments of land erosion, nautical safety and coastal protection (Pugh & Woodworth, 2014; Haigh et al., 2020). Tides not only control the navigability of some ports and sea routes, but also have a major influence on the intensity and timing of extreme sea levels during storm surges (e.g. Prandle & Wolf, 1978; Horsburgh & Wilson, 2007; Arns et al., 2020). For all of these reasons, it is apparent that for a very long time, mankind has had an increased interest in understanding the tides and its generating forces. It is therefore not surprising that the connection between tides and the Moon was already known 4,000 years ago (Stewart, 2008), even though it took until the 17th century to identify the importance of the relative position of Sun, Moon and Earth. The calculation and prediction of tides as a superposition of individual periodic oscillations was not even developed until the late 19th century. First accurate predictions were based on the Equilibrium Tides Theory, which incorporates the periodic and thus predictable nature of astronomical variations, regarding the orbits of Sun, Moon and Earth. These astronomical periods occur on both very short (< 1 d) and very long (> 20,000 yr) time scales, with the 14.77-day spring neap cycle and the 18.61-year nodal cycle being particularly important examples (Pugh & Woodworth, 2014). Given their close connection to the periodic and predictable nature of astronomical variations, the amplitudes and phases of tidal constituents as well as their corresponding tidal water levels were generally assumed to be periodic and stationary on time scales over which basin geometry undergoes only minor changes (i.e. decades to centuries). However, Keller (1901) showed increased tidal amplitudes due to reflection and local resonance changes as a result of building measures such as weirs (e.g. in the Ems River). Similarly, Doodson (1924) pointed to appreciable secular perturbations in the local tidal regimes of particular ports, weirs, and estuaries. More recently, the topic of changes in ocean tides has been revived and extended to the scales of shelves, basins and the global ocean - a development driven by the digitization and publication of global data sets of tide gauge records, see Woodworth et al. (2017). In fact, statistically significant tidal parameter trends in the range of a few percent are now well documented for many places around the world (e.g. Jensen, 1984; Führböter & Jensen, 1985; Woodworth et al., 1991; Flick et al., 2003; Ray, 2009; Jay, 2009; Mawdsley et al., 2015;

Talke & Jay, 2017). Fluctuations of similar magnitude and regional extent have further been observed on interannual time scales (e.g. Müller, 2011; Devlin et al., 2014; Feng et al., 2015; Ray & Talke, 2019).

Despite this ample evidence of changes in tidal water level series, the forcing factors and spatial extent of secular and short-term variability in tides are still uncertain, while the astronomical forcing was nearly constant over the observed period. Woodworth (2010) succeeded in detecting coherent patterns of amplitude and phase trends in primary constituents along the North American coasts, but found less regional consistency in data from Asia, the Australian Seas or Europe. However, some spatially coherent changes could still be observed in smaller and well-instrumented areas. A major problem identified by Woodworth (2010) is that small-scale (often site-specific) and large-scale changes may occur simultaneously, thereby impeding research of the underlying physical processes. Over wider coastal sections, and at sites open to the sea, the effects of a rise in mean sea level (MSL) on tidal wave propagation seems to explain only a fraction of the observed trends (Müller et al., 2011; Schindelegger et al., 2018). Accordingly, the assumption persists that other mechanisms - such as changes in stratification, turbulent dissipation, and variations in shoreline position or bed roughness - play major roles. The present consensus is that in many areas of the world a combination of different oceanographic processes may be involved. For instance, Ray & Talke (2019) suggest large secular changes of the lunar M_2 tidal constituent in the Gulf of Maine, caused by both sea level rise and persistent stratification changes. Yet, as implied above, any contributing mechanism will act on its own characteristic spatial and temporal scales, overlaying and possibly reinforcing other processes. This particularly applies to anthropogenic construction measures (e.g. building of dykes and tidal barriers) that can cause transient perturbations to the local tidal regime and affect adjacent stretches of coastline (Talke & Jay, 2020). Therefore, a major challenge is the separation of local effects and large-scale changes as well as their subsequent attribution to certain forcing factors.

An example of exceptionally tidal variations on both small and large spatial scales is the North Sea. Changes were first detected in the southeastern parts of the basin (German Bight) by Jensen (1984) for the three tidal parameters tidal low water, tidal high water and tidal range. Significant increases in tidal high water and tidal range as well as neutral trends in tidal low water were then documented in Führböter & Jensen (1985); for an updated overview see Jensen (2020a). Between 1958 and 2014, changes in tidal range as a proxy for divergent developments in tidal low and high water amount to approximately 3% (e.g. Helgoland, #55, numbering here and in the following with reference to Figure 12/Table 5) at some of the investigated tide gauges and to more than 11% at others (e.g. Wyk auf Föhr, #65, Figure 1). The latter is equivalent to a trend of 5.7 mm/yr at Dagebüll (#66) for example and outpaces the simultaneous local (~2 mm/yr, Dangendorf et al., 2015) and global MSL rise, which is approximately 3 mm/yr today (Dangendorf et al., 2019) and was at around 1.5 mm/yr between 1900 and 2012 (Oppenheimer et al., 2019). This magnitude of tidal range change is one of the highest in the world, only exceeded by developments in the Gulf of Maine (Ray & Talke, 2019).

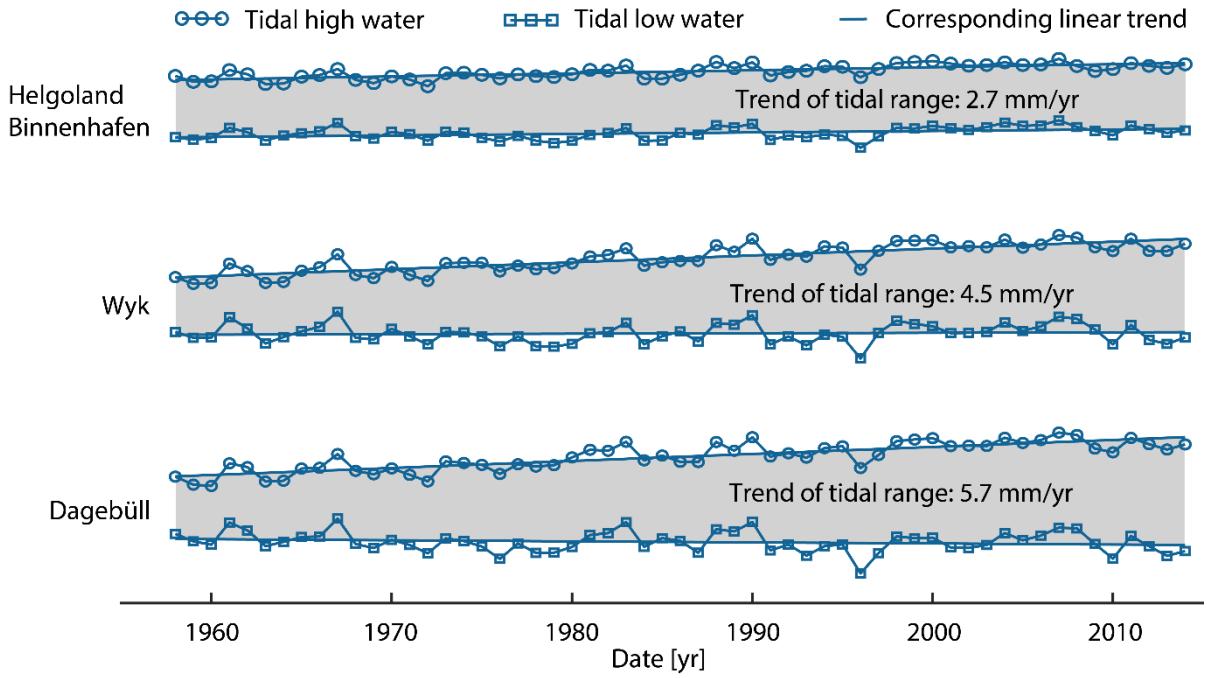

Figure 1: Time series of mean annual tidal low and high water levels for three exemplarily selected stations in the German Bight. For illustration purposes, all records are shown with different artificial vertical offsets. The increase in the tidal range is illustrated for the three sites as grey shaded areas between high and low water level time series.

Furthermore, the overlap between local and large-scale effects in the North Sea is particularly pronounced, possibly nurtured by the region's character as a shelf sea with its tide being generated in the Atlantic. Previous research (summarized in Jensen et al., 2014) has ruled out astronomical, large-scale morphological or tectonic causes (at least in the German Bight), but pointed to the generally nonlinear and non-uniform behavior of water levels in the North Sea. A general rise in the MSL and associated changes in the reflection and friction in the German Wadden Sea are cited as possible causes by Führböter & Jensen (1985), although Jensen (1984) already pointed out the possibility of a general change in tidal dynamics within the entire North Sea region. Both publications recommend the use of large-scale data sets for the entire North Sea basin in the near future. Jensen et al. (1991) extended these recommendations to include renewed investigations in the farer future, since sufficiently long time series for the entire North Sea basin were not yet available. Since these questions have not been conclusively answered to the present day, the aim of this thesis is to investigate the tidal changes in the study area North Sea and to detect possible physical causes. Therefore, the following questions will be addressed:

(1) Are the changes in tidal low water, tidal high water and the tidal range detected within the German Bight a localized phenomenon, or are they part of a large-scale development spreading over adjacent areas within the North Sea region?

(2) Is it possible to separate and quantify large-scale and small-scale effects from observed records?

(3) Can physical causes be attributed to the observed large-scale changes?

1.2 Structure and approach of this thesis

Due to the complexity of the research questions and the novel application and combination of otherwise unrelated statistical methods, both the structure of this thesis and the overall calculation procedure is described here, intending to serve as a guide. First, the general structure of the thesis is described without methodological details. Then the chosen approach to answer the research questions is explained and a survey of the methodology used is given.

In order to answer the above defined research questions, it is necessary to understand the theoretical background of tides and the underlying physical laws. For this purpose, Chapter 2 presents these backgrounds as well as the current state of research. Since the focus of this thesis is mainly on the changes occurring in tidal parameters of the North Sea and especially in the German Bight, the characteristics and peculiarities of this area are addressed at the beginning of Chapter 3. The data sets obtained, the data processing and the characteristics of the three tidal parameters tidal low water, tidal high water and tidal range are described here as well. In Chapter 4, the different statistical methods and their mathematical backgrounds are presented. Since a novel combination and application of these methods is applied in this thesis, not only the theoretical suitability of the methods is explained here, but also a practical validation is carried out and the fundamental suitability of the methods is demonstrated in Chapter 4.5. According to the results of the validation, Chapter 5 describes the results of the processing and adjustment of the initial data set. The answers to the research questions raised are afterwards given in the chapters 6 to 8. Chapter 6 describes the detectable changes of the tidal parameters in the North Sea basin and the first research question is answered. The separation and quantification of the detected tidal variations into large-scale and small-scale changes is presented in Chapter 7, responding to the second research question. Chapter 8 addresses the third research question and establishes a link between the detected large-scale effects and physical forcing factors. Even though the basic suitability of the methodology was validated in Chapter 4.5, a comparison between the originally measured data sets and the final results obtained is added in this chapter to rule out any artificial bias due to the applied methodology. However, as some aspects of these linkages border on the limits of the current state of the science, further possibilities for analysis emerge. These possibilities and current limitations are explicitly addressed in Chapter 9. Recommendations for achieving future knowledge gains are also given, after the results of the thesis are finally summarized in Chapter 10.

In order to explain the general approach of this thesis, it must first be noted, that most of the studies mentioned in Chapter 1 (e.g. Woodworth, 2010; Müller et al., 2011; Schindelegger et al., 2018; Ray & Talke, 2019, among others) examine changes in individual tidal constituents. This approach makes it difficult to exactly quantify how the changes in the individual tidal constituents combine to alter the observed tidal curve due to nonlinear interactions and the non-tidal residual (Mawdsley et al, 2015). Furthermore, tidal constituents are a rather abstract representation of the tides due to their origin in purely hypothetic celestial bodies and only the two dominant tidal constituents (M_2, S_2) represent an

actual physical reality (Pugh & Woodworth, 2014). Since each additional layer of abstraction basically further distorts the representation of reality and no clear advantages arise from the consideration of tidal constituents, a different approach was chosen here. In this thesis, only the M_2 and S_2 tidal constituents are considered and used primarily for control purposes and plausibility checks of the results, while the main analyses are based on direct measurements (i.e. total water levels). A survey of the methodology applied to the measured data basis can be taken from the flow chart in Figure 2.

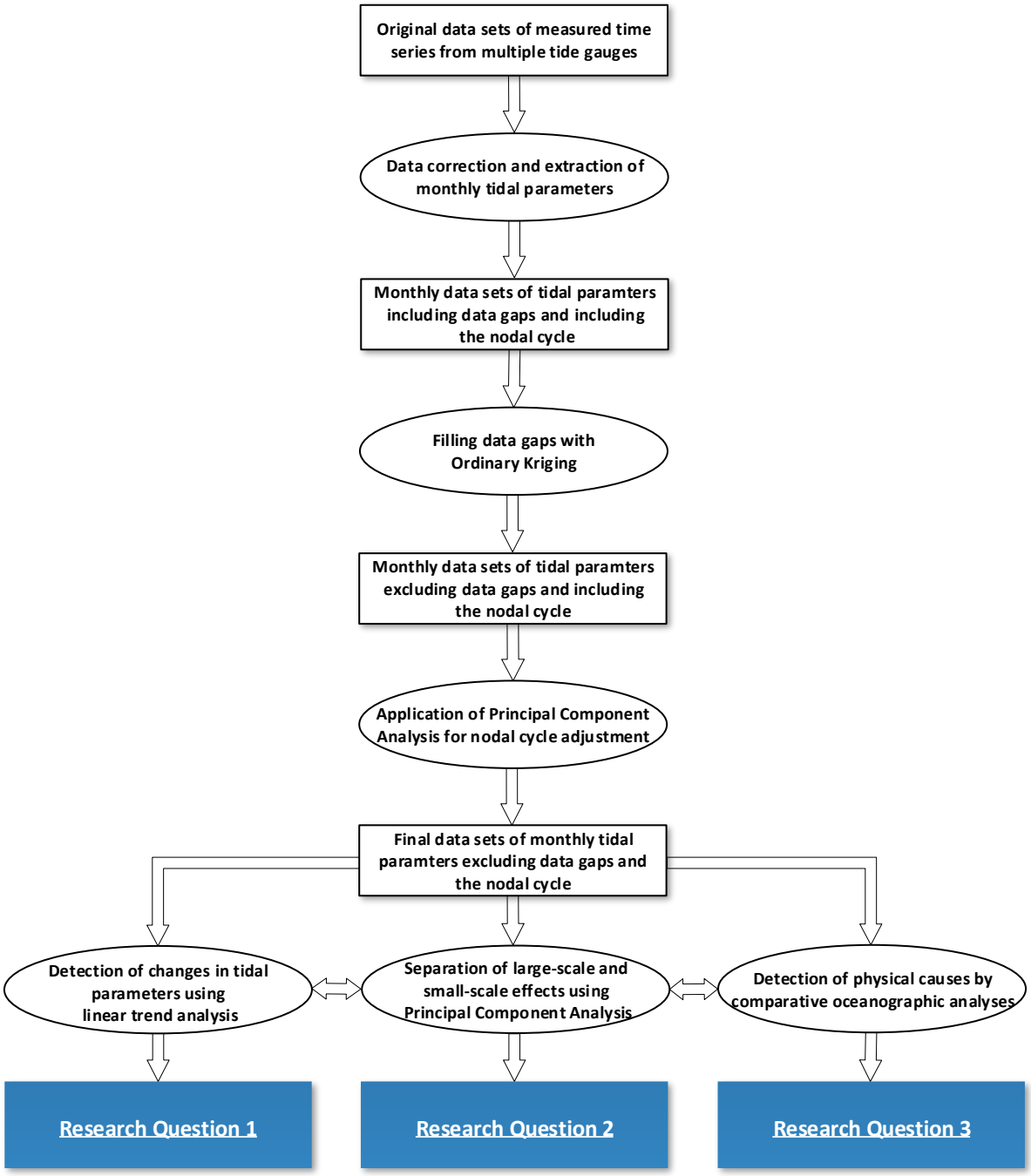

Figure 2: Flow chart of the chosen approach with reference to the research questions assigned.

The starting point for the explanation of the methodology is the collection of unaltered water level time series from North Sea tide gauges, containing incorrect values, influences of seasonality, data gaps and the nodal cycle. Before monthly time series of tidal parameters are calculated, these data sets are corrected for faulty values and impacts of seasonality, but still including data gaps and the nodal cycle. The data gaps are then closed by the interpolation procedure of Ordinary Kriging. Subsequently, the nodal cycle must be removed, using the statistical method of Principal Component Analysis (PCA). Please note that this procedure is applied recursively in 2 steps, first to eliminate the nodal cycle and in a later step to detect other large-scale signals. This approach in using PCA is based on the idea that if there are indeed large-scale signals affecting the tidal parameters in the North Sea, they should appear as coherent patterns visible at multiple sites, and be visible in the leading Principal Components (PCs). Simultaneously, spatially confined ("small-scale") anomalies in tidal parameters will be shifted into the higher PCs, making it possible to detect and separate different processes that influence the tidal parameters on different spatial scales. Since the nodal cycle as an astronomical parameter impacts all tide gauges in the North Sea, it can be defined as a large-scale effect and be separated and removed. Therefore, the final data basis for the following analyses is obtained.

These adjusted monthly data sets of tidal parameters excluding data gaps and the nodal cycle are used then for basin-wide linear trend analysis in order to answer the first research question. Furthermore, the final data basis is also used for re-running the PCA to determine the remaining large-scale signals other than the nodal cycle. Here, a link is established to the results of the trend analysis, since the large-scale signals must explain the large-scale trends sufficiently. The findings of these analyses are the answer to the second research question. The third and last research question is the analysis of possible physical causes. For this purpose, several oceanographic parameters are compared to the common, large-scale signals of the tidal parameters in order to identify commonalities and to understand the occurring physical processes. Again, this is linked to the first two research questions, since the physical causes must fit both the actual measured trends and the detected large-scale effects.

Please note: The results of the DFG-funded research project TIDEDYN (*Analyzing long term changes in the tidal dynamics of the North Sea*, project number 290112166), which I worked on from December 2016 to April 2020, are included in this thesis. Individual sections may therefore overlap with parts of the final report. Furthermore, parts of the results have already been published in the Journal of Geophysical Research: Oceans (Jänicke et al., 2020). The main work of this publication was done by the first author. The other authors were mainly involved in the research project TIDEDYN and/or participated in helpful technical discussions as well as giving valuable advices and comments for the preparation of the mentioned publication.

2 Theoretical background and state of the art

2.1 The astronomical generation of tides

Even though the existence of a causal relationship between Moon and tides was already known 4,000 years ago (Stewart, 2008), Johannes Kepler (1596–1650) was the first to verifiably suspect a gravitational attraction of the Moon to the oceans, even before Newton discovered his law of universal gravitation. Based on Kepler's ideas, Newton (1642–1727) was able to apply the laws he had discovered on water levels and Moon observations, proving the link between tidal water level oscillations and the position of the Moon and the Sun (Newton, 1687; Pugh, 1987). On a very general level, the tidal activity on Earth is described by Newton's law of universal gravitation, which was published in 1687 and is described in Eq. 1:

$$F = G \cdot \frac{m_2 \cdot m_1}{r^2} \qquad \textbf{Eq. 1}$$

Every mass m_1 [kg] regardless of its size attracts any other mass m_2 [kg] in the universe with a force F [N], depending on the product of the masses and the square of the distance r [m] between their centers. In this equation, G denotes the universal gravitational constant and amounts to $6.67 \cdot 10^{-11}$ $N \cdot m^2 \cdot kg^{-2}$ (Newton (1687). This commonly used explanation is slightly simplified, since Newton's law of universal gravitation is actually to be applied to each individual particle of the masses involved (Pugh, 1987). However, for the analyses concerning the gravitational effects on the tidal processes on the Earth, the following assumption in accordance with Gauss's law of gravitation is permissible, since relativistic gravitational effects are not of importance here: The involved masses are concentrated at a single point in the center of their spheres, for example Earth and Moon (Pugh & Woodworth, 2014).

In an Earth-Moon system, it is the gravitational pull of the Moon acting on the Earth and its oceans that causes the formation of tides. Since the masses of Earth and Moon can be considered constant as well as the gravitational constant G, Eq.1 demonstrates that the distance between Moon, Earth and the relative position to each other is the decisive factor in the formation of tides. The same effects occur analogously when including the gravitation of the Sun. Therefore, the tides of Earth's oceans are largely caused by the gravitational pull of the Moon and the Sun (Stewart, 2008). The resulting gradient of the gravity fields of Moon and Sun is often referred to as tidal potential. However, for the description of these basic principles and due to the analog impact of each added celestial body, only the Earth-Moon system is referred to for the moment.

In addition to the described purely gravitational effects, centrifugal forces caused by the rotation of the Earth-Moon system around their common center of mass also have a major impact on the tides and create an in motion, dynamical physical system. This dynamic ocean response to the gravitational forces of the Moon in a rotating system was first described by Laplace (1749–1827) at the end of the

18th century, using periodic and harmonic mathematical terms. The rotation of Earth's center of mass (mE_i) and Moon's center of mass (mM_i) around their common center of mass (CM) is shown in Figure 3 with the index i indicating the different points in time.

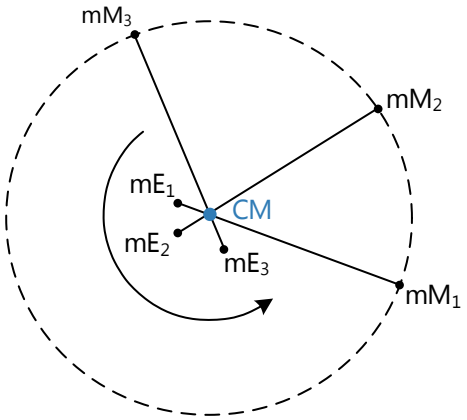

Figure 3: Schematic representation of the motion of Moon and Earth around their common center of mass (adapted form Pugh, 1987).

Due to the significantly higher mass of the Earth (~81 times the mass of the Moon), the common center of mass is still within Earth's radius, namely 4,671 km from its center (radius Earth: ~6,371 km). In contrast to the simplified representation here, note that Moon's orbit around the Earth is not circular, but elliptical. Following the explanations to Eq.1, CM is not only the common center of mass, but at the same time the center of the common gravity, around which the common rotation occurs and the centrifugal forces arise. Similar to the relative positions of Earth and Moon in the context of the gravitational pull, the common or relative rotation is the decisive factor here (Pugh & Woodworth, 2014), resulting in a superposition of centrifugal forces and gravitational forces (Figure 4).

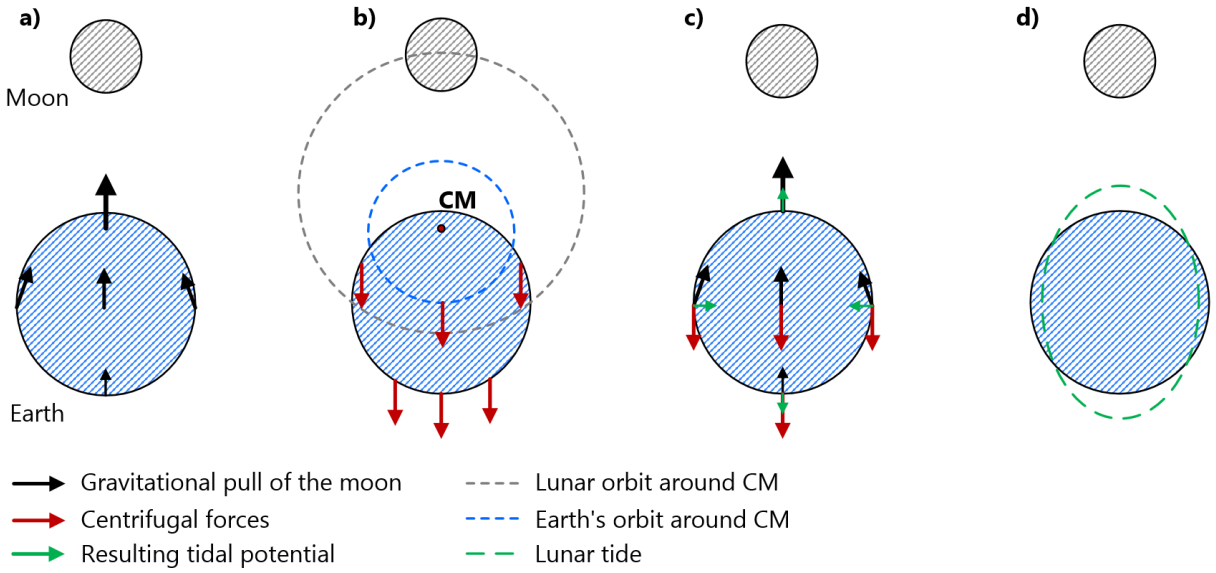

Figure 4: Simplified representation of lunar tidal forces, (a) gravitational pull of the Moon, (b) centrifugal forces and common center of mass of Moon and Earth CM, (c) forces from (a) and (b) and resulting tidal potential, (d) lunar tide as superposition of (a) and (b).

The gravitational pull of the Moon towards the side of the Earth facing the Moon (Figure 4-a) is opposed to the centrifugal forces (Figure 4-b) towards the side of the Earth facing away from the Moon. While the gravitational pull of the Moon according to Eq.1 is distance-dependent and differs at different places on Earth, the centrifugal force around CM remains constant (Pugh, 1987). The direction of the gravitation pull also differs from place to place at a given time, since it is always directed towards the center of mass of the Moon, while the direction of the centrifugal forces are equal at a given time. The superposition of these forces (Figure 4-c) translates then into the theoretical tidal potential of the Earth-Moon system (Figure 4-d).

For a better understanding of this superposition, a purely theoretical, oceanic Earth without land masses can be considered. On such an Earth, the superposition of the force vectors from Figure 4-c would produce only 2 large tidal waves, circling at opposite sides of the globe. This theoretical concept, in which only the forces of Moon and an oceanic Earth are taken into account, is often called Equilibrium Model with resulting Equilibrium Tides or more generally Equilibrium Theory of Tides. Laplace's calculations also refer to this system, since this was the only way to obtain an analytical solution for calculating the tide. The occurring amplitudes of the global tidal waves are very small, reaching only 0.24 m at their Earth-wide maximum on the equator (e.g. Pugh, 1987; Stewart 2008; Pugh & Woodworth, 2014). Even if this model idea does not correspond to reality due to the deflection of tidal waves by land masses, different water depths and many other effects which will be described in Chapter 2.2, it explains very precisely the theoretical impact of astronomical effects on the tidal dynamics of the Earth.

Up to now, primarily the Earth-Moon system was considered, which is now complemented by the Sun. The physical mechanisms of Sun’s influence on the oceanic tides of the Earth is analogous to the Moon’s influence, since the underlying physical principles remain the same for a rotational system of 2 or 3 celestial spheres. Again, centrifugal forces exist around the common center of mass (of Earth, Moon, and Sun) as well as gravitational forces. Under the approach of the Equilibrium Tide Theory, an Earth-Sun system can be considered analogous to the Earth-Moon system, in which the Sun then likewise causes two bulges on opposite sides of the Earth. In reality, of course, there is a superposition of the two impacts of Moon and Sun, which is demonstrated in Figure 5.

Since the centrifugal and the gravitational forces of the Sun and the Moon have different sizes and directions, the solar tide and the lunar tide are different in amplitude and phase (Figure 5-a). If the Earth-Moon-Sun system is analyzed under the specifications of the Equilibrium Tide Theory, the resulting solar amplitudes are smaller than the lunar amplitudes by a factor of 0.46, reaching 0.11 m on the equator (Pugh & Woodworth, 2014). The observed tides of Moon and Sun are in most cases much larger than the Equilibrium Tides due to the dynamic response of the ocean to the tidal forces and further assumptions of the Equilibrium Tide Theory (e.g. Pugh, 1987; Stewart 2008; Pugh & Woodworth, 2014). Nevertheless, the superposition of the observed (larger) lunar and solar tides explains most of the actual oceanic tides on Earth (Pugh, 1987), despite the reduction of the amplitudes as a result of the chosen simplifications. The dominant influence of these two celestial bodies on Earth's tides persists outside

the Equilibrium Tide Theory. Therefore, the extreme points of the system are of major importance, when the force vectors of Moon and Sun are horizontal to each other for an additive superposition (spring tide, Figure 5-b) or vertical to each other for a subtractive superposition (neap tide, Figure 5-c). In case of a spring tide, there is no phase shift between the vectors and the tides add up to larger water levels. In case of a neap tide, the phase shift is 90° and the resulting tide is minimized. The relative positions of the three celestial bodies to each other corresponding to these extreme points of the system are periodically recurring every 14.77 days and are called spring neap cycle (Pugh & Woodworth, 2014).

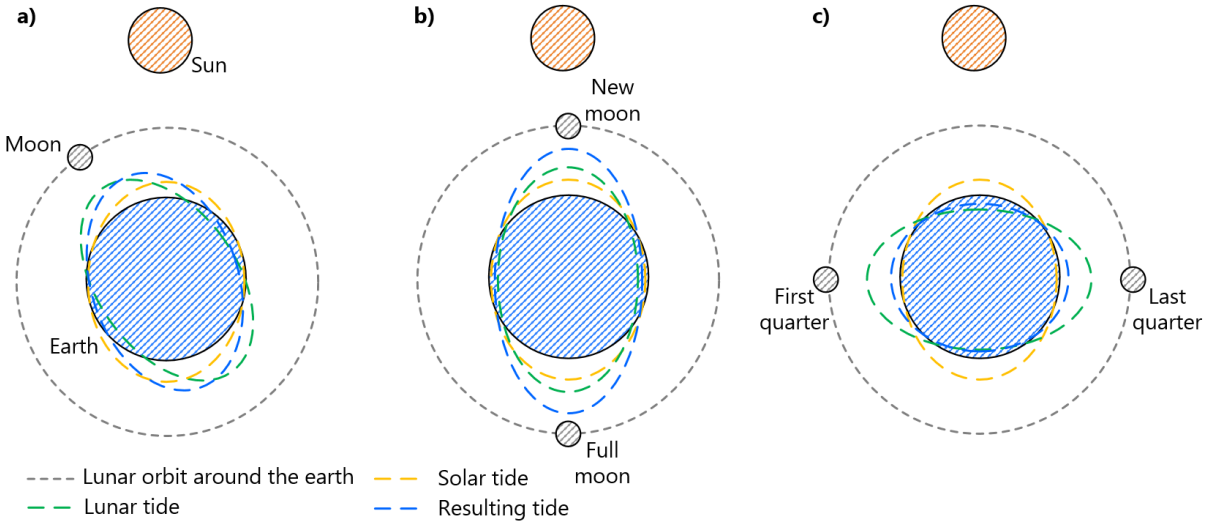

Figure 5: Simplified representation of lunar and solar tidal forces in the system Earth-Moon-Sun, (a) basic principle of superposition of lunar and solar tide, (b) extreme point spring tide, (c) extreme point neap tide.

In principle, the above considerations clarify that for a correct calculation and prediction of the tide, a superposition of several factors is necessary. Besides the different influences of Moon and Sun, the calculation is complicated by the fact that an analytical solution is only possible using periodic, harmonic mathematical terms as recognized by Laplace. This constraint is not matched by the actual orbits of the celestial bodies, since these are rather elliptical and irregular. For a correct analytical prediction of the tide, it is thus necessary to separate the acting forces not only according to the causal celestial body, but also according to different properties of the celestial body, e.g. different orbital irregularities. Since these occur periodically but at different times, not only the amplitude of the force but also the temporal components of the phase must be considered. Such a superposition of componentized tides of different origin, amplitudes and phases was first postulated by Lord Kelvin (1824–1907, civil name William Thomson), who referred to the components of the tide to be superimposed as tidal constituents. Kelvin presented the tide as the sum of various periodic mathematical terms and was the first to achieve an accurate prediction of the observed tides according to modern standards (Pugh & Woodworth, 2014). An exemplary calculation is given at the end of this chapter.

For the mathematical description of a periodic oscillation (which are the tidal constituents) in terms of harmonic analysis, information on amplitude and frequency is necessary. Based on the assumptions of the Equilibrium Theory, the tidal variation TV at a given time t and place can be expressed as finite sum of N of harmonic terms with the formula

$$TV(t) = \sum_{n=1}^{N} H_n \cdot \cos(\sigma_n \cdot t - g_n) \ [m] \qquad \textbf{Eq. 2}$$

H_n is the amplitude of the tidal constituent, g_n is the phase lag (also: tidal phase) of the tidal constituent compared to the Equilibrium Tide and σ_n is the angular frequency of the tidal constituent (adapted from Pugh & Woodworth, 2014).

At Kelvin's lifetime, many orbital variations of the Moon were still unknown and his work was pursued by Arthur Doodson (1890–1968), based on the progress of knowledge at his time. Doodson (1922) could not only improve the accuracy of the predictions, but also discovered the possibility of expressing the frequencies f_n of these variations as linear combinations of the 6 basic astronomical cycles of Sun and Moon:

$$f_n = n_1 \cdot f_1 \cdot n_2 \cdot f_2 \cdot n_3 \cdot f_3 \cdot n_4 \cdot f_4 \cdot n_5 \cdot f_5 \cdot n_6 \cdot f_6 \left[\frac{^\circ}{h}\right] \qquad \textbf{Eq. 3}$$

f_i denotes the frequencies (if the period p_n in hours is needed, $p_n = \frac{360}{f_n}$ applies) and n_i are the so called Doodson numbers (Stewart, 2008). The mathematical relationship to Eq. 2 is given by the angular frequency and reads as $\sigma_n = \frac{360 \cdot f_n}{2 \cdot \pi}$. It offers the enormous advantage of only needing the 6 basic astronomical cycles for tidal calculation, instead of various different frequencies. Tidal calculations are thus not only simplified up to this day, but numerical solutions could also be found in a short time using rudimentary mechanical calculating machines before the age of large computational power (Pugh & Woodworth, 2014). An overview of the astronomical cycles and their frequencies is given in Table 1.

Table 1: Fundamental tidal frequencies (adapted from Pugh & Woodworth, 2014).

f_i	Frequency [°/h]	Period	Source
f_1	14.49205211	1 lunar day	Mean lunar day
f_2	0.54901653	1 month	Sidereal Month
f_3	0.04106864	1 year	Tropical Year
f_4	0.00464184	8.85 years	Moon's perigee
f_5	0.00220641	18.61 years	Regression of Moon's nodes
f_6	*0.00000196*	*20,942 years*	*Sun's Perihelion*

The first astronomical cycle is the lunar day of 24 hours 50 minutes, which is the time the Moon needs to orbit the Earth once. It complies approximately to an angular movement and a frequency of $f_1 \approx \frac{360\,^\circ}{24.83\,\mathrm{h}} = 14.49\,\frac{^\circ}{\mathrm{h}}$ to achieve a full orbit of 360° within the period of 24 hours 50 minutes (Pugh & Woodworth, 2014). The second cycle is the Sidereal Month, denoting the period needed by the Moon to return to the same place in relation to the background of the stars (~27.32 d, frequency f_2). The tropical year is the third cycle (frequency f_3) and describes the orbit of the Earth around the Sun which takes 365.25 days. The fourth cycle is the gradual rotation of Moons orbit around the Earth (apsidal precession). It takes 8.85 years until the same Moon-Earth distance is reached again, an effect which is called Moon's perigee and is reflected in the frequency f_4. The regression of Moon's nodes is the fifth cycle and is often called the nodal cycle, a periodic change of angle between Moon and Earth (frequency f_5). The resulting change in tides is often referred to as nodal tide or nodal cycle. A practical discussion in the context of semidiurnal tides in the North Sea is given in Chapter 4.4 on the basis of the actual data situation and the methods used. Nevertheless, the physical background will be described here (Figure 6), since it is also necessary for the understanding of frequency f_5.

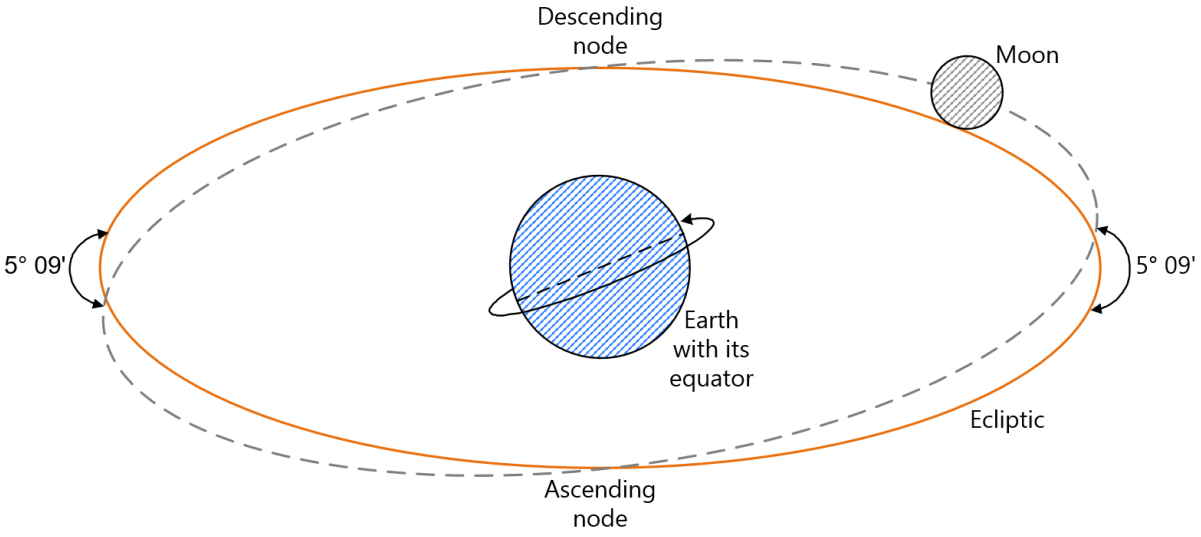

Figure 6: Simplified representation of the astronomical causes of the nodal cycle.

As shown in Figure 6, the main reference system in astronomy is the ecliptic, i.e. the plane at which the Earth orbits the Sun, which is inclined by 23° 27' to Earth's equator. The gradient between the Moons orbit and the ecliptic is around 5° 09'. As a result, within a period of 18.61 years an ascending node (up to the maximum nodal declination of 23° 27' + 5° 09' = 28° 32') and a descending node (down to the minimum nodal declination of 23° 27' - 5° 09' = 18° 18') are occurring. In the period covered by this thesis (1958–2014), theoretical maxima of the nodal amplitude occurred in 1959, 1978, 1997, and 2015 and theoretical minima in the years 1969, 1987, and 2006 (Pugh & Woodworth (2014). These changes in lunar declination have a high impact on lunar tidal components and can alter the semidiurnal lunar tidal components significantly, depending on water depth and position on earth (Pugh & Woodworth,

2014). The actual impact of the nodal cycle on measured water levels in context of the study area North Sea is assessed in Chapter 4.5.2.

Sun's perihelion refers to the sixth cycle and the effects of apsidal precession, a rotation of the entire earth orbit around the Sun, while shape and plane of the orbit remain the same. In the case of the Sun it takes 20,942 years until the same Earth-Sun distance appears again. In fact, the frequency f_6 is mostly not taken into account because its values are negligible for analyses with a temporal focus in era of instrumental measurements (Pugh, 1987) and it will be not considered any further in this thesis.

After the different frequencies f_i from Eq. 3 were discussed, the explanation of the Doodson numbers n_i is still missing. They are needed to represent the frequencies of the individual tidal constituents as a linear combination of the basic astronomical frequencies f_i. n_1 is used to define the tidal species. The range of possible values covers 0, 1 or 2, where 2 is used for semidiurnal tide, 1 for diurnal tide and 0 for long period tides with recurrence intervals of more than a day. The frequency of a lunar day is not important in that case and the frequency f_1 is omitted if n_1 is 0. The remaining values from n_2 to n_5 can adopt values between -5 and 5, jointly describing the proportions of basic astronomical cycles coded within f_n. Table 2 provides an overview of the most important and most widely used tidal constituents, while Doodson himself introduced 399 different tidal constituents. However, most of them have very small amplitudes and only the largest are displayed here.

Table 2: Principal Tidal Constituents (adapted from Steward, 2008).

Tidal Species	Name	Doodson numbers					Max. Equilibrium Amplitude	Period
		n_1 [-]	n_2 [-]	n_3 [-]	n_4 [-]	n_5 [-]	[m]	[h]
Semidiurnal	$\mathbf{n_1 = 2}$							
Principal lunar	M_2	2	0	0	0	0	0.24	12.42
Principal solar	S_2	2	2	-2	0	0	0.11	12.00
Lunar elliptic	N_2	2	-1	0	1	0	0.05	12.66
Lunisolar	K_2	2	2	0	0	0	0.03	11.97
Diurnal	$\mathbf{n_1 = 1}$							
Lunisolar	K_1	1	1	0	0	0	0.14	23.93
Principal lunar	O_1	1	-1	0	0	0	0.10	25.82
Principal solar	P_1	1	1	-2	0	0	0.05	24.07
Elliptic lunar	Q_1	1	-2	0	1	0	0.02	26.87
Long Period	$\mathbf{n_1=0}$							
Fortnightly	M_f	0	2	0	0	0	0.04	327.85
Monthly	M_m	0	1	0	-1	0	0.02	661.31
Semiannual	S_{sa}	0	0	2	0	0	0.02	4,383.05

Today's common nomenclature as used in Table 2 is based on the work of Darwin (1845–1912) and was first published in Darwin (1911). For a better understanding and to illustrate the correctness of the procedure, the following example is used: As described above, both Sun and Moon cause 2 tidal waves each on opposite sides of the Earth according to the principles of the Equilibrium Tide Theory. Since the rotation of the Earth around its own axis takes 24 hours, a solar-induced tidal wave must occur every 12 hours at every point on the Earth. Similarly, the Moon needs a lunar day of 24 hours 50 minutes for one rotation around the Earth and the corresponding tidal wave would occur every 12 hours 25 minutes or 12.42 hours. These two tidal constituents are referred to as M_2 and S_2 ('M' represents the Moon, 'S' the Sun and '2' is the n_1 Doodson number, indicating a semidiurnal tidal species). Since the periods for these two tidal constituents are known, it can now be verified whether they can be expressed with the 5 astronomical basis frequencies.

Using the values from Table 1 and Table 2 as input for Eq. 3, the following results are obtained:

$$f_{M2} = 2 \cdot 14.492 + 0 \cdot 0.549 + 0 \cdot 0.041 + 0 \cdot 0.004 + 0 \cdot 0.002 = 28.984 \ \frac{^\circ}{h}$$

and for the period $p_{M2} = \frac{360}{28.984} = 12.420$ h

$$f_{S2} = 2 \cdot 14.492 + 2 \cdot 0.549 - 2 \cdot 0.041 + 0 \cdot 0.004 + 0 \cdot 0.002 = 30.000 \ \frac{^\circ}{h}$$

and for the period $p_{M2} = \frac{360}{30.000} = 12.000$ h

These results are in agreement with the physically expected results and illustrates that the 5 basic frequencies can be used to describe the frequencies that actually occur. This conceptual approach makes it possible to relate individual tidal harmonics or tidal constituents to real astronomical behavior of Sun, Moon and Earth. Based on these findings and Eq. 2, it is possible to determine the theoretical amplitude for each tidal constituent for any given time and place.

While almost every tidal constituent serve to describe the non-circular parts of the orbits of Earth, Moon, and Sun, only the M_2 and S_2 constituents are assumed to represent a physical reality (Pugh & Woodworth, 2014). Malcherek (2018) also characterizes the use of tidal constituents as physically incorrect, but nevertheless useful. As explained above, a harmonic analysis is not feasible to reproduce the actual movements of the Earth, Moon, and Sun since it is based on the superposition of different wave functions and depends on a strictly circular behavior of the individual components. This is not the case due to the varying distances and angular speeds in their orbits. The additional tidal constituents already introduced solve this problem by adding what is called phantom satellites. These are imaginary celestial bodies of various masses, which move on various planes with various speeds in an orbit parallel to the equator or stand at fixed positions, regarding the background of the stars (Pugh & Woodworth, 2014). Thus instead of considering the non-harmonic variations in the orbit of the Moon around the Earth in the mathematical

equations, which would make a harmonic analysis impossible, purely theoretical celestial bodies are added. Their gravitation, when harmoniously superimposed, produces the same physical effects on the tides like the non-harmonic orbital variations. An example of such a superposition of the total amplitude is shown in Figure 7.

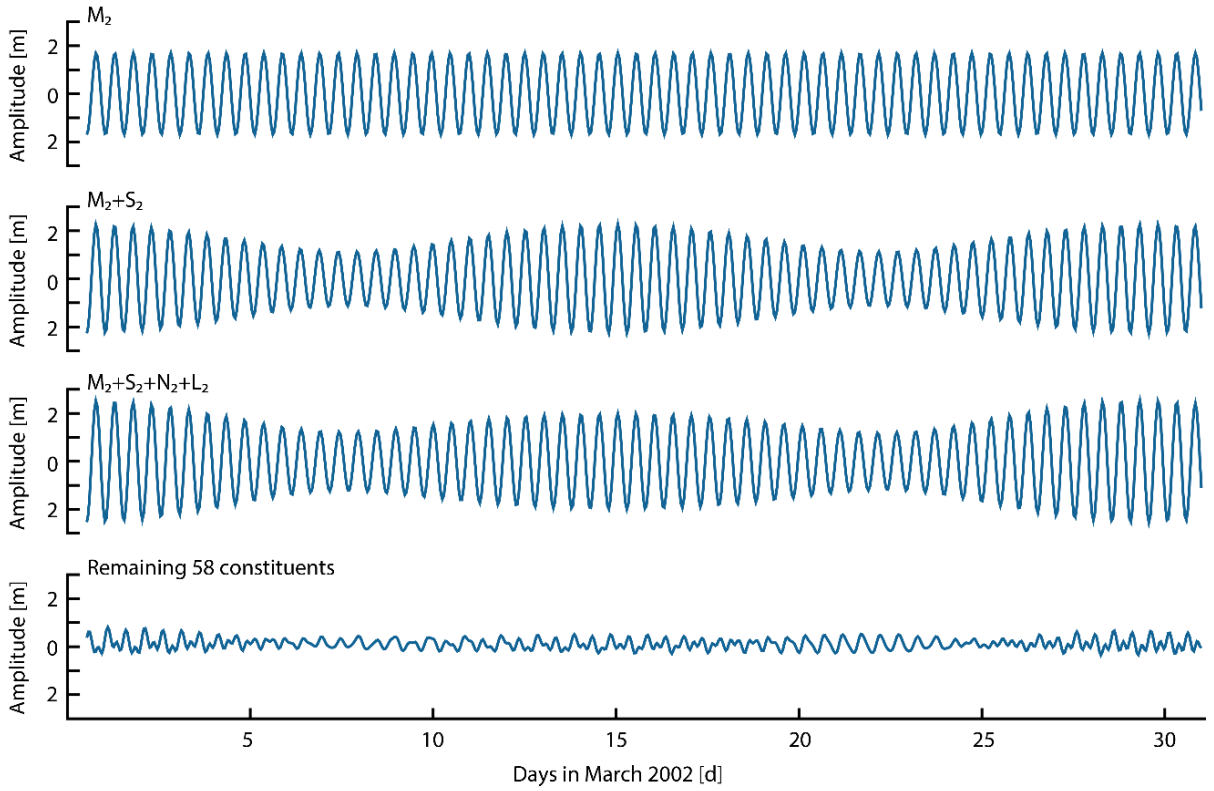

Figure 7: The effects of predicting tides with M_2, M_2+S_2, $M_2+S_2+N_2+L_2$ at Newlyn for March 2002. The bottom line shows the additional contribution to a full prediction, by a further 58 constituents (adapted from Pugh and Woodworth, 2014).

This method of superposition can be further illustrated using the example of N_2 and L_2 constituent (for the parameters of N_2 and L_2, see Table 2). In the above considerations for the derivation of the M_2 constituent, a perfect circular shape of the Moon orbiting the Earth is assumed, resulting in a constant distance between Moon and Earth and in constant tidal forces. In reality, this orbit is elliptical and consequently the distance between Earth and Moon varies over a 27.55 day period between the lowest (lunar perigee, stronger lunar tidal force) and the highest distance (lunar apogee, weaker lunar tidal force, Inman et al, 2005). This cycle exists independently of and in addition to the 8.85 year cycle discussed above, which reflects the distance changes between the Moon and the Earth due to apsidal precession. These 27.55 day deviations from the orbit cannot be neglected, as they can reach about 20% of the amplitude of the M_2 constituent. However, since an elliptical orbit cannot be described in a harmonic representation, a fictitious celestial body and a resulting fictitious tidal constituent N_2 were introduced. Moreover, the elliptical orbit of the Moon causes not only variations in the distance between the Moon and the Earth, but also changes the orbital velocity of the Moon. The result would be a phase shift of M_2 with a dependence of the amplitude to the orbital velocity. To account for this effect, another additional tidal constituent L_2 was introduced. If the tidal constituents M_2, N_2, and L_2 are combined, the result is a

tidal value, which takes into account the orbit of the Moon around the Earth on a lunar day as well as the orbital deviations of this orbit within a cycle of 27.55 days. The mentioned 8.85 year cycle for example would not be included in this tidal value. Such a combination of different tidal constituents is shown in Figure 7 using tidal constituents harmonically calculated from measurement data in Newlyn, United Kingdom (UK) in March 2002. In the upper part, only the tidal constituent M_2 is depicted, to which S_2 is added in the next step to display the dominant spring neap cycle. Next, N_2 and L_2 are calculated to represent the varying distance of the Moon from the Earth during a lunar month. In the bottom part of the figure, the remaining 58 tidal constituents are shown (in this analysis a total of 62 tidal constituents were determined). This exemplary calculation illustrates the functionality of the tidal constituents, however, the limitations of the method are also to be mentioned here.

It should be noted that even the use of all known tidal constituents does not fully describe the water level at a tide gauge and the predictions are never 100% accurate, since coastal water levels always contain non-tidal components such as meteorological impacts. One example is wind, which pushes water towards the coast or away from it, causing an increase or decrease in coastal water levels additional to the purely astronomical tidal signal. Another influence is the Inverse Barometer Effect (also: IBE or atmospheric loading), as the prevailing atmospheric pressure can further influence the water depth. These components are often referred to as non-tidal residual or meteorological residual (e.g. Pugh, 1987; Pugh & Woodworth, 2014; Haigh, 2017). It is also worth mentioning that the Highest and Lowest Astronomical Tides (often referred to as HAT & LAT), which are frequently used in nautical charts as the limit of navigability, are not determined as the sum of all maximum values of the tidal constituents, since physical dependencies exist here. For example, the semi-diurnal tidal water level tend to be smaller when the diurnal tidal water levels are reaching their maximum. To cope with these effects, statistical and empirical calculation methods for the computation of HAT & LAT were developed, which are not based on the principles of tidal constituents (Pugh & Woodworth, 2014). Another restriction concerning predictions from tidal constituents is the assumption of stationarity. Besides the well-known periodic variations from intra-annual to interannual to decadal and longer time scales, there are non-periodic changes on very long time scales. One example is the recession of the Moon from the Earth. According to Green et al. (2017), the lunar distance has increased by 4% in the last 252 million years, reducing the theoretical tidal generating potential by 13%. However, since the temporal focus in this thesis is much shorter, these non-periodic astronomical changes can be considered constant, as is the case in most studies over the era of instrumental measurements (Haigh et al., 2020).

Overall, despite these non-tidal residuals and the slightly non-stationary behavior on extensive timescales, it can be stated that both the theoretical, physical background and the actual predictions are based on the stationarity of the tides. There is a strong temporal change of the tides due to the change of the relative position of Earth, Moon and Sun, but these are of a purely periodic nature and the initial situation occurs again after a period of time that is fully known today. The six most important ones correspond to the Fundamental Tidal Frequencies from Table 1, e.g. 18.61 years for the regression of Moon's nodes

and the induced nodal cycle in tides. Consequently, significant long-term trends after exclusion of the known periodic behavior in tides are not created by astronomical influences, even considering the simplification of the Equilibrium Tide Theory. Occurring tidal changes can only be caused by changes in the response of Earth's oceanic system to the tidal potential, regardless of their specific cause. Therefore, an examination of the reactions of the Earth's oceanic system is provided in the next chapter.

2.2 The response of Earth's oceanic system to astronomical forces

The explanations of the previous chapter are based on the Equilibrium Theory of tides, assuming a purely oceanic Earth with a constant water depth and two symmetrical tidal bulges, resulting from the interactions of the Earth-Moon-Sun system. This approach is well suited to understand and mathematically explain the acting astronomical forces, but does not take into account the actual response of Earth's oceanic system including continental effects, channels, water depth and others. This response has a significant influence on the occurring tidal water levels, as can be easily observed from the larger values that actually emerge. While a superposition of all theoretical semidiurnal tidal amplitudes would reach their maximum of about 0.5 m at the equator according to Equilibrium Tide Theory, measured amplitudes of more than 10 m occur in reality far away from the equator. These enormous tidal amplitudes are found at several locations on Earth, for example at the Bay of Fundy, the Bristol Channel, the Bay de Mont Saint Michel or the Argentine Shelf (Pugh & Woodworth, 2014). The global distribution and the differing bathymetries and topographies of these areas exclude a local monocausality as possible cause. Therefore, there have to be numerous other factors affecting tidal expression on Earth on different spatial scales, making it evident that the response of the oceanic system to the astronomical forces causes significant variations compared to the idealized system of the Equilibrium Tide Theory. Since these variations differ in their spatial extent, it is useful to distinguish between local and regional to global reactions of the oceanic system, following the classification of Haigh et al. (2020). In the following, these reactions and effects are examined in more detail in order to explain the observed tides in contrast to the theoretical tides of the previous chapter.

At the global scale, manifold processes can contribute to tidal water levels. The most frequently cited processes are tectonics with their resulting amphidromic areas, water depth, marine ice sheet margins, nonlinear interactions and radiational forcing (e.g. Woodworth, 2010; Müller et al., 2011; Müller, 2012). A first-order influence are the tectonic properties of the Earth. In contrast to the Equilibrium Tide Theory, there is no oceanic Earth due to the presence of continental plates and land masses, but a multitude of interconnected basins. The only area where a contiguous sea surrounds the Earth in a circumpolar direction is the Antarctic Ocean (with the Drake Passage being still a narrow corridor). Since tidal waves can be characterized as periodic oscillations, they react sensitively to the size and shape of the basins. The occurring resonances and superposition of both individual and successive tidal signals lead to a significant increase in tidal amplitudes (Haigh et al., 2020). Conversely, Green et al. (2018) prove that due to the formation of supercontinents on geological time scales, i.e. the accumulation of almost all

land masses to form a continuous continent (e.g. Pangaea), the tides were very weak and almost equal to the Equilibrium Tide. These calculations demonstrate that a reduction of Earth's tidal impacting factors causes a convergence to the theoretical values of the Equilibrium Tide Theory.

Another phenomenon not considered by the Equilibrium Tide Theory is the appearance of amphidromic areas. Amphidromic areas are mainly determined by the geometry of the land masses and the Coriolis force, which results from Earth's rotation. According to Newton's first law, the motion of a body is only altered when an altering force occurs (Newton, 1687). Nevertheless, the direction of some physical bodies on large scales like tidal waves seem to change without such an external force. This effect is not caused by a changing of the velocity vector of the tidal wave, but by a change of the reference system Earth. Therefore, the Coriolis force is a pseudo-force in strict physical terms. Pseudo-forces are created by the movement of their surrounding reference system per definition, in this case the rotation of the Earth. In this context, however, this distinction is of academic nature, since the difference between force and pseudo-force does not matter for the observed deflection (Stewart, 2008). On a rotating Earth, an imaginary long progressive wave travelling in a channel moves in dependence to the Coriolis force, which deflects the wave towards the right boundary (in direction of motion) on the Northern Hemisphere and against the left boundary on the Southern Hemisphere.

That is why tidal waves feature a clockwise angular momentum in the Northern Hemisphere and counterclockwise angular momentum in the Southern Hemisphere. The resulting build-up of water leads to an altered surface elevation and a pressure gradient, which is in equilibrium with the Coriolis force. The arising gradient of the water level is dynamic and is called a Kelvin wave after its discoverer Lord Kelvin (Pugh & Woodworth, 2014). Kelvin waves create the balance between the Coriolis force and the nearest topographic boundary such as a coastline. The point around which the Kelvin wave rotates does not exhibit a displacement of the surface elevation and is defined as the amphidromic area. This area is often calculated theoretically for the individual tidal constituents and is then called amphidromic point. As mentioned above, the direction of rotation around the amphidromic point or area follows the effect of the Coriolis force, giving tidal waves a clockwise angular momentum in the Northern Hemisphere and a counterclockwise angular momentum in the Southern Hemisphere. Exceptions exist when the Coriolis force is superimposed by other influences such as the topography or large currents and an opposite rotational movement occurs, as for example in the South Atlantic. Another example occurs in the North Atlantic, where the northward tidal wave of the Atlantic turns right into the North Sea, but follows the coastline in the basin counterclockwise afterwards (Pugh & Woodworth, 2014).

Figure 8 shows the dynamics of an amphidromic point in outline form. On the left side of the figure it is shown that in an idealized system of Equilibrium Tide Theory without Earth's rotation and friction, no Kelvin wave and no amphidromic area exist. In an ideal system including Earth's rotation but excluding other effects such as friction or more complex geometries, the amphidromic point forms at equal distances from the left and right boundary (Figure 8, center). On the right side, friction is taken into account, but no complex or realistic geometry. The Kelvin wave then weakens due to energy loss by

friction during its rotational movement, causing shifts of the amphidromic points to the left on the Northern Hemisphere and to the right on the Southern Hemisphere (Pugh & Woodworth, 2014).

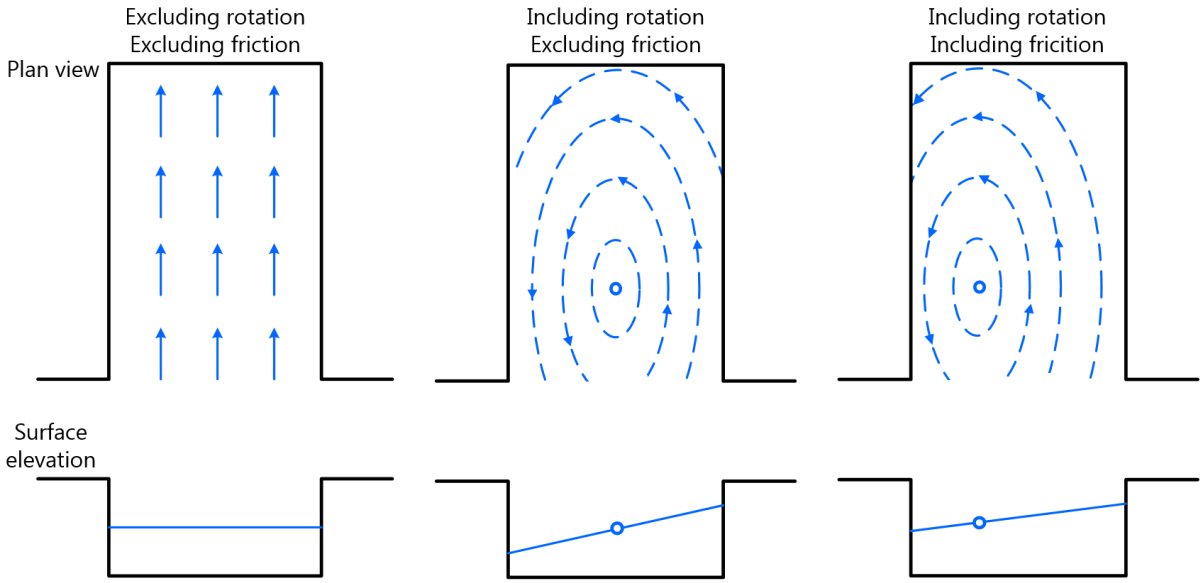

Figure 8: Dynamics of amphidromic points; Top: Direction of the tidal wave (arrows), co-range lines (dashed) and amphidromic point (circle); Bottom: Inclination of the surface elevation as a result of the Coriolis force and tidal friction (adapted from Pugh & Woodworth, 2014).

The discovery of Kelvin waves is of great importance for tidal studies as it allows the calculation of the tide as a rotation around an amphidromic point, given a sufficient distance from the boundaries for an unaffected rotary movement. Figure 9 shows the amplitudes of the dominant semidiurnal M_2 and diurnal K_1 tidal constituents, where K_1 represents the daily change of the declination of the Moon (i.e. simplifying the angle at which the Moon is above the equator), including their amphidromic points. The larger amplitudes of the semidiurnal M_2 compared to the diurnal K_1 are due to the distribution of land masses and for resonance reasons, since the ocean depth and the distribution of land masses are near-resonant to the semidiurnal tides today (Pugh, 1987). Overall, the sum of the described effects of land mass distribution and Coriolis force results in strong discrepancies to the equilibrium state.

The significant regional differences of M_2 and K_1 from their maximal theoretical values of 0.24 m and 0.14 m at the equator (Table 2) are evident in Figure 9. Also the above mentioned example can be considered. Especially for the west of the UK (Bristol Channel) and for the west of France (Bay de Mont Saint Michel), unusual large amplitudes of M_2 can be observed. Similarly, increased amplitudes are detectable in the area of Nova Scotia (Bay of Fundy) and the Argentine Shelf. However, these findings should not mask the fact that the unusually high tidal range in these areas, especially in the Bay of Fundy and the Bristol Channel, is heavily influenced by local factors like resonance, which are mentioned later in this chapter.

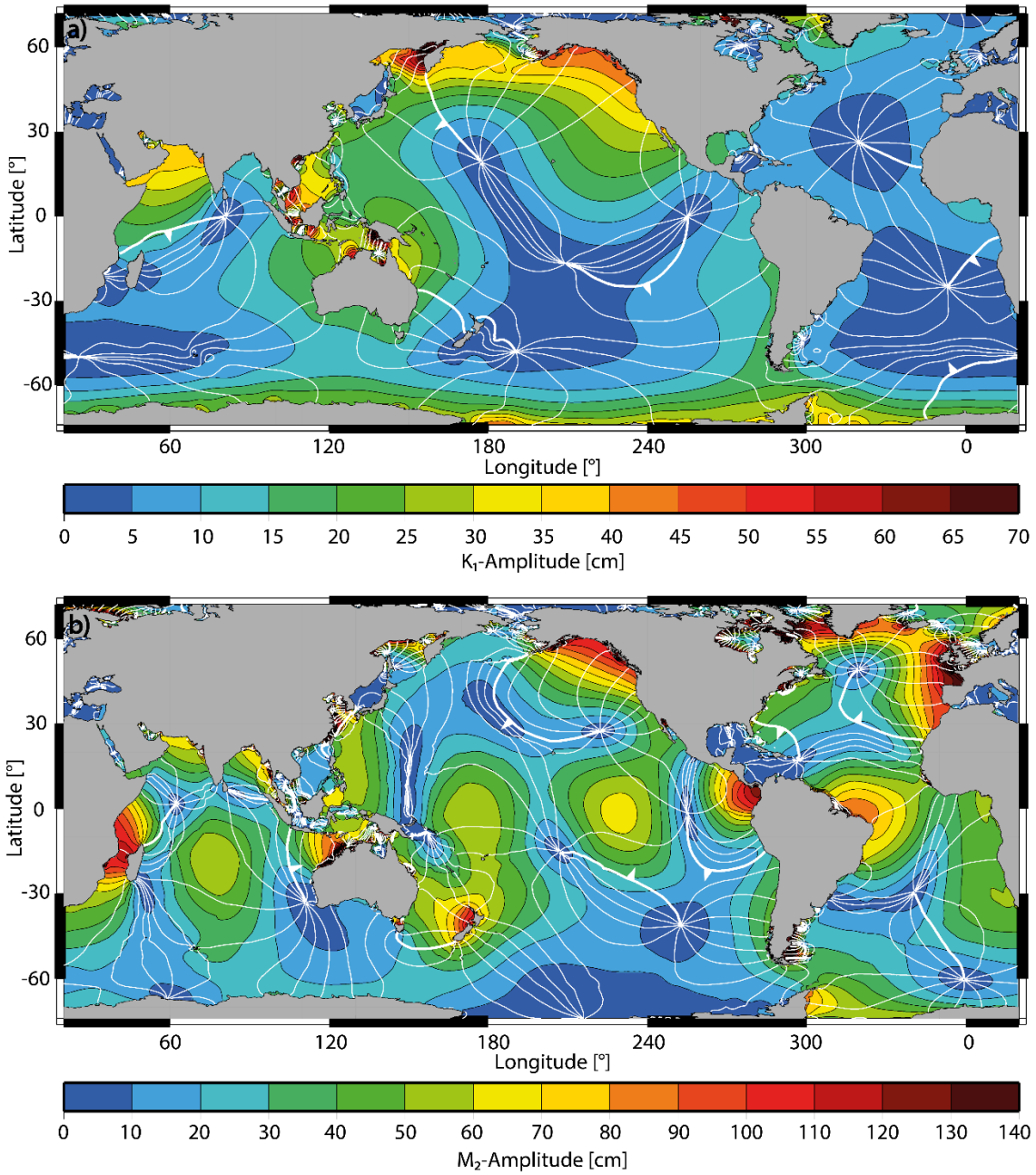

Figure 9: Co-tidal charts of the global K_1 (a) and M_2 (b) tide: global maps of lines joining places where amphidromic points of K_1 (a) and M_2 (b) occur (Pugh & Woodworth, 2014).

Another important point contributing to tidal water levels on a global scale in the context of Earth's oceanic basins is the limiting property of water depth. According to the Airy wave theory (often referred to as linear wave theory), waves can be described mathematically depending on the water depth h and the wavelength L (Malcherek, 2010):

$$v = \sqrt{\frac{g \cdot L}{2 \cdot \pi} \cdot \tanh\left(\frac{2 \cdot \pi \cdot h}{L}\right)} \left[\frac{m}{s}\right] \qquad \textbf{Eq. 4}$$

For very small x, tanh(x) = x and the equation simplifies to:

$$v = \sqrt{\frac{g \cdot L}{2 \cdot \pi} \cdot \tanh\left(\frac{2 \cdot \pi \cdot h}{L}\right)} = \sqrt{\frac{g \cdot \cancel{L}}{\cancel{2} \cdot \pi} \cdot \frac{\cancel{2} \cdot \pi \cdot h}{\cancel{L}}} = \sqrt{g \cdot h}\left[\frac{m}{s}\right] \qquad \textbf{Eq. 5}$$

This simplification is widely accepted for tidal waves (Pugh & Woodworth, 2014; Malcherek, 2018), where the wavelength is much larger than the water depth. However, it can also be derived very easily, using the North Sea as an example here. According to the Airy wave theory (Malcherek, 2010), the wavelength L of a tidal wave with the period p can be calculated as follows:

$$L = \sqrt{g \cdot h} \cdot p\left[\frac{m}{s}\right] \qquad \textbf{Eq. 6}$$

The average water depth of the North Sea basin is between 70 and 90 m (Huthnance, 1991; Quante & Colijn, 2016), while the M_2 tide has a period of 12.42 h or 44712 s (Table 2). The resulting wavelength is about 1170 to 1330 km. For these values, the difference between tanh(x) and x is smaller than 10^{-9} and thus negligible, making only the water depth relevant for the tidal wave velocity. Due to the low water depth compared to the large wavelength, tidal waves are therefore referred to as shallow water waves.

Since the wavelength would be much larger than the water depth according to Pugh & Woodworth (2014), the simplified wave equation (Eq. 5) can be used for a global approximate consideration of the influence of water depth on an oceanic Earth. Following this equation and assuming an average ocean depth of ~4,000 m on Earth, an average velocity of ~198 m/s of the tidal wave can be calculated. The difference between tanh(x) and x is then $-7.51 \cdot 10^{-9}$ and the use of the simplified equation is permissible. At the equator, however, a sub-lunar point moves westward at a speed of ~450 m/s because of the rotation of the Moon around the Earth. The result is a difference of about 252 m/s, since the velocity from the theoretical tidal potential is significantly larger than the tidal propagation speeds possible on Earth. The waves of the Equilibrium Tides could not keep up with the speed of the Moon due to the insufficient water depths of only 4,000 m on average. In fact, only in the very deep and contiguous Antarctic Ocean, the theoretical and observed velocities are almost identical (Pugh & Woodworth, 2014). Therefore, the amount of water available in Earth's oceans creates significant reductions in the speed of tidal waves compared to the Equilibrium Tide Theory, resulting in further deviations of the actual tidal response.

Another difference between the assumptions of the Equilibrium Tide Theory and the physical oceanic system is the existence and the extent of marine ice sheet margins. In principle, similar effects as explained regarding the distribution of land masses are involved here, since marine ice sheets also contradict the assumption of a purely oceanic Earth. Apart from the effects already described, ocean tides may also respond to the geometric configuration of the margins of marine ice sheets. This is particularly true for the extensive ice shelves surrounding the Antarctic ice sheet (Haigh et al, 2020). Padman et al. (2018) demonstrated that tidal currents near the Filchner-Ronne Ice Shelf and the southern Weddell Sea will

decrease significantly as the Ice Shelf thins, using a regional barotropic tidal model. The resulting slow-down is about 0.1 m/s for a hypothetical loss of 100 m of vertical ice extent. Even though Padman et al. (2018) described a possible change and not the actual state, the high impact of marine ice sheet margins becomes evident. Besides that, seasonal ice coverage in the cold regions of the Earth can also have a significant impact on tidal water levels. These effects are not treated at this point, since they occur periodically and are described in Chapter 2.4 as a possible cause for changing tides.

Besides these effects caused by the properties of Earth's oceanic system, the interaction of the acting tidal forces with other non-tidal processes can lead to significant changes of the equilibrium state. These are often summarized under the term nonlinear interactions or nonlinear feedbacks (Haigh et al, 2020). Especially in shelf areas like the North Sea, these effects tend to have a large impact. Rasquin et al. (2020) demonstrate the effects of time-varying bed roughness and bottom friction coefficients. Changes in turbulent dissipation and stratification (Müller, 2012) may also play a larger role. In addition, Arns et al. (2015a) point out the overall importance of various nonlinear relationships between the individual parameters in marginal seas, especially the dynamic response of the sea surface to meteorological forcing (see also Arns et al., 2020). Since meteorology is a separate field of research and there is also a large intersection with other geosciences, these interactions are not explained here in detail, but only the most important aspects are mentioned. Examples are storm events (e.g. Idier et al., 2019), seasonal variations of currents and winds (e.g. Devlin et al., 2018) as well as climate variations such as the El Niño-Southern Oscillation (ENSO, e.g. Devlin et al., 2014). Overall, the influence of nonlinear interactions between tidal and non-tidal parameters is not to be underestimated and is taken into account in the analysis part of this thesis (see Chapter 8.2 for example).

The last effect listed here describing the divergence between the response of the oceanic system and the astronomical forces acting on it, is the radiational forcing. It summarizes influences by the radiation of the Sun. This is explicitly not about the gravitation of the Sun which is represented in the S_2 tidal constituent for example and well accounted for by the Equilibrium Tide Theory, but about the effects of heating on a diurnal S_1 frequency (Haigh et al., 2020). The warming of the Earth by Sun's radiation has a potentially high impact on meteorological forces, such as variations in air pressure (pressure loading of the ocean) and the response of water levels to these changes (inverse barometer effect) as well as variations in land-sea breeze (Rosenfeld, 1988; Ray & Egbert, 2004). Since these meteorological effects are periodic as well on semi-annual and annual scales due to the different radiation of the Sun on day and night or in summer and winter, they are often referred to as radiational tides (Pugh & Woodworth, 2014).

Besides these global effects, there are many different local processes, modifying the impact of the astronomical tide on a smaller scale. Although there are great differences depending on the local conditions, two important processes can be named in general according to Haigh et al. (2020). These processes are dissipation and resonance or reflection. Regarding dissipation, Friedrichs & Aubrey (1994) as well as Jay (1991) demonstrate the leading order influence of the balance between frictional damping and

bathymetric funneling in estuaries and river influences areas. Frictional damping is an effect which reduces the tidal amplitudes by frictional losses, while bathymetric funneling leads to an increase in amplitudes by reducing the bottom friction. For example, different bottom friction in coastal areas (depending on the prevailing soil) can lead to different tidal characteristics despite identical tidal potential.

Reflection and resonance have already been mentioned in a global context, but are also of great importance on a local scale, especially in the context of estuaries. In general, abrupt changes in width and depth at a river boundary tend to increase the amplitude of incoming tidal waves (Jay, 1991; Chernetsky et al., 2010). The highest amplification is mostly assumed to occur at a ratio of 1:4 between estuary length and wavelength of the tidal wave. However, for this to be true, soil friction must lie within a certain, individually differing range. On the one hand, the bottom friction has to be large enough to broaden the resonant peak to enable resonance, on the other hand, a strong bottom friction leads to a drastic reduction of the amplitude, resulting in a prevention of a significant reflection (Haigh et al., 2020). These resonance effects can lead to very high amplitudes and contribute massively to them in the Bay of Fundy and the Bristol Channel for example (Pugh & Woodworth, 2014).

Overall, the large number of reactions, influences and effects in Earth's oceanic system make it evident that the response of this system to the astronomical tidal forces differ significantly from the theoretical values of the Equilibrium Tide Theory. The observable tidal dynamics reveal large discrepancies to the astronomical tidal potential. As shown in Chapter 2.1, the Equilibrium Tide Theory is excellently suited for the description of tidal forces and their causes, but as shown in this chapter, not adapted for the quantitative description of measured values. Since at the same time the astronomical forces and thus their tidal potential exhibit a strictly periodic and stationary behavior, the causes for long-term changes of tidal parameters searched for in this thesis can only be found in a changing response of the oceanic system. This changing response cannot be described by the Equilibrium Tide Theory and the necessity of using actual measured tide values becomes evident. These conditions support and reinforce the approach of this thesis of relying primarily on measured values and only secondarily on modeling and harmonic analysis. It will be discussed in the following chapters, which of the described responses of the oceanic system could be causal for the observed changes in the tidal parameters.

2.3 Changes in the observable tides

Most of the responses of Earth's oceanic system to astronomical forces explained in the previous chapter are not stationary, since changes in the oceanic system itself can cause varying responses. Only these varying responses can be causal for the tidal changes due to the periodic stationary character of the astronomical tidal forcing. Figure 10 provides a graphical summary of possible changes. The results of the individual changes are difficult to separate, as there are many interactions between them and it is often not possible to clearly distinguish between them. As explained in the Introduction of this thesis, this overlapping of different effects is a main challenge in the analysis of occurring changes. Similar to Chapter 2.2, it is useful to distinguish between local and global changes in the oceanic system, whereas

a close connection may be given, since global effects can have a significant impact on local changes. For this reason, only those effects acting exclusively on local scales will be labeled as local effects. In detail, changes of the oceanic system include tectonics in the context of the continental drift, changes in water depth and the resulting changes of shoreline position, the extent and the fluctuations of sea ice coverage, nonlinear interactions especially in the context of changes in ocean stratification and internal tides, as well as changes in radiational forcing.

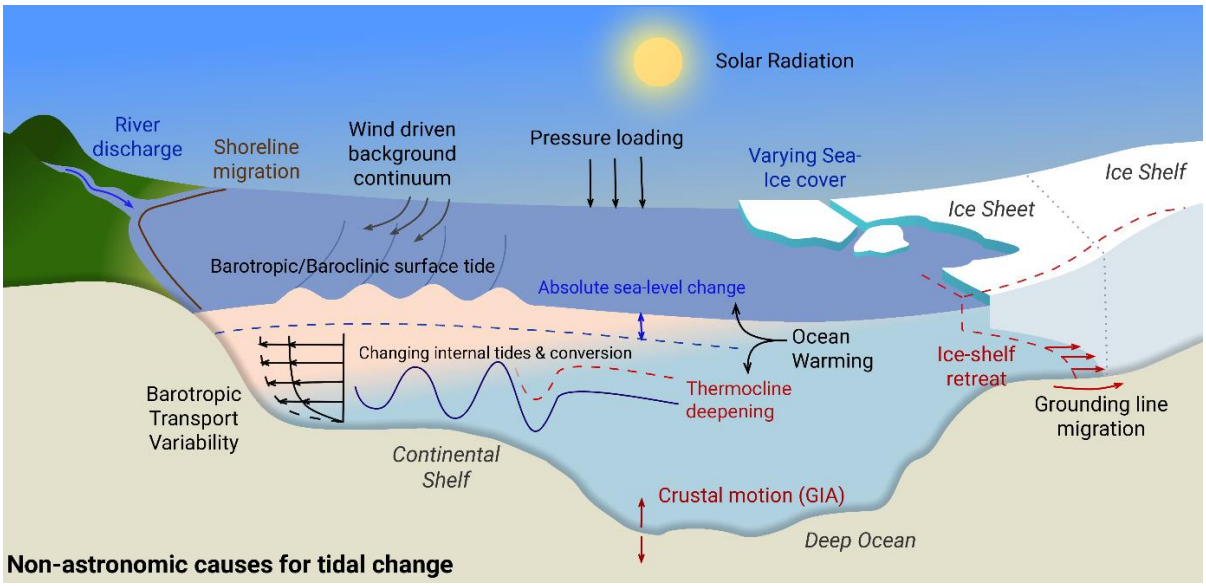

Figure 10: Illustration of the range of possible driving mechanisms that have been proposed to explain long-term changes in the tides on local, regional and global scale (Haigh et al., 2020).

In Chapter 2.2, tectonics are classified as a first-order influence, regarding their impact on the discrepancies between observed tides and tidal potential. As mentioned before, the oceans are close to the resonance state today for semidiurnal tides due to the current distribution of land masses. This state was established by the continental drift and is constantly altered by it, bringing regions in and out their specific resonance range on long time scales (Green et al., 2017). The cycles of the movement of tectonic plates between the formation of supercontinents (conditions similar to those of the Equilibrium Tide Theory) and their dissolution (with a potentially high tidal resonance) include periods between 400 and 450 million years (Green et al., 2018). Since these time scales are vast compared to the period of tidal measurement and especially to the study period, effects of continental drift are not taken into consideration in this thesis.

As explained in Chapter 2.1, tidal waves react very sensitively to changes in water depth due to their character as shallow water waves. These changes can be caused either by a geocentric (relative changes caused by level change of the tide gauge zero), by an absolute MSL rise or by long-term changes in the Earth's crust due to the melting of large glaciers (Glacial Isostatic Adjustment - GIA). The transmission of this changes to changes in the tidal wave occur through two different mechanisms. The first one is resonance, since the resonance frequency of a Kelvin wave depends on the basin length, which is changing according to the changes in water depth. The resonance range of the tidal wave can be both pushed

closer to its resonance state or it may be moved away from it (e.g. Pickering et al., 2012; Idier et al., 2017). The second mechanism corresponds to the amphidromic points. Following Eq. 5, a change in water depth alters the propagation speed of tidal waves and can cause a spatial reorganization of the amphidromic points, which leads to a potential change in tidal range. Furthermore, a change in water depth can modify the energy dissipation due to bottom friction, especially in shallow shelf seas (Taylor, 1922). This subsequent effect of a water level change is simultaneously a nonlinear interaction. Since the relative influence of bottom friction in shallow water waves depends on water depth, an increase in water depth tends to reduce the influence of bottom friction (Mudersbach et al., 2013; Arns et al., 2015a). Furthermore, a change in water depth, just like a changing extent of ice cover and the construction or deconstruction of coastal defense structures, may lead to shifts in shoreline positions. Here, too, the resonance changes and thus the tidal wave amplitude as a result of the modification of the basin length. The Basin length itself is in principle also influenced by changing shoreline dynamics (retreat, accretion), but these have not yet been investigated on a regional or global scale (Haigh et al., 2020). Changes in water depth or MSL changes have long been suspected as the origin of changes in tidal parameters, e.g. first from Führböter & Jensen (1985) for the North Sea and especially the German Bight or Woodworth et al. (1991) for the UK. Several other purely numerical studies also find this relationship to be feasible (e.g. Pickering et al., 2012; Idier et al., 2017; Green et al., 2018).

Another factor is the changing extent of Sea Ice. On intra-annual time scales, the isolation of the ocean surface from wind forcing as well as the occurring friction between ocean surface and sea ice can lead to a change in the tidal currents and the tidal amplitudes (Prinsenberg, 1988; St-Laurent et al., 2008). According to a modelling study of Müller et al. (2014), the seasonal variations of tidal amplitude in the Hudson Bay and Hudson Strait area is reduced by up to 0.1 m due to additional underice friction with an energy dissipation of 21 GW, which equivalents to about 10% of the total dissipation. Furthermore, a variable sea ice cover affects other parameters such as the water depth or the shoreline position. Although this effect has a potentially large impact in the higher latitudes of the Earth, it will not be analyzed further in this thesis due to the non-existence of extensive sea ice in the North Sea.

Variations of ocean stratification also have an impact on tidal dynamics, particularly in shallow water areas. Müller et al. (2012) demonstrated how seasonal variations in the stratification can trigger a change in tidal amplitude of up to 5% due to the changed viscosity distribution over the depth and the resulting change in the transformation of kinetic energy. Müller et al. (2012) could also provide a correlation between stratification and the surface expression of internal tides, while Colosi & Munk (2006) demonstrated an increase in the M_2 amplitude from 16.1 to 16.9 cm between 1915 and 2000 for a tide gauge from Honolulu, Hawaii. According to Haigh et al. (2020), these effects have also not been sufficiently researched. Due to the potentially high impact especially in shelf seas like the North Sea, a correlation between stratification and changes in tidal parameters is possible and needs to be investigated in this thesis.

The last point here is the radiational forcing with its potentially high impact on meteorological forces, which could cause changes in the tidal parameters via meteorological impacts. For this reason, as well as for the known high degree of nonlinear interactions between meteorology and tidal parameters (Mudersbach et al., 2013; Arns et al., 2015a), the consideration and analysis of meteorology in this thesis is necessary.

Even though the focus of this thesis is on large-scale effects, the potential superposition of these with small-scale effects requires consideration of possible changes on local or regional scale. The primary interest is a possible bias in the following analysis and how to avoid it. While the analytical methodology chosen in the following excludes local effects in general, such a consideration is still essential, since similar local effects at different tide gauges can be mistaken for large-scale effects without a basic understanding of the underlying processes. According to Haigh et al. (2020), particular noteworthy effects causing local tidal changes are river flow, turbulent mixing, the depth of channels and flats, and discrepancies between measured and actual development.

First of all, a qualitative, nonlinearly correlation between tides and river flow can be found at a local scale, especially in tidal rivers with a strong river flow (Hoitink & Jay, 2016). In this case, secular trends can occur in the tides, sometimes even in upstream locations far away from the coast (e.g. Moftakahri et al., 2013, for the San Francisco bay area). The mechanism of action is based on an increase in the effective frictional damping due to the landward increase in river flow velocity (Godin, 1986; Godin 1991; Jay, 1991; Godin, 1999). Since river levels are excluded from this study, this effect is only of interest if tide gauges are located directly at the mouth of a river. In order to avoid a distortion of the results on a large scale, it is ensured that the corresponding effects occur to the same extent at tide gauges without spatial proximity to rivers.

Another important impact factor on small spatial scales is turbulent mixing, which is significantly associated with large-scale stratification changes. It may have a significant influence on tidal dynamics and tidal range, especially in estuaries. In physical terms, the turbulent mixing of water layers leads to energy dissipation and thus to a reduction of the kinetic energy of the tidal wave. According to McLean & Smith (1979) and Talke et al. (2013), it is mostly caused by bottom roughness (dunes, ripples). However, a strong stratification reduces this mixing as well as the energy dissipation. In the area of the Ems River, for example, the formation of a 30 to 40 km long bank of mud caused a reduction in ground roughness, leading to a reduced turbulent mixing and an increase in the tidal range. This effect, occurring analogously to the stratification already described globally, is of potentially great importance and will be considered in the further analyses of this study, using the proxy of stratification changes (see Chapter 8.2).

A similar effect with the same physical mechanisms is produced by changes in the depth of local channels and flats, since the relative influence of friction decreases with increasing water depth and the tidal range may be enlarged. This effect can be triggered by natural variations in bathymetry, changes in MSL

(Arns et al., 2017), or channel deepening for shipping, and has already been detected in several estuaries (e.g. DiLorenzo et al., 1993; Jay et al., 2011; de Jonge et al., 2014), being classified by Haigh et al. (2020) as the primary factor for the long-term changes to estuary tides. Another problem can occur if tide gauges are located directly at such channels, as is often the case in the German Bight (Führböter & Jensen, 1985). A bathymetric change in the channel may alter the measured water depth and the tide gauges may no longer correctly reflect the tide in the surrounding area. This problem can occur especially in tidal low water and will be discussed in more detail in Chapter 3.3.

Apart from this effect in tidal low water, there can be discrepancies between measured and actual development at any tide gauge. If there are systematic errors in the measurement technique that go beyond statistical white noise, it may falsely appear as if the tide had changed. Woodworth (2010) cites three major factors, namely an undocumented change in tide gauge location (I), a change in measurement technology from conventional tide gauges (float/stilling) to acoustic, pressure or radar-based systems (II) and general data irregularities like timing or calibration errors (III). Factors I and III are usually detectable by a local tidal survey, since either spatial or temporal anomalies occur in the tidal parameters. Factor II, with its high potential impact caused by the many tide gauges affected, can be more problematic. Most tide gauge authorities have upgraded their recording technology in the decades up to 2010. A consistent comparison and correction of the time series before and after the upgrade was not always carried out. Since the different tide gauge authorities often operate all tide gauges within one region or even one country, a local tidal survey often cannot detect these errors. A plausibility check with data from other authorities in the same or even neighboring countries is necessary. Overall, Woodworth (2010) rates a local or regional comparison of consistency as the most important tool for detecting errors in individual records. For these reasons, the results presented later in this thesis have been checked for these points and the results presented are always based on tide gauges from different authorities or even different countries. Furthermore, Mawdsley et al. (2015) point out the possibility of different correction procedures used by various authorities. Consequently, in each case an own, individual control and correction procedure is recommended and applied.

In summary, it can be concluded that of the known possible global effects suspected of causing changes in tidal parameters, changes in water depth, changes in stratification, and meteorological changes are to be examined for the North Sea study area. Furthermore, potential overlaps with local effects as well as measurement errors have to be considered, especially in the area of estuaries. This is done in this thesis by the analytical methodology chosen here to exclude local effects as well as by checking the consistency of the results at a larger spatial distance to other tide gauges.

2.4 Classifications of observable tides

The amount, the impact and the large variations of oceanic responses to the astronomical tidal potential illustrate the complexity and variety of the tidal water levels actually occurring. Even though the ocean tides are the obvious terrestrial manifestation of the acting tidal forces, the local expression of tidal water

levels can vary considerably as previously shown. That is why there are various classification systems based on different criteria, which are presented here in the following. To begin with, Figure 11 depicts the terms used in this thesis to describe the tidal parameters. On the left side, the definitions of tidal high and tidal low water levels are displayed, while the right side of the figure presents the tidal range.

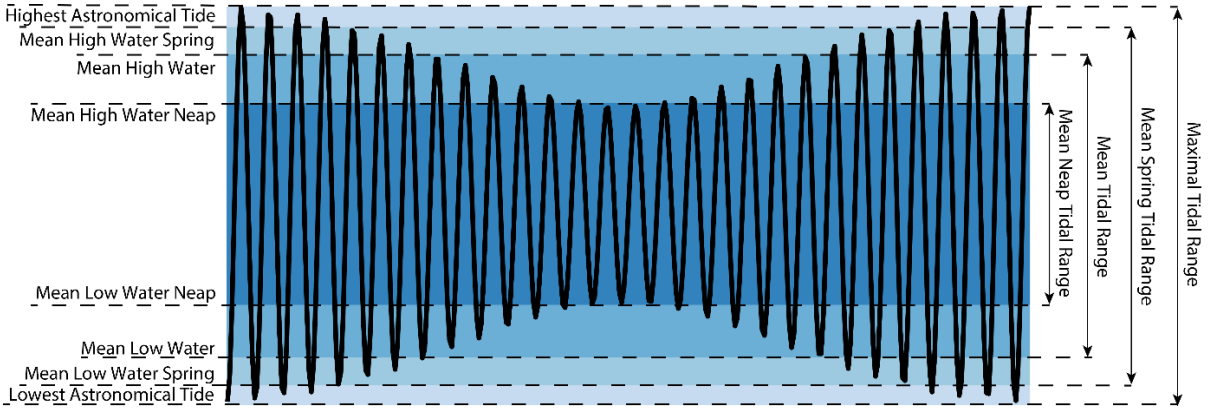

Figure 11: Illustration of the tidal parameters used in this thesis, derived from Pugh & Woodworth (2014) and Malcherek (2018).

Tidal low and high waters are defined as the highest and lowest periodically recurring water levels within a given cycle and the tidal range is often defined as the difference between high and low water (e.g. Pugh & Woodworth, 2014; Malcherek, 2018). However, in this thesis the tidal range is calculated according to the official German standard (DIN 4049-3, 1994) as the difference between each tidal high water and the mean of the previous and following tidal low water. The lowest tidal range occurs in the case of neap tides, because here the amplitude of the tidal curve is very low and tidal low and high water are close to each other. The influence of the spring-neap cycle is significant and leads to a doubling of the astronomical tidal range from 2 to 4 m within 7.4 days in Newyln (Figure 7) for example. In addition, HAT & LAT are often specified, since in certain astronomical constellations the spring tide can be exceeded in tidal high water and undercut in tidal low water. These values are usually obtained either by re-analysis of a period of time as long as possible or by harmonic analyses for years with known astronomical extremes (Pugh & Woodworth, 2014).

The measured tidal range is often used to classify coastal regions, since tidal low and high water are implicitly considered. Regions with a tidal range of less than 2 m are referred to as microtidal, with less than 4 m as mesotidal and with more than 4 m as macrotidal (Table 3).

Table 3: Classification of tidal regimes according to tidal range amplitude (Pugh, 1987).

Classification	Tidal range [m]
microtidal	$TR < 2.00$
mesotidal	$2.00 \leq TR \leq 4.00$
macrotidal	$TR > 4.00$

Another possibility is to quantify the influence of semidiurnal and diurnal tides. For this purpose, the amplitudes of the two most important semidiurnal tidal constituents M_2 and S_2 are set in relation to the most important diurnal tidal constituents K_1 and O_1 (which describe the varying declination of the Moon within one day). This concept originally goes back to Dietrich (1963) and describes a form number F with the following equation and classification (Foreman, 1977):

$$F = \frac{K_1 + O_1}{M_2 + S_2} \qquad \textbf{Eq. 7}$$

Table 4: Classification of tidal regimes according to form number (Foreman, 1977).

Classification	Form number [-]
semidiurnal form	$0.00 \leq F \leq 0.25$
mixed form	$0.25 < F \leq 3.00$
diurnal	$F > 3.00$

3 Study area and initial data basis

3.1 Study area North Sea

In the previous chapters, the astronomical basics of the tide, the response of Earth's oceanic system, possible causes for changes of the tide as well as the established classification of the tidal parameters were discussed. The study area of the North Sea will be described referring to these aspects in this chapter.

With a size of about 575,300 km², the North Sea is one of the largest shelf seas worldwide (Huthnance, 1991). Counted counter-clockwise, its margins comprise coastal sections of the UK, France, Belgium, the Netherlands, Germany, Denmark, and the south of Norway (Figure 12). The North Sea is connected to the North Atlantic via a large inlet between Scotland and Norway in the north and a narrow opening through the English Channel in the southwest. Further, it opens to the Baltic Sea in the east. Water depths in the North Sea are on average 90 m but vary greatly, generally increasing from south to north. While the southern parts are often shallower than 40 m with lowest depths in the German Bight, depth increase to about 300 m at the continental shelf toward the Norwegian Trench and the entry into the Norwegian Sea in the northwest. There are also extensive shallow water regions off the south-eastern coast of the UK known as the Dogger Bank complex, with their western part extending to the coasts of Norfolk and Suffolk (Quante & Colijn, 2016). It must be noted, however, that the depths given in the literature vary. Huthnance (1991), for example, assumes an average depth of only 70 m, but confirms the 300 m at the beginning of the Norwegian Trench slope, meaning that the order of magnitude is correct in general.

Following Eq. 7, the tide gauges used in this thesis feature form numbers between 0.04 and 0.19 and thus are classified as semidiurnal, which is confirmed by the data from literature (Sumich, 1996). The North Sea as a whole has only a small tidal potential of its own is strongly influenced by the astronomical tides entering the basin from the Atlantic in the most parts. The Atlantic semidiurnal tidal wave travels northwards, circling the amphidromic area in the central North Atlantic (see Figure 9-b) counterclockwise. A part of the wave propagates into the English Channel, while the Atlantic Wave continues north to the Shetlands, entering the North Sea basin between the Shetlands and Scottish mainland (Pugh & Woodworth, 2014). For the semidiurnal tides in the North Sea basin, three amphidromic systems result (Figure 12) with amphidromic points near to the English Channel, in proximity to the center of the basin and close to the Norwegian coast (Proudman & Doodson, 1924). The last one is often referred to as a degenerated or incomplete, because not all semidiurnal tidal components show a fully developed amphidromic point here (Pugh & Woodworth, 2014). Since the North Sea's basin shape is close to the resonance frequency in the semidiurnal spectral band, the superposition of the principal lunar and solar tides M_2 and S_2 leads to a significant spring neap cycle. The M_2 and S_2 constituents cause a potential tidal range between 1.00 and 5.00 m (Quante & Colijn, 2016). The observable impact of the spring neap cycle can vary considerably at individual tide gauges, but is generally in the decimal range for most

cases. For example, a difference between the mean high waters spring and neap as well as for the mean low waters spring and neap of about 0.50 m is assumed for Lerwick (NOC, 2020) and about 0.40 m for Cuxhaven (BSH, 2019). Higher values can occur in the English Channel area, such as about 1.00 m in Sheerness or 1.3 m in Dover (NOC, 2020). According to Table 3, the tidal regime of the North Sea can be classified as macrotidal (> 4.00 m), mesotidal (2.00 – 4.00 m) and microtidal (< 2.00 m), with the actual tidal range being strongly influenced by local factors. For example, the mean spring tidal range at the east coast of the UK varies between 3.60 m (Aberdeen) and 6.20 m (Immingham) (Horsburgh & Wilson, 2007). The mean tidal range in the data set used in this thesis is about 4.40 m at the east coast of the UK and the English Channel, 1.98 m at the Dutch west coast, 2.33 m at the Dutch north coast and 2.82 m in the German Bight. In general, all three tidal regimes are detectable with respect to the tidal range.

Overall, the North Sea is a large shelf sea without significant self-generated tides, featuring large shallow water areas in the south and deeper areas in the north. It contains three amphidromic points and borders on 7 European countries. Consequently, varying national tide gauge authorities with different standards exist, a fact that requires an intensive collecting and processing of the available data, which is explained in the next chapter.

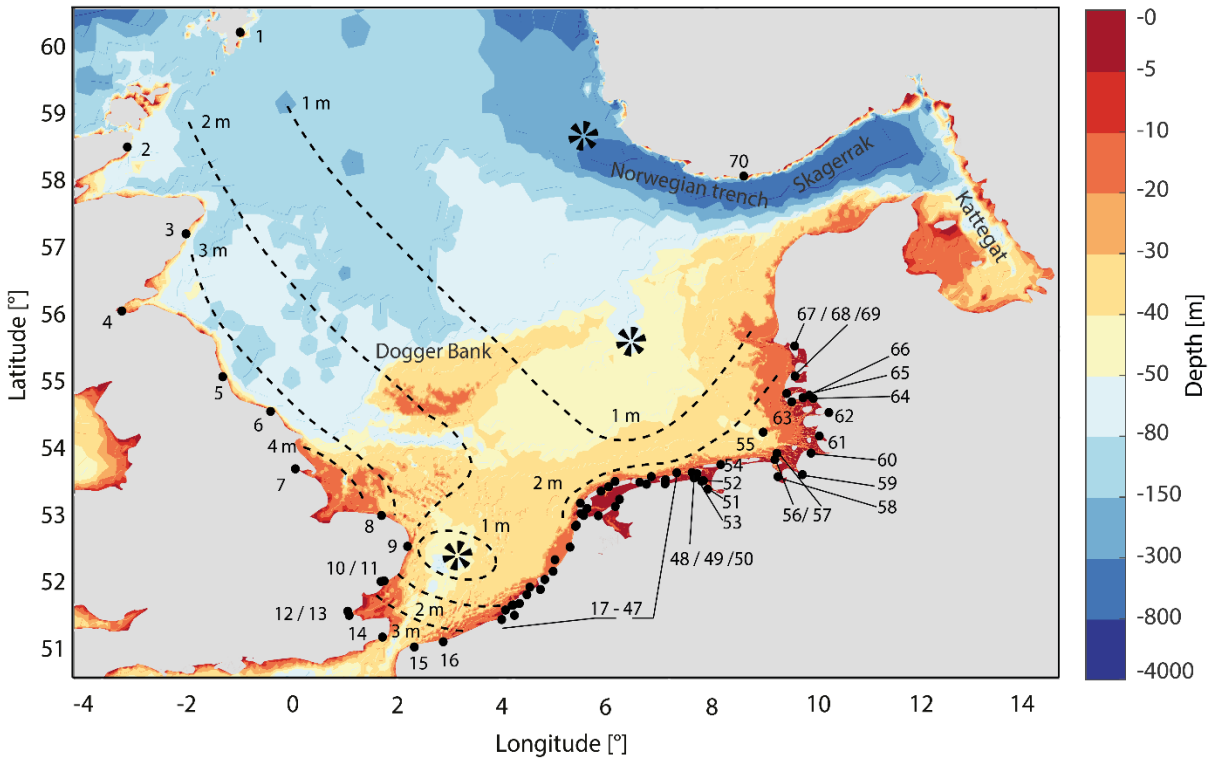

Figure 12: Bathymetry of the North Sea (Becker et al., 2009; Schrottke & Heyer, 2013). Also shown are the locations of tide gauges (black dots) used in this study including the chosen numbering (see also Table 3). The black propellers indicate the location of the three semidiurnal amphidromic areas (including the amphidromic points for the M_2 and S_2 constituent) and the black dotted lines indicate contours of equal mean tidal range (Sündermann & Pohlmann, 2011).

3.2 Initial data basis of the North Sea

Water level time series of 93 available tide gauges around the North Sea basin were collected from various sources. Data from GESLA (Global Extreme Sea Level Analysis, GESLA, Woodworth et al. 2017), Open Earth (Deltares, 2020) and the responsible German authorities for the German Bight (WSV, 2020) were collected. Additional data for the Dutch coast were provided by the Dutch Rijkswaterstaat on request. Since the quality control procedures of the different institutes are not identical, further data checks were performed at all sites, consisting for example of the identification and elimination of spikes and date or phase shifts. The data correction was done according to recommendations of Woodworth (2010) and Mawdsley et al. (2015), see also Chapter 2.3. The available time series vary considerably in length and completeness as well as in their spatial distribution density. The earliest measurements of tidal low and high water readings are from 1843 (Cuxhaven, Germany, #60), while on the Dutch coast data from some stations have only been digitally available since the 1980s. High-resolution data sets with an equidistant sampling between 1 and 60 minutes were used as well as time series of tidal low and high water. Equidistant time series with a resolution lower than 60 minutes were excluded, since supplemental analyses have shown that they insufficiently describe the height and timing of individual tidal low and high water levels. Considering the 18.61-year nodal cycle and the already known significant tidal changes of the German Bight from the end of the 1950s on (Jensen, 1985), an analysis period from January 1958 to December 2014 were adopted including approximately 3 nodal cycles. Tide gauges known to be located near to weir installations or in rivers were excluded, as these are at least partially separated from the oscillation system of the North Sea. 70 time series of tidal range remained in the data set, forming the basis for the following analysis (Table 5).

Besides the extent, the quality and the processing of the data itself, the spatial distribution of the data points may have a major impact on the selection of possible analysis methods. Considering the counter-clockwise propagation direction of the tidal wave, the tide gauges used in this study are counted by starting at Lerwick (Shetland Islands) and ending at Tregde (Norway). The database consists of 14 British, 2 French, 35 Dutch, 17 German, one Danish and one Norwegian and thus a total of 70 tide gauges. No data are available for the Belgian coast as the Belgian authorities do not provide sufficiently long time series. For the European coastlines, the actual lengths are difficult to determine due to both natural features such as bays, islands, estuaries, ebb and flow changes, and anthropogenic influences such as dyke construction. A precise determination of the spatial data density is thus not possible. Nevertheless, a rough orientation can be done and is feasible, since the aim here is a relative comparison between the countries coastlines. The lengths given here in the following are therefore based on linear approximation of the coastline. The 14 British tide gauges cover a coastline of about 1,600 km (including the linear distance between Lerwick (#1) and Wick (#2)) with a data density of one tide gauge per 115 km on average. The highest density is found in the Netherlands, where 35 tide gauges are located along less than 500 km of coastline, equivalent to one tide gauge per 14 km. The German North Sea coast is roughly 600 km long and features 17 tide gauges, leading to lower data density of one tide gauge per 35 km on

average. These lengths explicitly do not refer to coastal shape or islands in the foreland of the coasts but rather reflect the linear sea length in front of the coast. In spite of the lower density compared to the Netherlands, the German tide gauges feature an average completeness of about 88% in the study period, whereas only 65% in the Netherlands and 64% in the UK are reached. Besides these significant differences between the various countries, the data points reveal a distinct East-West and North-South gradient. While the North-South gradient results from the geometry of the North Sea and thus is unproblematic as a reflection of the natural conditions, the East-West gradient may be an issue when interpolating the missing values. If the westernmost station Leith (#4) at 3.18 °W is compared with the easternmost station Husum (#62) at 9.02 °E, the midline between them is at about 3 °E. Following Figure 12, it becomes evident that only 16 tide gauges are located left of this line in the western half of the study area, while 54 tide gauges are located right of this line in the eastern half of the study area. In addition, both data completeness and general data density are significantly lower in the western half. This fact has fundamental consequences for the interpolation of the missing data, since an interpolation procedure is needed that considers not only the spatial distances between the stations but also their spatial distribution and density. This issue was solved by choosing Ordinary Kriging (Chapter 4.2) as interpolation method. In addition, this uneven distribution makes it necessary to consider results of subsequent analyses for the entire study area as well as for individual segments, since the different number of data points can otherwise lead to an over- or underestimation of detected large-scale effects.

Table 5: Name, coordinates, period, and coverage of the 70 tide gauges used in this study (see also Figure 12).

	Tide gauge	LON [°]	LAT [°]	Period [yr]	Cov. [-]		Tide gauge	LON [°]	LAT [°]	Period [yr]	Cov. [-]
1	Lerwick	-1.14	60.16	1959–2011	0.83	36	Kornwerderzand-buiten	5.34	53.07	1958–2014	1.00
2	Wick	-3.09	58.44	1965–2014	0.79	37	Texel Noordzee	4.73	53.12	1990–2014	0.27
3	Aberdeen	-2.07	57.14	1958–2014	0.75	38	Harlingen	5.41	53.18	1958–2014	1.00
4	Leith	-3.18	55.99	1989–2014	0.39	39	Vlielandhaven	5.09	53.30	1958–2014	1.00
5	North Shields	-1.44	55.01	1962–2014	0.79	40	West-Terschelling	5.22	53.36	1958–2014	1.00
6	Whitby	-0.61	54.49	1981–2014	0.55	41	Terschelling Noordzee	5.33	53.44	1989–2014	0.45
7	Immingham	-0.19	53.63	1958–2014	0.90	42	Nes	5.76	53.43	1971–2014	0.77
8	Cromer	1.30	52.93	1988–2014	0.45	43	Holwerd	5.88	53.4	1971–2014	0.54
9	Lowestoft	1.75	52.47	1964–2014	0.86	44	Wierumer-gronden	5.96	53.52	1981–2014	0.60
10	Felixstowe	1.35	51.96	1982–2011	0.39	45	Lauwersoog	6.20	53.41	1971–2014	0.77
11	Harwich	1.29	51.95	1958–2014	0.29	46	Schiermonni-koog	6.20	53.47	1966–2014	0.86
12	Southend	0.72	51.5	1958–1981	0.40	47	Huibertgat	6.40	53.57	1973–2014	0.74
13	Sheerness	0.74	51.44	1958–2013	0.64	48	Borkum Fischerbalje	6.75	53.56	1963–2014	0.90
14	Dover	1.32	51.12	1958–2014	0.90	49	Borkum Südstrand	6.66	53.58	1958–2014	1.00

15	Calais	1.87	50.97	1965–2014	0.52	50	OudeWestereems	6.70	53.5	1981–1983	0.04
16	Dunkerque	2.37	51.05	1959–2014	0.68	51	Eemshaven Doekegat	6.86	53.46	1983–1987	0.07
17	Cadzand	3.38	51.38	1971–2014	0.77	52	Eemshaven	6.83	53.45	1979–2014	0.63
18	Westkapelle	3.44	51.52	1958–2014	1.00	53	Delfzijl	6.93	53.33	1958–2014	1.00
19	Oostkapelle	3.56	51.59	1971–2014	0.77	54	Norderney Riffgat und Hafen	7.16	53.7	1958–2014	1.00
20	Oranjezon	3.57	51.6	1979–1987	0.14	55	Helgoland Binnenhafen	7.89	54.18	1958–2014	1.00
21	Roompot-buiten	3.68	51.62	1972–1974	0.04	56	LT Alte Weser Roter Sand	8.13	53.86	1958–2014	1.00
22	Brouwers-ha-venscheGat08	3.81	51.75	1987–2014	0.49	57	Wilhelmshaven Alter Vorhafen	8.15	53.51	1958–2014	1.00
23	Haringvliet10	3.86	51.86	1980–2014	0.61	58	Bremerhaven	8.57	53.55	1958–2014	1.00
24	Haringvliets-luizenbuiten	4.04	51.83	1982–2014	0.54	59	Mellumplate	8.09	53.77	1963–2014	0.91
25	Hoek van Holland	4.12	51.98	1972–1987	0.26	60	Cuxhaven Steubenhöft	8.72	53.87	1958–2014	1.00
26	Scheveningen	4.26	52.1	1958–2014	1.00	61	Büsum	8.86	54.12	1958–2014	1.00
27	Noordwijk-meet-post	4.30	52.27	1961–2005	0.76	62	Husum	9.02	54.47	1958–2014	1.00
28	Ijmuiden-buiten-haven	4.55	52.46	1984–2006	0.36	63	Wittdün	8.38	54.63	1958–2014	1.00
29	Pettenzuid	4.65	52.77	1981–2014	0.60	64	Schlüttsiel	8.76	54.68	1961–2014	0.94
30	Petten	4.66	52.79	1978–2014	0.61	65	Wyk auf Föhr	8.58	54.69	1958–2014	1.00
31	Den Helder	4.74	52.96	1971–1974	0.05	66	Dagebüll	8.69	54.73	1958–2014	1.00
32	Oostoever	4.79	52.93	1958–2014	1.00	67	Hörnum	8.30	54.76	1958–2014	1.00
33	Den Oeverbuiten	5.05	52.93	1971–1981	0.15	68	List	8.44	55.02	1958–2014	1.00
34	Oudeschild	4.85	53.04	1958–2014	1.00	69	Esbjerg	8.43	55.47	1958–2014	0.92
35	Vlissingen	3.60	51.44	1958–2014	1.00	70	Tregde	7.55	58.01	1958–2014	0.40

The statistical analyses and procedures carried out in this thesis in Chapters 5, 6 and 7 are based exclusively on the tide gauge records described above. However, in Chapter 8, various external data sets of different physical quantities are used for comparison to answer research question 3 and detect possible links of tidal changes to physical effects. In the North Sea region, two different reconstructions of the MSL (Wahl et al., 2013; Niehüser et al., in prep), data on dike length over time (Lehmann, 2018), data on temperature and salinity distribution (Bersch et al., 2016) as well as the results of an established numerical model (Arns et al., 2015a/b) are used for this purpose. In addition, comparisons on larger spatial scales in the North Atlantic with the EN4.2.0 data set of temperature and salinity (Gouretski & Reseghetti, 2010) as well as indexes of the North Atlantic Oscillation (NOAA, 2020a), the East Atlantic Pattern (NOAA, 2020b), the Atlantic Meridional Overturning Circulation (NOAA, 2020a) and the Sub

Polar Gyre (Marinescotland, 2017) were made. Furthermore, in Chapter 8.2 the possible correlation between the records from the North Sea and the adjacent North Atlantic is examined. For this purpose, 24 additional North Atlantic tide gauges from the GESLA data set were used (Port-aux-Basques, Argentia, Saint John, Reykjavik, Cascais, Vigo, La Coruna, Santander, Saint Jean de Luz, Bayonne Boucau, Port Bloc, Les Sables D'Olonne, Saint Gildas, Port Tudy, Brest, Le Conquet, Newlyn, Roscoff, Devonport, Saint-Malo, Cherbourg, Le Havre, Newhaven and Dieppe, Woodworth et al., 2017). Overall, a comparison of the data from Table 5 and its derivatives is made with a total of 12 other data sets. Unlike the data collection presented in Table 5, all of these data sets are freely available, peer-reviewed and citable. Accordingly, no corrections were made here, but the original data sets were used. A comprehensive description can therefore be dispensed at this point, instead a description of the essential information in the context of their use is given in Chapter 7.

3.3 Data Processing and special characteristics

Apart from harmonic analyses requiring hourly values and an annual resolution of some benchmark data sets, monthly averages of tidal low water, tidal high water, and tidal range are used for the statistical analyses in this thesis. To produce monthly averaged values, the completeness of the data series for each month is required to be above 80%. In addition, less than 20% of the missing values may occur at a stretch, since otherwise the spring neap cycle could be underestimated or overestimated when the missing values are on an extreme point of the cycle, leading to discrepancies in the monthly values. In general, the use of monthly values offers various advantages for the research presented here, as it relates mainly to long-term changes which do not take effect on time scales within a month. Monthly averaging eliminates the many periodic intra-monthly fluctuations through averaging, such as the daily inequality between successive tidal high or low waters or the spring neap cycle, resulting also in a smaller impact of individual, shorter meteorological events.

In contrast to mean annual values, the distinct seasonal cycle of the North Sea still has to be eliminated for monthly values, but they offer the advantage of more usable data points for some highly incomplete tide gauges (e.g. if only 6 months of a year are available, since an 80% completeness criterion would result in the loss of the entire year). The seasonal correction was carried out by subtracting the average of all monthly values from each monthly value of a tide gauge, e.g. the average of all January values at a specific tide gauge was subtracted from each mean value of January at this tide gauge. Only in the comparison of tidal parameters with other long-term indicators such as temperature, salinity or MSL, annual values are used, since the data quality and completeness of these parameters does often not allow the use of monthly values. Furthermore, the use of annual values ensures the most comprehensive exclusion of seasonality and intra-annual meteorology, which is of high importance when comparing tidal values to other indicators (Führböter & Jensen, 1985).

For the further use of the tidal parameters in this thesis, their special properties and restrictions have to be considered. To begin with tidal low water, Führböter & Jensen (1985) describe the issue of tide

gauges in large Wadden Sea areas often not registering the lowest water level due to their location at Wadden channels, especially in the German Bight. The water level in the Wadden channel may not match the surrounding water level in case of tidal low water, as the water does not or only delayed discharge (Figure 13-a). Furthermore, an interaction between the tides and the morphology of the Wadden areas occurs, since the shape and depth of these channels depend on the tidal behavior (Knop, 1961; Jensen, 1985). As a result of these findings, the actual tidal low water in the surrounding areas can differ significantly from the measured values. For example, the tide gauge may be located in a water puddle and thus no longer correctly measure the further drop in the water level.

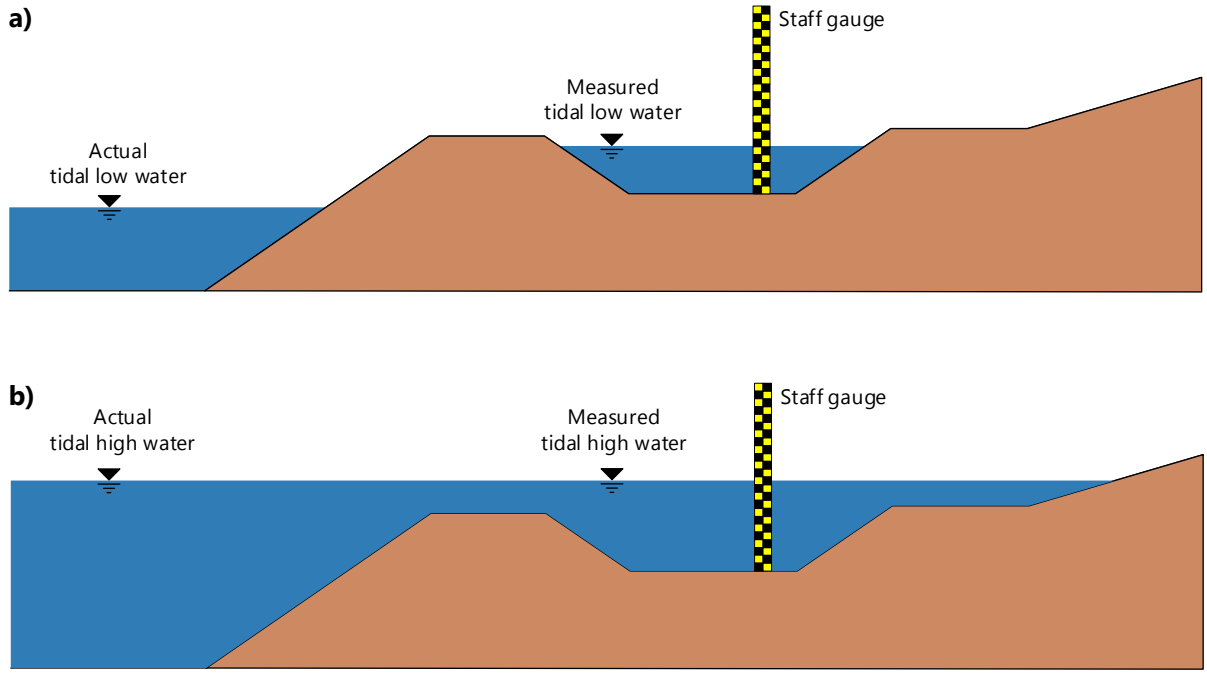

Figure 13: Non-scale principle sketch of discrepancy between actual and measured water levels for tidal low water (a) and equivalence between actual and measured water levels for tidal high water (b) according to Führböter & Jensen (1985).

For the tidal high water, however, the location of the tide gauges at Wadden channels causes no or only a minor effect due to the extensive flooding of the entire Wadden area. A delayed discharge or accumulation in Wadden channels is not relevant here (Figure 13-b). In addition, Jensen (1984) suggest a higher sensitivity of the tidal low water values to meteorology (e.g. wind surge) when compared with tidal high water values. Evidence of increased deviation of tidal low water readings due to wind influence can also be found in Gönnert (2003) in the context of storm surges. Overall, the tidal high water is less sensitive to interference at the individual tide gauge. Both Führböter & Jensen (1985) and Jensen (1985) concluded the better quality of tidal high water measurements in describing the general water level development.

These effects lead to conclusions for the tidal range, as it is the difference between tidal low and high water. The higher sensitivity of tidal low water to the meteorology compared to tidal high water is reduced by averaging two tidal low waters (see Chapter 2.3) and by using mean monthly values on short time scales. In addition, the meteorological part of the water level that is contained in both tidal low and

tidal high water is eliminated by the difference formation. Furthermore, Führböter & Jensen (1985) assume the meteorological influence on tidal low and tidal high water to be equal in the annual average, a statement which excludes a significant meteorological influence when using annual values of the tidal range. Other important advantages of using the tidal range are the elimination of systematic measurement errors occurring in both tidal low and tidal high water readings as well as the elimination of statistical white noise. Overall, the use of the tidal range offers the advantages of proportional equalization through differences analysis, although the inaccuracies of the tidal low water cannot be completely eliminated. However, the unfavorable aspect is that effects which are contained in both tidal low and tidal high water can no longer be detected in the tidal range. Inversely, any effect that is not identical in tidal low and high water is represented in the tidal range. This is especially useful for effects that are masked by other effects in tidal low and high water and are thus only detectable in the tidal range. Nevertheless, only effects originating from tidal low and/or tidal high water can occur in the tidal range, since it is a derived parameter. It is therefore necessary to analyze all three tidal parameters and to consider their differences, a procedure which was chosen in this thesis.

4 Methodology

After the characteristics of the North Sea study area and its tidal parameters were explained in the previous chapter and the initial data situation was described, the methods used are discussed in this chapter. In addition to the procedures explained in the following subsections in more depth, linear trend analysis, harmonic analysis of tidal constituents, wavelet coherence analysis and numerical modelling were carried out to characterize multiple features of the tide gauge records in the North Sea. None of these methods are explained here in detail due to their general recognition and widespread use, but are only briefly addressed. In contrast, less commonly used methods and methods with novel applications in this thesis are described in more detail. Due to this novel application of some methods in areas not corresponding to their original intended use, not only a theoretical description but also a validation of the basic suitability is given in Chapter 4.5.

Linear trends were calculated using ordinary least squares regression and their significance was assessed by considering normally distributed but serially correlated residuals following an autoregressive process of the order 1 (e.g. Mawdsley & Haigh, 2016). The assumption of a normal distribution is permissible here, since a sufficiently large sample of over 30 values is always given for the trend calculation in this thesis (Kuckartz et al., 2010). Annual amplitudes for the dominant tidal constituents M_2 and S_2 were determined by a harmonic analysis using the MATLAB toolbox U-Tide (Codiga, 2011), a procedure which is used to assess possible changes in the tidal constituents and enables the detection of amphidromic shifts. The wavelet analyses were conducted with the MATLAB package of Grinsted et al. (2004). This software does a cross wavelet transformation and an examination of two time series in the time frequency space in order to detect possible coherences between the signals becomes possible. For example, find common frequencies with a phase shift or at different points in time can be detected. Any significance statements made throughout this thesis are based on a 95% confidence level. In strict mathematical terms, the confidence level is the percentage of all cases in which a sample from the population of the parameter in question lies within the named interval. More often and perhaps more understandable, it is defined as the range in which a certain percentage of all possible results are found, a sufficiently precise definition for almost all applications (Kuckartz et al., 2010).

Furthermore, an existing two-dimensional, depth-averaged barotropic tide and surge model of the North Sea and the adjacent Atlantic Ocean (approximately from 48°N to 62°N and from 12°W to the transition between North Sea and Baltic Sea around 12°E) developed by Arns et al. (2015a, b) was used to simulate total water levels from 1958 to 2014. The original version of this model, based on the Danish Hydraulic Institute's (DHI) Mike21 FM (flexible mesh) model suite from 2014, was updated to the 2019 version for the analyses in this thesis. At the open boundaries, the Technical University of Denmark's DTU10 ocean tide model (Cheng & Andersen, 2010) is used as tidal input, and the MSL reconstructions of Wahl et al. (2013) were used to incorporate the effects of rise in MSL. The entire model domain was forced

with the 20th Century Reanalysis (20CR) data set of the US National Oceanic & Atmospheric Administration (NOAA) and the Cooperative Institute for Research in Environmental Sciences (CIRES) to describe the meteorologically induced effects on water levels (Compo et al., 2011).

4.1 Statistical fundamentals and basic methods

Since the statistical measure of Root Mean Square Error as well as correlation and (explained) variance or standard deviation are frequently used in the analyses part of this thesis, these concepts will be briefly explained here. The same applies to their usage for the detection as well as causal research of short-term and long-term changes in data series. Like the Mean Square Error (MSE), the Root Mean Square Error (RMSE) is a measure of the absolute, mean agreement between two data series. Both methods are widely used and recognized as standard procedures in statistical modeling (Hyndman & Koehler, 2006). The latter was chosen for this thesis, because the RMSE contains the same units and scales as the input variables, a feature which the MSE does not contain. With the RMSE it is possible to directly quantify the mean difference between two data series x and y of the number n (Willmott, 1984):

$$\mathrm{RMSE} = \sqrt{\frac{\sum_{i=1}^{n}(x_i - y_i)^2}{n}} \qquad \textbf{Eq. 8}$$

The coefficient of correlation or Pearson correlation coefficient (often as well as in this thesis only referred to as correlation) is a measure of the linear association between two variables x and y. The correlation can be both positive and negative and ranges from -1 to 1, where -1 indicates a perfect negative linear association and 1 indicates a perfect positive linear association. A value of 0 does not correspond to any linear dependency of x and y. In the case of trend including variables, a similar trend with the same sign can increase the linear relationship and the correlation significantly. In order to investigate a causal relationship between two variables, it is thus necessary to perform a trend adjusted analysis as well as an analysis including trends. The 95% confidence level of correlation is computed here by using the t-distribution with the degrees of freedom n – 2, which is better suited (more strict) for shorter time series than the normal distribution with identical results for longer time series (Maity, 2018). Since correlations are calculated which do not reach the minimum sample sizes of 30 for the application of the normal distribution, this stricter approach was chosen here in contrast to the trend calculation. The significance bounds (Upper Bound (UB) and Lower Bound (LB)) then result for a sample with the mean $\bar{x}$ and the standard error S_X to:

$$\begin{aligned} \text{Upper bound} &= \bar{x} + z \cdot S_X \\ \text{Lower bound} &= \bar{x} - z \cdot S_X \end{aligned} \qquad \textbf{Eq. 9}$$

z is the value of the t-distribution in case of correlation calculation or in case of trend calculation of the standard normal distribution (~1.75). In contrast to the standard normal distribution, the parameter of

the t-distribution depend on the sample size and cannot be specified in general form; tables of t-values can be taken from the corresponding literature, e.g. Kuckartz et al. (2010).

The correlation r of two variables x and y of the sample size n with the arithmetic means $\bar{x}$ and $\bar{y}$ and the standard deviations S_x and S_y is

$$r = \frac{1}{n-1} \cdot \sum_{i=1}^{n} \left(\frac{x_i - \bar{x}}{\sqrt{S_x}} \right) \cdot \left(\frac{y_i - \bar{y}}{\sqrt{S_y}} \right) \quad \textbf{Eq. 10}$$

The variance as square of the standard deviation measures the variation of a data series compared to its mean value. Mathematically speaking, the variance S^2 is the average squared deviation from the mean value of a sample with the length n (Maity, 2018):

$$S^2 = \frac{\sum_{i=1}^{n} (x_i - \bar{x})^2}{n-1} \quad \textbf{Eq. 11}$$

The quadratic relationship to the standard deviation S is:

$$S = \sqrt{S^2} = \sqrt{\frac{\sum_{i=1}^{n} (x_i - \bar{x})^2}{n-1}} \quad \textbf{Eq. 12}$$

The standard deviation and the variance are used in this thesis to quantify the influence of a periodic oscillation such as the nodal cycle on a time series. When an oscillation like the nodal cycle is removed from a time series, the level at which the short term oscillations occur changes and the standard deviation as well as the variance are reduced.

A related parameter in a different context is the explained variance. It is used in this thesis in order to quantify which part of the variance of a given signal x is described by another signal y. For this purpose, first a dependency between the signals has to be established by computing their correlation. In a next step, the difference (x–y) between the signals is formed and the residual may now show no more correlation to the original signal y. If there is still a significant correlation, no causal relationship can be assumed and no statement about the explained variance can be made. If no or only a non-significant remaining correlation can be detected, the variance reduction between x and the residual signal can be described as explained variance. Since the result is the proportion of the variance in x that is explained by y, it is often presented as a proportion of the original variance in signal x. The verification of the removal of the correlations between the residual and signal y is necessary, because a mere consideration of the reduction of the correlation can be random and the explained variance would then lose significantly in validity (Achen, 1982).

In the context of this thesis, the essential properties of data series are the short-term (interannual) and long-term (decadal) changes. Therefore, the various dependencies between two data series can appear on one or both time scales. Consequently, it is useful to distinguish between these two time scales in some parts of this thesis and especially in the investigation of physical causes in Chapter 8. Both explained variance and correlation are suitable for establishing a relationship on short time scales, but it is important to exclude long-term trends, making sure they do not outweigh the short-term connection. Long-term changes and their causes can be analyzed by the correlations including trends and the trends themselves. To prove a common non-random trend of two variables, two points must be considered: (I) the correlation excluding the trend must be significant and (II) lower or equal to the correlation including the trend. Otherwise, a reduction of the correlation when including trends would indicate an opposite development of the variables.

4.2 Ordinary Kriging

The procedure chosen here for the necessary interpolation of missing data points is the Ordinary Kriging algorithm. In general, Kriging (also Gaussian process regression) is a geostatistical method to linearly interpolate missing values based on information stemming from neighboring stations. Originally developed in the 1950s for mining purposes (Krige, 1951), this method has been used increasingly in other areas including the analysis and interpretation of incomplete surface air temperature fields (Rigor et al., 2000; Rohde et al., 2013). Missing values are determined according to a given covariance matrix, which is calculated from the existing observations and establishes a spatially relationship between the data points (Cressie, 1990). The basic idea was aptly summarized by Tobler (1970) with the words: "*...everything is related to everything, but near things are more related than distant things*", a property which is particular useful for spatially unequally distributed data sets such as the tide gauges used here. Due to the spatial non-uniformity of the data as described in Chapter 3.2, an interpolation method is needed that considers the spatial distances as well as the spatial distribution and density of the given data points (here: tide gauges). Problems regarding the clustering of measurement points are avoided by using statistical distances, which means that the spatial variance of the data set is taken into account. If clustering occurs in a region, the weights of the affected sample points are reduced by including the density distribution. If no clustering occurs in sparse regions, only the distance is considered. The procedure can be summarized with the formula

$$\hat{Z}_{(x_0)} = [w_1\ w_2 \dots w_{n-1}\ w_n] \cdot \begin{bmatrix} z_1 \\ z_2 \\ \vdots \\ z_{n-1} \\ z_n \end{bmatrix} = \sum_{i=1}^{n} w_i(x_0) \times Z(x_i), \qquad \textbf{Eq. 13}$$

where $\hat{Z}$ is the query value at the unobserved location x_0 and $i = 1 \dots n$ represents a running index over n observations. $\hat{Z}$ is computed from a linear combination of all observed values $z_i = Z(x_i)$, which are weighted by the parameter w according to distance and density.

Kriging provides some more important advantages over other interpolation procedures. The interpolated values change smoothly, always pass through the observed values at the sample points and the estimations tend to be conservative at every query point. The last aspect is particularly important because both the large-scale trend patterns and the underlying large-scale effects must not be artificially overestimated. This feature of Kriging is achieved by a convergence of interpolated values to the mean value of their region with increasing distance to the available samples. The interpolated values and trends tend to be less significant than the existing values and trends, guaranteeing that no significant interpolation-related trends occur. That is why Kriging estimates at query points tend to be conservative (Cowtan & Way, 2014) and as a results its prediction error variances are minimized (Oliver & Webster, 2015). All of these properties are crucial in the context of this thesis. Due to the highly non-uniform distribution of the tide gauges, the quality of the interpolated values strongly depends on tide gauge density in the area of the query point. However, for some of the procedures presented in the following, mathematically complete time series are indispensable. Since the number of available tide gauges is fixed and not changeable, other interpolation methods would possibly lead to severe overestimations. The use of Kriging guarantees that even in the case of insufficient initial data in regions with few measuring points and thus a poorer quality of interpolation, the overall result is not distorted with regard to small-scale changes, but corresponds to the mean value of its region. In this average of several tide gauges, large-scale signal are always included, since all tide gauges are impacted. This is not the case for small-scale signals, impacting only one or very few tide gauges. Therefore, the spatially uneven distribution of the data sets presented here is unproblematic. In keeping with this characteristic of a conservative interpolation, the general tidal behavior worked out in Chapter 6.1 and Chapter 6.2 is also valid when the Kriging step is omitted. The property of Kriging as a conservative estimator is additionally validated along with the overall statistical process sequence of this thesis in Chapter 4.5. Furthermore, for the separation of the large-scale effects (Chapter 7.2) as well as for the assignment of their physical causes (Chapter 8.1.3), a comparison is made with the unchanged data series in order to prove the accuracy of the procedure.

Overall, Ordinary Kriging is applied for two purposes in this theses. Firstly, temporal gaps in the tidal parameter data (see Chapter 3.2) were closed for each monthly time step in the study period. Secondly, additional data points along the coastline of the North Sea were interpolated for the tidal range, allowing not only to analyze the temporal evolution of each time series in terms of linear trends but also the spatial structure of these trends. This second procedure was not carried out for tidal high and tidal low water, because of the more pronounced uniformity of results, eliminating the need to delineate spatially contrasting developments. For both applications, the Ordinary Kriging algorithm of Schwanghart (2020) is used.

4.3 Principal Component Analysis (PCA)

In general, the Principal Component Analysis (PCA) is a method of multivariate statistics and often used to structure and simplify extensive data sets by approximating a large number of statistical variables with a smaller number of significant, non-correlated (orthogonal) linear combinations (Jolliffe, 2002). This type of analysis is often used today in Earth system sciences to identify spatial and temporal patterns of climate oscillations (e.g. Barnston & Livezey, 1987; Häkkinen & Rhines, 2004; Berx & Pain, 2017). Originally, the method was developed at the beginning of the 20th century and mainly used in psychology and social sciences (Überla, 1971). Schönfeld and Jensen (1992) date the increasing use in the natural sciences to the end of the 1950s, for example in meteorology (Lorenz, 1959), geology (Aubrey, 1979) or oceanography (Preissendorfer, 1988). Investigations of water level time series based on principal component analysis were first carried out by Tornevik (1977), Aubrey & Emery (1983), Nyberg (1983) and De Valk (1988) among others, with Schönfeld and Jensen (1992) first conducting analyses of tidal development in the German Bight.

If ve is a vector with n random variables, first a linear function $f_1(ve)$ - dependent on constant coefficients c_{1i} - is determined by calculating the eigenvector from the spatially weighted covariance matrix of ve. Then $f_1(ve)$ represents the largest possible overall (common) variance of all variables in ve:

$$f_1(ve) = c_{11} \cdot ve_1 + c_{12} \cdot ve_2 + \cdots c_{1n-1} \cdot ve_{n-1} + c_{1n} \cdot ve_n = \sum_{i=1}^{n} c_{1i} \cdot ve_{1i} \qquad \textbf{Eq. 14}$$

This decomposition process is repeated for a function $f_2(ve)$, which is uncorrelated with $f_1(ve)$ and describes the largest possible amount of the remaining common variance. It is possible to find n such functions, but the purpose is usually to explain as much variance as possible with significantly fewer functions $f_i(ve)$, known as Principal Components (PCs) (Jolliffe, 2002). For example, taking 100 time series without any commonality would result in 100 PCs, each explaining 1% of the total variance. However, if the 100 time series were identical, the result would be one PC explaining 100% of the variance. If all time series were one-half identical, PC1 would explain 50% of the variance and the remaining 50% would be distributed among the other PCs. Therefore, the PC of a temporally and/or spatially varying physical process represents orthogonal spatial patterns, in which the data variance is concentrated. Usually and in the following, the PCs are numbered according to the variance they contain, with PC1 explaining most of the variance of the original signals. Using the leading PC1, a reconstruction including only the largest common pattern of the observed variables can be generated. This is possible for any combination of PCs (e.g. for PC1 and PC2).

If all PCs are taken into account, the original time series y at time t and location x can be reproduced in the form of a sum with n being the number of PCs as follows:

$$y(t, x) = \sum_{i=1}^{n} f_i(t) \cdot e_i(x) \qquad \textbf{Eq. 15}$$

Therefore, a recursive calculation of the influence of an individual PC on parts of the initial data set is possible. The function f_i is the same for all locations and depends only on time, while the coefficients e_i depend only on location and represents a linear fit of the PC to the variable to be reconstructed. Therefore, this approach allows the spatial and temporal variability of a data set to be examined independently of each other (Schönfeld & Jensen, 1991).

In this study PCA is applied to the entire monthly de-seasoned data sets from the 70 tide gauges, whose gaps were previously filled through Ordinary Kriging. The procedure is applied separately for all three tidal parameters. If there are indeed large-scale signals affecting the tidal parameters in the North Sea, they should appear as a coherent pattern visible at multiple sites, and therefore be visible in the leading PCs. By contrast, spatially confined ("small-scale") anomalies in tidal parameters will be shifted into the higher PCs, as these can only be responsible for a small part of the overall variance. Such shifting includes not only the response of the local tidal system to, for instance, anthropogenic construction measures but also to changes in bathymetry or morphology. This approach can also reduce undetected tide gauge specific measurement errors, as these only occur at a single tide gauge and are thus not represented in the first dominating PCs. Local effects can explain more variance than large-scale effects at individual sites or small subsets, but never for the entire data set. It is therefore important to consider the explained variance of the PCs at each tide gauge individually to ensure that large-scale effects with a very small influence on the overall variance are retained. Another reason for considering each individual tide gauge is the uneven distribution of stations in the data basis. As described in Chapter 3.2, there are significantly fewer data points in the West of the study area than in the East. When making a quantitative comparison of the PCs, their spatial characteristics must be taken into account, since the absolute value of the explained variance also depends to a certain extent on the number of data points concerned. It is necessary to consider separate subsections of the study area as well as the individual tide gauges in the context of the explained variance, since an effect may appear to be significant for the entire study area only because of the large number of measurement points in a small subarea.

The issue related to the spatial extent of a local effect is illustrated in Figure 14. While the construction of the Afsluitdijk between 1927 and 1932 is certainly one of the larger, coherent construction measures with a length of about 32 km, its far-reaching influence on the tidal dynamics nevertheless illustrates the importance of spatial considerations. The changes in the mean value and the variance of the tidal range before and after the construction period are still clearly detectable at a distance of 50 km. However, the correlation between distance and change of these two parameters is not linear. While the variance in close proximity to the Afsluitdijk in Den Overbuiten increases by a factor of 3.2, the increase in Harlingen 37 km away is still about 2.1. In contrast, another 10 km further in Vlielandhaven, a factor of only 1.2 occurs, while in an overall distance of 50 km in West-Terschelling the construction is still corresponded to an increase by the factor 1.1. Here, without considering the individual tide gauges, a large-scale effect could be mistakenly assumed.

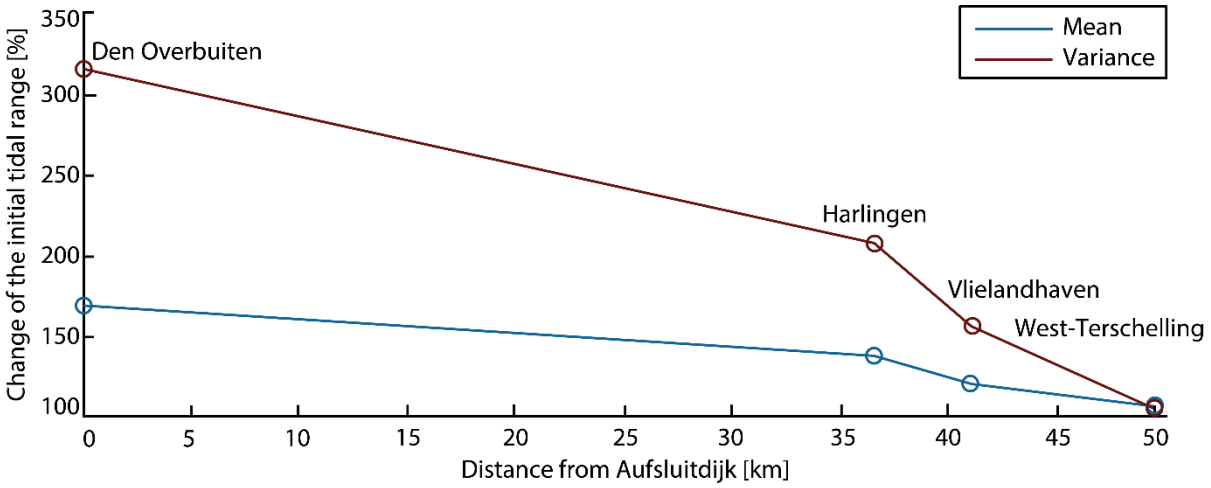

Figure 14: Relative changes in mean (blue) and variance (red) of tidal range at the named locations before (1926) and after (1934) the construction of the Afsluitdijk.

The actual separation of small-scale and large-scale effects is shown in the following Figure 15 using the example of Cuxhaven. The Figure depicts the measured values of tidal range, the reconstruction of the tidal range from leading PCs representing large-scale effects as well as their residuum. The residuum therefore represents the contribution of local effects.

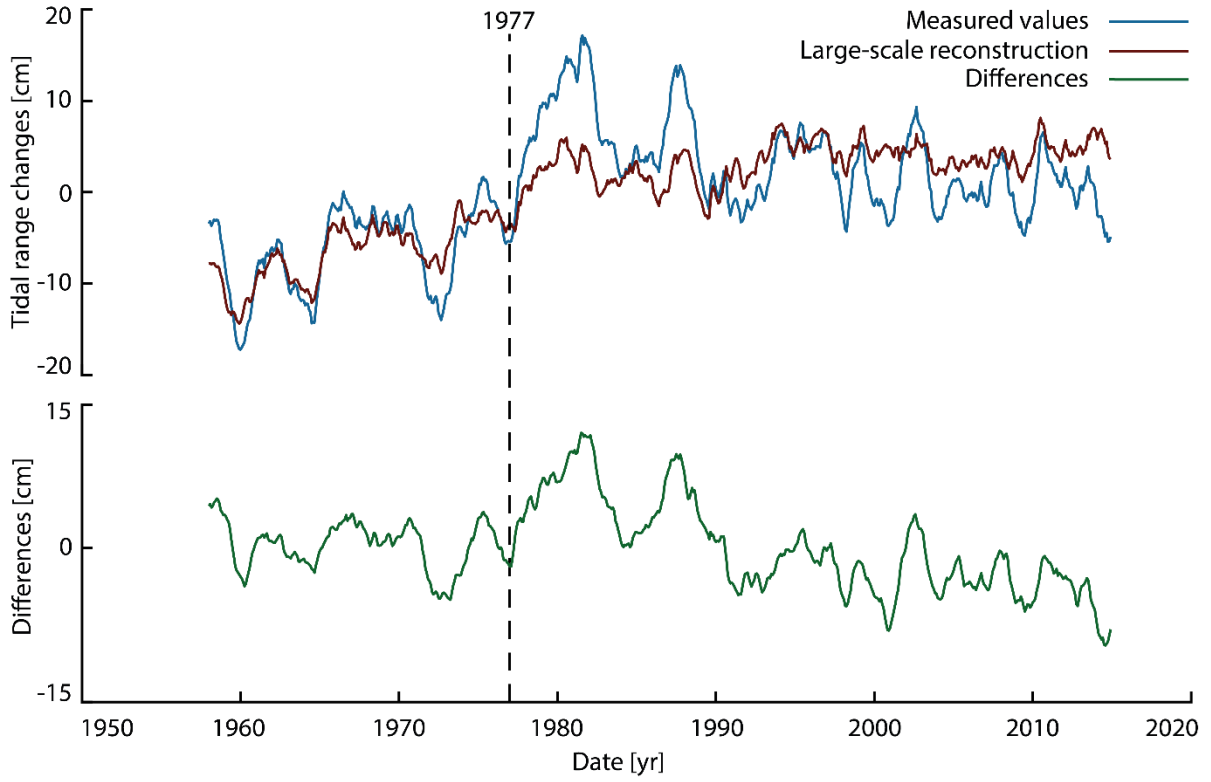

Figure 15: Measured values and large-scale reconstruction of the leading PCs of tidal range at the tide gauge Cuxhaven with dashed change point according to Ebener et al. (2020). A 12-month moving average is used to exclude seasonality and the nodal cycle was eliminated.

Until the year 1977 , a strong agreement between the two time series can be recognized. The correlation is 0.85 and the RMSE 2.5 mm/yr. After 1977, however, the time series diverge significantly, the correlation drops to 0.20 and the RMSE rises to 4.9 mm/yr. Ebener et al. (2020) use a similar methodology

to separate local effects and include a mathematical change point analysis to detect the causes of local changes. According to them, the expansion of the Lower Elbe between 1974 and 1978 is causative for a decrease in tidal low water and small variations in tidal high water, a combination that causes significant changes in tidal range. Independent of this causal research at local level, this example illustrates the methodology for separating small-scale and large-scale changes. Taking these considerations into account, the approach of PCA allows not only to attribute tidal parameter changes to small-scale and large-scale effects, but also to calculate the spatial extent and the temporal development of patterns that might reflect important environmental factors. Furthermore, PCA can be used to eliminate the nodal cycle utilizing its large-scale signal nature, a procedure described in the next chapter.

4.4 Elimination of the nodal cycle

The nodal cycle is one of the 6 basic astronomical cycles and have been described by Pugh & Woodworth (2014) as the leading tidal potential variation on decadal timescales, produced by the periodically changing declination of the Moon over an 18.61-year period. For the detailed astronomic background see Chapter 2.1 and Figure 6. The impact of nodal cycle variations on the tidal potential is assumed 3.7% on global average (Haigh et al., 2020) or 2.2 cm in global mean tidal amplitude (Baart et al., 2011). In shallow, narrow waters like the Gulf of Tonkin, the Bristol Channel or the English Channel, Peng et al (2019) found a nodal cycle driven change in the tidal high water of up to 30 cm, which reaches or even exceeds the predicted values of sea-level rise by 2050 for these areas. Haigh et al (2011) investigated the global influence of the nodal cycle on tidal high water levels and detected variations of up to 0.8 m. In the context of these water level variations, changes in tidal amplitudes driven by the nodal cycle are often referred to as nodal tide. However, this term should not lead to the misunderstanding that the nodal tide is a physical force or wave of its own. In fact, it is rather an oscillation of the tidal potential of the Moon and thus of all Moon generated tides. The term nodal cycle may therefore be less misleading and is used in this thesis.

The magnitudes of the nodal cycle driven amplitude changes mentioned above illustrate the need for the exclusion of the nodal cycle in any water level related studies, especially with regard to linear trend analysis (Pugh, 1987). Local effects can significantly change the impact of the nodal cycle (Haigh et al., 2011), whereby frictional effects, varying energy propagation and dissipation effects play a role here as well as varying water depths (Haigh et al., 2020). In addition to these individual points, overlapping and nonlinear interactions between them as well as data quality limitations and noise are obstructive (Rossiter, 1967; Trupin & Wahr, 1990). Therefore, the unknown amplitude and the spatial variability of the nodal cycle have to be determined. The widely used procedure of f-u correction (also: nodal correction) for the exclusion of the nodal cycle in the context of harmonic analysis (e.g. Trupin & Wahr, 1990; Codiga, 2011; Pugh & Woodworth, 2014) is based on the assumptions of the Equilibrium Tide Theory Pugh (1987). Within this theory, every tidal constituent consists of an amplitude and a phase, but only the tidal constituents of M_2 and S_2 have an actual physical background. The remaining tidal constituents

are mathematically based on imaginary celestial bodies, the phantom satellites. A more detail descriptions of this topic is given in Chapter 2.1. However, as a result of the Equilibrium Tide Theory's theoretical assumption of an oceanic Earth and a purely astronomical impacts, only the geographical position (lunar node longitude) of a tide gauge (Codiga, 2011) can be taken into account, but not the individual, local characteristics. That is why the assumptions of the Equilibrium Tide in the context of the nodal cycle have recently been questioned by various studies. The contrast between theoretical tidal potential and local system response is often significant and recognized for example by Cherniawsky et al. (2010), Feng et al. (2015) and Peng et al. (2019). A summary of this problem for the North Sea can be found in Hagen et al. (2021). Feng et al. (2015) prove that there are significant differences between the measured nodal tide and equilibrium tidal constituents for shallow continental shelf areas. Cherniawsky et al. (2010) come to a similar conclusion based on satellite altimetry, as the nodal amplitude ratios between different tidal constituents clearly exceeded the predicted values from the Equilibrium Tide Theory. As a result of these effect, several other approaches have recently been developed (Peng et al., 2019; Hagen et al., 2021) which are based on numerical as well as on analytical approaches like Taylor series. In both cases, high-resolution data sets (at least hourly resolution) are required, which are not available in most parts of the world, especially for data going back a long time. This is also the case in this thesis for most of the tide gauges and an alternative method have been developed that makes it possible to use tidal low and high water values for nodal correction.

To explain this approach, first the effect of the nodal cycle for the North See is shown exemplarily in Figure 16 for the tide gauges Felixstowe (#10), Westkapelle (#18), Helgoland (#55), and List (#68). Following the progression of the tidal wave from the deeper areas of the UK (Felixstowe) towards the shallower areas of the Netherlands (Westkapelle) and the German Bight (Helgoland, List), a decrease in the amplitude of the nodal cycle becomes apparent. It is particularly recognizable at its high points in 1959, 1978 and 1997, representing the spatial variance of the amplitude changes.

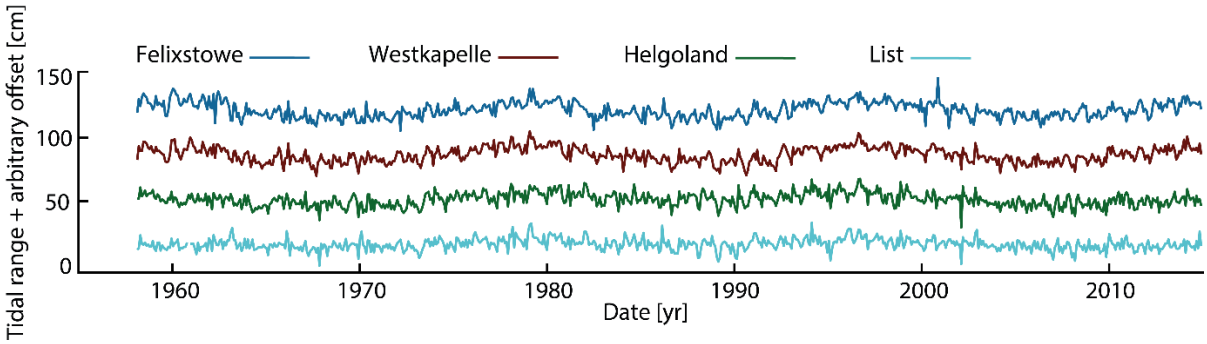

Figure 16: Time series of monthly tidal range of tide gauges Felixstowe, Westkapelle, Helgoland, and List, including the nodal cycle.

In principle, the extraction of the nodal cycle from the measured time series is accomplished with PCA. As mentioned above, the M_2 and S_2 tidal constituents are dominant in the North Sea area with only the M_2 being caused by the Moon. This is also true when using monthly values, even though the spring neap cycle is no longer relevant then. As a result, changes in M_2 will have a large influence on the water

levels at each tide gauge. With the nodal forcing acting in the entire study area, there is an impact on every tide gauge and on the overall variance. It is thus possible to identify and extract the impact of the nodal cycle as leading PCs according to the procedure presented in Chapter 4.3.

4.5 Validation and demonstration of the overall methodology

After explaining the statistical methods used in the previous subsections of this chapter, this subsection aims to demonstrate the fundamental suitability of the selected methods as well as the applicability of the overall statistical process sequence. In order to explain the statistical process sequence, it is useful to recall the initial problem in mathematical terms: The aim is to extract large-scale signals from a temporally incomplete data set consisting of 70 spatially unevenly distributed time series, each with up to 684 mean monthly values (corresponding to the study period from 1958 to 2014). This task is further complicated by the possible superimposition of several large-scale and small-scale signals at a varying extent, leading to a smudging of the signals. In addition, a correction must be made for the nodal cycle to ensure that this known large-scale effect does not distort the unknown large-scale effects due to its spatially varying impact.

This objective is mainly achieved by the combined application of Ordinary Kriging and PCA. The application of the PCA is recursive, since this procedure is used both to detect unknown large-scale effects and to correct the data set for the nodal cycle beforehand. To clearly distinguish these applications from each other, the correction of the nodal cycle is discussed separately in Chapter 4.5.2.

4.5.1 Ordinary Kriging and Principal Component Analysis

To address the aforementioned problems, PCA is used to detect large-scale signals identical at many tide gauges. The basic suitability and application of the methodology is demonstrated below. However, PCA requires complete data sets and an interpolation of the missing data must be performed first. As described in Chapter 4.2, the use of a conventional interpolation method such as a linear regression to a polynomial function for example is not applicable because of the superposition of small-scale and large-scale effects as well as the inhomogeneous spatial distribution. Local effects of neighboring tide gauges could be transferred when interpolating missing values and their impact would be spatially magnified, resulting in a potential overestimation. Furthermore, for an incomplete and strictly locally affected tide gauge, no correct interpolation of the missing values is mathematically possible, because the local effect only impacts the exact same tide gauge. The neighboring stations remain unaffected. However, the objective of this thesis is not to reconstruct missing tide gauges as accurately as possible, but to detect large-scale signals acting on my tide gauges. Since these signals are contained in every tide gauge of a certain region by definition, it is useful to use an interpolation method that is strictly conservative and therefore rather underestimates than overestimates local effects in the interpolation. Furthermore, the existing sampling points must not be manipulated by the interpolation, otherwise local influences could

also be overestimated. These properties are combined in the Kriging algorithm. Additionally, the obtained results are further ensured by this procedure, since all detected large-scale effects are rather underestimated than overestimated. A classical validation by filling artificial gaps in the initial data set and subsequent consideration of the correlation and the RMSE is therefore not useful, since this would work very well for tide gauges with small local signals and would result in a massive overestimation for tide gauges with large local signals. For the use in this thesis, it is much more important to demonstrate the overall conservative nature of Kriging for the actual data gaps in the existing data set. Hence, it must be proven that neither the reconstructed trends (after Kriging) nor the detected large-scale signals (after Kriging) overestimate the original trends (before Kriging) or the actual large-scale signal (before Kriging). This proof also includes the demonstration that a correct, rather conservative extraction of the large-scale signals is possible using PCA after the application of Kriging. This proof as well as the basic suitability of the methodology will be demonstrated in the following. In order to enable a comparison with measured data, where neither the gapless condition nor the large-scale signals are known, the results of the analyses are compared with unchanged measured data in the corresponding Chapters 7.2 and 8.1.3.

In order to validate the general procedure, 70 complete artificial time series are generated, each with 684 values. For a better comparability of the results, the calculation is done with reference to the unit circle between -1 and 1 (Figure 17).

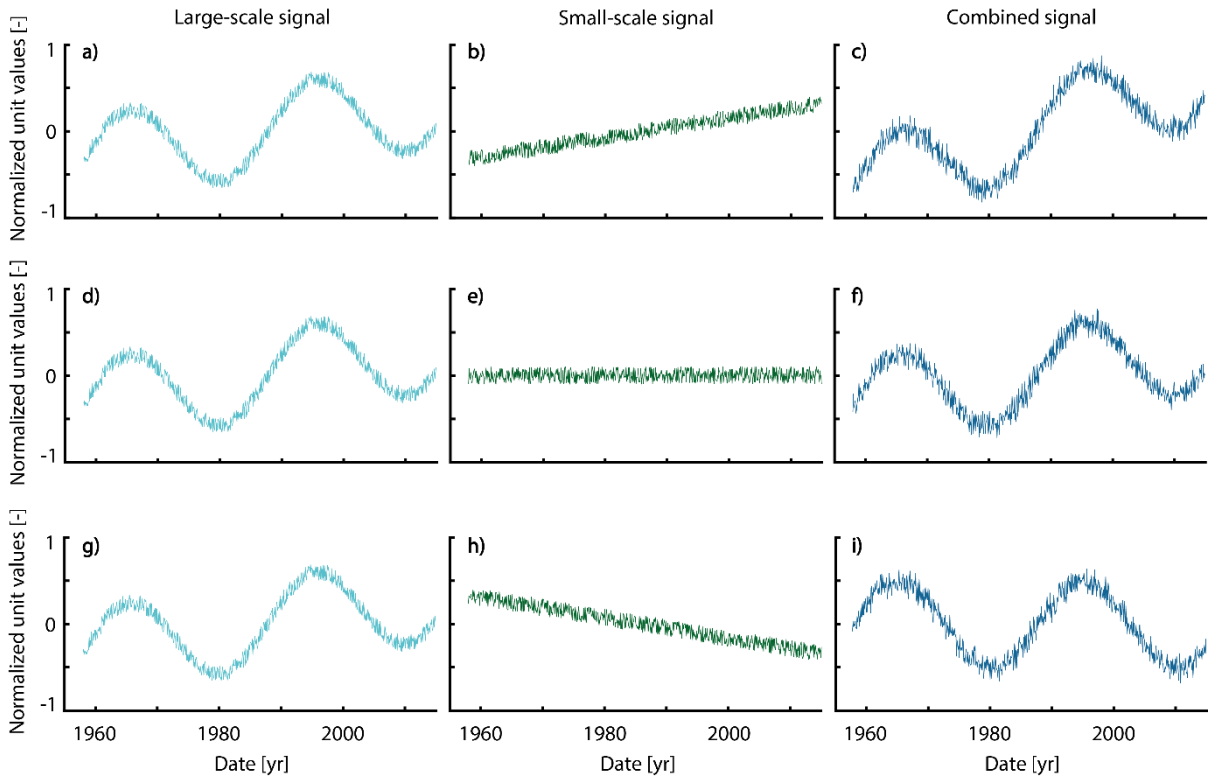

Figure 17: Artificial constant large-scale signal (a, d, g), artificial variable small-scale signal (b, e, h), and their combined signals (c, f, i).

Each time series contains a common sinus-based large-scale signal, which is overlaid with varying small-scale signals with a positive, a neutral or a negative trend. These local signals are randomly generated and can be up to a factor of 4 times larger than the large-scale signal in trend, since factor 4 is approximately the largest occurring trend difference in the original measured time series. The variance of both the large-scale and small-scale signals is randomly generated and equal in the average magnitude. Since PCA operates variance-based to separate the signals, this represents the worst case for the intended analysis. If the variance were significantly higher in one of the two, this would artificially simplify the separation. After the artificial signals are generated, all missing values in the measured data set are deleted in the artificial data set as well. Now the procedures used in the further course of this thesis can be applied to the artificial data set and the result can be compared with the initial situation, since the large-scale signal and the trends before deletion of the missing values are known. Kriging is performed first, followed by PCA to detect the large-scale signals. Afterwards, a comparison of both the reconstruction of the large-scale signal with the actual large-scale signal and the fully reconstructed trends (including all PCs) with the original trends is done.

Figure 18 compares the large-scale reconstruction of three tide gauges with the original combined signal from Figure 17 (c, f, i) for a positive, neutral and negative small-scale trend. It becomes evident that the local trend does not influence the detected large-scale signal in any of the three cases. In fact, a positive small-scale trend leads to a combined signal which is larger than the reconstruction of the large-scale signal and a negative small-scale trend leads to a combined signal which is smaller than the reconstruction of the large-scale signal. In no case the actual signal is overestimated by the reconstruction of PC1 regarding trends. The suitability of the methodology for separating the signals can therefore be confirmed in this step.

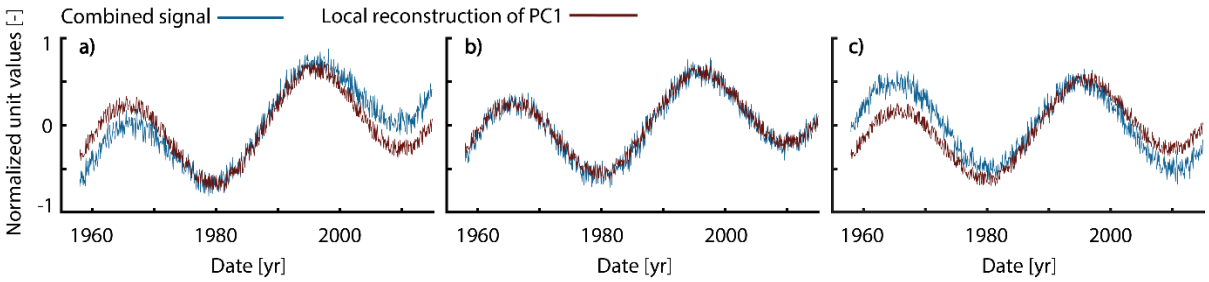

Figure 18: Comparison of the input time series (combined signal) with the local reconstruction of PC1 for a positive (a), neutral (b) and negative (c) small-scale trend.

This fact is further verified when comparing the detected large-scale signal with the original large-scale signal in Figure 19. The correlation between the two signals is 0.98 and it manages to explain about 97% of the variance of the original signal. Accordingly, the original large-scale signal explains just under 60% of the total variance in the data set, while the reconstruction explains only about 55%. Again, the procedures perform as expected and underestimates rather than overestimates the large-scale impact.

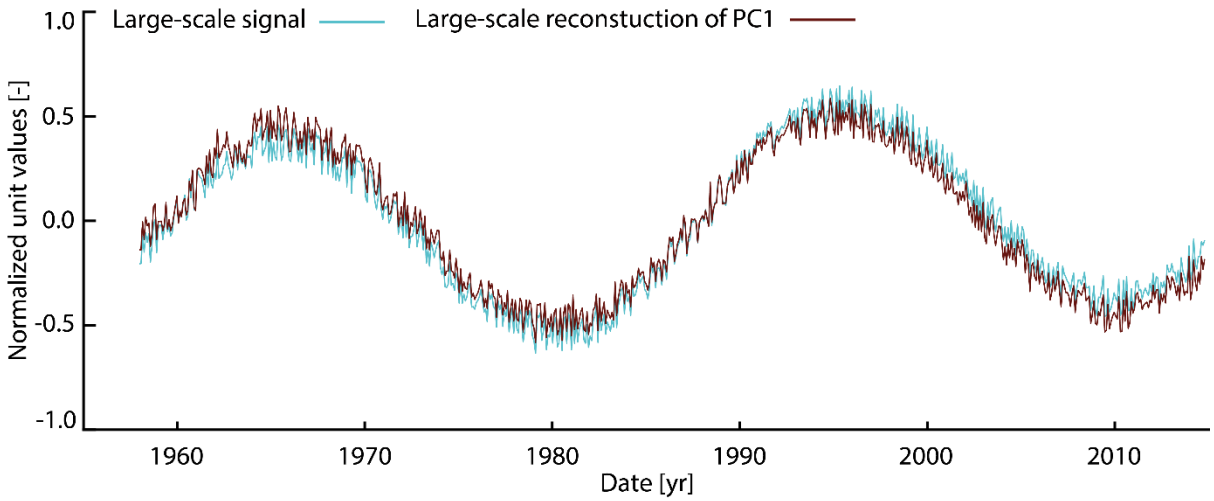

Figure 19: Comparison of the original large-scale signal and its reconstruction.

Finally, the conservative nature of the method regarding the trends at the individual tide gauges must be demonstrated. Figure 25 depicts the reconstructed trends after Kriging (red) and the original trends before Kriging (blue). Absolute trend values are used here to illustrate the conservative nature of Kriging, making the values smaller in moving them closer to zero. Only in 5 out of 70 cases, the reconstructed trend is minimally larger than the measured trend, with none of these deviations reaching significance on the 95% interval. Even the trends themselves are not significant in all 5 cases. Thus, not a single significant discrepancy is detected. Since the conservative nature of the methodology as well as its basic functionality regarding both variance and trends is proven, the procedures can be applied to the actual data set.

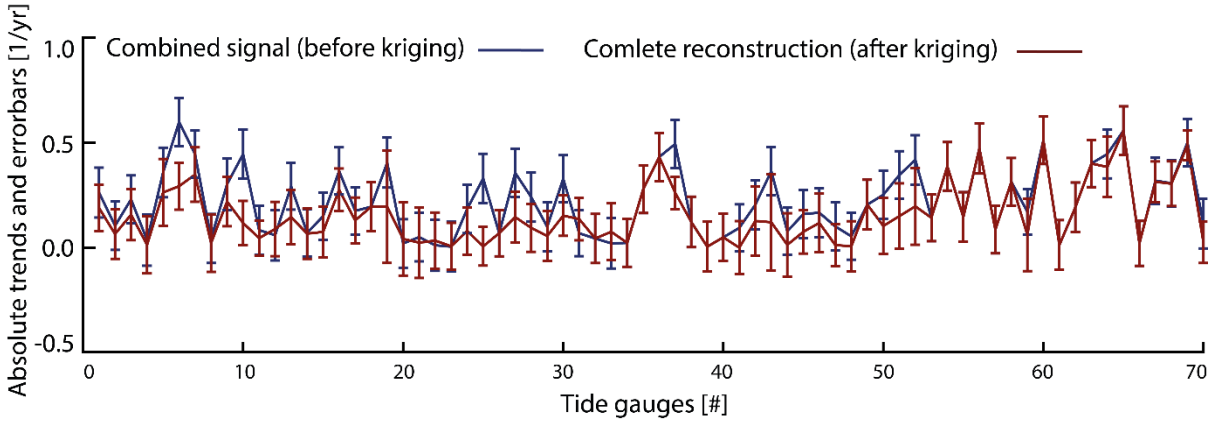

Figure 20: Comparison of the absolute trends of the input signal (before Kriging) and the complete reconstruction (after Kriging) with 95% confidence interval. Note that the full reconstruction time series are identical to the time series after Kriging.

4.5.2 Nodal cycle adjustment

Based on the procedure described in Chapter 4.4, the procedure for eliminating the nodal cycle is demonstrated and validated here. The extraction of the nodal cycle is presented in Figure 21 for tidal low water (a), tidal high water (b) and tidal range (c). The nodal cycle is clearly visible in the PCs, since overlaying effects, which mask the nodal signal often in measured data, only have a local impact or at least a smaller

impact on the overall variance. Obviously, the nodal cycle is most evident in the PCs of the tidal range. This is caused by 3 factors: (I) as explained in Chapter 3.3, measurement errors and overlaying effects such as seasonality and meteorology tend to be eliminated in the difference formation of the tidal range, (II) the significantly lower variance (Chapter 5) in tidal range allows a more precise analysis by PCA and (III), the nodal cycle in the North Sea region is by definition most evident in the amplitude of the M_2, which corresponds most closely to the tidal range (Chapter 4.4). Following these insights, it is possible to extract the nodal cycle by a nonlinear least squares fitting based on a sine function (Figure 21-d). No temporal grid points for the sine are used here, since otherwise the agreement with the theoretical high and low points would no longer be a quality indicator. The theoretical high and low points for tidal range described by Pugh & Woodworth (2014) based on the Moon's orbit confirm the results. Furthermore, it should be noted that even if the nodal cycle derived from tidal range is most consistent with the values from astronomy, the corrections were nevertheless also made for tidal low and high water. In this way, the parallel analyses of all three tidal parameters remain comparable and consistent.

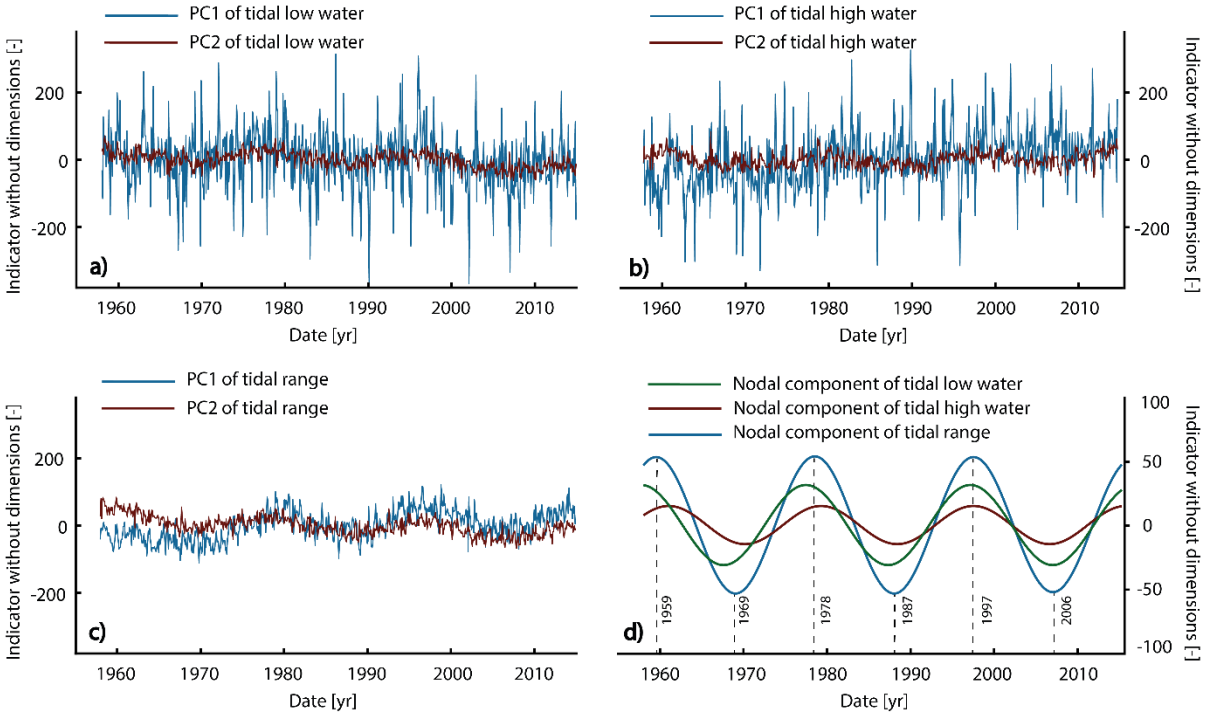

Figure 21: Results of the PCA for tidal low water (a), tidal high water (b), and tidal range (c). In part (d), the extracted functions of the nodal cycle and the highs and lows of the causative lunar declination (Pugh & Woodworth, 2014) are presented.

Based on the information about the nodal cycle in the leading PCs and their distribution, a tide gauge specific reconstruction and elimination of the nodal cycle from the measurement data is possible. The methodology can be applied to any of the 70 tide gauges in this study. For demonstration, this elimination is shown in Figure 22 for the tide gauges Felixstowe (#10), Westkapelle (#18), Helgoland (#55), and List (#68). The dotted lines illustrate the varying expression of the nodal cycle at different tide gauges. While the variances of the gauges Felixstowe (~39 cm^2 / ~20 cm^2) and Westkapelle (~35 cm^2 / ~18 cm^2) are almost halved, the reduction in Helgoland is less than 15% (~35 cm^2 / ~30 cm^2) and only

3% (~33 cm^2 / ~32 cm^2) on List. These varying reductions illustrate the deviant impact of the nodal cycle on different tide gauges. However, it does not allow any conclusion about the distortion of possible trend calculations, since trend calculation depends not only on the influence of the nodal cycle, but also on the time window under consideration. The largest possible error would generally occur when comparing an extreme point of the nodal cycle with the previous or subsequent extreme point. This maximum error in trend at the tide gauges would be 14 mm/yr in Felixstowe, 13 mm/yr in Westkapelle, 7 mm/yr in Helgoland and 4 mm/yr in List. The potentially highest error is often greater in amplitude than the inherent trends. This fact illustrates the importance of considering the nodal cycle in trend analyses with the application to the data sets used here presented in the following.

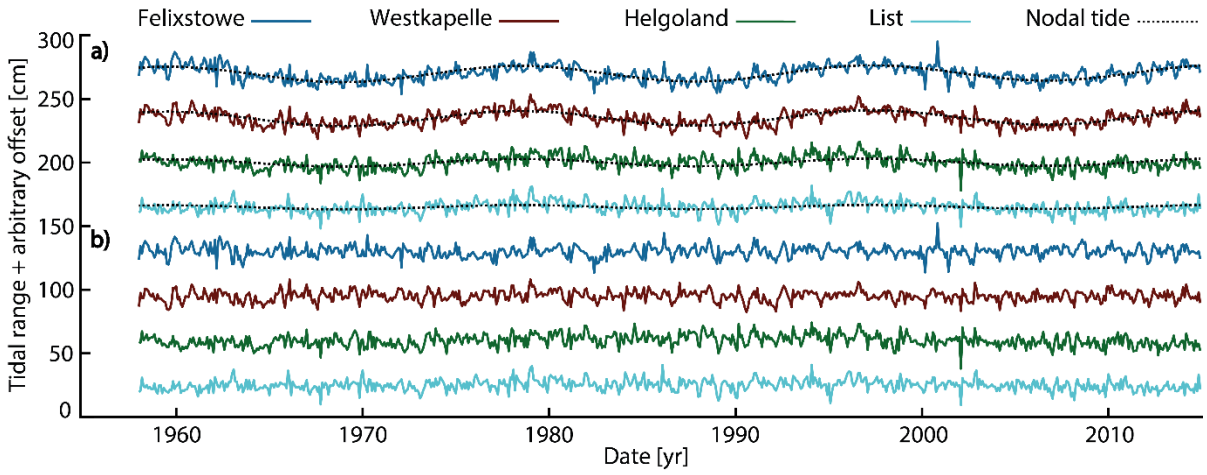

Figure 22: Time series of tide gauges Felixstowe, Westkapelle, Helgoland, and List including (a) and excluding (b) nodal cycle.

5 Setup of the final data basis

Having successfully validated the methodology in Chapter 4.5.1 and Chapter 4.5.2, these procedures are applied in this chapter to the entire data set of measured values. First, the application of Ordinary Kriging is carried out, followed by the elimination of the nodal cycle. The result as a complete data set excluding the nodal cycle then forms the final data basis on which the following calculations of the large-scale trends and the detection of the large-scale signals are performed. A distinction is made between tidal low and high water and the tidal range on the basis of their different characteristics. Please note that, as described in Chapter 3.2, the time series used have been adjusted for their mean so that changes can be analyzed at a common reference level of zero.

An overview of monthly tidal low and high water data is provided in Figure 23. The upper part of the figure represents the measured data without interpolation and the lower part represents the data after applying Ordinary Kriging. In addition to the numbering of the tide gauges, the corresponding national borders are marked to provide easier orientation.

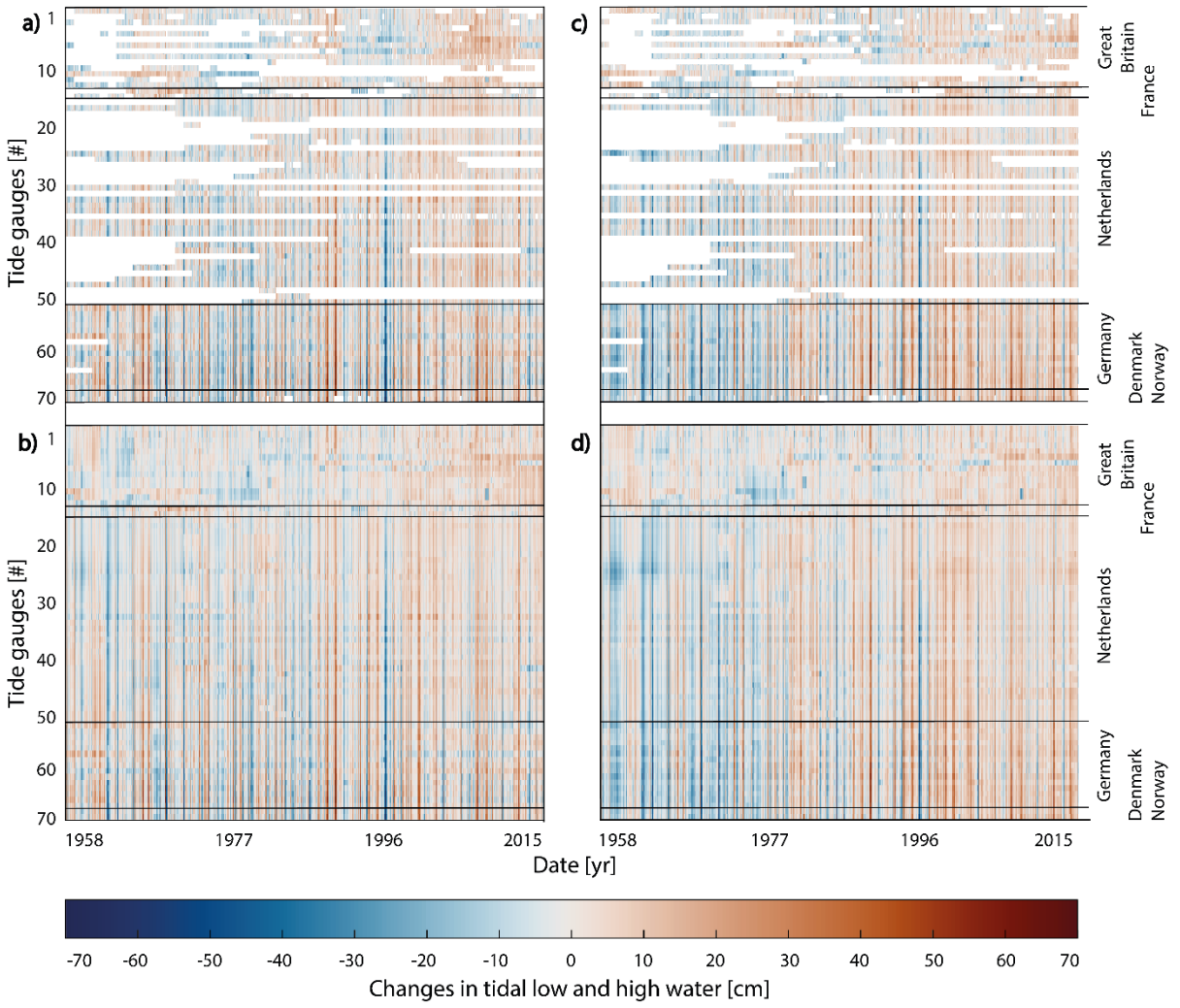

Figure 23: Changes in tidal low (a, b) and tidal high (c, d) water before (a, b) and after (b, d) applying Ordinary Kriging.

While the time series in Germany, Denmark, and Norway are almost complete, the gaps for tidal low water are more extensive in the UK, France, and the Netherlands. In particular, at many Dutch tide gauges records only started in the 1970s. Missing data here is interpolated from the longer-dated tide gauges, which comprise about one-third of all Dutch tide gauges. Due to the consideration of spatial dependence in the interpolation, the influence of longer British and German stations outside the immediate vicinity of the border is negligible. In the UK, the gaps cannot be assigned to a precise time, but the completeness increases with the beginning of the 1980s. Overall, data quality is lowest here, especially when the low tide gauge density is also considered. Across all borders, the database contains distinct inter and intra annual variations both before and after Kriging, although both the spring neap cycle and the seasonal cycle has been removed. A distinct nodal cycle is not apparent. The overall variance of tidal low water is about 138 cm² which corresponds to a standard deviation of about 11.7 cm. These values are not significantly changed by the Kriging algorithm (Figure 23-b). A slight increase of the reddish shades from left to right can be recognized, giving a first hint of an average rise in tidal low waters over the study period. This increase appears to be a bit more pronounced in the UK than in the other areas of the North Sea, with a tendency to decrease towards the German Bight. Overall, however, the increase appears to be relatively homogeneously distributed and rather moderate, compared to tidal high water.

In tidal high water, a more significant and less evenly distributed increase occurs. While the data gaps are almost identical to the tidal low water, larger positive trends are observable over the study period. The individual trends seem less pronounced in the UK and the southern parts of the Netherlands and more pronounced in the German Bight area (Figure 23-c/d). The blue tones are much more pronounced on the left side and the red tones are much more pronounced on the right side of the Figure, indicating an increase over the period between 1958 and 2014. Similar to the tidal low water, no distinct nodal cycle is visible, but the time series contain other distinct inter and intra annual variations. The overall variance here is 125 cm² with a standard deviation of 11.2 cm, falling short of the standard deviation of tidal low water by 0.5 cm. No significant change in variance due to Ordinary Kriging is found here either.

In summary, comparable properties exist between tidal low and high water regarding to intra and inter-annual variability, while the spatial distribution of temporal developments do not match. The tidal low water shows an overall moderate increase with a slightly higher impact in the UK area, while tidal high water depicts a more pronounced overall increase with a higher impact in the German Bight area. In addition, the overall variance of the tidal low water exceeds the overall variance of the tidal high water by about 10%.

As a quantity derived by difference formation, the data gaps in tidal range are very similar to those in tidal low and high water (Figure 24-a). For the same reason, the spatially varying developments in tidal low and high water are also reflected. The overall larger trend of tidal high water through vast parts of the study area results in a visible increase of tidal range in the German Bight and the northern parts of

the Netherlands. This increase is less pronounced in the southern areas of the Netherlands and non-existing in the UK, as can be recognized from the reddish color of the values in Figure 24-b. There seems to be a contrasting development between the UK in the west and the German Bight in the east of the North Sea, with the coast of the Netherlands forming a kind of transitional area. In contrast to tidal low (138 cm²/11.7 cm) and tidal high water (125 cm²/11.2 cm), the inter- and intra-annual variation and thus the variance is comparatively low with a value of 50 cm², which refers to a standard deviation of 7.1 cm. The low indicates that both level-specific influences and possibly remaining seasonal variations are eliminated by the process of difference formation, as those seem to occur in most cases in both tidal low and high water. In contrast to tidal low and high water, a more distinct nodal cycle is visible in the tidal range. This result is consistent with the results of the validation of the nodal cycle correction in Chapter 4.5.2.

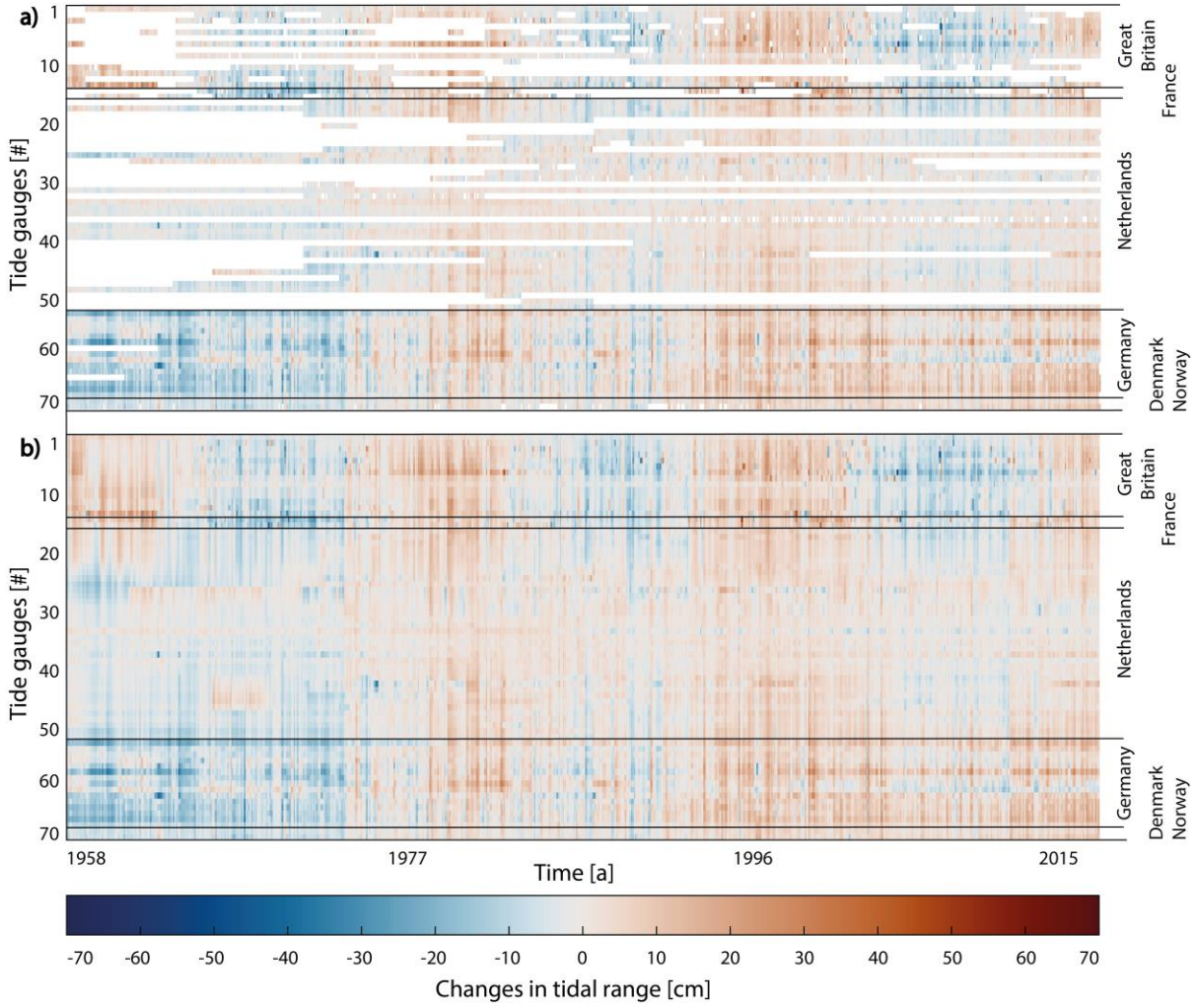

Figure 24: Changes in tidal range before (a) and after (b) applying Ordinary Kriging.

This completes the first step, applying Ordinary Kriging to the entire data set. The next step is to apply PCA to the interpolated data set to eliminate the effects of the nodal cycle. Even with no distinct nodal cycle being visible in the tidal low water (Figure 25-a), nevertheless a mathematical correction is applied to ensure comparability of the time series to the other tidal parameters. A slight smoothing due to nodal

correction is visible (Figure 25-a), which corresponds to a reduction of the variance by 3.5% or 2.4 cm in the standard deviation. Although hardly visually representable, this correction cannot be neglected, since a missing correction of 2.4 cm can cause additional trends of up to 0.4 mm/yr during the study period, assuming the worst case in which it exclusively reinforces the trend. Similar applies to the tidal high water where also no distinct nodal cycle is visible. Nevertheless, a mathematical correction leads to a reduction of the variance by 1.5% or 1.4 cm in the standard deviation here.

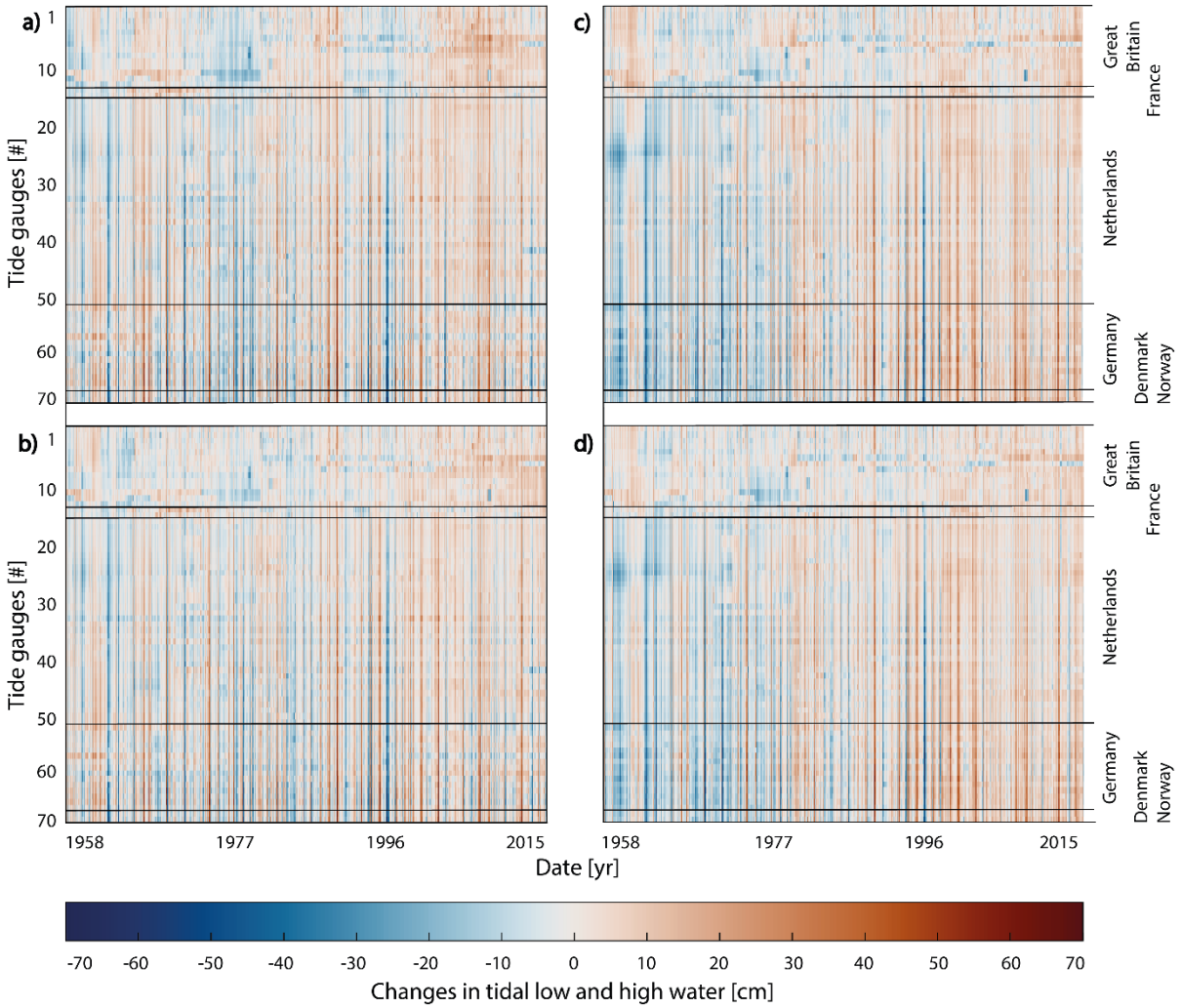

Figure 25: Changes in tidal low (a, b) and tidal high (c, d) water including Ordinary Kriging before (a, c) and after (b, d) elimination of the nodal cycle.

The opposite is the case for the tidal range, where a distinct nodal cycle occurs with clearly recognizable peaks around 1978, 1997 and 2014 (Figure 26-a). The peak around 1959 is only recognizable in the UK. It is striking that no such peak is present in the area of the German Bight, illustrating the potentially large spatial variability. Due to the massive data gaps a statement about the Netherlands can only be made to a limited extent, but in the time series ranging back long enough a clear nodal cycle can only be recognized in close proximity to the UK (Vlissingen, #35). Overall, the elimination of the nodal cycle (Figure 26-b) reduces the variance of the tidal range data set by 24% to 38 cm² and the standard deviation to 6.2 cm. The significantly greater reduction in variance of 24% when excluding the nodal cycle for the

tidal range (tidal low water 3.5%; tidal high water 1.5%) indicate a superposition of the nodal cycle by various effects such as remnants of seasonality or meteorology in tidal low and high water. Other important points eliminated in tidal range may be measurement errors or statistical white noise. These results correspond to the explanations in Chapter 3.3, where the advantages and the disadvantages of proportional equalization through differences analysis are described. Undesired effects are eliminated, which is beneficial, but other factors potentially causing tidal changes may be eliminated as well. This reinforces the approach of this thesis to search for common signals throughout the study area by applying PCA to all three tidal parameters. In summary, the final data set has now been generated that is temporally complete as well as adjusted for the nodal cycle, being the basis for the analyses in the next chapters.

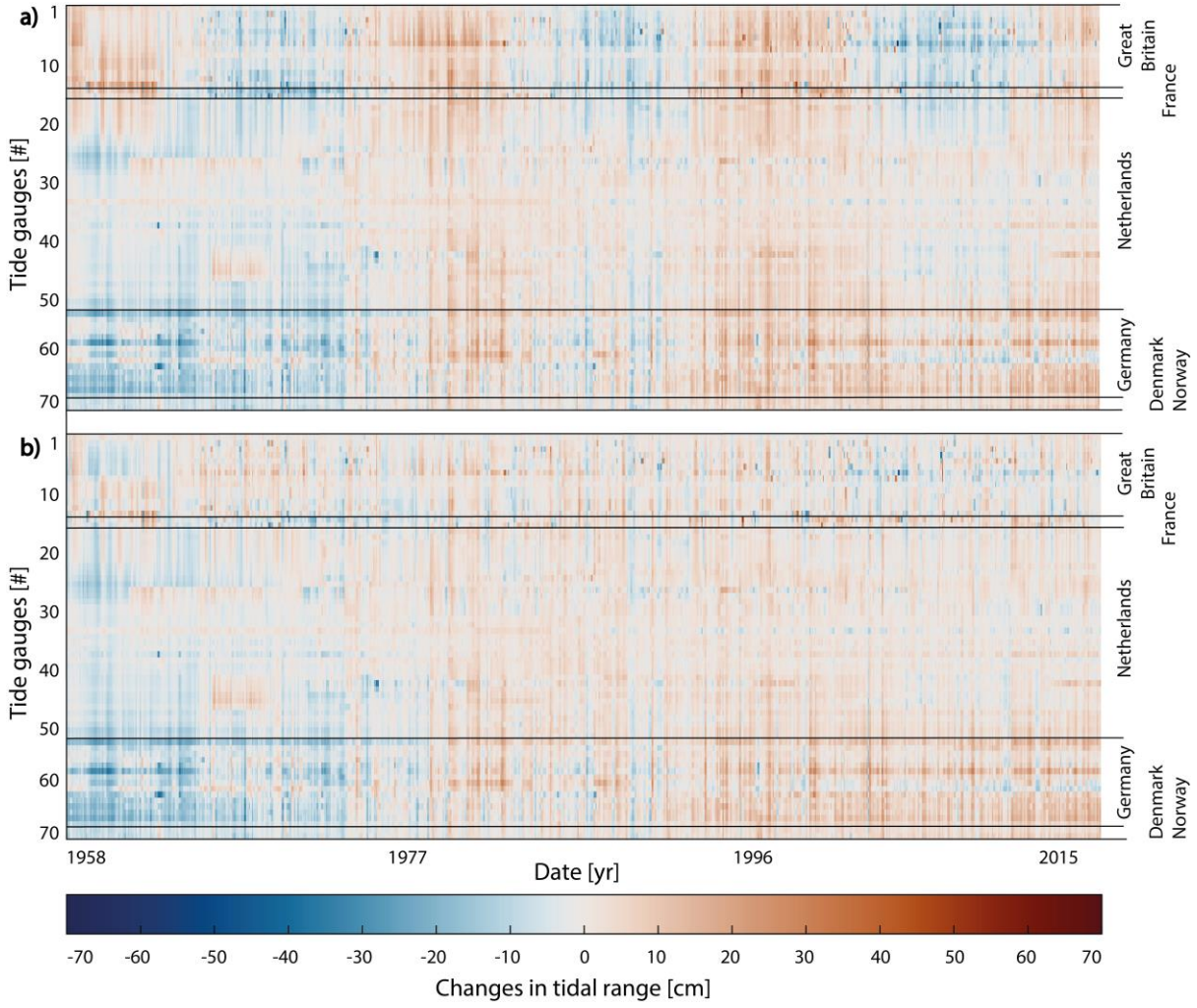

Figure 26: Changes in tidal range including Ordinary Kriging before (a) and after (b) elimination of the nodal cycle.

6 Tidal changes of the North Sea

Since the theoretical background of tidal changes, the current state of science as well as the methods and data sets used were explained in the previous chapters, it is now possible to process the first research question from the Introduction of this thesis: *Are the changes in tidal low and high water and the tidal range on different time scales detected within the German Bight a localized phenomenon, or are they part of a larger-scale development spreading over larger areas within the North Sea region?*

As already noted in the previous Chapter 5, spatial differences in the trends of tidal low and high water occur, resulting in tidal range changes. To investigate and quantify these discrepancies, the long-term changes of tidal parameters and their spatial variability in the study area have to be investigated. Therefore, the linear trend of each individual record and each parameter over a common period between 1958 and 2014 is calculated. In order to be able to represent large-scale changes as common spatial developments, the study area is divided into 3 regions, as can be found in Table 6 including their median trends.

The first region is the UK including the tide gauges Lerwick (#1) to Dover (#14), with the tide gauges from Lerwick to North Shields (#5) being categorized as UK North and the tide gauges from Whitby (#6) on as UK South. The tide gauges from Calais (#15) to Huibertgat (#47) are classified as the European West Coast, which merges into the German Bight at the station Borkum F. (#48). The tide gauges from Borkum F. to Cuxhaven (#60) are classified as German Bight South (GB South) and the tide gauges further to List (#68) as German Bight North (GB North). The two tide gauges Esbjerg (#69) and Tregde (#70) are not considered in this classification, since their isolated location does not allow any conclusions about large-scale developments. For the named areas, a median trend is given for each tidal parameter to quantify the occurring differences. The use of an arithmetic mean to describe the spatial distribution of trends is unsuitable because of its sensitivity to outliers and anomalies. Since these cannot be excluded due to the potentially significant local influences, the median is used here to describe the spatial characteristics of tidal parameters.

Table 6: Measured median linear trends in tidal low water, tidal high water and tidal range.

Location		Median linear trend [mm/yr]		
Region	**Tide gauges**	**Tidal low water**	**Tidal high water**	**Tidal range**
United Kingdom	Lerwick - Dover	1.6	1.3	-0.4
UK North	Lerwick - North Shields	1.2	1.0	-0.1
UK South	Whitby - Dover	2.4	1.4	-0.8
European West Coast	Calais - Huibertgat	1.3	2.0	0.8
German Bight	Borkum F. - List	0.8	3.8	3.0
GB South	Borkum F. - Cuxhaven	0.8	3.3	2.8
GB North	Büsum - List	0.8	5.2	4.3

6.1 Changes in tidal low and tidal high water

First, the linear trends of the tidal low and high water between 1958 and 2014 are calculated and presented in a general overview (Figure 27). With two exceptions, all significant trends are positive for both tidal low and high water in the study area. Some more tide gauges show negative trends, but these do not reach the 95% confidence level and are considered neutral, since they are not significantly different from zero. Furthermore, it is evident that the trends in tidal low water are less pronounced than in tidal high water with a median of 1.4 mm/yr compared to 2.2 mm/yr on a basin-wide scale. Overall, both tidal low and tidal high water trends are increasing, but at different rates.

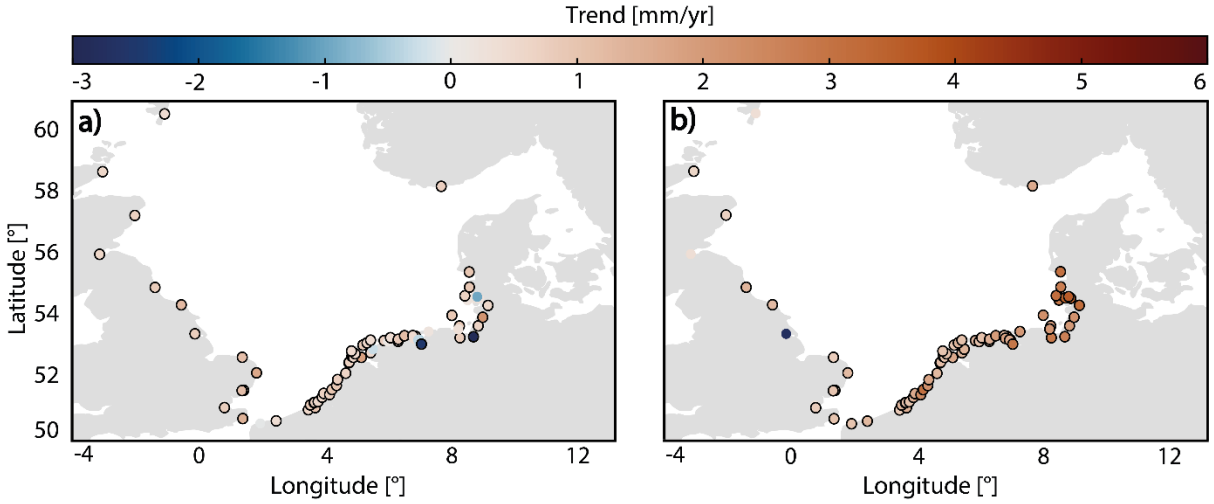

Figure 27: Linear Trends of tidal low (a) and tidal high (b) water between 1958 and 2014 (significant trends outlined).

Trends in tidal low water tend to be spatially more homogeneous than trends in tidal high water. The median tidal low water trends are identical in the German Bight and exhibit a maximum median divergence of 1.6 mm/yr to the UK (Table 6). This divergence is 4.2 mm/yr for the tidal high water and no identical values exist. However, if the spatial homogeneity is considered separately by region, it becomes apparent that the tidal low water trends diverge more strongly in the UK, while the tidal high water trends diverge more strongly in the German Bight. In tidal low water, only 57 of 70 trends reach the significance threshold with the German Bight being heavily overrepresented regarding non-significant trends. While less than 30% of all tide gauges are located here, nearly 70% of all neutral trends in tidal low water are located in this area. Contrary, 66 of the 70 tide gauges exhibit a significant tidal high water trend with the non-significant trends being located exclusively in the UK.

Overall, the trends of tidal low water are generally lower in the German Bight than in the UK. The European West Coast forms a kind of transitional area between the UK and German Bight, with the overall behavior of the tide gauges in this area being more similar to the German Bight. In contrast, the significant trends of tidal high water depict substantially higher values in the area of the German Bight and the eastern parts of the Netherlands than in the UK. Consequently, there is a clear contrast between the trends in the UK and the German Bight area, both for tidal low and high water. While the trends in

tidal high water are much higher in the German Bight area, the trends in tidal low water is more distinct in the UK area, forming a kind of a dipole.

In order to assess this contrasting development between the UK and the German Bight, these two areas are more closely presented in Figure 28 (for the associated regional trends, see Table 6). The regional classification of the study area is also presented, although the European West Coast is not shown here. While the trends are fully comparable, the geographical representation is purely qualitative and the scales do not match.

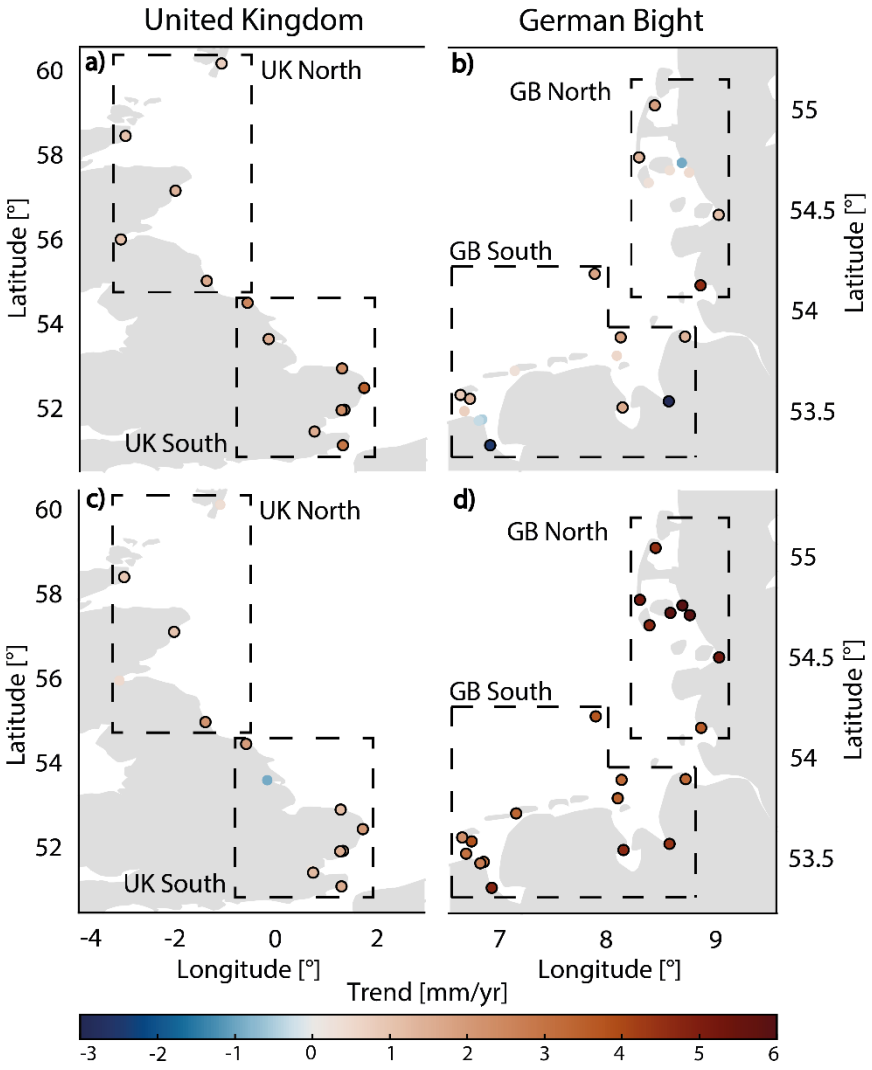

Figure 28: Linear Trends of tidal low water (a, b) and tidal high water (c, d) between 1958 and 2014 in the UK and the German Bight, including the area classifications used in this study (significant trends outlined).

The larger tidal low water trends in the UK reveal a median of 1.6 mm/yr, compared to only 0.8 mm/yr in the German Bight (Figure 28-a/b). The tide gauges of the European West Coast show a median trend of 1.3 mm/yr, matching the in-between character of this area. While no spatial variations are detectable in the German Bight with a median of 0.8 mm/yr both in the southern as well as the northern part, a distinct north-south divergence can be observed in the UK. The northern five stations from Lerwick (#1) to North Shields (#5) show a median trend of 1.2 mm/yr, the remaining stations from Whitby (#6) to

Dover (#14) depict a median trend of 2.4 mm/yr. It can be concluded that the overall trend of tidal low water in the UK and especially in UK South is larger than in the remaining study area. A contrary development can be observed for the tidal high water. The median trend in the UK is 1.3 mm/yr (UK North: 1.0 mm/yr, UK South 1.4 mm/yr) and 3.8 mm/yr in the German Bight (GB South: 3.3 mm/yr, GB North 5.2 mm/yr). On the European west coast, however, the median trend of tidal high water is 2.0 mm/yr, again matching the in-between character of this area.

Regarding the different developments of tidal low and high water within the regions, it must be noted that the different developments in tidal low and high water are distinct everywhere except in the north of the UK. While changes are also taking place here, they are rather small and almost identical. Thus, no significant change is to be expected for the tidal range. In contrast, the southern part of the UK exhibits the largest mean trend in tidal low water and the second lowest median trend in tidal high water. For the German Bight on the other hand, the median trends of tidal high water are remarkably high and the median tidal low water trends are very low.

In Figure 29, the trends of tidal high (red) and low (blue) water as well as their residuals are depicted at each station with the coloring indicating the larger trend.

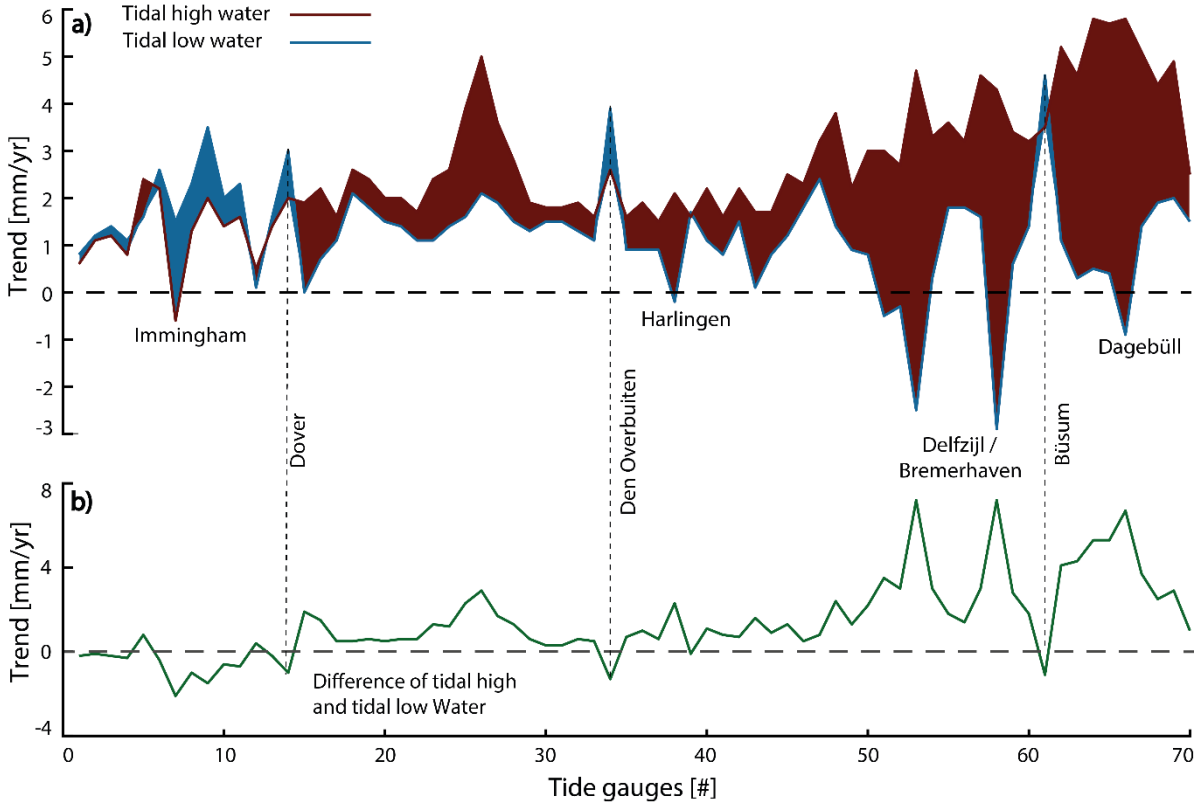

Figure 29: (a) Trends of tidal high (red) and low water (blue) at each station with the colored areas implying the larger trend. (b) Differences of trends; positive values indicate a larger trend in tidal high water, negative values indicate a larger trend in tidal low water.

It becomes evident, that at almost every UK tide gauge, the trends of tidal low water exceed the trends of tidal high water. This development is reversed on the continental side of the English Channel (after the tide gauge Dover), where the tidal high water tends to show larger trends. The only exceptions are

the two tide gauges Den Overbuiten (TLW = 3.9 ± 0.8 > THW = 2.7 ± 0.8 [mm/yr]) and Büsum (TLW = 4.6 ± 1.0 > THW = 3.6 ± 1.2 [mm/yr]), both subject to massive anthropogenic influences (Construction of Afsluitdijk and embankment of the Bay of Meldorf). In the UK, the tide gauge Immingham exhibits a (non-significant) negative trend in tidal high water (-0.9 ± 0.9 mm/yr), being the only tide gauge in the study area with a negative tidal high water trend. Negative trends in tidal low water occur at the tide gauges Harlingen (-0.2 ± 0.8), Delfzijl (-2.5 ± 0.9), Bremerhaven (-2.9 ± 1.0), and Dagebüll (-0.9 ± 1.4), from which only Delfzijl and Bremerhaven are statistically significant on the 95% confidence level.

Overall, the dipole-like spatial developments between the UK and the German Bight are identified again: the trends of tidal low water in the UK (especially in the south) are mostly larger than the trends in tidal high water, while the opposite is observable for most of the German Bight and to a smaller extend for European West Coast. The differences between the trends of tidal low and high water are rather small in the north of the UK and in parts of the Netherlands. A change between from larger trends in tidal low water to larger trends in tidal high water is evident along the continental coastline. Furthermore, it is important to note that small difference between these two tidal parameters does not imply that there have been no changes, but only that tidal low and high water are subject to similar trends. This again supports the approach of this thesis to investigate not only the tidal range, but also tidal low and high water. Nevertheless, different changes are of particular interest and the strong differences in the trends of tidal low and high water appear to be particularly pronounced in the south of the UK, in the eastern parts of the Dutch coast and in the German Bight, a development that should also be reflected in the tidal range.

6.2 Changes in tidal range

The parameter tidal range were calculated as the difference between each tidal high water and the mean of the two surrounding tidal low waters according to the German standard (DIN 4049-3, 1994). Based on this calculation method, tidal range can be regarded as the combination or the result of the developments in tidal low and high water. 60 of 70 tide gauges depict a significant trend between 1958 and 2014. As already indicated by the similar development of tidal low and high water, only 2 out of 5 tide gauges show significant trends in the north of the UK and their statistical difference from zero is rather small with -0.4 ± 0.3 mm/yr in Lerwick (#1) and 0.8 ± 0.5 mm/yr in North Shields (#5). In the south of the UK, however, 7 of 9 trends are significant. The remaining neutral trends are mostly distributed along the European West Coast, underlining the transitional character of this area between UK and German Bight with 5 neutral trends between Cadzand (#17) and Roompot-buiten (#21).

Overall, a variety of trends with a particularly pronounced spread in the southern parts of the basin can be identified (Figure 30). Immingham (#7) in the south of the UK shows the largest negative, statistically significant trend (-2.3 ± 0.5 mm/yr) of all sites, while the smallest significant negative trend of -0.7 ± 0.3 mm/yr is found in Felixstowe (#10). In contrast, trends turn positive on the continental side of the

English Channel and the European West Coast. The assessment reveal increasing trends following the coastlines of France (1.3 ± 0.4 mm/yr at Dunkerque (#16)), Belgium, and the western Netherlands up to the tide gauge at Huibertgat (0.8 ± 0.2 mm/yr, #47), near to the German-Dutch border. Maximum trends of 7.3 ± 0.5 mm/yr are reached in Bremerhaven (#58) in the south and 6.8 ± 0.3 mm/yr in Dagebüll (#66) in the north of the German Bight.

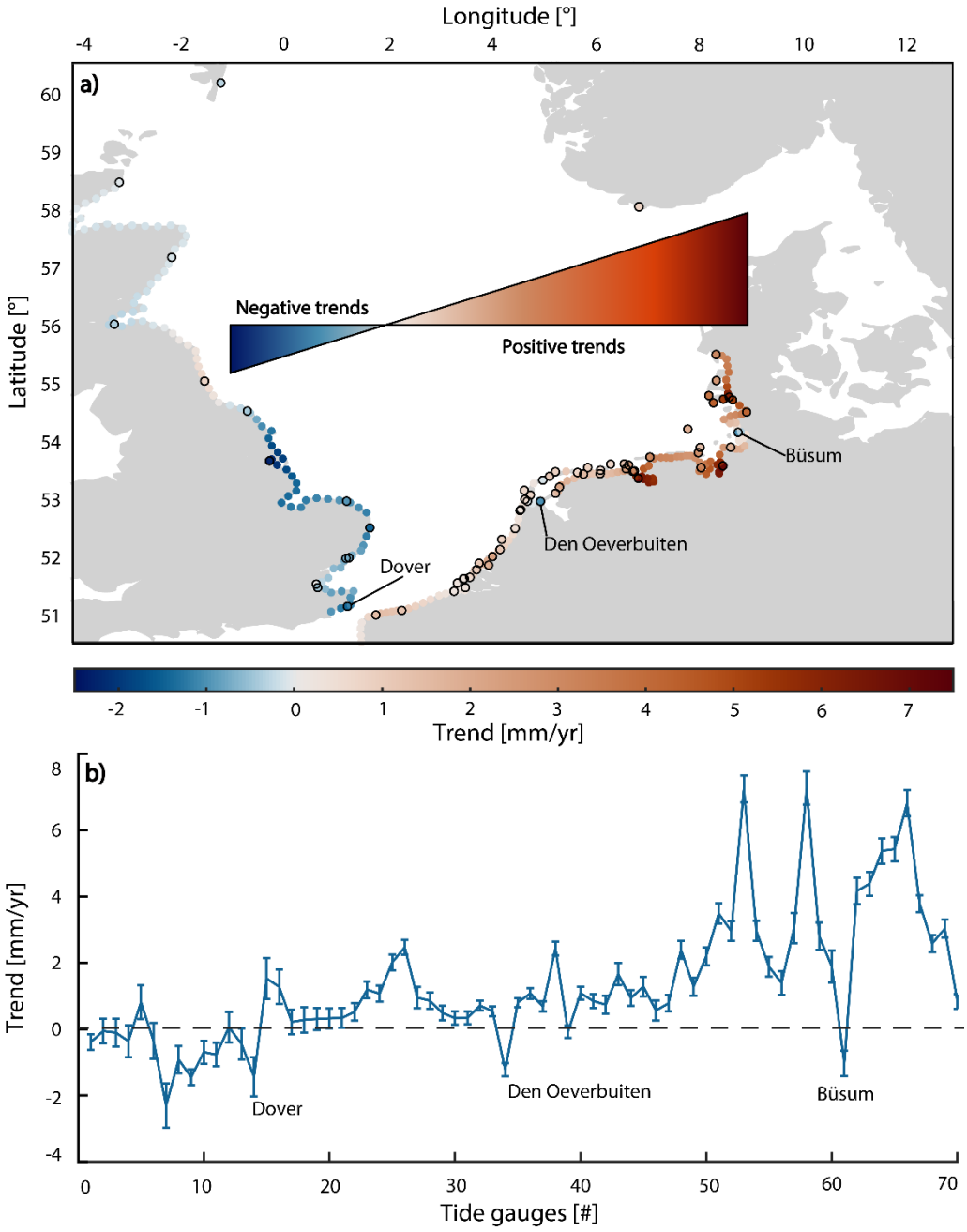

Figure 30: Linear Trends of tidal range between 1958 and 2014: (a) mapped spatially for the study area (measured values outlined, markers without edges were added by Kriging) and (b) with individual 95% confidence interval.

This development is also reflected in the median trends. While the median trend of tidal range is negative in the entire UK (-0.4 mm/yr) with -0.1 mm/yr in the north and -0.8 mm/yr in the south, a positive median trend of 0.8 mm/yr occur at the European West Coast. Hereafter, sharp trend increases are found

within a short distance, reaching values of 2.8 mm/yr in the south and 4.3 mm/yr in the north of the German Bight (3.0 mm/yr). Local changes affect some tide gauges like Den Oeverbuiten (-1.2 ± 0.4 mm/yr, #34) or Büsum (-1.0 ± 0.7 mm/yr, #61), which at first sight seem to contradict this spatial pattern. It can be suggested (e.g. Ebener et al., 2020, see also Figure 14) that these local exceptions are mainly caused by anthropogenic interventions such as the building of the Afsluitdijk at Den Oeverbuiten or dredging and dike constructions near to Büsum, which coincide with anomalies in the local tidal range series.

6.3 Changes in major tidal constituents and amphidromic areas

As described in Chapter 2.1, the decomposition of the observed tides into its individual tidal constituents is a harmonic procedure where amplitude and phase are obtained as results. Due to the harmonic nature of the process, the amplitude oscillates homogenously around its average and is rather comparable to the tidal range than to tidal low or high water. A large part of the non-tidal residual is no longer included here (Chapter 3.3), and the behavior corresponds more to astronomical forcing, as can also be shown, for example, by the detection of the nodal cycle (Chapter 4.5.2). In addition, there is a close relationship between changes in tidal range and altered location of the amphidromic areas (see Chapter 2.2), analogous to the tidal constituents and the amphidromic points. A calculation of the tidal constituents in addition to the tidal range offers the advantage that the obtained results can be compared with current numerical studies as well as with theoretical approaches to the change of amphidromic points.

The identified dipole-like trend pattern most evident in tidal range has its node approximately at the longitude of the English Channel (Figure 30) and suggests a westward displacement of the main low amplitude areas (including amphidromic points of M_2 and S_2) located in the central North Sea and near the English Channel (Figure 12). To obtain further indications of such a shift, a harmonic analysis to determine the dominant semi-diurnal M_2 and S_2 tidal constituents was performed, which make the largest contributions to the tides in the North Sea. Since high-resolution hourly time series with a coverage of at least 75% between 1958 and 2014 are required for a tidal analysis (Codiga, 2011), only a subset of 28 tide gauge records is appropriate for the assessment. The available database is thus reduced and fewer stations show significant trends (20 for M_2, 14 for S_2). Nevertheless, the overall finding (Figure 31) are similar to the assessment focusing on tidal ranges highlighted in Figure 30; that is for both constituents (though with larger magnitude for M_2), negative trends occur in the southeast of the UK and the highest positive trends are found in the German Bight area. A westward displacement of the M_2 and S_2 amphidromic point is, therefore, also implicated. This can also be derived theoretically on the basis of Chapter 2.2. The observed changes in the tidal range can be considered in the context of the elaborations of Taylor (1922) on amphidromic systems. Based on simple analytical solutions, Taylor demonstrated an altered propagation speed due to increased water depth, leading to a shift of the amphidromic point towards the open boundary in a semi-enclosed basin. As a result, the tidal range at the opposite (dissipative) end of the basin increases. In that case, this statement implies a shift of the amphidromic points

towards the north, seemingly contradicting the changes (i.e. an east-west shift) observed here. However, as pointed out in Haigh et al. (2020), increasing the tidal range and thus the tidal currents at the dissipative end could lead to a higher frictional energy loss. This would cause a leftward deflection of the tidal wave and the amphidromic point, see Figure 5 in Haigh et al. (2020). For the North Sea, MSL rise and an increased frictional dissipation would ultimately shift the amphidromic point towards the west, reducing the tidal range on the left side of Figure 30 (the east coast of the UK) and increasing the tidal range on the right side of the basin (the German Bight).

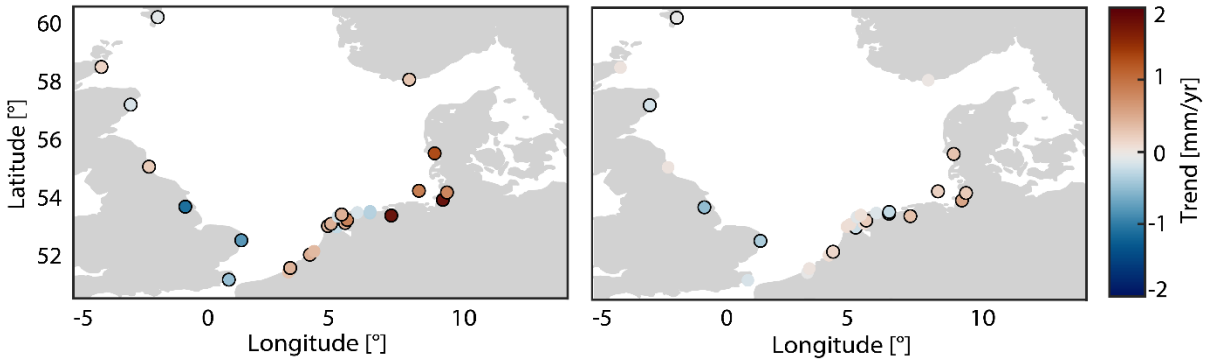

Figure 31: (a) Linear trends of the M_2 and (b) S_2 tidal constituents between 1958 and 2014 (significant trends outlined).

This argumentation is supported by several numerical modelling efforts (Pickering et al., 2012; Idier et al., 2017; Schindelegger et al., 2018), in which the impact of large (0–10 m) MSL increases on leading constituents (mainly M_2) were investigated. Complementary to this empirical assessment, they all detected (at least qualitatively) similar patterns as shown in Figure 30 and Figure 31. However, closer examination also reveals some discrepancies and the model results do not correspond exactly to the measured data. For instance, both Pickering et al. (2012) and Schindelegger et al. (2018) predict an increase in M_2 amplitude in the southwestern part of the North Sea, between Suffolk/Essex and the Netherlands, while here negative trends in Suffolk/Essex and positive trends in the Netherlands are detected. In-depth studies of the influence of sea level rise on European Shelf tides (Pelling and Green, 2014; Idier et al., 2017) point to sensitivities of the tidal response to the magnitude of sea level rise and whether or not low-lying land is inundated in the numerical simulation (flooding or no-flooding). In addition to these two extreme cases of shoreline treatment, Pelling and Green (2014) investigated the M_2 response to partial flooding, roughly based on the actually existing protective structures. This last option provides the greatest agreement with the results presented here, but again does not reflect the negative trends in the South UK. In fact, the tide around Suffolk/Essex exhibits little sensitivity to the shoreline scenario (Idier et al., 2017). More to the point, the assumption of no-flooding seems to be plausible in the areas of the greatest changes (German Bight and the northern parts of the Netherlands) and here the results agree with all existing modelling studies. No final assessment can thus be made here as to whether and which models are most consistent with the observations. In this context, effects may be involved that are not included in numerical models so far. As Arns et al. (2015a) pointed out, various nonlinear relationships between the individual parameters in marginal seas are of particular importance,

especially the dynamic response of the sea surface to meteorological forcing (see also Arns et al., 2020). In addition, time-varying bed roughness and bottom friction coefficients (Rasquin et al., 2020) and changes in turbulent dissipation with stratification (Müller, 2012) may play a role. Possible causes for these changes are discussed in detail in Chapter 8. Overall, it becomes evident that the detected changes in the tidal range indicate a change in amphidromic areas, which would fit the theoretical considerations of an increase in MSL. This provides further evidence for increases in MSL as a possible cause for the change in tidal parameters.

6.4 Answer to the first research question

As defined in the Introduction of this thesis, the first research question is: *Are the changes in tidal low water, tidal high water and the tidal range on different time scales detected within the German Bight a localized phenomenon, or are they part of a larger-scale development spreading over larger areas within the North Sea region?*

Based on the analyses conducted in the above chapter, this question can now be answered. The linear trends of the tidal parameters (tidal low water, tidal high water, and tidal range) depict significant changes between 1958 and 2014 in large part of the study area, as shown in Figure 27 and Figure 30. Over the entire study area, median tidal high water trends are larger (2.2 mm/yr) than median tidal low water trends (1.4 mm/yr), but varying regionally coherent patterns exist (Table 6). To describe these regional patterns, the study area is divided into the regions UK, European West Coast and German Bight. In total, 57 of the 70 tide gauges show a significant trend in tidal low water and 66 of 70 in tidal high water. The neutral trends of tidal high water are located entirely in the UK, while the German Bight is highly overrepresented in the neutral trends of tidal low water. This is also reflected in the median trends of the regions. While the increase in tidal low water (1.6 mm/yr) is larger than the increase in tidal high water (1.3 mm/yr) in the UK, the tidal high water trends exceed the trends of the tidal low water in the rest of the study area. On the European West Coast and in the area of the German Bight, only small trends of tidal low water (0.8 mm/yr) are detectable, while the trends of tidal high water rise almost constantly to over 2.0 mm/yr or even 5.2 mm/yr in the north of the German Bight. In summary, there is a clear contrast between the trends in the UK and the German Bight area, both for tidal low and high water. While the trends in tidal low water are larger in the UK area, the trends in tidal high water are much more distinct in the German Bight, forming a kind of a dipole. This development is also reflected in the tidal range. While in the north of the UK the median tidal range is almost constant, in the south of the UK clearly negative trends are detectable (-0.8 mm/yr). In contrast, following the coastline of the European West Coast, median trends are rising from 0.8 up to 4.3 mm/yr in the northern parts of the German Bight. A dipole-like behavior of the trends is thus also evident here.

Apart from the trend analysis itself, it is important to note that the detected spatial patterns for all tidal parameters are still consistent when checked for instrument errors according to Woodworth (2010) and Mawdsley et al. (2015), as described in more detail in Chapter 2.4. Since some of the detected patterns

are homogenous across the borders of different countries and tide gauges authorities (e.g. Germany - Netherlands for tidal high water), while others being inhomogeneous within the same country (e.g. UK for tidal range), it is certain that the detected changes are not caused by measurement errors at least for the largest part.

In summary and with reference to the first research question, it can be stated that in all investigated tidal parameters predominantly significant trends occur at most of the tide gauges of the study area, making changes of tidal parameters a basin-wide phenomenon. Nevertheless, there is no homogeneous or uniform pattern across the entire North Sea Region, but significant regional patterns exist, resulting in opposing developments between the UK and the German Bight. The changes first described in Jensen (1984) and Führböter & Jensen (1985) for the tide gauges of the German Bight occur in reduced intensity also throughout the European West Coast, while in the UK contrary trends appear. With few exceptions, changes in tidal low and high water do not develop in a comparable manner, resulting in a changing tidal range and making regional coherent differences apparent.

7 Separation of large- and small-scale tidal changes

As described in the previous chapter, the results of the linear trend analysis point towards distinct, regionally coherent, spatial patterns, occasionally interrupted by diverging trends at individual locations: The rise in tidal high water exceeds the rise in tidal low water outside the UK at almost every tide gauge, resulting in an increase in tidal range. In parts of the UK on the other hand, the increase in tidal low water is significantly larger than in tidal high water, reducing tidal range. Evidently, several large-scale (and small-scale) patterns exist and therefore the second research question will be discussed in this chapter. It was defined as: *Is it possible to separate and quantify large-scale and small-scale effects from observed records?*

In order to further distinguish between the large- and small-scale effects of the observed tidal changes - comprising both long-term trends and short-term variability - PCA is applied to the time series of tidal low water, tidal high water and tidal range. While Chapter 7.1 focuses on the identification of large-scale signals based on the explained variance, Chapter 7.2 examines the resulting long-term trends as well as the short-term variability in the context of quantification. If there are indeed verifiable large-scale signals affecting the tidal parameters, they will appear as a coherent pattern at multiple sites, and will be visible in the leading PCs. By contrast, spatially confined (small-scale) anomalies will be shifted into the higher PCs, as these can only be responsible for a small part of the overall variance.

7.1 Identification of large- and small-scale tidal changes

Figure 32-a/b shows the results of PCA for tidal low and high water. The first intriguing observation is the high oscillation of PC1 for both tidal parameters, resulting in a variance of 7921 and 7744. The variance in PC2 is only about 454 in tidal low and 380 in tidal high water. Since these values are devoid of units and difficult to assess, it should be noted for context that the corresponding values of the tidal range are only 1541 (PC1) and 380 (PC2). In fact, the high differences in variance between PCs of tidal low and high water compared to the tidal range confirm the considerations from Chapter 3.3, according to which both meteorological influences as well as possibly remaining seasonal variations are eliminated (at least to a large extend) by calculating the tidal range. Consequently, these effects can no longer be included in the tidal range PCs. That said, the physical processes sought here may also be affected and the necessity for a comparable analysis of all three tidal parameters becomes evident again, even though the tidal range is a derived quantity from tidal low and high water. The consistently higher variance in PC1 is caused the computing procedure, as PCA always transfers as much of the overall variance as possible to the first principal component. Local anomalies or measurement errors can be excluded as major influences on PC1 and PC2, since these would not be depicted in the first PCs. Therefore, a comparison between the PC1 of the tidal parameters is the most informative in this context.

The first two PCs of tidal low water explain about 89% of the total variance in the entire data set (PC1: 84%, PC2: 5%), while each of the remaining 68 PCs only holds contributions of 0.001–2%, supporting

the assumption of systemic large-scale effects such as a MSL rise. This makes PC1 and to a smaller extent PC2 dominant for describing the variance of the tidal low water. A similar pattern can be detected in tidal high water. The first two PCs explain about 89% of the total variance in the entire data set (PC1: 85%, PC2: 4%), while each of the remaining 68 PCs accounts for 0.001–2% of the overall variance.

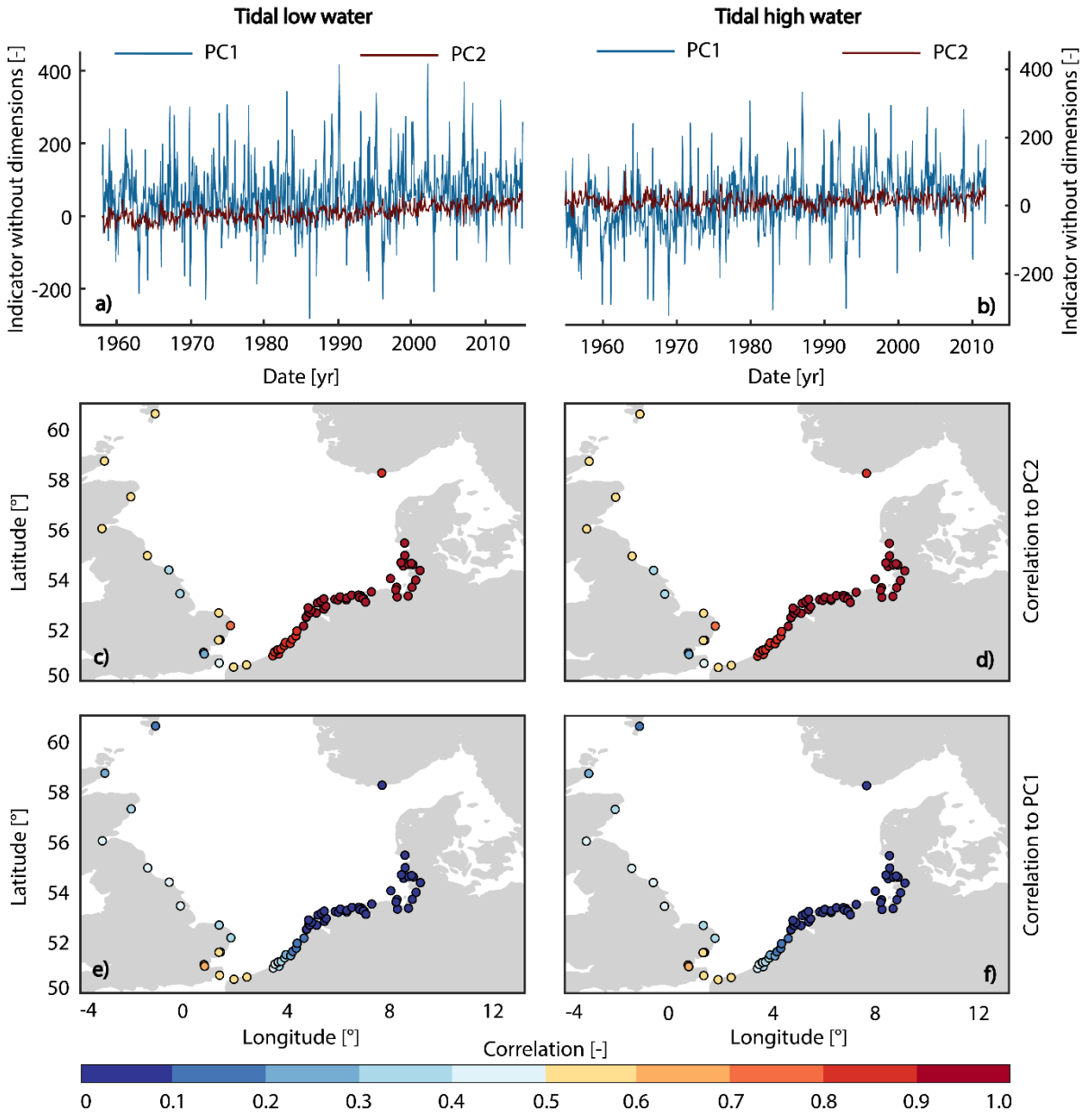

Figure 32: Results of the PCA for tidal low (left side) and high water (right side). Shown are PC1 and PC2 (a, b) with their spatial patterns in terms of correlation between PC1 (c, d) and PC2 (e, f) with tidal low and high water for each tide gauge.

Since the contribution of the overall explained variance depends to some extent on the spatial distribution of the tide gauges, it is necessary to consider the PCA results at each tide gauge individually in order to detect spatial patterns. In Figure 32 c) to f), the correlations between the first PCs and the time series of the tidal low and high water are shown. This two representations are well suited to determine in which spatial areas the detected large-scale signals have their greatest impact. A distinct, dipole spatial

pattern between the UK and the German Bight is detected for both tidal parameters, similar to the results of the trend calculation. While for PC1 correlations are above 0.9 on large parts of the European West Coast and the German Bight, lower but still significant values between 0.4 and 0.7 are reached in the UK. PC2 is more dominant in this area, but with lower correlations and almost no significant correlation in the rest of the study area. These spatial distributions suggest that the leading PC1 reflects a coherent large-scale effect in the entire North Sea Basin, which impact is considerably larger on the European West Coast and especially on the German Bight, compared to the UK. The almost identical spatial patterns of PC1 in tidal low and high water as well as their positive trends described in Chapter 6.1 indicate a common cause of the occurring changes. PC2, on the other hand, is only relevant in the UK, which can be explained either by a separate causal physical effect or by a varying system response to the same large-scale impact.

For the tidal range, the first two PCs presented in Figure 33 explain about 69% of the total variance in the entire data set (PC1: 55%, PC2: 14%), while each of the remaining 68 PCs contributes between 0.01% and 4%. Additionally, only PC1 and PC2 represent significant parts of the variance at a larger number of tide gauges and are the only PCs not local in character. For example, PC3 does explain about 4% of the total variance, but this is largely attributable to only two tide gauges and thus a purely local effect (Cuxhaven (#60) and Büsum (#61)). Figure 33-c show moderate but significant correlations of 0.3–0.5 for PC1 at the south-western boundary of the North Sea and displays the highest values (~0.9) in the area of the German Bight. A contrasting picture emerges again for PC2. In the area of the German Bight, correlations with tidal range changes are non-significant and close to zero but almost consistently above 0.7 and significant in the UK (Figure 33-d). This spatial distribution of correlations again suggests two coherent large-scale effects, reflected in the two leading PCs, while local effects are retained in the lower PCs. Like discussed above, the variance here is substantially lower than in the other two tidal parameters with 1541 (PC1) and 380 (PC2). Due to the significantly higher share in the total variance of PC2 as well as an even more pronounced split between the UK and the German Bight, a consideration of the coefficients is useful here. PC1 describes an increase in tidal range over time, as evident from its positive slope and the consistently positive values of the associated coefficients at all sites (Figure 33-b). The magnitudes of the coefficients reveal that the PC1 signal increases as one travels counter-clockwise throughout the basin reaching its strongest expression in the German Bight. PC2 exhibits a negative trend and is most pronounced in the area of the southeastern coast of the UK. The coefficients of PC2 change sign from positive values along the UK coast to negative values in the area of the German Bight (Figure 33-b). Similar to the trends of measured tidal range (Figure 30), a dipole-like temporal evolution with a node in the area of the English Channel is detected. In general, PC1 accounts for the increase in tidal range in the German Bight and PC2 represents the decrease in tidal range at the south-eastern coast of the UK.

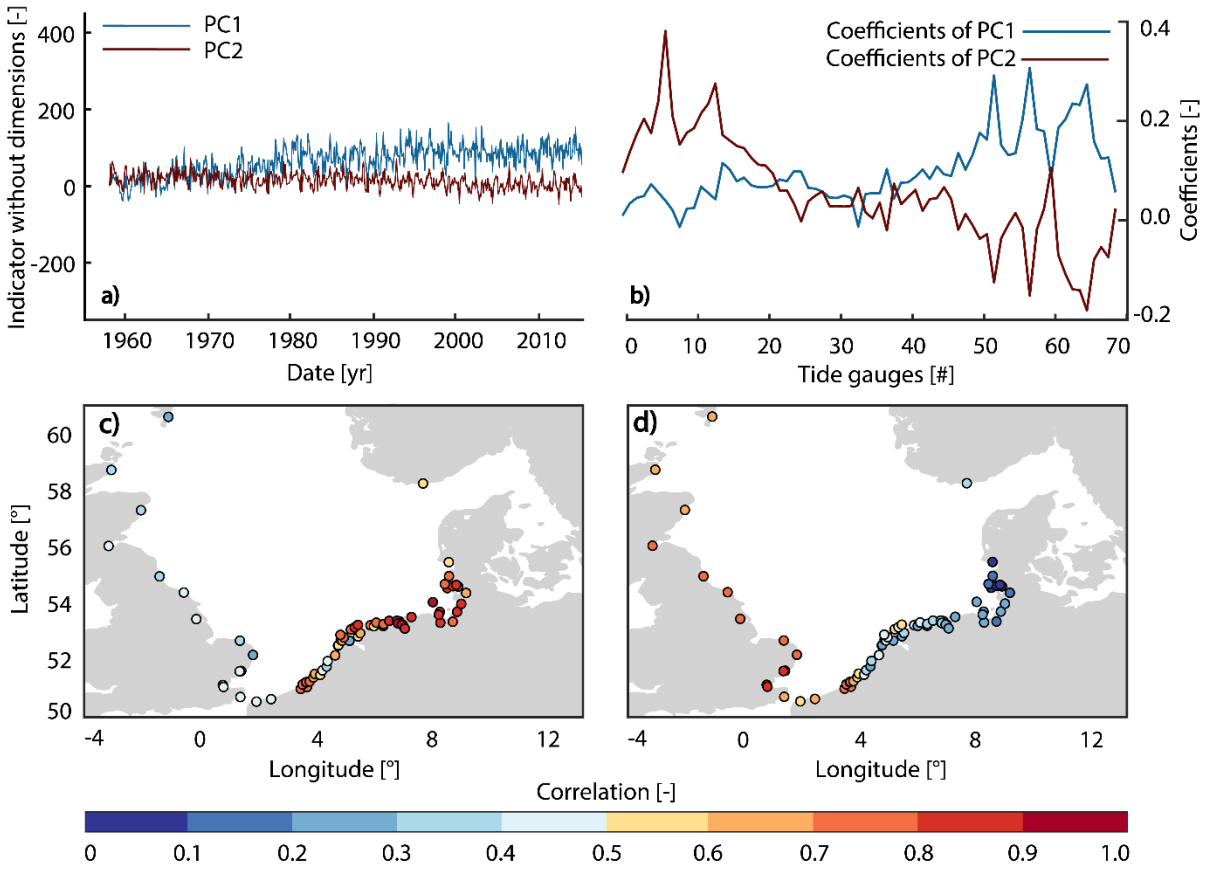

Figure 33: Results of the PCA for tidal range. Shown are time series of PC1 and PC2 (a) and their spatial patterns (b). Panels (c) and (d) map the correlations between observations and PC1 (c) and PC2 (d).

In addition to the identification of the signals via PCA, it is necessary to compare the relationship of the identified, leading PCs to each other. This serves not only to verify the process, since by definition there must be no correlation between the individual PC1 of a tidal component, but it also can be used to detect indications of common physical causes. For this purpose, the correlations of the leading PCs to each other are investigated (Table 7).

Table 7: Correlation between PC1s of tidal parameters (excluding trends / including trends).

PC1 of	Tidal low water	Tidal high water	Tidal range
Tidal low water	1.00 / 1.00	0.92 / 0.94	-0.17 / -0.36
Tidal high water	0.92 / 0.94	1.00 / 1.00	0.22 / 0.00
Tidal range	-0.17 / -0.36	0.22 / 0.00	1.00 / 1.00

Since in tidal low and high water PC1 is largely dominant in the overall variance, this comparison is limited to PC1. In accordance with the principles of PCA, there are no significant correlations between the PCs of a single tidal parameter. While the correlations of PC1 for tidal low and high water to the PC1 of tidal range are rather low, ranging from -0.36 to 0.22, both including and excluding trends, the correlation between PC1s of tidal low and high water is exceptionally high. It reaches values of 0.92

including trends and 0.94 excluding trends. In addition to the previous considerations, this again indicates a common, large-scale cause of the changes in tidal low and tidal high water in the entire study area. A further indication here is the lack of high correlations between PC1 of the tidal range and the other two tidal parameters, since a common large-scale signal of tidal low and high water would be equalized by the formation of differences in the calculation of the tidal range. Thus, this suggests at least two large-scale effects, with one being visible in tidal low and high water similarly, and another one becoming visible the tidal range. If including the more pronounced differences between the UK and the rest of the study area in the first two PCs of the tidal range, at least three different large-scale effects become assumable.

In a final step, the extent to which the identified signals depend on the data basis is examined. The purpose is to verify whether basin-wide signals can actually be identified independently in each subarea (UK, European West Coast, and German Bight). The PCA is therefore repeated based on these three subareas for all tidal parameters and the leading, large-scale PCs are compared between the two data sets. Explained variance is used here as a measure of agreement between PCs. If the detected PCs represent indeed basin-wide signals, the dominant PCs would also have to be detectable in each subarea as well.

Since PC1 of the complete data set is dominant in tidal low and high water on the European West Coast and in the German Bight (Figure 32), it must also be reproducible based on these two subareas. PC2 of the complete data set has a very small impact in these areas, so no agreement is to be expected here. In the UK, both PCs should be detectable since PC1 and PC2 exert an influence of approximately the same magnitude. Therefore, the individual agreement of each PC has to be smaller. For the tidal range on the other hand, the agreement of PC1s must be large in the German Bight and small in the UK, since PC1 is mainly dominant in the German Bight (dipole). Accordingly, the opposite is true for PC2. The agreement of the European West Coast as transition area must be in between the values of the German Bight and the UK. However, since significantly more tide gauges are located in the impact zone of PC1 than PC2 (Figure 33), the agreement should be closer to the values of the German Bight. The results are shown in Table 8 and are exemplified by PC1 of the tidal high water in Figure 34.

Table 8: Agreement among PC1 and PC2 of all three tidal parameters from the complete data set with PC1 and PC2 from a regional subarea of the complete data set

Agreement in PC1 / PC2 based on the regional subarea	Tidal low water [%]	Tidal high water [%]	Tidal range [%]
United Kingdom	43 / 42	45 / 40	16 / 79
European West Coast	96 / 2	96 / 2	79 / 13
German Bight	98 / 1	98 / 1	93 / 3

It is evident that the results are as expected and thus not distorted by the selected tide gauges. PC1 of all three tidal parameters can be replicated by 98% from the German Bight data, while no significant agreements exist for PC2. At the European west coast, approximately the same applies to PC1 and PC2 of tidal low and high water, while the tidal range indicates the dipole of the study area. This inversion between PC1 and PC2 is completed in the tidal range of the UK with agreements of only 16% for PC1 and 79% for PC2. Values for tidal low and high water are nearly identical, reflecting the similar influence of PC1 and PC2 in the UK. Figure 34 illustrates this using PC1 of the tidal high water. It is evident that only PC1 of the UK (red) differs visibly from the other PCs, since PC1 is less dominant here. The agreement to the overall PC1 of tidal high water amounts to 45% (Table 8). The agreement between the overall PC1 and the European West Coast is 96% and 98 % for the German Bight.

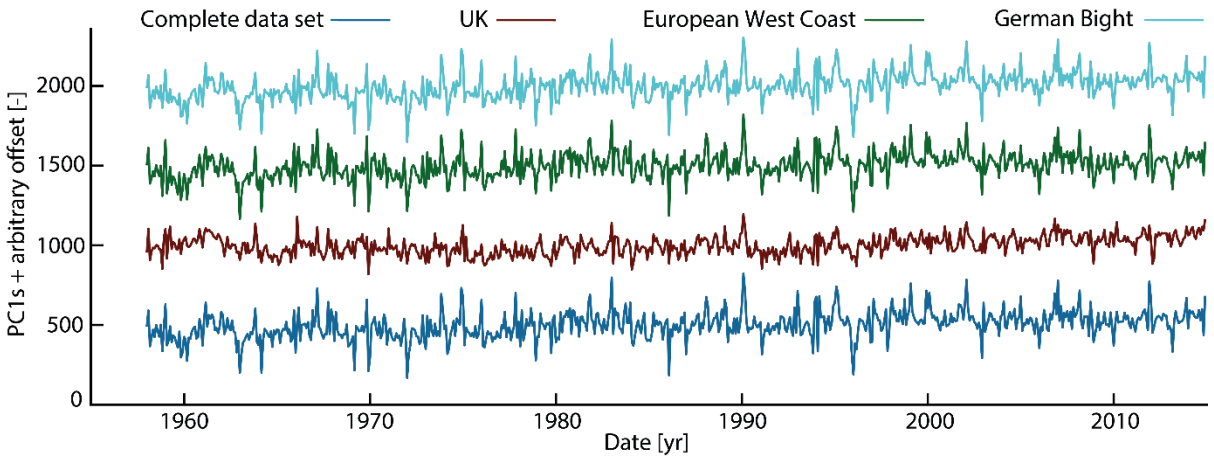

Figure 34: Tidal high water PC1s based exclusively on the tide gauges of the UK (red), European West Coast (green), German Bight (cyan), and the complete data set (blue) for comparison.

7.2 Quantification of large- and small-scale tidal changes

The detected spatial patterns of PC1s and PC2s impacts are also confirmed when considering the explained variance for particular clusters of tide gauges the in context of quantification (Figure 35). An assessment of the variance explained by PC1 and PC2 at each individual tide gauge reveals distinct spatial patterns and allows for the calculation of the percentages at a regional level.

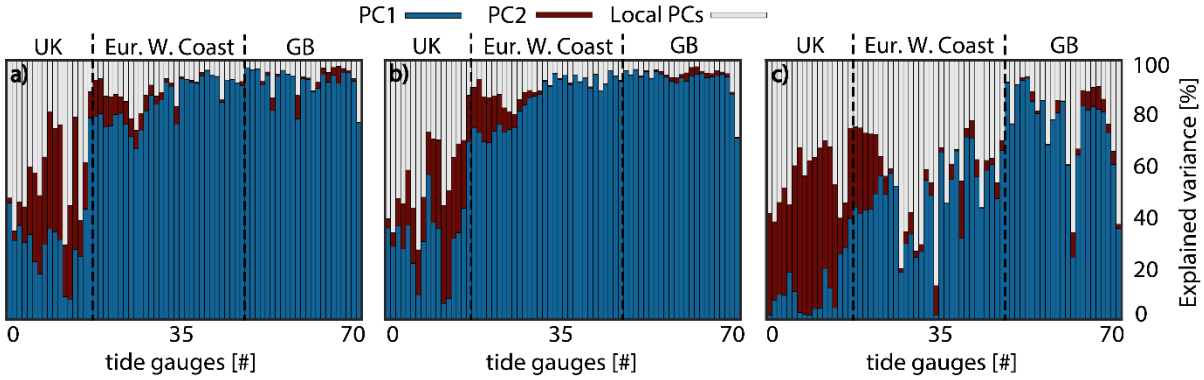

Figure 35: Tide gauge specific partitioning of the explained variance of PC1, PC2, and the local PCs for tidal low (a) and high water (b) and tidal range (c).

It becomes evident that PC1 and PC2 explain only a moderate proportion of the variance in the UK, adding up to just 55% (Table 9) for tidal low water. Conversely, this implies that 45% of the variance is controlled by local effects here. On the European West Coast, this value decreases to 14% and is only 6% throughout the German Bight with PC1 explaining over 92% of the variance. It can be concluded, that locally limited effects on small scales seem to have a much higher impact in the UK than in the German Bight and the European West Coast, areas which are strongly dominated by PC1. Simultaneously, PC2 explains less than 5% of tidal low water variance in these areas. In the UK, however, 28% of the variance can be explained by PC2, with a clear difference between the North (11%) and the South (38%). Overall, this results in a most evident contrast between the UK, where only about 55% of the tidal low water variability can be explained by large-scale effects of PC1 and PC2, and the German Bight, where 94% of the variability can be explained by large-scale effects, primarily PC1.

For tidal high water, values of 28% (PC1) and 22% (PC2) in the UK and of 94% (PC1) and 2% (PC2) in the German Bight are detected. Overall, 50% of the variability in tidal high water is dominated by local effects in the UK and only 4% in the German Bight. Again, the magnitudes of PC1 and PC2 are comparable in the UK, whereas PC1 is dominant in the German Bight and the European West Coast (PC1 82%; PC2 6%). When interpreting these results with respect to the apparently high contribution of local effects in the UK, it must be noted that the data basis (see Chapter 3.2) is poorest in the UK. Both the density of tide gauges and their completeness are significantly lower than on the European West Coast or the German Bight. While this does not affect the principle existence and detectability of large-scale effects, it may reduce their quantitative impact on the total variance.

Along southeastern UK coastlines, where negative trends were found, the explained variance of tidal range's PC1 amounts to only 7%, while PC2 explains about 55%. On the European West Coast, the mean explained variance for PC1 is 45% and only 10% for PC2. The contribution of the second mode drops to 3% in the German Bight, whereas PC1 explains 78% of the variance on average. Overall, the impact of PC2 is much more dominant on tidal range than on the other two tidal parameters in the UK.

Table 9: Explained variance in tidal low water, tidal high water and tidal range.

Region	Explained variance tidal low water [%]			Explained variance tidal high water [%]			Explained variance tidal range [%]		
	PC1	PC2	Local PCs	PC1	PC2	Local PCs	PC1	PC2	Local PCs
United Kingdom	27	28	45	28	22	50	8	48	44
UK North	35	11	54	33	11	56	10	35	55
UK South	23	38	39	26	28	46	7	55	38
Euro. W. Coast	81	5	14	82	6	12	45	10	45
German Bight	92	2	6	94	2	4	78	3	19
GB South	92	2	6	94	2	4	82	1	17
GB North	92	3	5	94	3	3	71	6	23

After having quantified the extracted signals in terms of short-term variability and explained variance, the resulting reconstructions including their trends will be analyzed now. In addition to quantifying the influence of the large-scales effects, a comparison to the measured trends is also made here in order to re-check the methodology (see Chapter 4.2). The following analyses are similar to the analysis of PCs, but here only the trends are considered. In contrast to the dimensionless PCs, a true to scale comparison to measured values is then possible. In order to separate the influences of large-scale and small-scale effects, the reconstruction of each tidal parameter is calculated collectively from leading components PC1 and PC2. The result is the reconstruction of the tidal parameter excluding local effects, making it possible to derive the influence of large-scale effects on the linear trends. If an overlap of these two trends can be detected taking into account their confidence intervals, the large-scale influence can be classified as dominant. This classification is a chosen threshold and seems to be reasonable due to its mathematical objective calculability.

In Figure 36 (left), the trends of the large-scale reconstruction of all three tidal parameters are compared to the trends of the measured values. On the right side of the figure, the spatial development of the reconstructed trends can be found.In the reconstruction of the tidal low water, there is no overlap detectable for 6 tide gauges and strong local influence can therefore be assumed. These tide gauges are Southend (#12), Calais (#15), Dunkerque (#16), Delfzijl (#53), Bremerhaven (#58), and Büsum (#61), whereas with Büsum, Bremerhaven, and Delfzijl a strong anthropogenic influence by building measures is already well-known (Ebener et al., 2020). In contrast, only the two tide gauges Immingham (#7) and

Hoek van Holland (#25) are not reproduced within their significance intervals in tidal high water. Despite the fact that a slight overestimation of the measured values throughout the European West Coast can be detected the tidal high water, a significant agreement is given at 68 out of 70 stations in contrast to the tidal low water with only 64 out of 70 stations. The RMSE between the reconstructed trends and the measured trends for tidal low and high water is very similar with 0.75 mm/yr and 0.78 mm/yr, reconfirming that the underlying physical effect could be identical for both. The overall mean values of the reconstructions are 1.6 mm/yr for the tidal low water and 2.7 mm/yr for the tidal high water, implying in combination with the nearly identical RMSE and the different number of significant agreements a lower influence of local effects on the tidal high water on average. This confirms once more the higher sensitivity of the tidal low waters to local conditions as explained in Chapter 3.3.

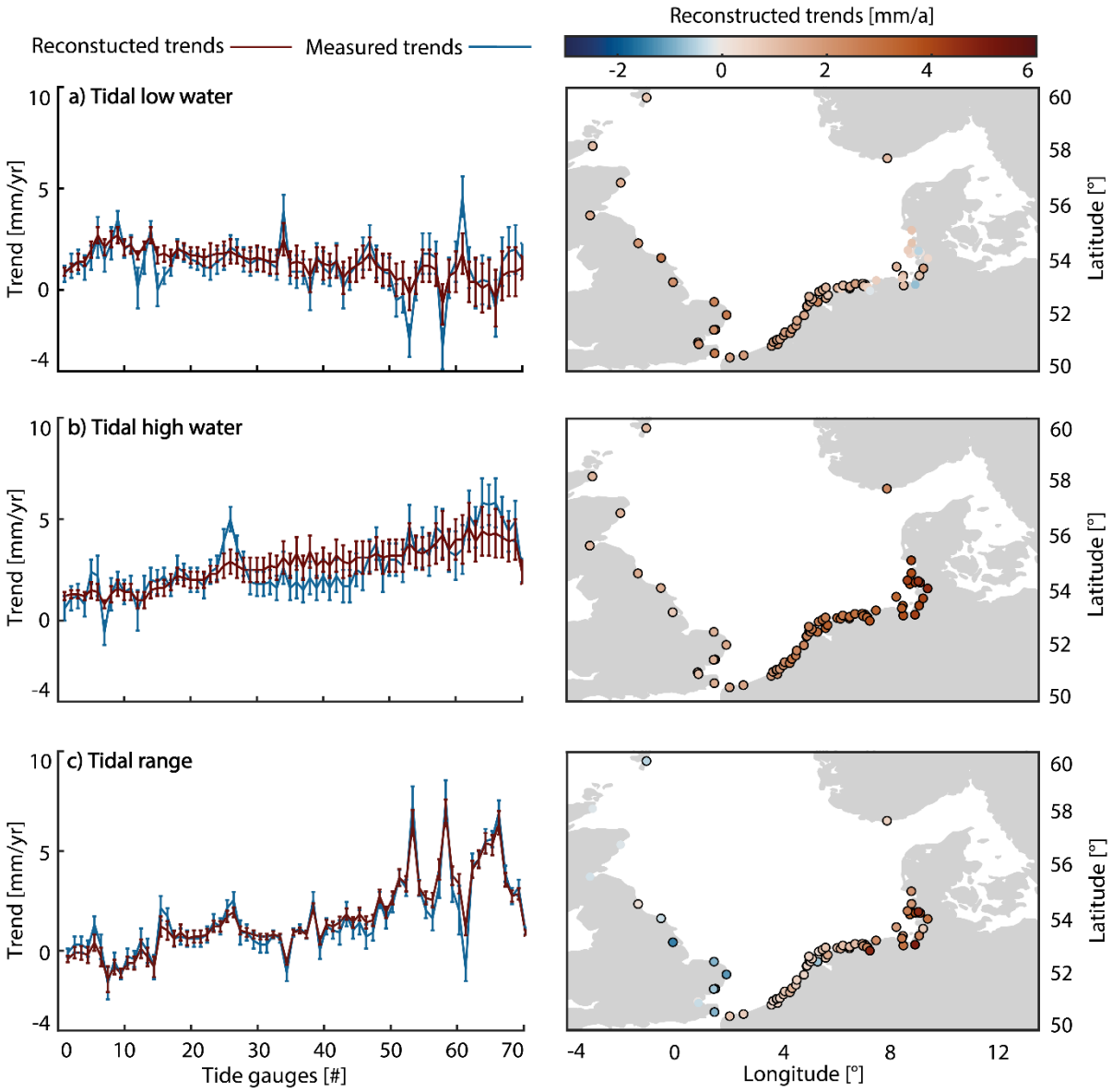

Figure 36: Linear trends in tidal low water (a), tidal high water (b) and tidal range (c) with 95% significance intervals from measurements (blue) and reconstructions (red) based on PC1 and PC2 on the left side and spatial distribution of the linear trends from reconstructions (significant trends outlined) on the right side.

When considering the developments in the different regions (UK, European West Coast, German Bight) of the study area (Table 10, Figure 36 right), a distinct picture emerges for the tidal low water in which all significant trends are positive and non-significant trends occurring mostly in the German Bight. This is essentially in line with the findings for trends of measured data in Chapter 6.1. The same consistency can be found for the tidal high water, since the trends here are much more distinct and there are only two non-significant trends. For the tidal low water, the measured median trend in the German Bight is 0.8 mm/yr and the reconstructed median trend is 0.9 mm/yr, resulting in an overestimation of 0.1 mm/yr. The absolute differences are higher in the northern German Bight with an underestimation of 0.4 mm/yr than in the southern German Bight with an overestimation of 0.1 mm/yr. In the UK, the median trends differ in the north by 0.2 mm/yr (overestimation) and in the south by 0.1 mm/yr (underestimation). On the European West Coast, the trends are overestimated with 0.2 mm/yr. In accordance with the measured trends, the reconstructed trends of tidal low water in the UK (2.0 mm/yr) are significantly higher than in the German Bight (0.9 mm/yr) with the European West Coast as a kind of transitional area (1.5 mm/yr). A comparable dipole-like pattern is found in the reconstructions of the tidal high water. In the southern German Bight there is only a slight overestimation of 0.1 mm/yr, while in the northern German Bight an underestimation of 1 mm/yr occurs. In the South of the UK, no deviation can be found and a minor overestimation results in the north of the UK (0.2 mm/yr). The overall trends are 1.3 mm/yr in the UK, which is below those of the European West Coast (2.6 mm/yr) and well below those of the German Bight (3.8 mm/yr). As a result, it can be stated, that after the exclusion of the local effects in tidal low and high water, the dipole-like overall picture remains and thus must be caused by a large-scale effect.

For the tidal range, the confidence bounds show even clearer overlaps for most cases. Exceptions to this are the tide gauges North Shields (#5) and Büsum (#61) with only small overlaps in Den Overbuiten (#34), Büsum, and Cuxhaven (#60), all of which are subject to substantial building measures (construction of the Afsluitdijk, Embankment of the Bay of Meldorf, anthropogenic expansion of the Lower Elbe, see Ebener et al., 2020). However, the general trends at most gauges can be qualitatively and quantitatively reproduced by PC1 and PC2. Figure 36-c (right) underlines this statement by a spatial map of the reconstructed trends, highlighting the dipole-like pattern between UK and German Bight sites. The RMSE between the reconstructed trends and the measured trends of the tidal range is smaller (0.49 mm/yr) compared to tidal low (0.75 mm/yr) and tidal high water (0.78 mm/yr), with the mean trend being only 1.6 mm/yr. The reduction of the RMSE by more than a third is a further indicator of the advantages of proportional equalization through differences analysis, eliminating systematic measurement errors and statistical white noise (see also Chapter 3.3). Comparing with the estimates in Chapter 6.2, the median trend of the reconstruction is -0.1 mm/yr in the North and -0.6 mm/yr in the South of the UK and thus corresponds approximately to the measured values (-0.1 mm/yr and -0.8 mm/yr). This is also the case for the European East Coast with a reconstructed median trend of 1.0 mm/yr compared to 0.8 mm/yr in the measured data. While in the northern German Bight the trends are identical,

the trend in the southern German Bight from the reconstruction is 3.3 mm/yr, overestimating the measured trend by 0.5 mm/yr (Table 10).

Table 10: Median linear trends in tidal low water, tidal high water, and tidal range (measured & reconstructed).

Region	Median linear trends of tidal low water [mm/yr]		Median linear trends of tidal high water [mm/yr]		Median linear trends of tidal range [mm/yr]	
	Measured	Recon.	Measured	Recon.	Measured	Recon.
United Kingdom	1.6	2.0	1.3	1.3	-0.4	-0.3
UK North	1.2	1.4	1.0	1.2	-0.1	-0.1
UK South	2.4	2.3	1.4	1.4	-0.8	-0.6
European West Coast	1.3	1.5	2.0	2.6	0.8	1.0
German Bight	0.8	0.9	3.8	3.8	3.1	3.5
GB South	0.8	0.9	3.3	3.4	2.8	3.3
GB North	0.8	0.4	5.2	4.2	4.3	4.3

Overall, the appropriate applicability of PCA for time series of the tidal range in terms of finding large-scale signals is evident. The reconstructed trends agree on a 95% significance level with their measured counterparts in over 97% of all tide gauges for tidal high water and tidal range. In tidal low water, this value is somewhat lower at 91%, with predominantly no agreement for tide gauges with known high impact local effects (e.g. Delfzijl (#53), Bremerhaven (#58) or Büsum (#61)). While the RMSE is 0.75 mm/yr for tidal low and 0.78 mm/yr for tidal high water, only an error of 0.49 mm/yr for tidal range is detectable. However, these values do not indicate a misrepresentation of the tidal low and high water, but rather the considerable influence of local effects at individual tide gauges. These are highlighted even more clearly in the tidal range as for example particularly striking at tide gauges Den Overbuiten (#34), Cuxhaven (#60) and Büsum (#61) in tidal range. These tide gauges already stood out in the calculation of the measured trends as being strongly locally influenced. PCs of higher order capture more than 80% of the remaining variance at tide gauge Den Overbuiten, more than 50% in Büsum and around 30% at Cuxhaven in tidal range. This anomaly is reflected in the comparison of the measured trends with those from the reconstruction of PC1 and PC2 (Figure 36-c). However, it must be noted that the common variance of tidal low and high water, including local effects having a similar effect on both parameters, already have been eliminated by calculating tidal range. Due to these effects, the overall variance in measured tidal low and high water is more than 2.5 times larger (see Chapter 5) than the variance in in the tidal range, amplifying the impact of local effects acting differently on tidal low and high water. Overall, it can be stated that local effects have a very large influence on the explained variance at individual sites, but not on the overall picture. At the same time, the significant reduction of the RMSE in terms of tidal range strongly suggests the presence of the same local effects in both tidal parameters, cancelling each out in the formation of the tidal range. A further possible explanation for

the higher RMSE in tidal low and high water is the meteorological component, since despite being a large-scale effect, the measurable impact at each tide gauge differs on the local scale. Therefore, it could only be partially reflected in the first principal components, but still be canceled out in the tidal range. A combination of both effects seems most likely here, which would also explain the significant reduction in variance explained before.

7.3 Answer to the second research question

On the basis of the analyses conducted in this chapter, the second research question concerning a *possible separation and quantification of large-scale and small-scale effects from observed records* can now be answered. For this purpose, a PCA was applied to the time series of tidal low water, tidal high water and, tidal range and indeed, the first two PCs turned out to be dominant for all three tidal parameters, confirming the idea of separating large-scale effects in the leading PCs.

In tidal low and high water, the overall explained variance for PC1 and PC2 is 89%, with PC2 being slightly smaller at 4% in tidal high water than in tidal low water at 5%. For both tidal parameters, the other PCs explain only between 0.001 and 2% of the overall variance and occur at very few tide gauges. The same applies to the tidal range. Here, 55% of the variance is explained by PC1, 14% by PC2 and a maximum of 4% by other PCs, which again affect only few tide gauges at once. Hence, it can be concluded that the separation of small-scale and large-scale signals was successful. This is also supported by the long-term trends, where most of the reconstructed large-scale trends agree on a 95% significance interval with their measured counterparts (Figure 36). In a complete reconstruction, there is a perfect match at all tide gauges.

Furthermore, a distinct, dipole spatial pattern similar to the results of the trend calculation of measured can be identified between the UK and the German Bight, with PC2 being mostly significant in the UK. While PC2 explains only 2-3% of the variance in the German Bight for all tidal parameters, it explains around 22% and 48% in the UK, reaching or surpassing PC1 in this area. At the same time, PC1 is extremely dominant in the German Bight with values between 78% and 92% and PC2 peaking at only 6% of overall variance (Figure 35, Table 9). This dipole image is also confirmed when looking at the correlations between measured time series and PCs. It can be consistently observed that PC2 shows the highest impact in the UK, decreases strongly on the European West Coast and exhibits only very low values in the German Bight, while the converse is perceptible for PC1 (Figure 32). In addition, the signals of the leading PCs were compared to each other and a high correlation of 0.92 (including trends) and 0.94 (excluding trends) between PC1 of the tidal low and high water could be detected, while no high correlations exist to the tidal range. This allows two conclusions: (I) it confirms that common effects in tidal low and high water are no longer present in the tidal range and (II) the changes in tidal low and high water are possibly driven by the same physical effect, differing from the effect becoming visible in tidal range. These conclusions are validated when looking at the long-term trends. The RMSE as a measure of the agreement between measured and reconstructed values is nearly identical for tidal low

and high water with 0.75 mm/yr and 0.78 mm/yr. This agreement reconfirms that the underlying physical effect contained in PC1 could be identical for both parameters (II), since the RMSE corresponds to the unexplained component. Simultaneously for the tidal range, the RMSE decreases to 0.49 mm/yr with a median trend of 1.6 mm/yr, indicating again a contribution of common effects and their elimination when calculating tidal range (I). Besides that, the different mean values of reconstructions (1.6 mm/yr for tidal low water and 2.7 mm/yr for tidal high water) imply in consideration of the similar RMSE a significantly lower influence of local effects on the tidal high water. It seems to confirm the higher sensitivity of the tidal low waters to local conditions as explained in Chapter 3.3. Furthermore, the number and location of non-significant tidal low water trends indicate a significantly lower sensitivity of tidal low water to changes in water level regarding the large Wadden areas, as the German Bight is heavily overrepresented in the number of neutral trends. This observation was already made in the trend analysis of the measured values, but local effects could not be excluded as possible cause. However, due to the use of large-scale reconstruction in this chapter, these are omitted and a systemic effect affecting several tide gauges in the Wadden Sea area can be assumed. In principle, this observation confirms the findings of Jensen (1984) and Führböter & Jensen (1985), which attribute the lower sensitivity of tidal low water measurements to measurement conditions and interactions of tide and Wadden areas (see Chapter 3.3).

Overall and in response to the second research question can be noted, that a separation and quantification of large-scale and small-scale effects based on short-term variance and long-term trends has been achieved. A quantification of both tide gauge and region specific separations can be found in Figure 35, Figure 36, Table 9, and Table 10. These results indicate both a common cause of the changes in tidal low and high water. Independent of this common cause, two further effects seem to exist, which only become visible in the tidal range. Even though these effects are assigned to the tidal range by the chosen methodology of the PCA here and in the following, it must be noted that they physically have originate from tidal low and/or high water. The physical causes of these different large-scale signals will be analyzed in the next chapter, answering the third and last research question.

8 Physical causes of large-scale tidal changes

After large-scale changes in tidal low water, tidal high water and tidal range were detected in Chapter 6 and separated from small-scale interference in Chapter 7, the assignment of causal physical effects to these changes is made in this chapter. The corresponding third and final research question about the *assignability of physical effects to the observed changes* is thus to be addressed.

When proving such a causation between two time series in context of this study, it is necessary to assign two essential properties of each time series. When searching for a connection between the leading PCs of each tidal parameter and physical effects, the short-term (interannual) as well as the long-term (decadal) variations have to be correlated, whereby these obviously merge into each other. For this purpose, the correlations excluding and including the long-term trends are considered separately, the former to detect a causal relationship and the latter to determine whether this relationship is strengthened or weakened by the long-term behavior. An exact and formula-based description of the mathematical procedures can be found in Chapter 4.1. In contrast to most analyses of this thesis, this analysis is based on mean annual values instead of mean monthly values, because the required physical indicators are often not available in a higher resolution. In addition, annual values offer the advantage of excluding both seasonal effects and intra-annual meteorology, making an adjustment for these effects obsolete (see also Chapter 3.3).

As described in the Introduction to this thesis as well as in Chapter 2.4, changes in the MSL have been suspected for some time to correspond to changes in tidal parameters. While Führböter & Jensen (1985) first pointed out this fact for the German Bight, Woodworth et al. (1991) described a possible connection between tidal range and changes in the MSL for the UK. Further studies with different focuses, e.g. on numerical simulation of changing tidal constituents (e.g. Pickering et al., 2012; Idier et al., 2017), in parts even on geological time scales (Green et al., 2018), come to similar, but purely numerical, theoretical results, although they roughly match the patterns of M_2 and S_2 detected here (see Chapter 6.3). Nevertheless, the results of this thesis presented in Chapters 6 and 7 do also indicate a relationship between tidal parameter changes and the MSL. The presumably common cause of changes in tidal low and high water and the (mathematical) independent behavior of the tidal range indicated by the PCA point in this direction. The supposed impacts of a changing MSL could be detectable in tidal low and high water, but eliminated in the calculation of the tidal range. In addition, the large-scale nature of the observed patterns excludes other known explanatory patterns at least in the area of the German Bight, as first stated by Jensen (1984). For these reasons, it is reasonable to investigate a possible relationship between tidal parameters and MSL changes at first, but not exclusively. The causes of the changes becoming visible only in the tidal range are then investigated on the basis of further indicators. The applied approaches and their results are described in the following chapter.

8.1 Physical causes of changes in tidal low and tidal high water

In order to detect a possible causation between changes of tidal parameters and MSL changes in the North Sea, reconstructions of the MSL for the study period between 1958 and 2014 must be available. As it was described in Chapter 6, several spatial patterns of tidal changes exist, with the opposing trends between the UK and the German Bight (and parts of the European west coast) being particularly striking. Even though this dipole-like pattern covers the entire range of longitude of the study area, it is still a rather small region in global terms. Since variations of the MSL vary greatly from region to region or on even smaller scales (e.g. Milne et al., 2009; Jensen et al., 2014; Pugh & Woodworth, 2014), global studies like Dangendorf et al. (2019) or Oppenheimer et al. (2019) are not suitable for these analyses. Therefore, if available, local reconstructions of the MSL should be used for the assignment aimed for here. Unfortunately, local reconstructions are only available for individual parts, but not for the entire North Sea basin. While continuous time series extending over a long periods can be found for the German Bight, this is not so much the case in the UK, at least at its eastern coast (see Chapter 3.2). The most aggravating factor is the low level of data completeness in this area. While more than 88% of tidal water level values are available for the German Bight in the study period between 1958 and 2014, the level of completeness is only 64% in the UK. As a result, an error accumulation when comparing tidal parameters and MSL cannot be precluded, since both quantities are calculated differently and could be variously distorted by large data gaps. In principle, a large number of studies exist that take the MSL developments on the eastern coast of the UK in account, but these are of limited use here, since either they are based on incomplete or very short time series, ignore large parts of the region or are purely numerical in nature (e.g. Woodworth et al., 1991; Pickering et al., 2012; Wahl et al., 2013; Dangendorf et al., 2015; Idier et al., 2017; Schindelegger et al., 2018). By contrast, a large number of local or regional studies in the area of the German Bight or at least with a focus on large parts of the German Bight exist analyzing long-term tidal water series and sea level rise. These studies have been published for example by Rietschel (1933), Lüders (1936), Gaye (1951), Dietrich (1954), Rohde (1975), Liese & Luck (1978), Liese (1979), Jensen (1984), Jensen (1985), Führböter & Jensen (1985), Siefert & Lassen (1985), Jensen et al. (1991), Heyen et al. (1996), Langenberg et al. (1999), Wahl et al. (2010, 2011, 2013), Albrecht et al. (2011), Jensen et al. (2011), Hein et al. (2011), Dangendorf et al. (2012), and Jensen et al. (2014). An extensive overview of previous research in this context can be found in Jensen (2020a). Particularly noteworthy in the context of this thesis are Jensen et al. (2011), as they computed tide gauge specific reconstructions of the MSL for various stations in the German Bight.

Most recently, Niehüser et al. (in prep.) have made another important contribution in this context and developed an update of Jensen et al. (2011). Niehüser et al. (in prep.) were able to reconstruct level-specific values for the MSL at selected tide gauges in the German Bight by using neural networks based on tidal low and tidal high water values as well as minutely measured values. The limitations in the quality of the tidal low water measurements (see Chapter 3.3) apply here as well, but inclusion of minutely values at least reduces the relative impact of the tidal low water and thus the total error in the

time series. Yet, a complete exclusion of the comparative error between tidal low water and the MSL is not to be expected, since large-scale and systematic inaccuracies in the tidal low water may be fully contained in PC1. It is to be expected that a possible correlation between the tidal parameters and the MSL can be detected less significantly in tidal low water than in tidal high water.

Unfortunately, the method of Niehüser et al. (in prep.) cannot be applied to the eastern UK due to insufficient data. Therefore, comparisons with individual tide gauges reconstructions could only be made for the German Bight on the basis of the existing data. Nevertheless, a causal analysis for the UK is also aimed at and a reconstruction of the North Sea-wide MSL by Wahl et al. (2011) based on 30 tide gauge location around the basin is used as a second best solution. Here, it must be noted, that even if a direct correlation between tidal parameters and MSL exists, a rather mediocre agreement can be expected due to the non-consideration of spatial patterns and local variations of the MSL. Consequently, a possible causation between MSL and tidal parameters based on the reconstructions of Niehüser et al. (in prep.) will be investigated firstly in the German Bight. Afterwards, a possible similar interaction is assessed for the UK based on the data of Wahl et al. (2011). A separate investigation in the area of the European West Coast is omitted due to its transitional character (e.g. Table 9, Figure 35) between the two poles of the dipole pattern of the UK and the German Bight. An explanation of the two poles implicitly includes the area between them.

8.1.1 German Bight

To enable a consistent comparison, the following analyses that refer to Niehüser et al. (in prep.) are based exclusively on the coinciding tide gauges, which are: Norderney (#54), Helgoland (#55), LT Alte Weser (#56), Wilhelmshaven (#57), Cuxhaven (#60), Husum (#62), Wittdün (#63), Dagebüll (#66), Hörnum (#67), and List (#68), a sample that is spatially evenly distributed over the German Bight. This selection of 10 tide gauges is significantly smaller than the 22 German Bight tide gauges used in the rest of this thesis. Nevertheless, a sufficient amount of data can be assumed, since dominant PC1 reflects over 90% of the overall variance for each tidal parameter in the entire German Bight and over 80% of the median variance at the selected tide gauges. A correlation to the MSL would therefore tend to be rather smaller than being too large, excluding the possibility of an artificially high value. Since the trends are also reproduced with sufficient accuracy (see Chapter 7.2), PC1s can be regarded as representations of tidal parameters in the context of large-scale developments in the German Bight. To further ensure comparability of the results, the individual MSL reconstructions of Niehüser et al. (in prep.) were averaged to an index time series, making the data comparable to the large-scale PC1s of the tidal parameters. Hence, a sufficient representation of the overall situation for the German Bight can be assumed.

In order to assess the short-term changes, dominant PC1s of the tidal parameters and the MSL index are presented on the left side of Figure 37, excluding their trends. High correlations of 0.88 for tidal low and 0.90 for tidal high water are found. The variance of tidal low water is 26 cm² with about 80% being explainable by the MSL index, while the variance of tidal high water is 16 cm² with the MSL index

containing about 70% of the variance. In both cases, the remaining variance is about 5 cm², indicating that the large-scale variance of both tidal parameters is related to the MSL for the most part. This connection is further consolidated when looking at the tidal range. Considering the high correlation between PC1s of tidal low and high water, it is evident that changes in MSL are related to the same parts of variance in tidal low and tidal high water. The tidal range would then not be correlated to the MSL index, since these shares of variance would cancel each other out. In addition, the variance of tidal range would have to be smaller or equal to the remaining variance of 5 cm² in tidal low and high water, as only this part of the variance is not caused by MSL changes. Following this argumentation, Figure 37-e indeed displays no correlation (Corr. = 0.00), proving that the distinct correlation detected in large-scale tidal low and high water changes does not exists in the tidal range. Furthermore, the variance for the tidal range is only 3 cm², while the variances of tidal low and high water are still around 5 cm² after MSL index adjustion, indicating that the difference of 2 cm² are caused by the meteorological influence contained both in tidal low and high water (Führböter & Jensen, 1985). Since these cancel each other out in the calculation of the tidal range, 3 cm² remain as non-meteorological variance, being contained in PC1 of tidal range. Consequently, the short-term developments of the tidal range and its variance have to be dependent on factors apart from meteorology and MSL changes, which will be searched for in Chapter 8.2.

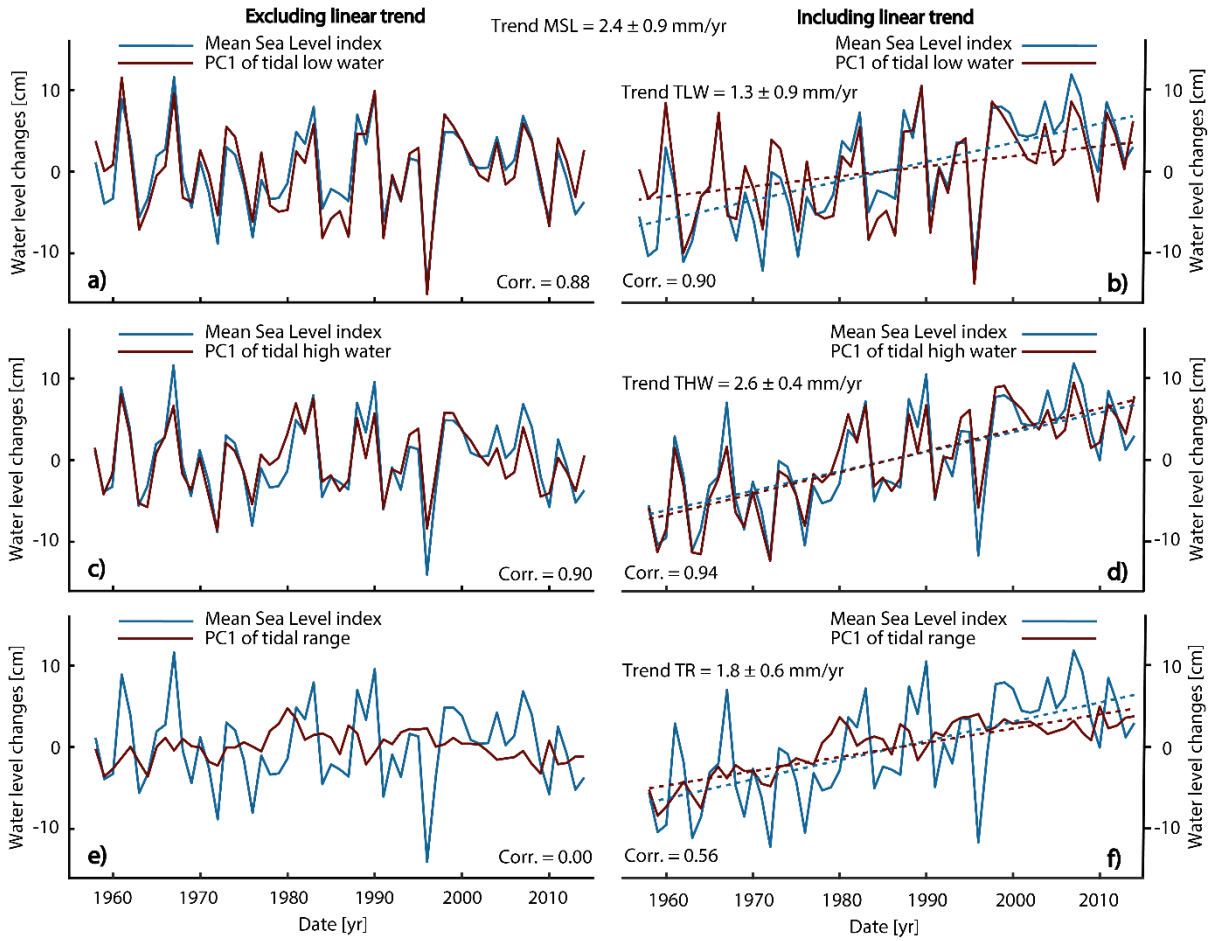

Figure 37: Mean Sea Level index and PC1 (scaled) of tidal low water (a, b), tidal high water (c, d), and tidal range (e, f) in the German Bight excluding (left) and including (right) linear trends.

Apart from these short-term considerations, it is necessary to examine the long-term developments. The linear trends of MSL index and tidal parameters are presented on the right side of Figure 37, exhibiting values of 2.4 ± 0.9 mm/yr for the MSL index and 1.3 ± 0.9 mm/yr, 2.6 ± 0.4 mm/yr and 1.8 ± 0.6 mm/yr for the tidal parameters on a 95% confidence interval. Since the significant correlations between MSL and PC1 reconstructions of tidal low and high water have already been demonstrated excluding trends, only the question of common or divergent long-term trends remains: by considering the linear trends, the correlation is further enhanced, increasing from 0.88 to 0.90 in tidal low and from 0.90 to 0.94 in tidal high water. For PC1 of the tidal range, the correlation increases by a large margin of over 0.56, strongly indicating a common long-term development to the MSL. However, since no correlation exists excluding the trend, no direct causation can be proven with this indicator. Overall, these results are in line with expectations, since a direct correlation between both tidal low and high water with the same large-scale impact (of a changing MSL) can be established, an effect, which is not detectable in tidal range. The absence of a direct correlation excluding trends would suggest that the changes in tidal range are caused by other large-scale effects, but the huge magnification of correlation when including trends may nevertheless indicate a connection to the MSL.

In addition to this unresolved question, temporal divergences between the linear trend of the MSL index and PC1 trends of the tidal parameters can be found. There seems to be a tipping point in the mid-1980s, where the formerly exceeding progression of tidal ranges PC1 falls below the rise of the MSL index. Simultaneously, a similar and even more pronounced effect is evident in tidal low water's PC1, revealing an identical tipping point. For the tidal high water, only a small and reversed effect is occurring, with the divergence to the MSL being very small and mostly not significant. These relative differences between the residuals of tidal low and high water to the MSL index could explain the long-term progression of tidal range. The relative difference of the large residual in tidal low water and the small residual in tidal high water would then cause the trends in tidal range, a possibility which is also indicated by the common tipping points. Evidently, tidal low water levels track less closely than tidal high water levels the long-term development of the MSL, making the long-term sensitivity of both tidal parameters to the MSL the decisive fact. This long-term agreement between tidal range and MSL would then be caused by the remaining trend component of the MSL index, which is not eliminated by the difference formation due to the lower sensitivity of the tidal low water. This theory applies explicitly only to the long-term developments, since the elimination of the common MSL caused variance in tidal low and high water has already been proven. It is now necessary to ascertain whether this considerations are physically plausible as well as quantitatively and qualitatively verifiable in the next step.

For this purpose, the divergent large-scale developments of tidal low and high water are considered in a physical context first. The trend of large-scale tidal high water changes exceed the trend of the MSL index by 0.2 mm/yr, which is in principle a well-known effect and have already been documented in several studies, e.g. in the German Bight by Mudersbach et al. (2013) and Arns et al. (2015a). Both studies assign nonlinear interactions between water depth, meteorology and bottom friction as causes

for a larger increase in tidal high water than in MSL, whereas Arns et al. (2015a) succeeded in demonstrating these effects within a numerical model. Therefore, a direct causation between the increase in the MSL and the tidal high water is physical possible despite slightly different trends. The trends of the large-scale tidal low water developments, however, are significantly lower than the trends of the MSL. To clarify this apparent contradiction, the measurement constraints of the two quantities have to be considered again. As explained in Chapter 3.3, there are several limitations regarding the sensitivity of tide gauges to local disturbances, with the individual location of the tide gauge being decisive here. As noted in Führböter & Jensen (1985) and Jensen (1985), the location of tide gauges at Wadden channels in large Wadden areas like the German Bight leads to higher tidal low water readings than actually present in the surrounding area due to non-existent or delayed runoff within these channels. In addition, the interdependence between tide and morphology in Wadden areas can lead to falsified values, which are not present in tidal high water and are thus not equalized in the tidal range (Knop, 1961; Jensen, 1985). One conclusion from these effects is the need for a sufficiently high increase in tidal low water to a level at which it is measured correctly by the tide gauges. If a constant bathymetry is assumed, a tide gauge on a Wadden channel would only then show correct tidal low water values, if the MSL was already raised to a level where the surrounding water level matches the Wadden channels water level. However, this effect would not affect the development of the tidal high waters (see also Figure 13). Furthermore, these considerations are supported by the spatial distribution of non-significant tidal low water trends in the North Sea. In both the measured (Figure 27) and the reconstructed (Figure 36) time series, the German Bight is clearly overrepresented in terms of non-significant trends. While in both cases rising tidal low waters tend to be recorded in the entire North Sea, neutral (measured) or even negative (reconstructed) values occur almost exclusively in the German Bight. Simultaneously, none of the non-significant tidal high water trends are located in this area. Overall, the divergent large-scale trends in tidal low and high water can be interpreted as distinct responses to changes in MSL, excluding possible local anomalies.

Therewith the physical plausibility is proven, leading to a quantitative verification in the next step. Here, the accumulated residuum of the large-scale trends of tidal low and high water to the trend of the MSL is compared with the large-scale trend of the tidal range. This will clarify whether the different responses to the increase in MSL are suitable to explain the trend of the tidal range. Including the 95% boundaries UB and LB, the residuals of the linear tidal low ($UB_{MSL-TLW}$, $LB_{MSL-TLW}$) and tidal high water ($UB_{MSL-THW}$, $LB_{MSL-THW}$) trends to the trend of the MSL index (UB_{MSL}, LB_{MSL}) is calculated. Subsequently, it is checked whether these residuals correspond to the large-scale trend of the tidal range. Please note that for this calculation a higher accuracy is necessary and a higher number of decimal places is used than for example in Figure 37.

$$\begin{aligned} \mathrm{UB_{MSL-TLW}} &= \mathrm{UB_{MSL}} - \mathrm{UB_{TLW}} \\ &= (2.39 + 0.92) - (1.25 + 0.89) \\ &= 3.31 - 2.14 \\ &= 1.17\ [\mathrm{mm/yr}] \end{aligned}$$

$$\begin{aligned} \mathrm{LB_{MSL-TLW}} &= \mathrm{LB_{MSL}} - \mathrm{LB_{TLW}} \\ &= (2.39 - 0.92) - (1.25 - 0.89) \\ &= 1.47 - 0.36 \\ &= 1.11\ [\mathrm{mm/yr}] \end{aligned}$$

Thus, the residual trend for tidal low water is between 1.11 and 1.17 mm/yr.

$$\begin{aligned} \mathrm{UB_{MSL-THW}} &= \mathrm{UB_{MSL}} - \mathrm{UB_{THW}} \\ &= (2.39 + 0.92) - (2.61 + 0.39) \\ &= 3.31 - 3.00 \\ &= 0.31\ [\mathrm{mm/yr}] \end{aligned}$$

$$\begin{aligned} \mathrm{LB_{MSL-THW}} &= \mathrm{LB_{MSL}} - \mathrm{LB_{THW}} \\ &= (2.39 - 0.92) - (2.61 - 0.39) \\ &= 1.47 - 2.22 \\ &= -0.75\ [\mathrm{mm/yr}] \end{aligned}$$

The residual trend in tidal high water trend is between -0.75 and 0.31 mm/yr. The large-scale tidal range trend ($\mathrm{UB_{TRMSL}}$, $\mathrm{LB_{TRMSL}}$) explained by tidal low and tidal high water trend residuals would be at:

$$\begin{aligned} \mathrm{UB_{TRMSL}} &= \mathrm{UB_{MSL-TLW}} - \mathrm{UB_{MSL-THW}} \\ &= 1.17 - 0.31 \\ &= 0.86\ [\mathrm{mm/yr}] \end{aligned}$$

$$\begin{aligned} \mathrm{LB_{TRMSL}} &= \mathrm{LB_{MSL-TLW}} - \mathrm{LB_{MSL-THW}} \\ &= 1.11 + 0.75 \\ &= 1.86\ [\mathrm{mm/yr}] \end{aligned}$$

Therefore, the value of the tidal range trend exclusively resulting from the different response of tidal low and high water to the changing MSL is between 0.86 and 1.86 mm/yr. These values indeed show a high agreement with the actual large-scale development of the tidal range, which reveals trends between 1.19 mm/yr and 2.35 mm/yr. The calculated trends thus overlap in a range from 1.19 mm/yr to

1.86 mm/yr with the large-scale trends, corresponding to an agreement of 0.67 on a 95% confidence interval. Conclusively, the trend of the large-scale development of the tidal range reflected in PC1 or at least the larger part of it is quantitatively connected to the divergent responses of tidal low and high water to the MSL rise.

Since the connection of tidal low and high water to the MSL index now has been demonstrated for the German Bight physically as well as quantitatively, the qualitative proof remains. In Figure 37, significant temporal changes of the time series become apparent. Due to the linearity of the trend analyses, temporal changes cannot be accounted for in the quantitative proof, which allows only for a stationary consideration. The adding of another degree of freedom to the trend lines is necessary. Due to the high variance compared to the relatively small trends and the short length of the time series, no comparative, quantitative analysis for a second degree function is possible and no confidence interval can be formed. Therefore, it is indeed a purely qualitative analysis. However, this is considered unproblematic, since the quantitative part of the analysis was carried out in Figure 37 and the focus here is on the changes over time. In Figure 38, the large-scale development of tidal parameters and the MSL index are shown with their second degree polynomial functions. This illustration allows a much better representation of the individual differences to the progression of the MSL index.

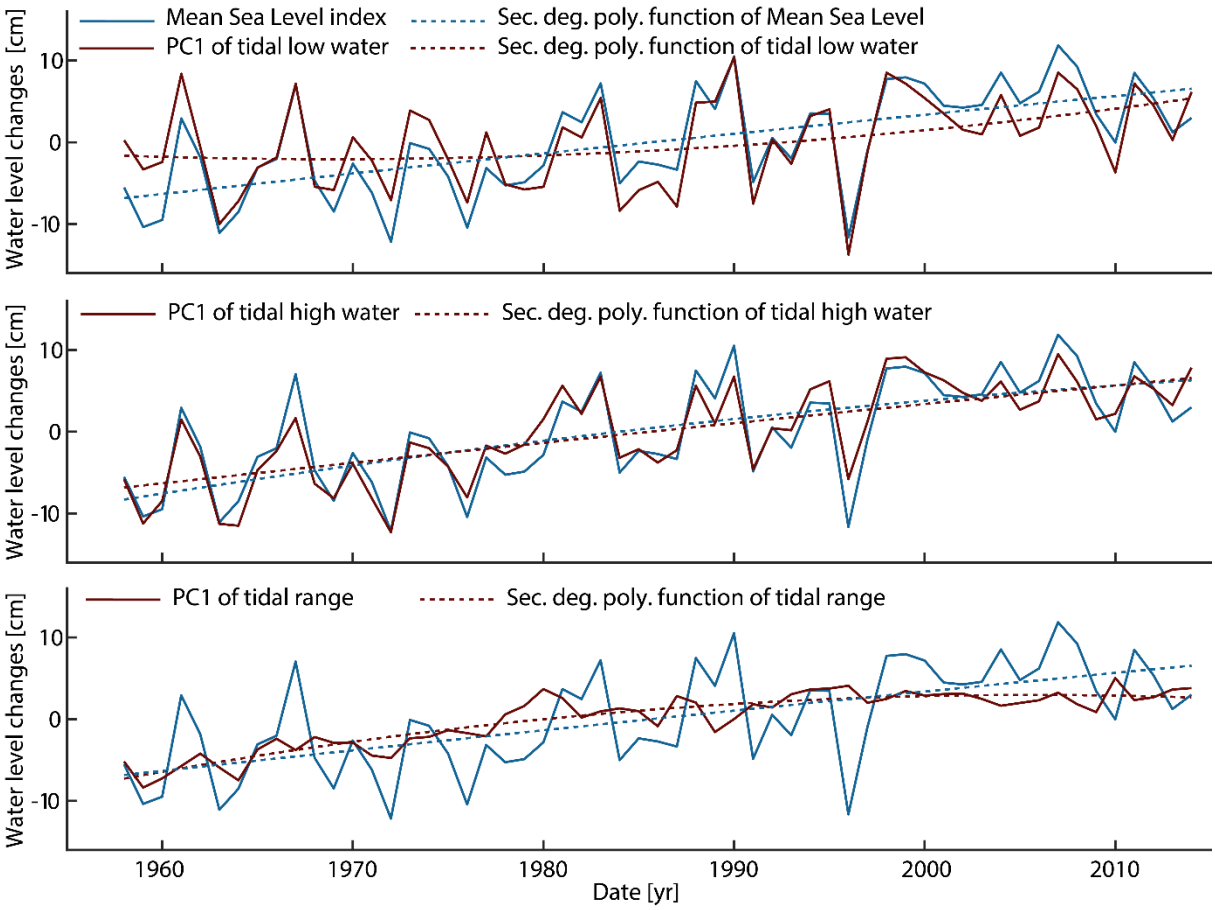

Figure 38: Mean Sea Level index according to Niehüser et al. (in prep.) and index of tidal low water (a), tidal high water (b) and tidal range (c) with their second degree polynomial functions in the German Bight.

First of all, the almost linear increase of the MSL index becomes apparent despite the addition of another degree of freedom, which proves the linear character of this development. In contrast, a much more nuanced development is now visible in the large-scale tidal low water development. Initially, almost no trend can be detected between 1958 and the end of the 1970s. During the 1980s, the tidal low water begins to rise, reaching a parallel development to the MSL index at the end of the 1980s which is maintained approximately until the end of the time series. This parallel development demonstrates that a very similar trend in tidal low water and MSL has occurred since the late 1980s. In contrast to this temporal changes, the increase of the tidal high water is nearly linear and follows the development of the MSL index. Only at the beginning of the time series smaller differences are visible. The development of the tidal range is closely connected to these changes. It follows the development of the MSL index up to the end of the 1980s, with only small deviations at the beginning of the records. From the early 1990s onwards, however, tidal range trends fall behind the MSL and remain constant from the year 2000. This is consistent with the increase in tidal low water parallel to the MSL from the end of the 1980s on. Overall, the change in the tidal range seems to depend largely on the development of the tidal low water, as tidal high water follows the MSL index almost constantly, confirming the results from the physical and quantitative analysis.

Overall, all of the applied analyses prove a strong relationship between MSL changes and changes in tidal low and high water on both short and long time scales. In contrast, no correlation can be found for the tidal range on short time scales, yet the trend of the tidal range seems to result from the divergent responses of the tidal low and high waters to the increase in MSL. The causes of the tidal range changes on short time scales are discussed in more detail in Section 8.2.

8.1.2 United Kingdom

After establishing the causal relationship between MSL and the large-scale changes in tidal low and high water in the German Bight, the question of a comparable effect in the UK naturally arises. The investigation here is more difficult, since for tidal low and high water both PC1 and PC2 represent a significant part of the variance. In the German Bight, PC1 was dominant with over 90% of the variance in tidal low and high water compared to only 2% in PC2. PC1 contains about 27% in tidal low and 28% in tidal high water of the overall variance in the UK, a component that can already be assigned to the changes in the MSL in analogy to the developments in the German Bight. Therefore, at least a partial influence of the MSL is given, since the physical connection between MSL rise and PC1 has been proven in the previous chapter. The question remains as to whether extend the MSL is the dominant signal or if PC2 has a different origin, explaining around 28% of tidal low and around 22% of tidal high waters overall variance. That is why the analyses performed in the following refer exclusively to PC2. The limitations on data quality and the non-consideration of the regional features of the MSL in the existing sources described at the beginning of this chapter do apply here. The North Sea-wide MSL reconstruction of Wahl et al. (2011) is used. An overview similar to Figure 37 is given in Figure 39, where the

MSL is derived from Wahl et al. (2011) instead of Niehüser et al (in prep.). It becomes apparent that the correlations between the MSL index and tidal low and high water are much lower than in the German Bight area for PC1, but still significant.

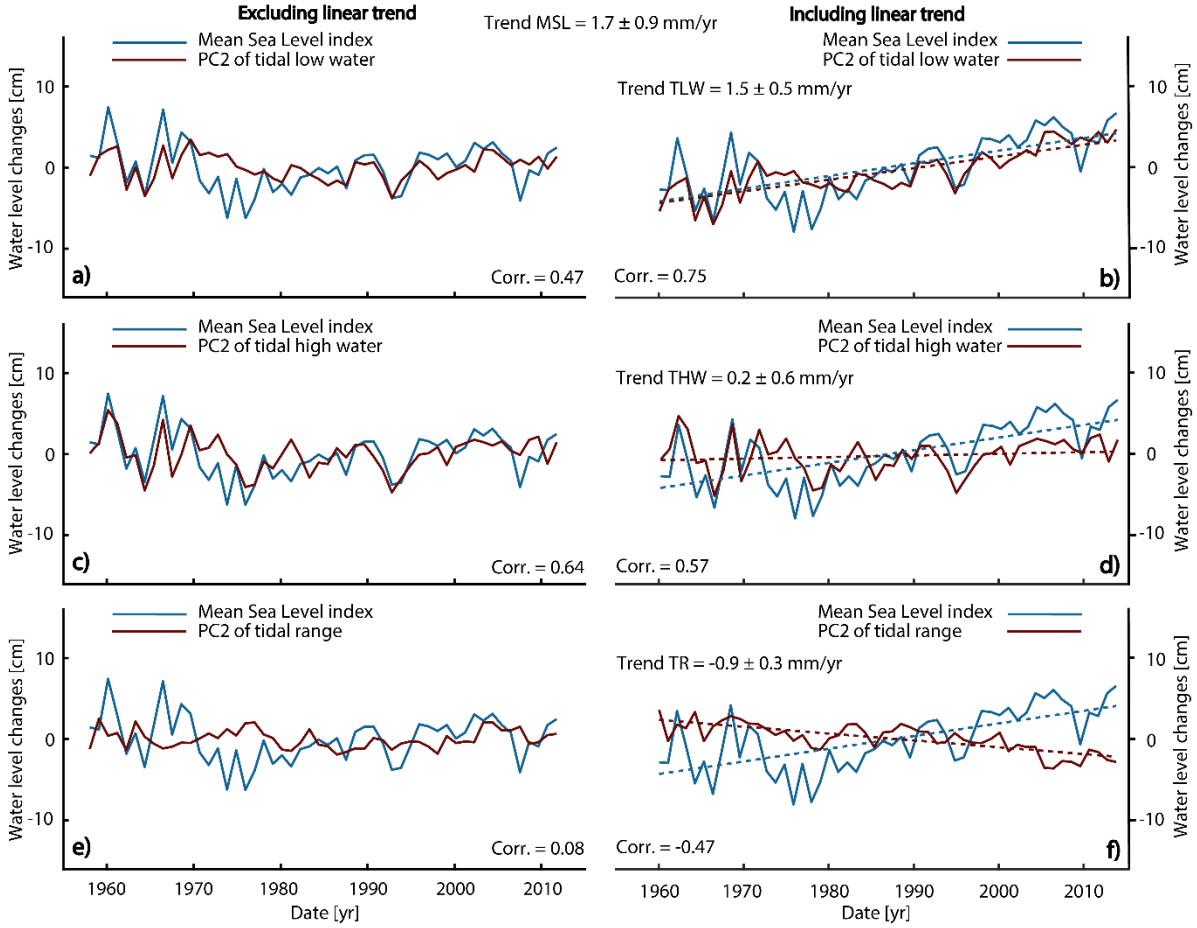

Figure 39: Mean Sea Level index according to Wahl et al. (2013) and index of tidal low water (a, b), tidal high water (c, d), and tidal range (e, f) in the UK excluding (left) and including (right) linear trends.

The correlation between the MSL and the tidal low and high water excluding trends are 0.47 and 0.64. No significant correlation is detectable in the tidal range excluding trends. In contrast to the behavior in the German Bight, a negative correlation results for the tidal range including trends, although here, too, no causal relationship can be detected. The trend of the tidal low water (1.5 ± 0.5 mm/yr) matches the trend of the MSL index (1.7 ± 0.9 mm/yr) with significantly overlapping confidence intervals, resulting in an increase of the correlation to 0.75. The low correlation of only 0.47 excluding trends appears too low to establish a causal relationship, but the large increase seems to imply it. This high agreement does not contradict but confirms the developments in the German Bight, as there are no large Wadden areas off the coasts of the UK. In tidal high water, the consideration of the trends leads to a reduction of the correlation from 0.64 to 0.57, since tidal high water does not show a significant trend here. This result also tends to contradict a direct correlation, although the correlations are too high and, moreover, significant to ignore. Overall, a causation between MSL and PC2 cannot rejected, but it is much less profound than for PC1. A distinct proof does not succeed here. However, the results also do not contradict

the results from the German Bight, especially since the evidence between PC1 and MSL has already been established and almost 30% of the short-term variations in the UK can be explained by them.

There are several possible reasons that could mask a more distinct connection between PC2 and the MSL besides data completeness. The reconstruction of the MSL (Wahl et al., 2011) does not correspond to regional conditions but to a basin-wide average, possibly causing significant discrepancies. Furthermore, local effects vary the tide gauges in the UK significantly and the impact of local variance at individual tide gauges is significantly higher than in the German Bight (Figure 35; Table 9). Additionally to locally produced anomalies, there may also be varying reactions to an increase in the MSL, since tide gauges do only measure the local system response. If there is a distinctly different local response of the individual tide gauges, a shift to the higher PCs can theoretically occur, since the physical cause may be large-scale, but the measurable response of the system is local. This effect is negligible in the German Bight, since only about 6% of the variance in the tidal low water and only about 4% of the variance in the tidal high water on the time scales considered here are caused by local effects. In the UK, on the other hand, local effects contribute 45% in tidal low water and 50% in tidal high water to overall variance and could include local reactions to the increase in MSL. The cumulative impact of these effects prevents a more detailed examination, as it was done for the German Bight, especially with regard to the long-term trends of the tidal range. Overall, it is evident that the developments in tidal low and high water in the German Bight depend significantly on the increase in MSL. In principle, this relationship can also be demonstrated for the UK, but it remains unclear how distinct this relationship is. Due to the lack of reliable, local MSL reconstructions of the UK as well as due to the large data gaps, no quantification can be performed here. Nevertheless, it can be stated that there are strong indications for a causal relationship also for PC2 in the UK, so that at least no contradiction to the German Bight arises.

8.1.3 Reverification of the theoretical results with measured values

Since the effects observed in this thesis are mainly of a large-scale nature including complex theoretical analysis, it seems useful to compare the agreement of the measured values to the results presented here, especially regarding trends. This comparison is intended to complement the demonstration of the fundamental suitability of the methodology in Chapter 4.5 as well as the quantitative plausibility check of the large-scale trends based on measured trends in Chapter 7.2. In particular, the intended underestimation of trends by Ordinary Kriging can lead to deviations, an error whose correction would, however, increase the significance of the results. To further plausibilize the results obtained, a comparison between large-scale signals and unaltered, measured values at individual tide gauges is carried out for the German Bight. This region was chosen, because the correlation between MSL and tidal parameters is most clearly provable here.

As the highest discrepancies between the trends of PC1s and MSL occur in tidal low water, the development of the tidal low water should be reviewed for each individual tide gauge in the German Bight and compared to PC1. Basically, two causes inherent in the methodology could have caused deviations

in the trends: the Ordinary Kriging could underestimate developments at individual tide gauges or locally deviating responses (for example as a result of anthropogenic interventions) of individual tide gauges to the increase of the MSL could be shifted to a higher PC and thus be unrepresented in PC1. Both sources of error can be analyzed using Figure 40-a, which depicts the measured time series (without any interpolation of missing values) of all 22 tide gauges in the larger German Bight area with a moving average of 19 years excluding the nodal cycle.

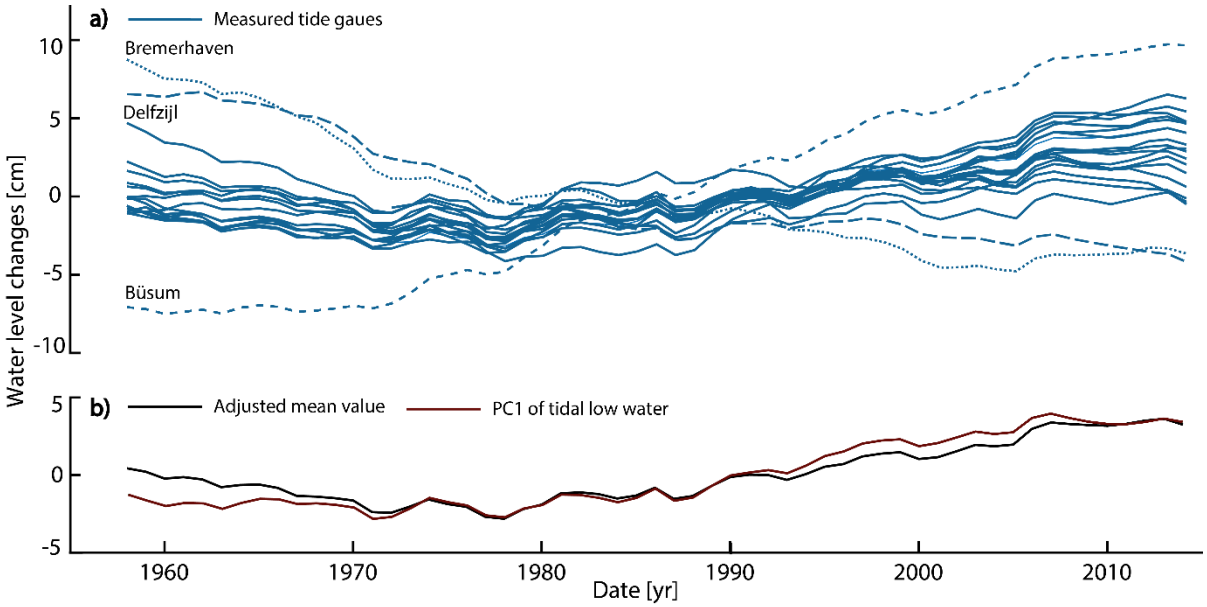

Figure 40: (a) Annual time series of tidal low water at all tide gauges in the German Bight (blue); (b) Mean value excluding (adjusted for) the locally affected tide gauges Bremerhaven, Delfzijl and, Büsum (black) and tidal low waters PC1 (red). All time series were smoothed by a 19-year moving average to exclude the nodal cycle.

Regarding potential source of error, indeed three tide gauges Delfzijl (#53), Bremerhaven (#58), and Büsum (#61) display a visually divergent development. However, a clear increase in the trends starting between 1970 and 1980 can be detected at all stations visually, including these three. While Bremerhaven and Delfzijl previously showed strongly declining trends, these subsequently become almost neutral. Büsum resembles the development at the other tide gauges, but inhibits a much more pronounced increase in the 1970s. Overall, a similar qualitative behavior can be observed at all tide gauges, despite of the quantitatively deviations concerning the three mentioned tide gauges. These discrepancies indicate a significant overlay of the detected large-scale signal by local effects at these tide gauges, which indeed was proven by Ebener et al. (2020) and Hollebrandse (2005). In Bremerhaven, various deepening measures of the outer Weser have taken place, port development projects have influenced the values of tidal low water in Delfzijl and a time-related connection to the embankment of the Bay of Meldorf can be verified for Büsum. This apparent superimposition is a further confirmation of the applied methodology, as the quantitative variations can be explained. These considerations do not exclude the existence of local effects with smaller impacts at other tide gauges, which were also demonstrated by Ebener et al. (2020). Figure 40-b represents the mean value of all time series without the three diverging tide gauges and compares it with the development of tidal low waters PC1. A high correlation of over 0.93

(excluding trends) and over 0.96 (including trends) is detectable. The joint downward trend in tidal low waters is slightly underestimated at the beginning of the 1960s and a similar effect occurs in the mid-1990s. However, even in these areas the graphs run parallel for the most part, indicating that short-term effects at a few gauges could be the causative factor. In addition, different local effects at various tide gauges with similar effects on measurement values could deviate the mean value from the tidal low water index, since they would be excluded in the PCA. In summary, the calculated large-scale development of tidal low water with its significant increase since the 1970s can be confirmed on the basis of the actual measurement data, since and no major, unexplained discrepancies to PC1 are detectable.

For the tidal high water, a discrepancy to the trend of the MSL occurs only to a smaller extend. However, the underlying comparison was made with the mean MSL index and not with the individual MSL reconstructions to account for the large-scale character of PC1. Therefore, a comparison is made here at individual tide gauges between the MSL calculated from measured data by Niehüser et al. (in prep.) and the large-scale reconstruction (PC1) to verify the large-scale results and to define the limits of the procedure at local scale. This comparison is made for all tide gauges in the German Bight from Niehüser et al. (in prep.) and is exemplary illustrated using the 4 tide gauges Norderney (#54), Helgoland (#55), Cuxhaven (#60), and List (#68) in Figure 41. A complete presentation of all tide gauges can be found in the Appendix. The measured values of tidal high water are also displayed in addition to the MSL and the large-scale reconstruction to allow a cross comparison of all three values. The correlation between MSL and large-scale reconstruction is about 0.9 at each of the individual gauges and roughly corresponds to the comparison of the large-scale signals in Figure 37, proving a significant correlation also at the scale of individual tide gauges. In contrast, the trends do not correspond as well as in the large-scale comparison, but remain in the same order of magnitude. While the trends of reconstructions and the trends of the measurements show clear overlaps of their significance intervals (see also Figure 36), the agreement is smaller compared to the trend of the MSL. For example, a linear trend of 2.5 ± 1.1 mm/yr can be determined from the data of Niehüser et al. (in prep.) at the tide gauge Helgoland, whereas both the reconstruction with 3.3 ± 0.8 mm/yr and the measured values 3.6 ± 0.9 mm/yr exceed this value. In principle, this exceeding of MSL trends is not surprising, since it corresponds to the effects described by Mudersbach et al. (2013) and Arns et al. (2015a), which were discussed in Chapter 8.1.1.

Nevertheless, the deviations are larger than in the large-scale analysis and the possible procedural causes have to be addressed, namely the properties of the MSL time series as well as the PCA itself. Regarding the MSL time series it must be noted, that the local MSL was searched for by Niehüser et al. (in prep.). As a result, the calculation of the MSL time series does not contain any corrections for local effects, which are therefore also included in the MSL trend calculation. For example, the individual system response to the MSL rise at a single tide gauge would not be corrected, but is excluded in the PCA-based large-scale reconstruction. This problem appears less severe in the large-scale comparison, as an averaged MSL index is much less sensitive to local effects. In addition, the large-scale reconstruction

calculated by PCA has to be scaled to the individual levels of tide gauges to enable a comparison, causing further deviations. These deviations are not present with large-scale considerations, since no scaling to local conditions is necessary. Given that scaling does not impact the correlation and thus the causation excluding trends is still intact, the trends themselves can be altered. Overall, larger discrepancies are to be expected at the single tide gauge than in the large-scale context due to both the methodology of Niehüser et al. (in prep.) and the limitations of PCA. However, despite these discrepancies caused by physical effects, the different consideration of local effects and the limitations of the PCA, a clear correspondence between MSL, measured values and reconstructions remains detectable also at individual tide gauges. In total, a high agreement of the measured values to the results of this thesis can be verified for the tidal low water as well as for the tidal high water.

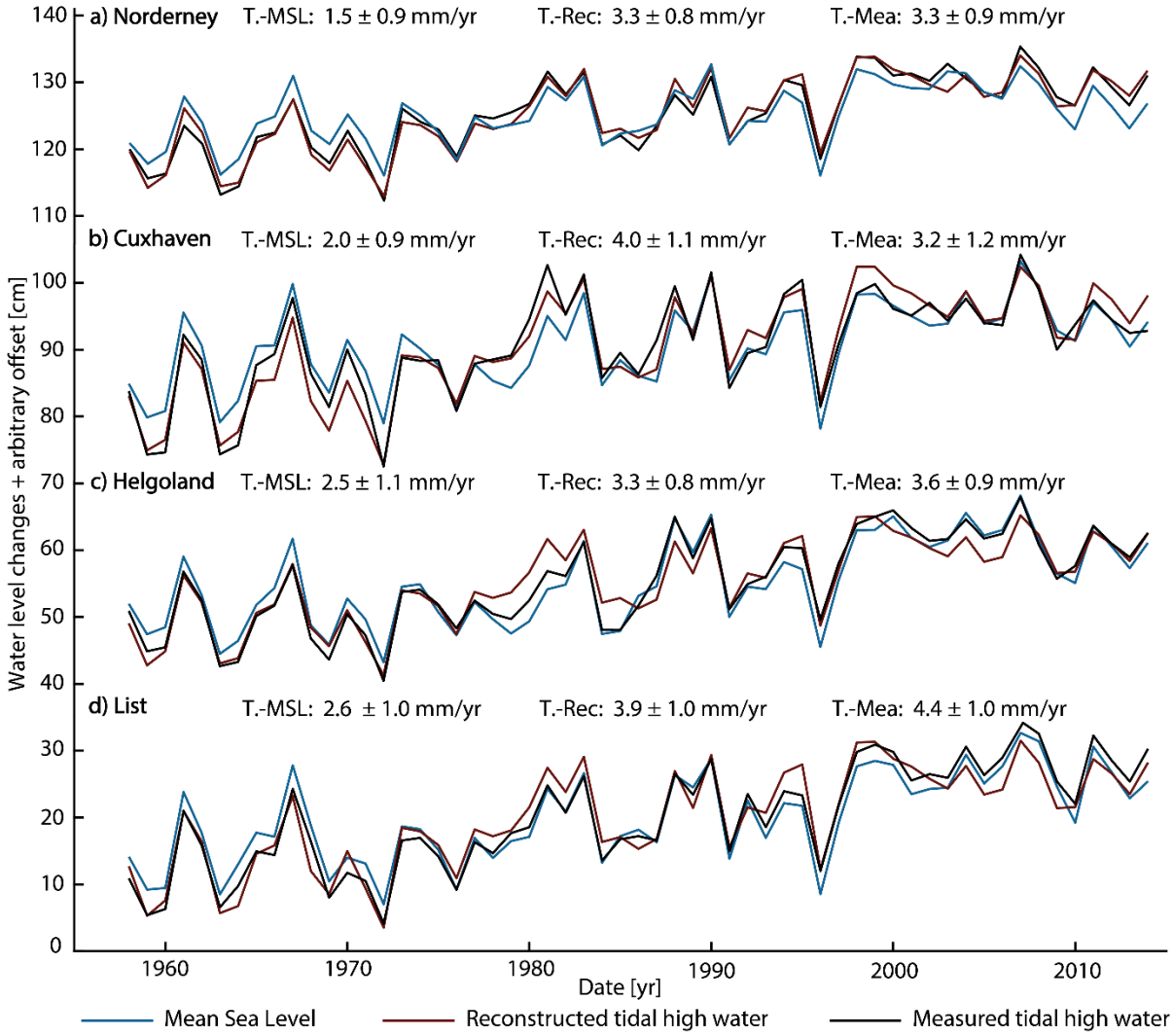

Figure 41: Annual time series and trends (T.-) of MSL according to Niehüser et al. (in prep.), reconstructed tidal high water of PC1 (Rec) and measured tidal high water (Mea). The correlations between the reconstructions and the MSL are about 0.90 for the presented tide gauges of Norderney (a), Cuxhaven (b), Helgoland (c) and List (d), a depiction of all tide gauges can be found in the Appendix.

8.2 Physical causes of changes in tidal range

Up to here, the trends of tidal low and high water were demonstrated to correlate significantly to the MSL with the trends of the tidal range resulting from the different response of the other tidal parameters to the MSL rise. Both the linear trends as well as the nonlinear development and of the tidal range can be largely explained, especially in the German Bight and to a smaller degree in the UK. In the preceding analyses it was further proven, that large parts of the variance of both tidal low and high water are caused by changes of the MSL. Nevertheless, those parts of the variance which are not identical in tidal low and high water are not eliminated by difference formation and needs to be further analyzed. They are depicted in the tidal range. As an additional complicating factor, only 8% of the variance of tidal range is explained by PC1 in the UK (PC2: 48%) in contrast to 78% in the German Bight (PC2: 3%). This dipole indicates two different large-scale signals, being masked in tidal low and high water and becoming visible only in the tidal range. As demonstrated in Chapter 7.1, the PCA suggests two modes of variability for tidal range that appear coherently at the investigated sites in the North Sea. In contrast to the analyses of tidal low and high water, it is not possible to find a direct oceanographic index including MSL indices as physical cause for the variance of the tidal range. Therefore, the only part remaining utterly unknown at this point is the physical cause of short-term changes in tidal range for the German Bight as well as for the UK.

To narrow down possible causes, the first question arising is whether PC1 and PC2 of tidal range are produced within or outside the North Sea basin. If the former is the case, then the PCs should show no correlations to tide gauge records from the adjacent North Atlantic, while an external forcing would possibly provide some sort of coherence with those records. Therefore, PC1 and PC2 generated from tide gauges inside the North Sea basin were compared with selected tide gauges from outside the North Sea basin in the North Atlantic, which were not included in the PCA. Here, the additional 24 North Atlantic tide gauges from the GESLA data set described at the end of Chapter 2.2 are used. No coherence is found for PC1 and it can be concluded that the signal is produced within the basin or at least not in the North Atlantic, a factor which will be addressed later. The opposite applies to PC2. A comparison between PC2 and available tide gauge records along the European Atlantic coast, Iceland, and Canada is shown in Figure 42. Figure 42-c indeed documents high and significant correlations of about 0.7 on average between PC2 (calculated exclusively on the basis of North Sea data set) and Atlantic tide gauge records spanning the region from the English Channel southward to Spain. Moreover, there are significant correlations of 0.64 in the north (Reykjavik, Iceland), and even in the Northwest Atlantic (still reaching 0.46 in Port-aux-Basques, Newfoundland) (Figure 42-a/c). Further south towards the Gulf of Maine, these correlations disappear (not shown). A supplemental wavelet analysis (not shown) further reveals that the common oscillations between PC2 and the measured tidal range changes mainly occur on time scales from 6 to 24 months with particularly high coherence at around 12 months. This finding can be interpreted as an indication for a common high-frequency signal in the North Atlantic of unknown origin, causing widespread changes in tidal range. In order to further narrow down the possible causes

for the PC2 signal, outputs from the barotropic shallow-water model run by Arns et al. (2015a/b) over the period from 1958 to 2014 were used. To facilitate a rigorous comparison with the in situ data, simulated time series at the locations of the 70 tide gauge stations were extracted. A PCA revealed that the PC2 pattern is represented well in the simulated data. Similarly high correlations between the model-based PC2 and the observations of the Atlantic tide gauges occur. While the mean correlation of the European tide gauge records (Figure 42-b) with North Sea PC2 from observations is 0.70, it is only marginally lower for the barotropic model outputs with a correlation of 0.66. If the simulated signal is removed from the model, the correlation becomes insignificant and even disappears at most sites. In consequence, PC2 must be driven by a process initially included into the boundary conditions from the numerical model.

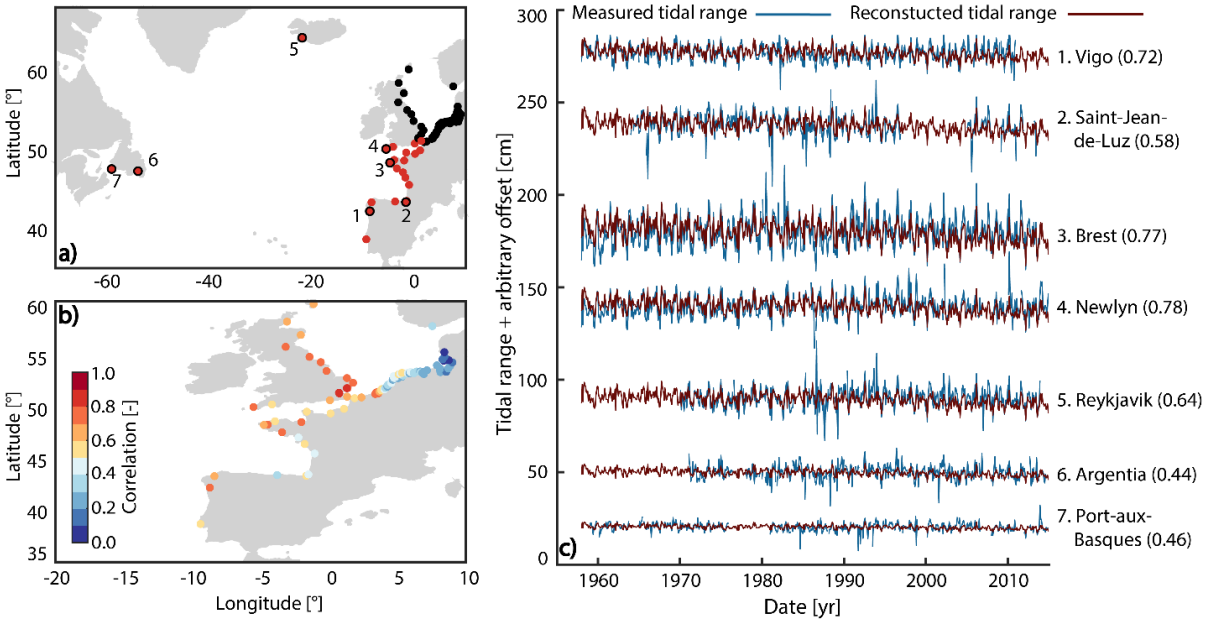

Figure 42: (a) Extended network of tide gauges (black dots) with additional stations shown in red, (b) correlations of all tide gauges (except 5–7) with PC2 and (c) comparison between measured and reconstructed values of tidal range at the newly added tide gauges 1–7. The reconstructions in c) are based on PC2, and the numbers in parentheses indicate the correlations.

Since a barotropic formulation without buoyancy forcing and thermodynamic calculations were used, a purely barotropic relationship can be concluded. Amongst the possible relevant factors, the tidal input to the model can safely be neglected. The used DTU10 tide model consists of ten tidal constituents, stationary in time and modulated only by the 18.61-year nodal cycle (Arns et al., 2015a/b). The high correlations on the east coast of the UK and in the North Atlantic are unrelated to this forcing, since purely tide-induced changes would be periodic and present in the remaining parts of the North Sea. The effects of bottom friction are more involved, but some simple geometric considerations are instructive. As the tidal wave enters the extensive shallow water areas of the southern North Sea, energy losses due to friction become dominant, yet the influence of PC2 is increasingly attenuated in the direction of propagation (Figure 33-d). This discrepancy suggests that frictional effects do not represent the physical

cause of PC2, although they might play a role in suppressing the magnitude of PC2 in the highly dissipative eastern North Sea region. As the simulations were performed with an invariant bathymetry and constant friction parameters, sea level rise and meteorological forcing remain as possible causes. Accordingly, the correlations between PC2 and these factors (MSL rise, atmospheric pressure loading, wind velocities and directions) were analyzed but no clear and significant linear relationship could be detected. In this context, Arns et al. (2015a) already referred to the numerous nonlinear relationships between the individual parameters in marginal seas. Specifically, the nonlinear interaction between tide and sea level rise as well as the dynamic response of the sea surface to meteorological forcing are important (see also Arns et al., 2020). Further numerical analyses in the future, in particular sensitivity studies taking into account altered tidal boundary conditions and time variable friction coefficients, will perhaps allow for a final identification of the ultimate driving factors (e.g. Rasquin et al., 2020).

While the signal of PC2 of tidal range is reproducible, PC1 cannot be detected in the simulated data, which means PC1 is absent in the barotropic model. Above it was stated that there is no coherence to the Atlantic tide gauges for PC1, which suggests an origin of the signal within the basin. It seems plausible that a baroclinic, density-related effect inside the North Sea is responsible for PC1. Based on the state of the art regarding the possible baroclinic causes of changes in the observable tides (see Chapter 2.3), the known relationships between tidal currents and turbulent energy losses in varying stratification conditions appears as a promising explanation. This attribution primarily arises from considerations at seasonal time scales. Using hydrographic casts and baroclinic model simulations, Müller et al. (2014) linked M_2 elevation changes of 1–5 cm in the southern North Sea to the see-sawing of continental shelf stratification between statically stable summer and well-mixed winter conditions. Strong buoyancy gradients in mid-depths (20–30 m) of shallow waters arise during summer months (e.g. van Haren et al., 1999) and stabilize the water column against energy losses to vertical mixing. The associated increase in barotropic tidal transport and surface elevations was found to be most pronounced in very shallow areas and for cyclonic rotation of strong tidal currents (Müller, 2012) - conditions that are all present in the North Sea. To relate at least parts of the PC1 content to this process, temporal evolution of the North Sea's density structure based on gridded temperature and salinity profiles from the KLIWAS data set were analyzed (Bersch et al., 2016). These data are provided as annual values through to 2013 at comparatively high spatial resolution (0.25° x 0.5° latitude-longitude boxes, 2–5 m depth intervals). For consistency, the monthly PC1 series was binned to annual values (1958–2013 with respect to the length of the KLIWAS data set) and cleaned from secular changes with periods longer than 30 years. Because it is unknown how well KLIWAS represents the smaller, more subtle secular trends of density across the water column, the comparison between stratification and PC1 is limited to changes on interannual time scales. To suppress noise in the climatology, vertical density profiles from a particular set of grid points around the German Bight were averaged to a mean water column structure per year (Figure 43-a). These query points, indicated by black dots in Figure 43-b, lie within 2° of 54.5°N/6.0°E and have an exact depth of 35 m in the KLIWAS data set. The sampled area is shallow, hosts strong tidal currents,

and is not permanently mixed, thus favoring a potential effect of stratification on tides. The time-averaged density profile (Figure 43-a) indicates a pycnocline at 20–25 m, conforming in principle to modeling results (e.g. van Leeuwen et al., 2015; Guihou et al., 2018). While this agreement is reassuring, the intake of profiles in various states of stratification through the crude spatial averaging has to be noted (i.e. homogeneous, seasonally or intermittently stratified conditions, see van Leeuwen et al., 2015). Given the tendency for in situ measurements being taken in summer, the KLIWAS data set may, however, mainly represent the seasonally stratified case.

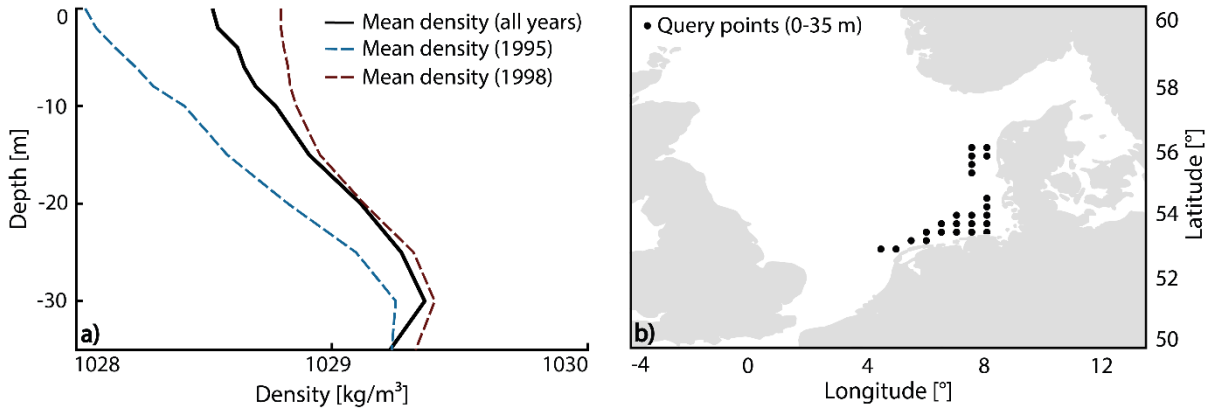

Figure 43: (a) Vertical profiles of potential density as averaged over all query points in (b) at depths from 0 to 35 m for the years 1958 to 2013 (black), the year 1995 (blue) and the years 1998 (red). The two selected years feature the greatest deviation from the mean density profile.

Some interannual variability in density gradients is already evident from Figure 43-a, where individual profiles are plotted for the years 1995 and 1998, which differ markedly near the surface by almost 1 kg/m^3. An extension to the full depth-time sequence (1958–2013, upper 35 m, see Figure 43-a) suggests that fluctuations of this magnitude are common but the density perturbations are often mixed throughout the water column, making it difficult to align stratification changes in particular years to highs or lows in the PC1 series. Therefore an approximate stability index as top-to-bottom stratification is defined (cf. Eq. 2.9 of Knauss & Garfield, 2017)

$$\text{Stability} = \frac{\rho_{\text{top}} - \rho_{\text{bed}}}{\delta H} \qquad \textbf{Eq. 16}$$

where ρ_{top} is the averaged density over depths 0, 2, and 4 m, ρ_{bed} is a mean density across 25, 30, and 35 m, and $\delta H = 28$ m. The adopted metric is akin to the potential energy anomaly advocated by Simpson (1981) and expresses the shape of the density profile through its first derivative. From Figure 44-b, it can be seen that the stability index exhibits some noticeably similarity with interannual tidal range changes in PC1. It closely follows the PC1 curve until 1979, echoes the broad peaks around the years 1987 and 1995, and features multiple reversals in sign from 2007 onward. Alongside this qualitative agreement, the observed changes in density gradients amount to about 0.3 kg/m³ per 10 m of depth and thus correspond to the order of magnitude that maintains the seasonal cycle of M_2 in this region (Müller et al., 2014). Therefore, all indications are that changes to the intensity of summer stratification and/or the time spent in a stratified (or mixed) regime over the course of a year cause the variance in tidal range

represented by PC1. When PC1 is multiplied by its coefficients, for a variation in the stability index of 1-σ the tidal range at tide gauges in the southern German Bight changes by 2.4–2.7 cm, depending on location.

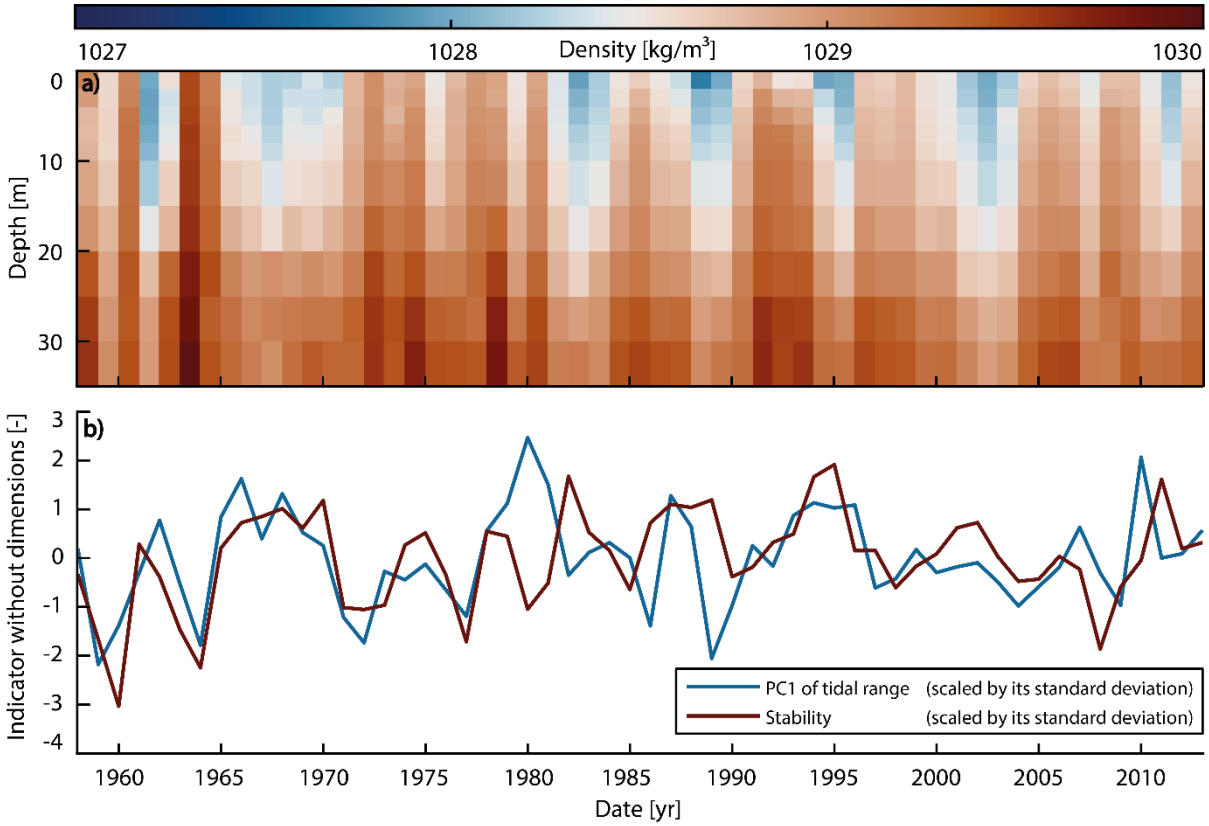

Figure 44: (a) Spatially averaged density profiles (0–35 m) from the query area in Figure 43-b spanning the period 1958 to 2013. (b) Comparison between PC1 changes and the stability index (see main text), where both time series were scaled by their standard deviation and adjusted for long-term trends.

8.3 Answer to the third research question

Based on the analyses in this chapter, the question of the *assignability of physical effects to the observed changes* can now be answered. For this purpose, both the short-term variability and the long-term trends of each tidal parameter were attributed to physical effects. The short-term variability in tidal low and high water as well as the long-term trends in all tidal parameters are, generally spoken, explained by changes of the MSL. The short-term variability of the tidal range on the other hand is caused by stratification effects in the German Bight and by large-scale, barotropic changes originating from the North Atlantic in the UK. Since the tidal range is a derived parameter, the latter effects must also be present in tidal low and or tidal high water, but could not be detected in these parameters due to superposition with other effects.

For a more detailed answer, distinctions must be made not only between the short-term variance and the long-term trends, but also between the three tidal parameters and the geographical location in the study area North Sea as well. Starting with an assessment for a connection to the MSL, the calculations were first carried out for the German Bight, because of the much better data availability and quality in this

area. Afterwards, the findings were compared with the existing data from the UK. For the German Bight, significant correlations between the dominant large-scale signals (PC1s) and a MSL index based on the work of Niehüser et al. (in prep.) were found. On short time scales (excluding linear trends), correlations of 0.88 for the tidal low and 0.90 for the tidal high water were detected, while no correlation exists for the tidal range. Including linear trends, the correlation in the tidal low water increases to 0.90 and to 0.94 in the tidal high water, proving a causation as well as a common trend. For the tidal range, the correlation increases to 0.56 at least indicating a common trend (Figure 37). Since PC1s of tidal low and high water are also highly correlated to each other (>0.90, see Table 7) and thus a common underlying cause has already been demonstrated in Chapter 7, a close relationship between short-term changes in MSL and short-term changes of these two tidal parameters is thereby proven. The non-existent correlation between MSL and tidal range excluding trends confirms this connection, since the contribution of MSL changes to both the variance of tidal low and high water is eliminated in the calculation of tidal range. At first glance, this considerations seem to be contradicted by the common trend between tidal range and MSL in the long-term view. This apparent paradox can be resolved by looking at the long-term sensitivity of tidal low and high water to MSL changes. It was successfully demonstrated, that while the tidal high water responds highly sensitive and nearly linear to MSL changes, the tidal low water exhibits a deviating reaction and runs parallel to the MSL only since the end of the 1980s, causing a non-stationary trend in the tidal range between 1958 and 1990 (Figure 38). The effects cited by Führböter & Jensen (1985) and Jensen (1985) are considered to be causal for this divergent response of the tidal low water: the location of tide gauges at Wadden channels in large Wadden areas leads to higher tidal low water readings than actually present in the surrounding area due to non-existent or delayed runoff within Wadden channels. If a constant bathymetry is assumed, a tide gauge at a Wadden channel will only then show correct tidal low water values, when the surrounding water level and the water level in the Wadden channel are identical. This is not the case until the rise in MSL has already sufficiently increased the surrounding water level. A quantitative analysis confirms these results with an agreement of 0.67 on a 95% confidence interval.

Due to the poorer data basis, such a consideration is unfortunately not possible in the UK, where PC2 is much more important. However, since PC1s of the tidal parameters also depict a significant impact here (Table 9), at least a partial connection to MSL is implicitly proven. Further complicating things, only a numerical North Sea-wide reconstruction of MSL (Wahl et al., 2013) is available for comparison in the UK. This comparison is highly error-prone due to local variations of the MSL within the North Sea. Consequently, rather low correlations of 0.47 or 0.75 (excluding/including trends) in tidal low water and of 0.64 or 0.57 in tidal high water are obtained (Figure 41). No significant correlation in the tidal range is to be found, although a common long-term trend seems to exist here as well. More detailed analyses are not possible because of the poorer data basis, resulting in only a partial proof via the contribution of PC1. However, no evidence to the contrary could be found and PC2 may represent another regional

system response to the MSL rise, deviating from PC1 due to the absence of large shallow water areas in the UK for example.

After that, only the short-term variance of the tidal range remains to be determined, which physically corresponds to the non-identical and unexplained parts of the variance from tidal low and high water. A comparison of the two leading PCs of tidal range with tide gauges from the North Atlantic shows high agreement with PC2, but not with PC1 (Figure 42). A supplemental wavelet analysis further reveals a high coherence around 6 to 24 months, indicating a common high-frequency signal in the North Atlantic of unknown origin. In order to narrow down the possible causes for the PC2 signal, outputs from the barotropic shallow-water model run by Arns et al. (2015a/b) over the period 1958 to 2014 were used and PC2 could be detected in the simulated data. Because the model is based on an invariant bathymetry and constant friction parameters, as possible causes remain nonlinear interaction between tide and sea level rise as well as the dynamic response of the sea surface to meteorological forcing. In contrast, PC1 could not be identified in the model and there is no significant correlation with the North Atlantic, which suggests a baroclinic, density-related effect originated inside the North Sea basin. It was demonstrated that local stratification changes have a large impact on the tidal range in the shallow water areas of the German Bight: a stronger pycnocline stabilizes the water column against turbulent dissipation and allows for higher tidal elevations at the coast. To quantify this effect, a stability index is used to represent the stratification of the upper water layers. It could be proven that, for a variation in the stability index of 1-σ, the tidal range at tide gauges in the southern German Bight changes by 2.4–2.7 cm, depending on location (Figure 43, Figure 44). Overall, it can be concluded that both short-term and long-term changes in the tidal parameters tidal low water, tidal high water and tidal range are fully explained for the German Bight. This applies only limited to the UK, but no contraindications to these connections could be found either and at least a principle connection to the MSL was proven for tidal low and high water.

9 Further possible links and current limits of science

In the previous Chapter 8, physically plausible and mathematically verifiable causes were assigned to the observed large-scale tidal changes. However, in the course of the analyses on which this thesis is based, further fascinating correlations and possible impacts on general tidal behavior in a wider context were identified. These effects can only vaguely be explained due to a lack of sufficient data and limitations regarding the current state of science. These less significant or even unproven connections as well as the limits set by the current scientific knowledge are discussed in this chapter.

9.1 Tidal range changes and oceanographic or meteorological indices

As described in Chapter 3.1, there is a close causal relationship between the tidal dynamics of the North Sea and the North Atlantic, with the tides of the North Sea being produced almost exclusively in the North Atlantic. Taking into account the proclaimed baroclinic character of PC1 and the causal relationship to stratification, it seems reasonable to look for possible connections to the developments in the adjacent North Atlantic. A breakdown into different modes of stratification variability is tempting but beyond the scope of this thesis and the available data, as it would call for consideration of several factors, including freshwater buoyancy input, variable local wind stirring, and the inflow of Atlantic water masses through the northern and southern boundaries (Mathis et al., 2015). Nevertheless, long-term hydrographic data of the North Atlantic was analyzed in order to be able to describe a large-scale context.

According to Segar (2018), stratification is primarily dependent on the density of water. The key factors of water density in the ocean are temperature and salinity. These in turn are controlled to a large extent by ocean currents, which transport water of different temperature and salinity. Since many of the Earth's major current systems are at least partly wind driven, meteorology is taken into account (e.g. Buckley & Marshall, 2016). In order to search for possible links of tidal ranges PC1 to the North Atlantic, data on temperature and salinity as well as indices of the major ocean currents and meteorological patterns are investigated. Most of the underlying data for the following analyses were obtained from the National Oceanic and Atmospheric Administration (NOAA) of the United States of America. Therefore, the definitions and explanations of NOAA are mostly used and only complemented by other sources, such as Marine Scotland data, an agency of the Scottish Government in case of the subpolar gyres index.

The two most important indices of low frequency variability in meteorology over the North Atlantic are the North Atlantic Oscillation (NAO) and the East Atlantic Pattern (EAP) (Barnston and Livezey, 1987; NOAA, 2020a/b). These are often referred to as teleconnection patterns, which are defined as climate anomalies being related to each other at large distances. In accordance to Wallace & Gutzler (1981), the NOA connects parts of the East Atlantic and West Atlantic atmospheric pressure patterns, consisting of a north-south dipole of atmospheric pressure between the Icelandic Low in the north and the Azores High in the south. One center is overlying Greenland and one center of opposite sign is covering the

central latitudes between 35° N and 40° N over the North Atlantic. Changes in the NAO are associated with basin-wide changes in the intensity and location of the North Atlantic jet stream and storm trajectory as well as large-scale modulations of the existing heat and moisture transport patterns (Hurrell, 1995). These changes lead to variations in temperature and precipitation patterns, often extending from eastern North America to Western and Central Europe (Walker & Bliss, 1932; van Loon & Rogers, 1978; Rogers & van Loon 1979). Because of the large-scale influence of the NAO, a corresponding index was obtained from NOAA to show a possible correlation between meteorology and the variance of the tidal range (NOAA, 2020a). The second important pattern of low frequency variability in meteorology over the North Atlantic is the EAP, which was retrieved analogously as the index of the NAO. The EAP resembles the NAO pattern and also consists of a north-south dipole of air pressure anomaly centers spanning the North Atlantic from east to west. However, the southern pole is shifted further southeast and is often interpreted as a "southward shifted" NAO pattern, with the southern pole containing a strong subtropical connection and distinguishes the EAP from the NAO (NOAA, 2020b).

The two systems of ocean currents most interesting in this context are the Atlantic Meridional Overturning Circulation (AMOC, data obtained from NOAA, (2020c)) and the Sub Polar Gyre (SPG, data obtained from Marine Scotland data, an agency of the Scottish Government (Marinescotland, 2017)). The AMOC is a large system of ocean currents that carry warm water from the tropics northwards into the North Atlantic via the Gulf Stream, which transports warm water from the Gulf of Mexico to Greenland. Its continuation is the North Atlantic Current, resulting from a mixing of the tropical water of the Gulf Stream with the arctic water of the Labrador Current. The variability in AMOC is large and primarily reflects the response to local wind forcing on intra-annual time scales, while the interannual to decadal variability is mainly linked to geostrophic equilibrium. The AMOC and its corresponding index used here are commonly defined as the zonally and vertically integrated northward volume transport of ocean water (Buckley & Marshall, 2016). A comparison of the AMOC Index with the results of the PCA could provide insight into a possible correlation between a change in volume transport in the North Atlantic and changes in the tidal dynamics of the North Sea. The SPG (and also the subtropical gyre not treated here due to missing indices and large spatial distance to the subtropical south) is the dominant feature of the surface circulation of the North Atlantic Ocean. It is driven by the combination of meteorology, variation of heat input with changing latitude as well as the global overturning circulation and can be regarded as gyroscopic connection between the North Atlantic, East Greenland, and the Labrador Current. Variations of the SPG in strength and extend can be linked to variations in advection of water masses (Häkkinen & Rhines, 2009) and their properties (Holliday et al., 2008). The data set of the SPG was originally created by Berx & Paine (2017), who, following the methodology of Häkkinen & Rhines (2004), performed a PCA of the sea level anomaly field of the North Atlantic based on altimeter products and defined the leading component as index of the SPG. Accordingly, the principal explanations in this thesis follow the explanations of Berx & Paine (2017).

Figure 45 depicts PC1 of tidal range in context with the discussed meteorological and oceanographic indices both with and without the linear trend, analogous to the comparisons in Chapter 8.1. For none of the mentioned indices a significant correlation can be recognized excluding linear trends. The correlation to the NAO is almost 0 both excluding and including trends. The same applies to the EAP, but here the correlation rises to 0.52 including the trends. Since no causal relationship can be shown, this higher correlation is probably due to generally rising trends in both time series. Based on these indices, no correlation between the variance of the tidal range in the North Sea and large-scale meteorological patterns can be found. Weak correlations to AMOC and SPG can be depicted at least, although even these are too small to prove a common causal development. Since temperature and salinity are not yet considered in these analyses, they are examined in the next step.

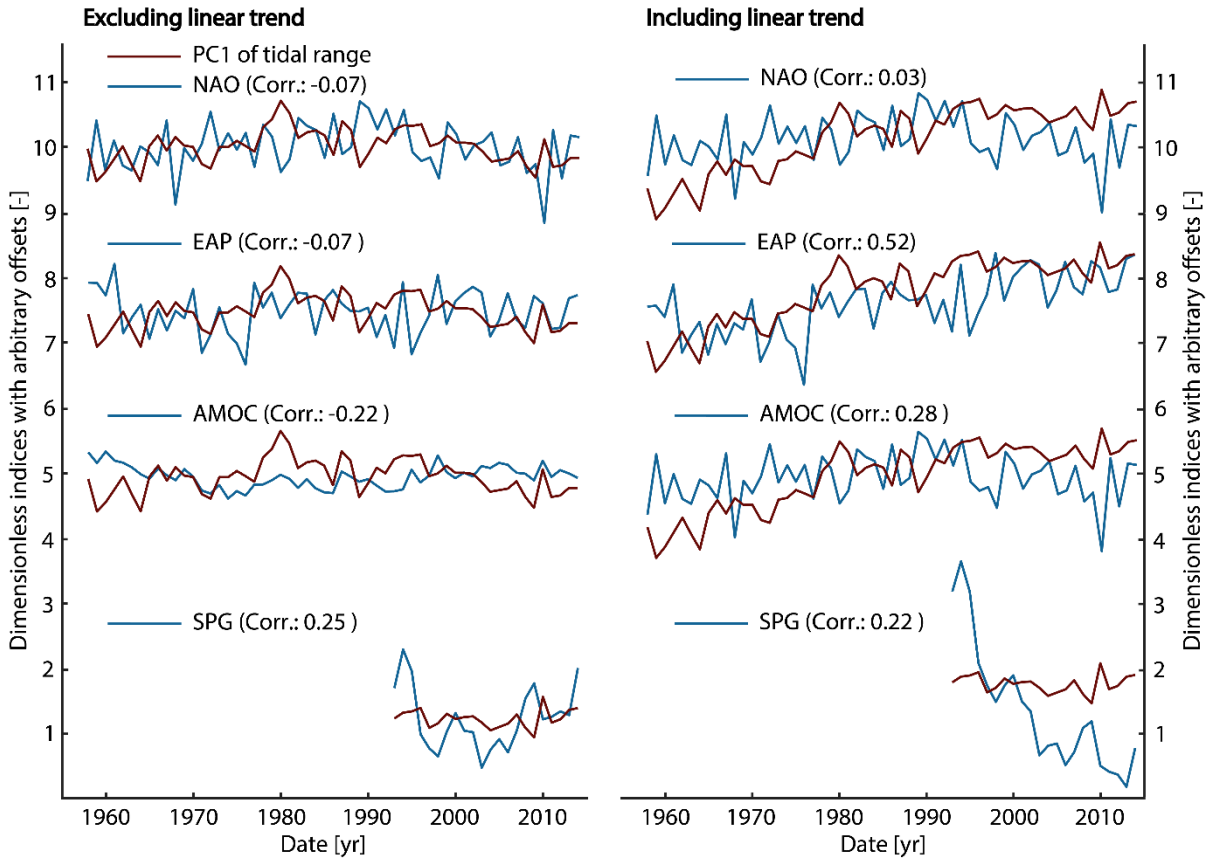

Figure 45: PC1 of tidal range compared to meteorological and oceanographic indices of North Atlantic Oscillation (NAO), East Atlantic Pattern (EAP), Atlantic Meridional Overturning Circulation (AMOC), and the Sub Polar Gyre (SPG) excluding (left) and including (right) linear trends. Correlations (Corr.) are given in brackets.

The possible correlations between temperature, salinity and tidal range are investigated based on the EN4.2.0 data set (Gouretski & Reseghetti, 2010). The resulting correlations are three-dimensional and depend on both location and depth. As no significant correlations between tidal range and salinity were found, this comparison is not presented here. However, there are significant negative correlations between tidal range and temperature. The highest values occur in the area of the Norwegian coast and north of Scotland, where correlations of almost -0.9 are reached (Figure 46). In the surrounding areas, the correlation is also above -0.7. Some exemplary temperature curves are shown together with PC1 in

Figure 46-b. The negative correlation is most pronounced in individual years prior to the 1990s and still persists on decadal time scales. It is evident that the temperature changes in these areas show a high degree of agreement with PC1. The highest correlations appear in relatively shallow areas at depths of up to 150 m, except for the area near Scotland, where the highest anti-correlation can be found in depths of up to 300 m (Figure 46-c). An additional correlation field is located off Portugal. Here, correlations of about -0.72 occur, which are found at depths of 350 to 500 m. The correlations described here were calculated excluding trends of temperature and PC1 and are lower including the trends, so there is no contradiction to the explanation of the tidal range long-term trends being caused indirectly by MSL changes. Following these observations, the variance of the tidal range could then be controlled by temperature changes and the long-term trend of the tidal range by changes of the MSL.

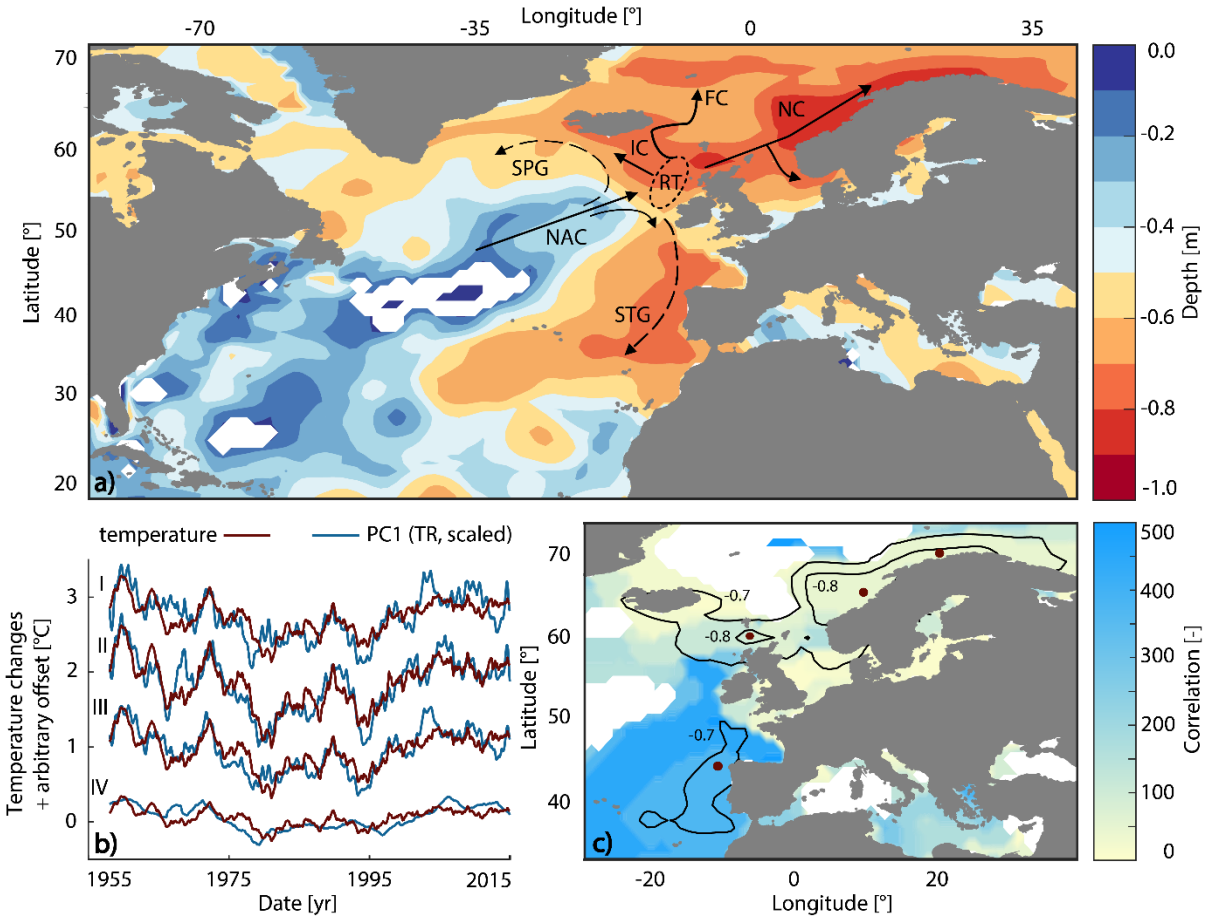

Figure 46: (a) Maximum magnitude correlations (significance level > 95%) between PC1 and temperature: NAC: North Atlantic Current, SPG: Sub Polar Gyre, STG: Sub Tropical Gyre, IC: Irminger Current, RT: Rockall Trough, NC: Norwegian Current. (b) Selected temperature curves with high correlations north (I) and west (II) of Norway, north of Scotland (III), and west of Portugal (IV). (c) Geographical position of the selected locations and depth of the maximum correlation, depth greater than 500 m are shown in white. The areas with the magnitude of correlations higher than -0.7/-0.8 are shown in black lines.

The contiguous region of high correlations begins about the northeastern end of the Rockall Trough near Scotland. In this area subpolar and subtropical waters meet, which leads to a complementary presence of the SPG towards Greenland and the Sub Tropical Gyre towards the Canary Current. These currents are continuations of the North Atlantic Current. The subpolar and subtropical waters mix and enter into

the Arctic Mediterranean. This mixed water as well as the detected high fields of correlation follow the Irminger Current, the Faroe Current and in particular the Norwegian Current to the North. The area off Portugal also fits into this pattern, since water from the North Atlantic Current is also transported here by the Sub Tropical Gyre via the Canary Current (Hátún et al., 2005). The shape of the correlation fields corresponds to the three main mass input flows of the Arctic Mediterranean (Irminger Current, Faroe Current, and Norwegian Current), which are all driven by the North Atlantic Current. Hátún et al. (2005) have shown this mass input from the North Atlantic Current into the Arctic to be mainly controlled by the activity of the SPG on interannual to interdecadal time scales. Asbjørnsen et al. (2019) confirm this fact for the Norwegian Current and extend it by the interaction between the SPG and the Sub Tropical Gyre. They also successfully demonstrate that the temperature distribution in the near surface layers of the Norwegian Sea is significantly controlled by the mass input of North Atlantic Current and consequently by the interaction of SPG and Sub Tropical Gyre. This phenomenon occurs primarily on interannual time scales, as it is partly overlaid by local effects such as air-sea heat fluxes, Ekman forcing or ocean advection on shorter time scales. Furthermore, they state, that the temperature after the upheavals in the area of the Rockall Trough is not so much determined by the temperature of the inflowing water of the North Atlantic Currents, but by the strength of the inflow, i.e. the mass transport (Asbjørnsen et al., 2019). This mixing of water from different sources and the associated change of water temperature could be the reason why the high correlations between PC1 and temperature only occur after the Rockall Trough. Therefore, the spatial coincidence of the subsequent currents with the correlation fields could be caused by the mass transport of the North Atlantic Current.

According to these findings, two different physical explanation patterns can be derived. Firstly, it is possible that the mass input itself changes the tidal behavior in parts of the North Sea. In this scenario, there have to be detectable correlations to the MSL, which is indeed the case for the tidal low and the tidal high water. However, as a result of the difference forming when calculating the tidal range, this connection is no longer detectable here. The same is true for the variance and since high correlations are still detectable, there have to be another cause. This leads to the second explanation, where the altered temperature distribution in the Norwegian Sea via the Norwegian Current is reflected in the North Sea, which is largely controlled by the same mass input. The altered stratification and the proven relationship to the variance of the tidal range point in this direction. In this case, the changing temperature patterns would be reflected in the stratification of the North Sea and thus cause a change in the tidal dynamics.

A further indication of this is provided by Figure 47, showing a wavelet analysis between PC1 and an index of the SPG. Despite an adjustment for seasonal effects (12-month moving average), only discontinuous coherences in the period of up to 0.5 years can be detected. In the range up to 1.5 years, more continuous correlation fields appear. The high coherences on interannual time scales and the numerous interruptions on shorter time scales are similar to the results of Asbjørnsen et al. (2019) regarding temperature anomalies in the Norwegian Sea caused by the SPG. The relationship between SPG and tidal

variation is therefore similar to the relationship between SPG and temperature variations in the Norwegian Sea. It provides another indication that the variance of the tidal range is correlated to the near-surface temperature in some parts of the North Atlantic. However, it must be explicitly stated that that a high degree of uncertainty remains. The results are plausible based on the current state of knowledge, but must be constantly adapted and expanded to the future state of knowledge. The underlying oceanographic processes are the subject of current research and are not yet understood. Asbjørnsen et al. (2019) explicitly point out the limited knowledge and predictability of these interrelationships due to the excessive superposition of the measured values by local surface forcing such as air-sea heat fluxes and Ekman forcing.

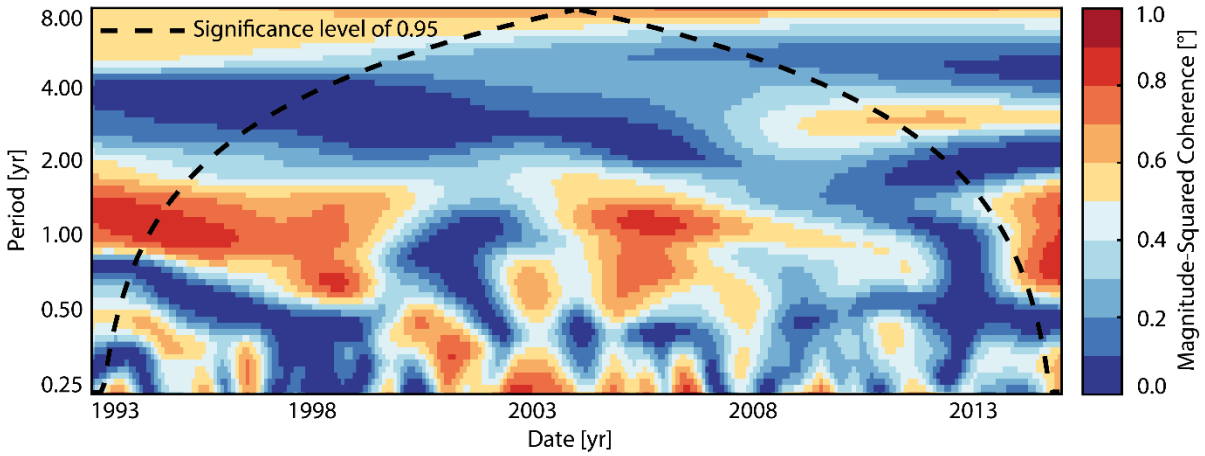

Figure 47: Wavelet analysis of PC1 and the SPG index (Berx & Payne, 2017) with a 12-month moving average.

Overall, connections between PC1 of tidal range and the NAO, the EAP, the AMOC, and the SPG were searched for, but no significant correlations were detected (Figure 45). Likewise, no correlation could be found to the salinity distribution of the North Atlantic. For the temperature, however, high correlations of up to 0.9 occur in some areas with a spatial association to the North Atlantic Current, leading to a possible explanation for changing stratification: the altered temperature distribution in the Norwegian Current, which is largely controlled by the mass input of the North Atlantic Current, is possibly changing the stratification and therefore the tidal regime in the North Sea (Figure 46, Figure 47).

9.2 Tidal low water changes and anthropogenic construction activity

As already explained in the Introduction of this thesis and in more detail in Chapter 4.3, a major problem in the analysis of tidal changes is the overlap of small-scale (e.g. construction measures) and large-scale (e.g. MSL rise) effects. This issue was handled in this thesis by using PCA and the results described in Chapter 7 and Chapter 8 were obtained, including evidence of a direct relationship between MSL changes and tidal parameter trends. It was further shown that the tidal low water measurements are less sensitive than the tidal high water measurements to changes of MSL in the German Bight, especially for long-term linear trends up to the 1970s. This was explained in Chapter 3.3 and Chapter 8.1.1 with the localization of tide gauges at Wadden channels, but another, unproven effect could be involved here as

well: the cumulative impact of the sum of all anthropogenic construction measures. It cannot be excluded, that in addition to the small-scale effects of anthropogenic interventions such as those identified and described by Ebener et al. (2020) or Hollebrandse (2005), the increasing overall length of constructions on the coast lines features a cumulative impact. In this scenario, the sum of the locally acting construction measures might have produced a response of the entire tidal system, which might not be detectable by the leading PCs. Such an effect could have very little impact on the variance on small-scales as well as on large-scales and would thus be invisible for the PCA, but could still cause significant changes in the long-term trends. The physical background would consist of a reduction in total tidal volume due to embankments and a resulting change in tidal dynamics, which would be compensated by an increase in the MSL after some time. Because of the large number and the large spatial and temporal distribution of the individual construction measures as well as the poor data situation, it is not possible to provide quantitative evidence or counterevidence for this theory. Nevertheless, a short qualitative consideration of this possibility seems appropriate at this point.

For the German Bight, the coasts of the two federal states Lower Saxony and Schleswig-Holstein would be affected. Unfortunately, the state of Lower Saxony does not publish data on coastal construction measures (Jensen et al., 2020b). Schleswig-Holstein provides their data collection, but only the newly built dike lengths since 1900 are available here with sufficient accuracy. Data on blocked tidal volumes or areas are only sporadically available (Lehrmann, 2018). Therefore, the newly constructed dike length is taken here as a rough proxy for the reduced tidal volume. This assumption is highly prone to error as there is not necessarily a linear relationship between dike length and reduced tidal volume and the correlation between these sizes could be instationary. Nevertheless, it is the only possible option for comparison based on the available data. Another source of error is the difference in the data basis to compare. While both the MSL index and the PCA results take into account the developments in the entire German Bight including the developments in Lower Saxony, these data can only be compared with Schleswig-Holstein. An elimination of the tide gauges from Lower Saxony is not possible due to procedural reasons, since the PCA is based on the overall system variance and random separation of the initial system is prohibited. Figure 48 depicts the cumulative lengths of the dike constructions in Schleswig-Holstein (blue bars) between 1958 and 2014 as well as the changes to the previous year (red bars). There is a constant, steep increase in dike length detectable until the mid-1990s, followed by a plateau with a subsequent slight increase. Comparing this development with the residual water level between the polynomic functions of the MSL and the tidal low water from the quantitative analysis in Chapter 8.1.1, i.e. the development of the tidal low water that cannot be described by the MSL, a common development is initially discernible. The flattening of the residual curve coincides with the plateau of the dike length, but the dike length increases further afterwards, while the residual curve remains rather constant. However, the additional construction measures are much smaller and may not have a large impact on the behavior of the overall system. Despite these qualitative similarities, no reliable correlation can be

demonstrated here for the reasons described above. Therefore, it can only be stated here that the existence of a cumulative large-scale impact on long-term trends as the sum of all small-scale impacts of anthropogenic construction measures cannot be excluded on the basis of the existing data basis. Further research Lower Saxony's data could allow for a better comparison.

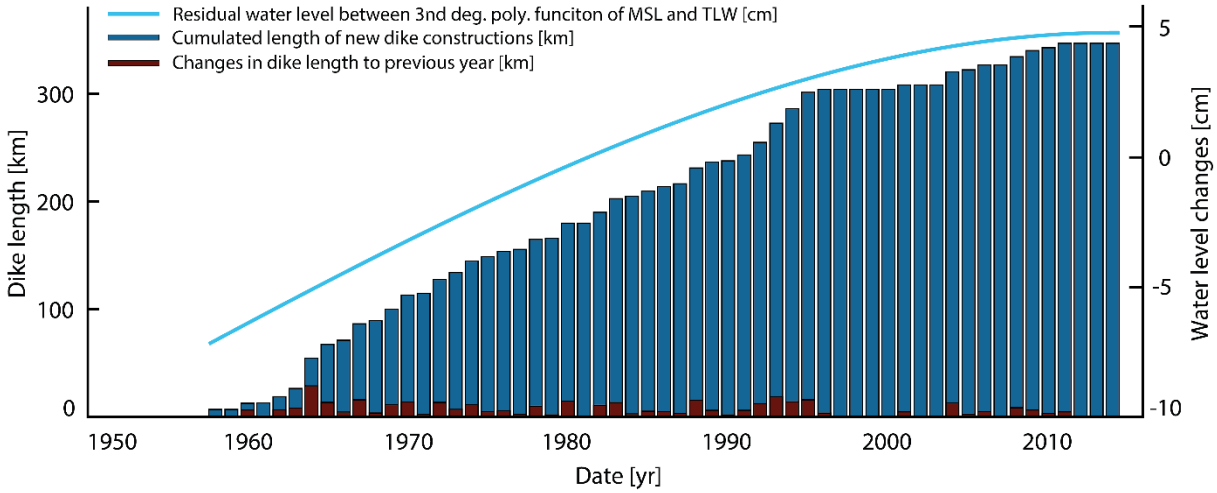

Figure 48: Comparison between anthropogenic construction measures in kilometers of new dike length per year in Schleswig-Holstein according to Lehmann (2018) and discrepancy between the rise in MSL and tidal low water for the tide gauges in Schleswig-Holstein.

10 Summary and discussion

Perhaps because of the close connection between the periodic and predictable nature of astronomical variations and the corresponding tidal water levels, the tidal parameters of tidal low water, tidal high water and tidal range were generally assumed to be constant on time scales over which basin geometry undergoes only minor changes (i.e. decades to centuries, Jänicke et al., 2020). Apart from isolated, local studies (e.g. Keller, 1901; Doodson, 1924), this assumption was not questioned again until the second half of the 20th century. Although some studies have previously investigated tidal water changes in the German Bight area (e.g. Gaye, 1951; Dietrich, 1954; Jensen, 1984), Führböter & Jensen (1985) were the first to discuss large-scale, potentially even basin-wide, changes in tidal parameters in the second half of the 20th century using the North Sea as study area. Today, statistically significant changes in tidal parameters are well documented around the world (e.g. Woodworth et al., 1991; Flick et al., 2003; Ray, 2009; Jay, 2009; Mawdsley et al., 2015; Talke & Jay, 2017). Nevertheless, the spatial extend of short-term and long-term changes as well as the forcing factors remains uncertain (Woodworth, 2010; Haigh et al., 2020; Talke & Jay, 2020), considering the stationarity of astronomical forcing over the period of tide gauge observations.

An example of exceptionally tidal variations on both small and large spatial scales is the North Sea with the magnitude of tidal range changes being one of the highest in the world. Previous research (summarized in Jensen et al., 2014) has ruled out astronomical, large-scale morphological or tectonic causes as forcing factors, citing a MSL rise as possible cause without providing final evidence. Especially Jensen (1984) and Führböter & Jensen (1985) recommend renewed investigations in the farer future, because sufficiently long time series for the entire North Sea region were not available at that time. Since these questions have not been conclusively answered to the present day, the aim of this thesis is to investigate the changes in tides in the North Sea study area and to detect possible physical causes, answering the following questions:

(1) Are the changes in tidal low and high water and the tidal range detected within the German Bight a localized phenomenon, or are they part of a larger-scale development spreading over adjacent areas within the North Sea region?

(2) Is it possible to separate and quantify large-scale and small-scale effects from observed records?

(3) Can physical causes be attributed to the observed changes?

10.1 Summary and conclusions

To access these research questions, a data set of 70 tide gauges (Figure 12, Table 5) of the North Sea basin was compiled and a study period from 1958 to 2014 was defined, based on the known tidal changes in der German Bight from the end of the 1950s on (Jensen, 1985) and the 18.61-year nodal cycle. A correction and validation of the resulting data set according to Woodworth (2010) and Mawdsley et al.

(2015) was performed and the occurring data gaps were filled by applying Ordinary Kriging (Chapter 4.2). A special property of the Kriging procedure is the conservative nature of its estimates at query points, resulting in under- rather than overestimation of the general system behavior. An artificial overestimation of the detected trends caused by the data interpolation could thus be avoided. The data set was then adjusted for the impact of the nodal cycle using PCA, a method developed specifically in this thesis for the North Sea area (Chapter 4.4). The adjusted, final data set is presented in Chapter 5. A general overview of the methods used in this thesis as well as a validation of their novel applications can be taken from the Chapters 1.2 and 4.5.

In order to answer the first research question about the spatial expansion of the occurring tidal changes, linear trend analyses of the three tidal parameters tidal low water, tidal high water, and tidal range were conducted and various developments were detected (Chapter 6). In the median of the entire study area, both tidal low and tidal high water are increasing with the trend of tidal low water (~1.4 mm/yr) falling below the trend of tidal high water (~2.2 mm/yr). A basin-wide change for both tidal parameters could thus be demonstrated. However, significant regional differences and contradicting developments were observed. Therefore, the study area was divided into 3 sections of similar tidal changes: The UK, the European West Coast (France, Belgium, and Netherlands) and the German Bight. In contradiction to the overall development, the median increase in tidal low water exceeds the increase in tidal high water in the UK, while the trend of tidal high water is significantly larger than the trend of tidal low water in the German Bight (Figure 27, Figure 28). The European West Coast forms some kind of transitional area between these opposing poles, with overall tidal high water trends exceeding tidal low water trends slightly. Accordingly, this dipole-like pattern between the UK and the German Bight was also detected in the tidal range, representing the difference between tidal low and high water. Here, a negative median trend in the UK (-0.4 mm/yr) contrasts with a positive trend of 3.0 mm/yr in the German Bight, while the European West Coast exhibits a positive trend of only 0.8 mm/yr. This spatial pattern is confirmed when looking at the tide gauges with non-significant trends. In total, all non-significant, neutral trends of tidal high water are located in the UK, while the German Bight contains an above-average number of those for tidal low water. Simultaneously, more than half of the neutral trends of the tidal range, representing an equal development in tidal low and high water, occur in the area of the European West Coast (Figure 30), underlining its character as some kind of transitional zone. In summary, it was proven that the three tidal parameters exhibit predominantly significant, regional coherent changes at most of the observed tide gauges between 1958 and 2014, making variations in tidal parameters a basin-wide phenomenon. Regarding the first research question specifically, it can be stated that the tidal changes in the German Bight first described in Jensen (1984) and Führböter & Jensen (1985) occur in reduced intensity also throughout the European West Coast, while in the UK contrary trends appear. The question of the spatial extent of tidal changes is thus answered: there is no homogeneous or uniform pattern observed across the entire North Sea basin, but a dipole-like pattern that delineates the opposing developments between the UK and the German Bight with the European West Coast being a kind of transitional area.

To separate and quantify these patterns and their underlying processes (research question 2), PCA was applied in the next step to each tidal parameter (Chapter 7). The aim of PCA in this context is not only to treat both long-term trends and short-term variability in a unified framework, but also to distinguish between small-scale and large-scale processes and effects. The first two PCs turn out to be dominant for all three tidal parameters, explaining about 89% of the variance in tidal low and high water and 69% in tidal range. The remaining overall variance is attributed to local effects, since the remaining PCs occur at very few tide gauges and explain only small percentages of the overall variance, making them entirely local phenomena. In addition to the explained variance, the highly significant correlations between the extracted signals and measured data prove the success of the methodology, with the reconstruction of a single tide gauge from all PCs resulting in 100% agreement both on long-term and short-term scales. The high impact of large-scale effects was demonstrated, as the reconstructed trends agree with their measured counterparts for over 97% of all tide gauges for tidal high water and tidal range on a 95% significance level. In tidal low water, this value is somewhat lower at 91%, with predominantly no agreement for tide gauges with known high local impacts, e.g. Delfzijl (#53), Bremerhaven (#58) or Büsum (#61).

For all three tidal parameters, a distinct, dipole spatial pattern in the PCs similar to the results of the trend calculation (measured values) was identified between the UK and the German Bight. It was consistently observed, that PC2 depicts the highest impact in the UK, decreases strongly on the European West Coast and exhibits only very low values in the German Bight, while the opposite is true for PC1 (Figure 32, Figure 33, Figure 35). This dipole image is also confirmed when looking at the correlations between measured time series and PCs. In addition, high correlations were detected between the leading PCs of tidal low and high water (0.92 including and 0.94 excluding linear trends), but no correlations occurred for the tidal range. This high correlation offered a first hint at a common, large-scale physical cause of the changes in tidal low and high water, which, however, does not appear to explain the changes in tidal range. When analyzing the long-term trends of the large-scale reconstructions (Figure 36), it is noticeable that the RMSE between measured and reconstructed values for tidal low and high water is almost identical, but significantly higher than in the tidal range. Since the RMSE corresponds to the unexplained component of tidal water levels, it provides another indication that the trends in tidal low and high water have a common cause and that this cause, among other influences, is eliminated in the calculation of the tidal range. Besides that, the different mean values of reconstructions imply in consideration of the similar RMSE a significantly larger impacts of local effects on the tidal low water than on the tidal high water values. For this reason, Führböter & Jensen (1985) attributed a significantly more accurate measurement of water level changes to tidal high water. Furthermore, the number and location of non-significant trends in the large-scale reconstructions indicate a significantly lower sensitivity of tidal low water to large-scale changes compared to tidal high water in the large Wadden areas, as the German Bight is heavily overrepresented in the number of neutral trends. This distribution also corresponds to the results of the trend analysis of the measured values. In principle, these observations are

consistent to the findings of Jensen (1984) and Führböter & Jensen (1985), which attribute the lower sensitivity of tidal low water measurements in this area to measurement conditions and interactions between tide and Wadden morphology (Chapter 3.3). However, in response to the second research question can be noted, that a separation and quantification of large-scale and small-scale effects based on short-term variance and long-term trends was achieved. This separation indicates both a common cause for the changes in tidal low and high water and other, unrelated causes for the changes in tidal range. Although the last mentioned changes must already be present in the tidal low and high water, they seem to be masked here and therefore only become visible in the tidal range. A quantification of both tide gauge and region specific separations can be found in Table 9 and Table 10.

To answer the third research question, physical causes were assigned to the patterns of the large-scale PCs. For this purpose, first a comparison was made between the dominant PC1s in the German Bight and the MSL reconstructions of Niehüser et al. (in prep.). High correlations of 0.88 for the tidal low and 0.90 for the tidal high water were detected on short time scales (excluding linear trends), while no correlation exists for the tidal range. The correlation increases to 0.90 for tidal low water and to 0.94 for tidal high water when including linear trends, proving a common development between tidal parameters and MSL (Figure 37). Both the short-term and the long-term variations in tidal low and high water on large spatial scales are thus attributable to the developments in MSL, which represents the already assumed common physical cause. However, when including linear trends, the correlation between tidal range and MSL also increases significantly, implying a common trend and seeming to contradict the obtained results at first sight. This effect is explained by the lower sensitivity of tidal low waters to large-scale water level changes already detected in the measured trends and the large-scale reconstructions: the location of many tide gauges at Wadden channels in the German Bight leads to higher tidal low water readings than actually present in the surrounding area due to non-existent or delayed runoff (Jensen, 1984; Führböter & Jensen, 1985; see also Figure 13). Since the tidal range is basically formed as the difference between tidal low and high water, an underestimation of the tidal low water leads to an artificial positive trend in the tidal range. These resulting artificial trends were mathematically quantified and confirmed with an agreement of 0.67 on a 95% confidence interval, comparing the assumed artificial trend from the underestimation of tidal low water with large-scale tidal range trends. Furthermore, a comparative nonlinear trend analysis of second degree (Figure 38) reveals the highly sensitive response of tidal high water to MSL changes, while the tidal low water exhibits a deviating reaction and runs parallel to the MSL only since the end of the 1980s. This effect causes a non-stationary positive trend in the tidal range between 1958 and 1990. Consequently, the large-scale trend in the tidal range disappears around 1990. Thus, it can be demonstrated physically (underestimation of tidal low water caused by tide gauge locations), quantitatively (assumed artificial trends and large-scale tidal range trends show significant overlapping) and qualitatively (temporal changes of the tidal range correspond to the temporal changes of the residual between tidal low water and MSL) that the long-term trend of the tidal range is significantly caused by the residuals between MSL trends and tidal low water trends. In order

to exclude unknown procedural errors concerning Ordinary Kriging or PCA, these results were verified and confirmed on the basis of unchanged measured values at the individual tide gauges (Figure 33, Figure 34, and Appendix).

Due to the poorer data basis and the high impact of both PC1 and PC2, such a consideration is unfortunately not possible for the east coast of the UK. No sufficiently long, high-resolution time series exist here and the methodology of Niehüser et al. (in prep.) cannot be applied. However, as more than 25% of the variation in the UK is explained by PC1s, a significant influence of the MSL was implicitly proven here as well. Since a direct proof is not possible, an attempt was made by comparing PC2 with a North Sea-wide reconstruction of the MSL from Wahl et al. (2013) to find a causal relationship. Because of regional variations of MSL within the North Sea and low data completeness in the UK, this comparison is highly error-prone. Nevertheless, smaller but still significant correlations of 0.47 and 0.75 (excluding/including trends) in tidal low water and of 0.64 and 0.57 in tidal high water were obtained (Figure 39). No significant correlation to the tidal range were detected, but a common long-term trend could be existing here as well and thus PC2 may also represent a regional system response to the MSL rise.

As the last unsettled question, the short-term variance of the tidal range remains to be determined. This short-term variance contains the non-identical and unexplained parts of the variance from tidal low and high water. To further narrow down possible causes on large scales, a comparison of the detrended two leading PCs of tidal range with tide gauges from the North Atlantic was done and a high agreement to PC2 was found, indicating an origin of the PC2 signal outside the North Sea (Figure 42). Furthermore, outputs from the barotropic shallow-water model run by Arns et al. (2015a/b) were compared to the leading PCs. PC2 was identified in the model and the possible causes could be narrowed down via the model inputs to barotropic, nonlinear interactions between tide and sea level rise or to the dynamic response of the sea surface to meteorological forcing. In contrast, PC1 could not be detected in the barotropic model nor in measured data from the North Atlantic, suggesting a baroclinic, density-related effect originated inside the North Sea basin. This effect was identified as an impact of altered stratification: a stronger pycnocline stabilizes the water column against turbulent dissipation and allows for higher tidal elevations at the coast, an effect that could be quantified as a stability index. For a variation in the stability index of 1-σ, the tidal range at tide gauges in the southern German Bight changes by 2.4–2.7 cm, depending on location (Figure 43, Figure 44). Therefore, the physical background of both short-term and long-term changes in the three tidal parameters in the German Bight can be considered fully explained, as changes in MSL and stratification are causal. Strong indications exist for similar effects in the UK, but larger uncertainties remain here and a direct impact from the North Atlantic seems also to exist.

In summary, this thesis succeeded in detecting significant changes of the tidal parameters tidal low water, tidal high water, and tidal range in the North Sea between 1958 and 2014 as well as in separating and quantifying them. Thus, not only was the request of Jensen (1984) and Führböter & Jensen (1985)

for a basin-wide investigation and quantification of tidal changes in the North Sea fulfilled, but for the first time a large-scale separation of small-scale and large-scale changes was achieved. This separation has been identified by many studies in the past as the most important unsolved obstacle in identifying physical causes and attributing them to observed tidal changes (Woodworth, 2010; Haigh et al., 2020; Talke & Jay, 2020). And indeed, after successful separation, physical causes could be assigned to the various changes, mostly in accordance to earlier, purely theoretical considerations (Müller et al., 2011; Schindelegger et al., 2018; Haigh et al., 2020) for the first time. For the German Bight, the large-scale developments of tidal parameters can be fully explained by changes in MSL and stratification, while in the UK the influence of the MSL and North Atlantic impacts was proven, but no full explanation is possible on the basis of the available data.

10.2 Recommendations for further research

Within the scope of this thesis, a large number of results have been obtained that answer the defined research questions. Nevertheless, some results and approaches are in the margins of the current state of science and further research needs can be defined. Additionally, the results of this thesis provide new possible approaches for the investigation of further unresolved questions.

Regarding the first research question of spatial trend developments, the recommendation of Führböter & Jensen (1985) is repeated with respect to renewed large-scale analyses in the future. Even though a comprehensive analysis could be performed for most of the coastline of the North Sea, further sufficiently long, high-resolution time series from Denmark, Sweden, and Norway could complete the spatial analyses. The same applies to tide gauges in the UK with respect to research question 3. If complete, high-resolution time series of the east coast were available through further time series digitization in the future, a comparison could also be made here with MSL reconstructions using the method of Niehüser et al. (in prep.).

In the context of the third research question, changes in stratification are a global but not yet conclusively researched phenomenon and partly contradictory results have been obtained (e.g. Sallée et al, 2021). Since a connection to tidal range changes has been established at least for the shallow margins of the North Sea basin in the German Bight, it seems useful to carry out these investigations also on a global scale. In particular, the impact of stratification changes on the transition of tidal waves from deep water to shallow shelf seas could provide further interesting results and should be researched for shelf seas other than the North Sea. Another essential point here is the establishment of a large-scale baroclinic model in which, similar to PC2 of tidal range, numerical sensitivity studies could be performed to describe the influence of temperature distribution. The results regarding PC1 of tidal range clearly indicate a causal temperature distribution, as was described in Chapter 9.1. The physical mechanisms of action could be clarified in detail in following studies. Furthermore, the origin mechanisms of the temperature changes as well as their occurrence in other coastal regions could be clarified. Important questions here are: Do trends in ocean stratification affect tides in specific environments at basin-to-shelf scales? How

large is the total contribution from enhanced or weakened turbulent energy losses in shallow surface layers and altered baroclinic dynamics? These questions are particularly important and they are subject of ongoing research not only in the context of the tide, but also in the context of occurring temperature anomalies in the Norwegian Sea. The underlying oceanographic processes are not yet fully understood. Asbjørnsen et al. (2019) explicitly point out the limited knowledge and predictability of these interrelationships due to the excessive superposition of the measured values by local surface forcing such as air-sea heat fluxes and Ekman forcing. A large-scale, numerical approach as well as the aforementioned questions (among others) form a central component of the already approved follow-up project to TIDEDYN, which is launched under the title "Scoop" in May 2021. Another consideration in the context of numerical modeling would be a detailed, barotropic examination of the German Bight to allow for a possible impact of cumulative dike lengths on the development of tidal low waters, as it was discussed in Chapter 9.2.

In addition to this further deepening of the results with respect to the three analyzed tidal parameters tidal low water, tidal high water and tidal range, an investigation of other tidal parameters in the future seems promising. While the analyzed tidal parameters describe vertical variations of the water level curve, the horizontal, i.e. temporal, variation of this curve could also be analyzed. In Chapter 2.2 (Eq. 5), it was shown that the velocity v of the tidal wave can be simplified to $v = \sqrt{g \cdot h}$, following the airy wave theory. Simultaneously, basin-wide positive trends for both tidal low and tidal high water could be demonstrated, which differ mainly only in their magnitude (Chapter 6). Since the gravitational acceleration g is constant, a possible increase in tidal wave velocity due to an increase in water depth h is indicated, especially since the reconstructions of Niehüser et al. (in prep.) also suggest an increase in MSL. It would be of particular interest to see whether only the propagation time of the tidal wave through the North Sea basin is accelerated and the difference in entry times between tidal low and tidal high water remains constant, or if the interval between the entry of the tidal water levels at the individual tide gauge is also changed due to deviating accelerations.

Besides these follow-up studies to further improve the understanding of the change in tidal dynamics, this thesis also provides approaches for specific, practical use of the results in the future. While the detection of large-scale signals of all three tidal parameters was used here exclusively for causal research, an impact assessment based on these results could also be made. One conceivable application would be a forecast of tidal developments. At least in the area of the German Bight, an analytical, quantitative correlation between MSL and tidal changes was established. Based on the predictions of the MSL rise, the future change of the tidal parameters could be estimated analogously. Such a consideration could provide a significant contribution to future coastal protection, especially concerning the tidal high water. Another use could be a cause and effect analysis of changes in bathymetry. Even though morphological changes of bathymetry were excluded as causal for the tidal changes (Jensen et al., 2014), a reverse impact chain is very likely. Numerous studies (e.g. Mudersbach et al., 2013; Zijl et al., 2013;

Arns et al., 2015a; Wang et al., 2018; Rasquin et al., 2020) point to the importance of the nonlinear and yet unexplained relationship between (tidal) water levels and a varying bathymetry, in particular but not exclusively in the context of numerical modelling. Since time series of the isolated large-scale developments of the tidal parameters are now available, a connection to changes of bathymetry could be investigated here at least on large spatial scales. Thus, a qualitative and quantitative correlation could possibly be calculated. In combination with a forecast of future tidal changes based on MSL trend predictions, both tidal water levels and bathymetries could then be estimated. Besides the most important aspect of coastal protection, this would also have positive effects for the maritime economy, shipping in general and all kinds of marine actors, for example port operators. These stakeholders would be enabled to recognize, anticipate and, if necessary, counteract corresponding developments, also in the context of operating within a profitable margin. This is particularly true in the context of keeping shipping lanes navigable, for example in the extensive shallow water areas of the German Bight (Roeland and Piet, 1995; Kirichek et al., 2018; Wölfl et al., 2019; Kirichek et al., 2020; Sievers et al., 2021).

11 References

Achen, C. H. (1982). Interpreting and Using Regression. Thousand Oaks, CA: SAGE Publications, Inc. https://doi.org/10.4135/9781412984560

Albrecht, F., Wahl, T., Jensen, J., & Weisse, R. (2011). Determining sea level change in the German Bight. *Ocean Dynamics*, 61(12), 2037–2050. https://doi.org/10.1007/s10236-011-0462-z

Arns, A., Dangendorf, S., Jensen, J., Talke, S., Bender, J., & Pattiaratchi, C. (2017). Sea-level rise induced amplification of coastal protection design heights. *Scientific Reports*, 7, 40171. https://doi.org/10.1038/srep40171

Arns, A., Wahl, T., Dangendorf, S., & Jensen J. (2015a). The impact of sea level rise on storm surge water levels in the northern part of the German Bight. *Coastal Engineering*, 96, 118–131. https://doi.org/10.1016/j.coastaleng.2014.12.002

Arns, A., Wahl, T., Haigh, I., & Jensen J. (2015b). Determining return water levels at ungauged coastal sites: a case study for northern Germany. *Ocean Dynamics*, 65 (4), 539–554. https://doi.org/10.1007/s10236-015-0814-1

Arns, A., Wahl, T., Wolff, C., Vafeidis, A. T., Haigh, I. D., Woodworth, P., Niehüser, S., & Jensen, J. (2020). Nonlinear interaction modulates global extreme sea levels, coastal flood exposure, and impacts. *Nature Communications*, 11, 1918(2020). https://doi.org/10.1038/s41467-020-15752-5

Asbjørnsen, H., Årthun, M., Skagseth, O., & Eldevik, T. (2019). Mechanisms of Ocean Heat Anomalies in the Norwegian Sea. *Journal of Geophysical Research: Oceans*, 124(4), 2908–2923. https://doi.org/10.1029/2018JC014649

Aubrey, D. G. (1979). Seasonal Patterns of Onshore/Offshore Sediment Movement. *Journal of Geophysical Research: Oceans*, 84(C10), 6347–6354. https://doi.org/10.1029/JC084iC10p06347

Aubrey, D. G. & Emery, K. O. (1983). Eigenanalysis of recent United States Sea levels. *Continental Shelf Research*, 2(1), 21-33. https://doi.org/10.1016/0278-4343(83)90020-1

Baart, F., van Gelder, P. H.A.J.M., Ronde, J. d., Koningsveld, M. v., & Wouters, B. (2011). The Effect of the 18.6-Year Lunar Nodal Cycle on Regional Sea-Level Rise Estimates. *Journal of Coastal Research*, 2012, 511-516. https://doi.org/10.2112/JCOASTRES-D-11-00169.1

Barnston, A. G., & Livezey, R. E. (1987). Classification, Seasonality and Persistence of Low-Frequency Atmospheric Circulation Patterns. *Monthly Weather Review*, 115, 1083–1126. https://doi.org/10.1175/1520-0493(1987)115<1083:CSAPOL>2.0.CO;2

Becker, J. J., Sandwell, D.T., Smith, W. H. F., Braud, J., Binder, B., Depner, J., Fabre, D., Factor, J., Ingalls, S., Kim, S-H., Ladner, R., Marks, K., Nelson, S., Pharaoh, A., Trimmer, R., von Rosenberg, J., Wallace, G., & Weatherall, P. (2009). „Global Bathymetry and Elevation Data at 30 Arc Seconds Resolution: SRTM30_PLUS“. *Marine Geodesy* 32(4), 355–371. https://doi.org/10.1080/01490410903297766

Bersch, M., Hinrichs, I., Gouretski, V., & Sadikni, R. (2016). Hydrographic climatology of the North Sea and surrounding regions – version 2.0, Center for Earth System Research and Sustainability (CEN), University of Hamburg, icdc.cen.uni-hamburg.de/daten/ocean/knsc-hydrographic.html

Berx, B., & Payne, M. (2017). The Sub-Polar Gyre Index – a community data set for application in fisheries and environment research. *Earth System Science Data*, 9, 259–266. https://doi.org/10.5194/essd-9-259-2017

BSH (2019). Gezeitentafeln 2020: Europäische Gewässer, Bundesamt für Seeschifffahrt und Hydrographie, ISSN 0084-9774

Buckley, M. W., & Marshall, J. (2016). Observations, inferences, and mechanisms of the Atlantic Meridional Overturning Circulation: A review. *Reviews of Geophysics*, 54 (1), 5–63. https://doi.org/10.1002/2015RG000493

Cheng, Y., & Andersen, O. B. (2010). Improvement in global ocean tide model in shallow water regions. Poster, SV.1-68 45, OSTST, Lisbon, Oct.18-22.

Chernetsky, A. S., Schuttelaars, H. M., & Talke, S. A. (2010). The effect of tidal asymmetry and temporal settling lag on sediment trapping in tidal estuaries. *Ocean Dynamics*, 60, 1219–1241. https://doi.org/10.1007/s10236-010-0329-8

Cherniawsky, J. Y., Foreman, M. G., Kang, S. K., Scharroo, R., & Eert, A. J. (2010). 18.6-year lunar nodal tides from altimeter data. *Continental Shelf Research*, 30(6), 575–587. https://doi.org/10.1016/j.csr.2009.10.002

Codiga, D. L. (2011). Unified tidal analysis and prediction using the UTide Matlab functions. Technical Report 2011-01. Graduate School of Oceanography, University of Rhode Island, Rhode Island. https://doi.org/10.13140/RG.2.1.3761.2008

Colosi, J. A., & Munk, W. (2006). Tales of the venerable Honolulu tide gauge. *Journal of Physical Oceanography*, 36(6), 967–996. https://doi.org/10.1175/JPO2876.1

Compo, G. P., Whitaker, J. S., Sardeshmukh, P. D., Matsui, N., Allan, R. J., Yin, X., Gleason, B. E., Vose, R. S., Rutledge, G., Bessemoulin, P., Brönnimann, S., Brunet, M., Crouthamel, R. I., Grant, A. N., Groisman, P. Y., Jones, P. D., Kruk, M. C., Kruger, A. C., Marshall, G. J., Maugeri, M., Mok, H. Y., Nordli, Ø., Ross, T. F., Trigo, R. M., Wang, X. L., Woodruff, S. D., & Worley, S. J. (2011). The Twentieth Century Reanalysis Project. *Quarterly Journal of the Royal Meteorological Society*, 137, 1–28. https://doi.org/10.1002/qj.776

Cowtan, K., & Way, R. G. (2014). Coverage bias in the HadCRUT4 temperature series and its impact on recent temperature trends. *Quarterly Journal of the Royal Meteorological Society*, 140, 1935–1944. https://doi.org/10.1002/qj.2297

Cressie, N. (1990). The origins of kriging. *Mathematical Geology,* 22, 239–252. https://doi.org/10.1007/BF00889887

Dangendorf, S., Marcos, M., Müller, A., Zorita, E., Riva, R., Berk, K., & Jensen, J. (2015). Detecting anthropogenic footprints in sea level rise. *Nature Communications*, 6, 7849. https://doi.org/10.1038/ncomms8849

Dangendorf, S., Wahl, T., Hein, H., Jensen, J., Mai, S. & Mudersbach, C. (2012). Mean Sea Level Variability and Influence of the North Atlantic Oscillation on long-term trends in the German Bight. *Water*, 4(1), 170–195. https://doi.org/10.3390/w4010170

Darwin Sir G.H. (1911). The Tides and Kindred Phenomena in the Solar System. 3rd ed. London: John Murray

De Jonge, V. N., Schuttelaars, H. M., van Beusekom, J. M. M., Talke, S. A., & de Swart, H. E. (2014). The influence of channel deepening on estuarine turbidity dynamics, as exemplified by the Ems estuary. *Estuary, Coastal and Shelf Science*, 139, 46–59. https://doi.org/10.1016/j.ecss.2013.12.030

De Valk, C. (1988). Hoofdkomponenten-analyse van meetreeksen. *Waterloopkundig laboratorium*, H0535

Deltares (2020). Open Earth database, http://opendap.deltares.nl/thredds/catalog/opendap/rijkswaterstaat/waterbase/27_Waterhoogte_in_cm_t.o.v._normaal_amsterdams_peil_in_oppervlaktewater/nc/catalog.html, accessed on 09/01/2021

Devlin A. T., Jay D. A., Talke S. A. and Zaron E. (2014). Can tidal perturbations associated with sea level variations in the western Pacific Ocean be used to understand future effects of tidal evolution?. *Ocean Dynamics*, 64(8), 1093–1120. https://doi.org/10.1007/s10236-014-0741-6

Devlin, A. T., Zaron, E. D., Jay, D. A., Talke, S. A., & Pan, J. (2018). Seasonality of tides in Southeast Asian Waters. *Journal of Physical Oceanography*, 48, 1169–1190. https://doi.org/10.1175/JPO-D-17-0119.1

Dietrich, G. (1954). Ozeanographisch-meteorologische Einflüsse auf Wasserstandsänderungen des Meeres am Fallbeispiel der Pegelbeobachtungen von Esbjerg. *Die Küste*, 2, 130–156

Dietrich, G. (1963). General Oceanography. John Wiley & Sons Inc: Third Printing Edition. Interscience Publisher, ISBN 0470214503

DiLorenzo, J. L., Huang, P., Thatcher, M. L., & Najarian, T. O. (1993). Dredging impacts on Delaware Estuary tides. Presented at Proceedings of the 3rd International Conference on Estuarine and Coastal Modeling III

DIN 4049-3 (1994). Hydrologie, Teil 3: Begriffe zur quantitativen Hydrologie. ICS 07.060; 01.040.07

Doodson, A. T. (1922). Harmonic development of the tide-generating potential. *Proceedings of the Royal Society,* 100, 305–329. https://doi.org/10.1098/rspa.1921.0088

Doodson, A. T. (1924). Perturbations of harmonic tidal constants. *Proceedings of the Royal Society*, 106, 513–526. https://doi.org/10.1098/rspa.1924.0085

Ebener, A., Arns, A., Jänicke, L., Dangendorf, S., & Jensen, J. (2020). Untersuchungen zur Entwicklung der Tidedynamik an der deutschen Nordseeküste - Ein Ansatz zur Identifizierung und Quantifizierung von Tideveränderungen durch lokale Systemänderungen. ALADYN-A: Analyses of observed tidal dynamics; Abschlussbericht zum KFKI-Projekt ALADYN (03F0756A). https://www.kfki.de/en/projekte/details?id=ed13c2f78ec74a298beab4c3c97cb609, accessed on 29/10/2020

Feng, X., Tsimplis, M. N., & Woodworth, P. L. (2015). Nodal variations and long-term changes in the main tides on the coasts of China. *Journal of Geophysical Research: Oceans*, 120(2), 1215–1232. https://doi.org/10.1002/2014JC010312

Flick, R. E., Murray, J. F., & Ewing, L. C. (2003). Trends in United States Tidal Datum Statistics and Tide Range. *Journal of Waterway, Port, Coastal, and Ocean Engineering*, 129(4), 155–164. https://doi.org/10.1061/(ASCE)0733-950X(2003)129:4(155)

Foreman, M. G. G. (1977): Manual for Tidal Heights Analysis and Prediction. *Pacific Marine Science Report* 77-10 (2004 revision)

Friedrichs, C. T., & Aubrey, D. G. (1994). Tidal propagation in strongly convergent channels. *Journal of Geophysical Research*, 99(C2), 3321–3336. https://doi.org/10.1029/93JC03219

Führböter, A., & Jensen, J. (1985). Säkularänderungen der mittleren Tidewasserstände in der Deutschen Bucht. *Die Küste*, 42, 78–100

Gaye, J. (1951): Wasserstandsänderungen in der Ostsee und in der Nordsee in den letzten hundert Jahren. *Die Wasserwirtschaft*, Sonderheft: Vorträge der gewässerkundlichen Tagung 1951 in Hamburg

Godin, G. (1986). Modification by an ice cover of the tide in James Bay and Hudson Bay. *Arctic*, 39(1), 65–67. https://doi.org/10.14430/arctic2048

Godin, G. (1991). Compact approximations to the bottom friction term, for the study of tides propagating in channels. *Continental Shelf Research*, 11(7), 579–589 https://doi.org/10.1016/0278-4343(91)90013-V

Godin, G. (1999). The propagation of tides up rivers with special considerations on the Upper Saint Lawrence River, *Estuarine. Coastal and Shelf Science*, 48(3), 307–324. https://doi.org/10.1006/ecss.1998.0422

Gönnert, G. (2003). Sturmfluten und Windstau in der Deutschen BuchtCharakter, Veränderungen und Maximalwerteim 20. Jahrhundert. *Die Küste*, 67, 185–365

Gouretski, V., & Reseghetti, F. (2010). On depth and temperature biases in bathythermograph data: development of a new correction scheme based on analysis of a global ocean database. *Deep-Sea Research I*, 57(6), 812–833. https://doi.org/10.1016/j.dsr.2010.03.011

Green, J. A. M., Huber, M., Waltham, D., Buzan, J., & Wells, M. (2017). Explicitly modelled deep-time tidal dissipation and its implication for Lunar history. *Earth and Planetary Science Letters*, 461, 46–53. https://doi.org/10.1016/j.epsl.2016.12.038

Green, J. A. M., Molloy, J. L., Davies, H. S., & Duarte, J. C. (2018). Is there a tectonically driven supertidal cycle? *Geophysical Research Lett*ers, 45, 3568–3576. https://doi.org/10.1002/2017GL076695

Grinsted, A., Moore, J. C., & Jevrejeva, S. (2004). Application of the cross wavelet transform and wavelet coherence to geophysical time series. *Nonlinear Processes in Geophysics*, 11, 561–566. https://doi.org/10.5194/npg-11-561-2004

Guihou, K., Polton, J., Harle, J., Wakelin, S., O'Dea, E. & Holt, J. (2017). Kilometric Scale Modeling of the North West European Shelf Seas: Exploring the Spatial and Temporal Variability of Internal Tides. *Journal of Geophysical Research: Oceans*, 123(1), 688–707. https://doi.org/10.1002/2017JC012960

Häkkinen, S., & Rhines, P. B. (2004). Decline of Subpolar North Atlantic Circulation during the 1990s. *Science*, 304(5670), 555–559. https://doi.org/10.1126/science.1094917

Häkkinen, S., & Rhines, P. B. (2009). Shifting surface currents in the northern North Atlantic Ocean. *Journal of Geophysical Research Oceans*, 114(C4). https://doi.org/10.1029/2008JC004883

Hagen, R., Plüß, A., Jänicke, L., Freund, J., Jensen, J., & Kösters, F. (2021). A combined modelling and measurement approach to assess the nodal tide modulation in the North Sea. *Journal of Geophysical Research: Oceans*, 126(3). https://doi.org/10.1029/2020JC016364

Haigh, I. D. (2017). Tides and Water Levels. *Encyclopedia of Maritime and Offshore Engineering*, 248, 1–13

Haigh, I. D., Eliot, M., & Pattiaratchi, C. (2011). Global influences of the 18.61-year nodal cycle and 8.85-year cycle of lunar perigee on high tidal levels. *Journal of Geophysical Research*, 116 (C6), 25249. https://doi.org/10.1029/2010JC006645

Haigh, I. D., Pickering, M. D., Green, J. A. M., Arbic, B. K., Arns, A., Dangendorf, S., Hill D., Horsburgh, K., Howard, T., Idier, D., Jay, D. A., Jänicke, L., Lee, S. B., Müller, M., Schindelegger, M., Talke, S. A., Wilmes, S.-B., & Woodworth P. L. (2020). The Tides They Are a-Changin': A comprehensive review of past and future non-astronomical changes in tides, their driving mechanisms and future implications. *Review of Geophysics*, 58(1). https://doi.org/10.1029/2018RG000636

Hátún, H., Sandø, A.B., Drange, H., Hansen, B., & Valdimarsson, H. (2005). Influence of the Atlantic Subpolar Gyre on the Thermohaline Circulation. *Science*, 309, 1841–1844. https://doi.org/10.1126/science.1114777

Hein, H., Mai, S., & Barjenbruch, U. (2011). What tide gauges reveal about the future sea level. *Proceedings of the Aqua Alta*, Hamburg

Heyen, H., Zorita, E., & von Storch, H. (1996). Statistical downscaling of monthly mean North Atlantic air-pressure to sea level anomalies in the Baltic Sea. *Tellus*, 48(2), 312–323. https://doi.org/10.1034/j.1600-0870.1996.t01-1-00008.x

Hoitink, A. J. F., & Jay, D. A. (2016). Tidal river dynamics: Implications for deltas. *Reviews of Geophysics*, 54, 240–272. https://doi.org/10.1002/2015RG000507

Hollebrandse, F. A. P. (2005). Temporal development of the tidal range in the southern North Sea. *Dissertation*, Faculty of Civil Engineering and Geosciences, TU Delft; 2005.

Holliday, N. P., Hughes, S. L., Bacon, S., Beszczynska-Möller, A., Hansen, B., Lavín, A., Loeng, H., Mork, K. A., Østerhus, S., Sherwin, T., & Walczowski, W. (2008). Reversal of the 1960s to 1990s freshening trend in the northeast North Atlantic and Nordic Seas. *Geophysical Research Letters*, 35(3). https://doi.org/10.1029/2007GL032675

Horsburgh, K. J., & Wilson, C. (2007). Tide-surge interaction and its role in the distribution of surge residuals in the North Sea. *Journal of Geophysical Research*, 112(C8). https://doi.org/10.1029/2006JC004033

Hyndman, R. J., & Koehler, A. B. (2006). Another look at measures of forecast accuracy. *International Journal of Forecasting*, 22(4), 679–688. https://doi.org/10.1016/j.ijforecast.2006.03.001

Hurrel, J. W. (1995). Decadal Trends in the North Atlantic Oscillation: Regional Temperatures and Precipitation. *Science*, 269, 676–679. https://doi.org/10.1126/science.269.5224.676

Huthnance, J. M. (1991). Physical Oceanography of the North Sea, *Ocean & Shoreline Management*, 16, 199–231. https://doi.org/10.1016/0951-8312(91)90005-M

Idier, D., Bertin, X., Thompson, P. & Pickering, M., D. (2019). Interactions Between Mean Sea Level, Tide, Surge, Waves and Flooding: Mechanisms and Contributions to Sea Level Variations at the Coast. *Survey in Geophysics* 40, 1603–1630. https://doi.org/10.1007/s10712-019-09549-5

Idier, D., Paris, F., Cozannet, G. L., Boulahya, F., & Dumas, F. (2017). Sea-level rise impacts on the tides of the European Shelf. *Continental Shelf Research*, 137, 56–71. doi:10.1016/j.csr.2017.01.007

Inman, D. L., Jenkins, S. A., McLachlan, A., Orme, A. R., Leatherman, S. P., Whitman, D., Zhang, K., Laborel, J., Belknap, D. F., Han, G., McMinn, A., Stickney, R. R., Stright, M. J., Johnson, L. L., Hamel, J.-F., Mercier, A., Walker, H. J., Stive, M. J. J., Macintosh, D., Eisma, D., Sanlaville, P., Prieur, A., Fairbridge, R. W., Hansom, J. D., Hopley, D., Edyvane, K. S., & Bird, E. (2005). Encyclopedia of Coastal Science. Springer Science + Buisness Media B.V., Ed.: Maurice L. Schwartz. https://doi.org/10.1007/1-4020-3880-1_1

Jänicke, L., Ebener, A., Dangendorf, S., Arns, A., Schindelegger, M., Niehüser, S., Haigh, I. D., Woodworth, P., & Jensen, J. (2020). Assessment of Tidal Range Changes in the North Sea from 1958 to 2014. Journal of Geophysical Research, 126(1). https://doi.org/10.1029/2020JC016456

Jay, D. A. (1991). Green's law revisited: Tidal long wave propagation in channels with strong topography. *Journal of Geophysical Research*, 96(C11), 20585–20598. https://doi.org/10.1029/91JC01633

Jay, D. A. (2009). Evolution of tidal amplitudes in the eastern Pacific Ocean. *Geophysical Research Letters*, 36(4). https://doi.org/10.1029/2008GL036185

Jay, D. A., Leffler, K., & Degens, S. (2011). Long-term evolution of Columbia River tides. Journal of Waterway, Port, *Coastal, and Ocean Engineering*, 137(4), 182–191. https://doi.org/10.1061/(ASCE)WW.1943-5460.0000082

Jensen, J. (1984). Änderungen der mittleren Tidewasserstände an der Nordseeküste. *Mitteilungen Leichtweiß-Institut für Wasserbau*, 83, TU Braunschweig, Braunschweig

Jensen, J. (1985). Über instationäre Entwicklungen der Wasserstände an der deutschen Nordseeküste. *Mitteilungen Leichtweiß-Institut für Wasserbau*, 88, TU Braunschweig, Braunschweig

Jensen, J. (2020a). Retrospektive der Meeresspiegelforschung in Deutschland. Hydrografische Nachrichten, 115, 18–26. https://doi.org/10.23784/HN115-03

Jensen, J., Arns, A., Ebener, A., Weisse, R., Yi, X., Wurpts, A., Berkenbrink, C., & Hubert, K. (2020b). ALADYN: Analysing long-term changes of tidal dynamics in the German Bight, Schlussbericht zu 3.2 BNBest-BMBF 98 https://www.kfki.de/en/projekte/details?id=ed13c2f78ec74a298beab4c3c97cb609, accessed on 29/10/2020

Jensen, J., Dangendorf, S., Wahl, T., & Steffen, H. (2014). Meeresspiegeländerungen in der Nordsee: Vergangene Entwicklungen und zukünftige Herausforderungen mit einem Fokus auf die Deutsche Bucht. *Hydrologie und Wasserbewirtschaftung*, 58(4), 304–323. https://doi.org/10.5675/HyWa_2014,6_1

Jensen, J., Mügge, H.-E., Schönfeld, W., & Visscher, G. (1991). Final report of the KFKI-project Wasserstandsentwicklung in der Deutschen Bucht, 1991, Hamburg, Germany

Jensen, J., Wahl, T., Frank, T., & Dangendorf, S. (2011). Ermittlung des MSL (Mean Sea Level) und Analyse von hochaufgelösten Tidewasserständen an der deutschen Nordseeküste. Abschlussbericht AMSeL http://vzb.baw.de/publikationen.php?file=kfki_projekte/0/097_2_1_e35918.pdf, accessed on 09/12/2020

Jolliffe, I. T. (2002). Principal Component Analysis, Springer Series in Statistics, Springer, New York. https://doi.org/10.1007/b98835

Keller, H. (1901). Weser und Ems, ihre Stromgebiete und ihre wichtigsten Nebenflüsse: eine hydrographische, wasserwirtschaftliche und wasserrechtliche Darstellung, Verlag von Dietrich Reimer, Berlin

Kirichek, A., Chassagne, C., Winterwerp, H., & Vellinga, T. (2018). How navigable are fluid mud layers?. *Terra et Aqua: International Journal on Public Works, Ports and Waterways Developments*, 20, 2546-2552.

Kirichek, A., Shakeel, A., & Chassagne, C. (2020). Using in situ density and strength measurements for sediment maintenance in ports and waterways. *Journal of Soils and Sediments*, 20, 2546-2552. https://doi.org/10.1007/s11368-020-02581-8

Knauss, J. A., & Garfield, N. (2017). Introduction to Physical Oceanography. *Waveland Press*, 3rd Edition, ISBN 147863250X, 978-1-4786-3250-4

Knop, F. (1961). Untersuchungen über Gezeitenbewegung und morphologische Veränderungen im nordfriesischen Wattgebiet als Vorarbeiten für Dammbauten. Dissertation. Mitteilungen des Leichtweiß-Instituts für Wasser- und Grundbau der TH Braunschweig

Krige, D. G. (1951). A statistical approach to some basic mine valuation problems on the Witwatersrand. *Journal of the Southern African Institute of Mining and Metallurgy*, 52, 119–139

Kuckartz, U., Rädiker, S., Ebert, T., & Schehl, J. (2010). Statistik. SpringerVS, 2nd Edition, ISBN 978-3-531-19890-3

Langenberg, H., Pfizenmayer, A., von Storch, H. & Sündermann, J. (1999). Storm-related sea level variations along the North Sea coast: natural variability and anthropogenic change. *Continental Shelf Research*, 19(6), 821–842. https://doi.org/10.1016/S0278-4343(98)00113-7

Lehmann, C. (2018): Baumaßnahmen an der Westküste Schleswig-Holsteins seit 1900; Landesbetrieb für Küstenschutz, Nationalpark und Meeresschutz Schleswig-Holstein (LKN.SH); 2018

Liebsch, G. (2009). Was bedeutet Normal Null? Unser Höhensystem und der Meeresspiegel. *GIZ-Vortragsprogramm Meeresspiegelschwankungen - Teil III*, Bundesamt für Kartographie und Geodäsie, http://www.giz.wettzell.de/Vortraege/20090507_MeeresspiegelNormalNull/WasBedeutetNormalNull.pdf, accessed on 08/05/2020

Liese, R. (1979). Veränderungen von Tidehochwasser, Tideniedrigwasser und Tidehub seit 1946. Jahresbericht 1978. Forschungsstelle für Insel- und Küstenschutz der Niedersächsischen Wasserwirtschaftsverwaltung, Band 3

Liese, R. & Luck, G. (1978). Verfahren zum Nachweis von Veränderungen der Tidehochwasserstände in der Deutschen Bucht. *Deutsche Gewässerkundliche Mitteilungen*, 22 (5), 133–145

Lorenz, E. N. (1959). Prospects for Statistical Weather Forecasting. Final Report, Statistical Forecasting Project, Department of Meteorology. Massachusetts Institute of Technology, Boston, 1959.

Lüders, K. (1936). Über das Ansteigen der Wasserstände an der deutschen Nordseeküste. Jahresbericht 1969, Forschungsstelle für Insel- und Küstenschutz Norderney, Band XX

Maity, R. (2018). Statistical Methods in Hydrology and Hydroclimatology. *Springer Transactions in Civil and Environmental Engineering.* https://doi.org/10.1007/978-981-10-8779-0

Malcherek, A. (2010). Gezeiten und Wellen. Die Hydromechanik der Küstengewässer. Springer Fachmedien Wiesbaden. https://doi.org/10.1007/978-3-8348-9764-0

Malcherek, A. (2018). Gezeiten und Wellen In Küsteningenieurwesen und Ozeanographie. Springer Fachmedien Wiesbaden. https://doi.org/10.1007/978-3-658-19303-4

Marinescotland, (2017): https://data.marine.gov.scot/data set/sub-polar-gyre-index, accessed on 12/10/2020

Mathis, M., Elizalde, A., Mikolajewicz, U., & Pohlmann, T. (2015). Variability patterns of the general circulation and sea water temperature in the North Sea, *Progress in Oceanography*, 135, 91–112. https://doi.org/10.1016/j.pocean.2015.04.009

Mawdsley, R. J., Haigh, I. D., & Wells, N. C. (2015). Global secular changes in different tidal high water, low water and range levels. *Earth's Future*, 3(2), 66–81. https://doi.org/10.1002/2014EF000282

Mawdsley, R. J., & Haigh, I. D. (2016). Spatial and Temporal Variability and Long-Term Trends in Skew Surges Globally. *Frontiers in Marine Science,* 3:29. https://doi.org/10.3389/fmars.2016.00029

McLean, S. R., & Smith, J. D. (1979). Turbulence measurements in the boundary layer over a sand wave field. *Journal of Geophysical Research*, 84(C12), 7791–7808. https://doi.org/10.1029/JC084iC12p07791

Milne, G. A., Gehrels, C. W., Hughes, C. W. & Tamisiea, M. E. (2009). Identifying the causes of sea-level changes. Nature Geoscience, 2, 471–478. https://doi.org/10.1038/ngeo544

Moftakahri, H. R., Jay, D. A., Talke, S. A., Kulkulka, T., & Bromirski, P. D. (2013). A novel approach to flow estimation in tidal rivers. *Water Resources Research*, 49, 1–16. https://doi.org/10.1002/wrcr.20363

Mudersbach, C., Wahl, T., Haigh, I.D., Jensen, J. (2013). Trends in high sea levels of German North Sea gauges compared to regional mean sea level changes. *Continental Shelf Research,* 65, 111–120. https://doi.org/10.1016/j.csr.2013.06.016

Müller, M., Arbic, B., & Mitrovica, J.X. (2011). Secular trends in ocean tides: observations and model results. *Journal of Geophysical Research*, 116 https://doi.org/10.1029/2010JC006387

Müller, M. (2011). Rapid change in semi-diurnal tides in the North Atlantic since 1980. *Geophysical Research Letters*, 48, 107–118. https://doi.org/10.1029/2011GL047312

Müller, M. (2012). The influence of stratification conditions on barotropic tidal transport and its implication for seasonal and secular changes of tides. *Continental Shelf Research*, 47, 107–118. https://doi.org/10.1016/j.csr.2012.07.003

Müller, M., Cherniawsky, J., Foreman, M., & von Storch, J.-S. (2014). Seasonal variation of the M2 tide. *Ocean Dynamics*, 64(2), 159–177. https://doi.org/10.1007/s10236-013-0679-0

NOAA (2020a). National Oceanic and Atmospheric Administration. https://www.cpc.ncep.noaa.gov/data/teledoc/nao.shtml, accessed on 12/10/2020

NOAA (2020b). National Oceanic and Atmospheric Administration. https://www.cpc.ncep.noaa.gov/data/teledoc/ea.shtml, accessed on 12/10/2020

NOAA (2020c). National Oceanic and Atmospheric Administration. https://www.psl.noaa.gov/data/correlation/amon.sm.long.data, accessed on 12/10/2020

NOC (2002). National Oceanography Center of the University of Liverpool. https://www.ntslf.org/tides/hilo, accessed on 08/07/2020

Newton, I. (1687). Philosophiae Naturalis Principia Mathematica, London

Niehüser, S., Arns, A., Jänicke, L., & Jensen, J. (in prep). Reassessment of mean sea level in the North Sea region.

Nyberg, L. (1983). Sea Level Forecasts with an EOF Model. North Sea Dynamics, Springer-Verlag, Berlin, Heidelberg

Oliver, M. A. & Webster, R (2015). Basic Steps in Geostatistics: The Variogram and Kriging. SpringerBriefs in Agriculture. Springer International Publishing. https://doi.org/10.1007/978-3-319-15865-5

Oppenheimer, M., Glavovic, B., Hinkel, J., Van de Wal, R. S. W., Magnan, A. K., Abd-Elgawad, A., Cai, R., Cifuentes-Jara, M., DeConto, R. M., Ghosh, T., Hay, J., Isla, F., Marzeion, B., Meyssignac, B. & Sebesvari, Z. (2019). Sea level rise and implications for low lying Islands, coasts and communities. *IPCC special report on the ocean and cryosphere in a changing climate*, Cambridge University Press, Cambridge, UK

Padman, L., Siegfried, M. R., & Fricker, H. A. (2018). Ocean tide influences on the Antarctic and Greenland ice sheets. *Reviews of Geophysics*, 56, 142–184. https://doi.org/10.1002/2016RG000546

Pawlowicz, R., Beardsley, B., Lentz, S. (2002). Classical tidal harmonic analysis including error estimates in MATLAB using T_TIDE. Computers & Geosciences, 28(8), 929–937. https://doi.org/10.1016/S0098-3004(02)00013-4

Prandle, D., & Wolf, J. (1978). The interaction of surge and tide in the North Sea and River Thames. *Journal of the Royal Astronomical Society*, 55. https://doi.org/10.1111/j.1365-246X.1978.tb04758.x

Peng, D., Hill, E. M., Meltzner, A. J., & Switzer, A. D. (2019). Tide gauge records show that the 18.61-year nodal tidal cycle can change high water levels by up to 30 cm. *Journal of Geophysical Research: Oceans*, 124 (1), 736–749. https://doi.org/10.1029/2018JC014695

Pelling, H. E., & Green, J. A. M. (2014). Impact of flood defences and sea-level rise on the European Shelf tidal regime. *Continental Shelf Research*, 85, 96–105. https://doi.org/10.1016/j.csr.2014.04.011

Preissendorfer, R. (1988). Principal Component Analysis in Meteorology and Oceanography. Elsevier, Amsterdam, ISBN 0444430148

Prinsenberg, S. (1988). Damping and phase advance of the tide in western Hudson Bay by the annual ice cover. *Journal of Physical Oceanography*, 18(11), 1744–1751. https://doi.org/10.1175/1520-0485(1988)018<1744:DAPAOT>2.0.CO;2

Proudman, J., & Doodson, A.T. (1924). The principal constituent of the tides of the North Sea. *Philosophical Transactions of the Royal Society*, 224, 616–625. https://doi.org/10.1098/rsta.1924.0005

Pickering, M. D., Wells, N. C., Horsburgh, K. J., & Green, J. A. M. (2012). The impact on the European Shelf tides by future sea-level rise. *Continental Shelf Research*, 35, 1–15. https://doi.org/10.1016/j.csr.2011.11.011

Pugh, D. T. (1987). Tides, surges and mean sea-level: A handbook for engineers and scientists. Hoboken, NJ: John Wiley, ISBN 047191505X

Pugh, D., & Woodworth, P. (2014). Sea-level science: Understanding tides, surges, tsunamis and mean sea-level changes. Cambridge University Press, Cambridge, ISBN 9781107028197

Quante, M., & Colijn, F. (2016). North Sea Region Climate Change Assessment. Springer Nature, New York. https://doi.org/10.1007/978-3-319-39745-0

Rasquin, C., Seiffert, R., Wachler, B., & Winkel, N. (2020). The significance of coastal bathymetry representation for modelling the tidal response to mean sea level rise in the German Bight. *Ocean Science*, 16, 31–44. https://doi.org/10.5194/os-16-31-2020

Ray, R. D. (2009). Secular changes in the solar semidiurnal tide of the western North Atlantic Ocean. *Geophysical Research Letters,* 36(19). https://doi.org/10.1029/2009GL040217

Ray, R. D., & Egbert, G. (2004). The global S1 tide. *Journal of Physical Oceanography*, 34(8), 1922–1935. https://doi.org/10.1175/1520-0485(2004)034%3C1922:TGST%3E2.0.CO;2

Ray, R. D., & Talke, S. A. (2019). Nineteenth-Century Tides in the Gulf of Maine and Implications for Secular Trends. *Journal of Geophysical Research: Oceans*, 124(10), 7046–7067. https://doi.org/10.1029/2019JC015277

Rietschel, E. (1933). Neuere Untersuchungen zur Frage der Küstensenkung. *Deutsche Wasserwirtschaft,* 5.

Rigor, I. G., Colony, R. L., & Martin, S. (2000). Variations in surface air temperature observations in the arctic. *Journal of Climate*, 13, 1979–1997. https://doi.org/10.1175/1520-0442(2000)013<0896:VISATO>2.0.CO;2

Roeland, H, & Piet, R. (1995). Dynamic preservation of the coastline in the Netherlands. *Journal of Coastal Conservation*, 1(1), 17-28. https://doi.org/10.1007/BF02835558

Rogers, J. C. & Loon, H. v. (1979). The Seesaw in Winter Temperatures between Greenland and Northern Europe. Part II: Some Oceanic and Atmospheric Effects in Middle and High Latitudes. *Monthly Weather Review*, 107, 509–519. http://dx.doi.org/10.1175/1520-0493(1979)107<0509:TSIWTB>2.0.CO;2

Rohde, H. (1975). Wasserstandsbeobachtungen im Bereich der deutschen Nordseeküste vor der Mitte des 19. Jahrhunderts. *Die Küste*, 28, 1–96

Rohde, R. A., Muller, R. A., Jacobsen, R., Perlmutter, S., Rosenfeld, A., Wurtele, J., Curry, J., Wickham, C., & Mosher, S. (2013). Berkeley Earth temperature averaging process. Geoinformatics & Geostatistics: An Overview. http://dx.doi.org/10.4172/gigs.1000103

Rosenfeld, L. K. (1988). Diurnal period wind stress and current fluctuations over the continental shelf off northern California. Journal of Geophysical Research, 93(C3), 2257–2276. https://doi.org/10.1029/JC093iC03p02257

Rossiter, J. R. (1967). An Analysis of Annual Sea Level Variations in European Waters. *Geophysical Journal International*, 12 (3), 259–299. https://doi.org/10.1111/j.1365-246X.1967.tb03121.x

Sallée, J. B., Pellichero, V., Akhoudas, C., Pauthenet, E., Vignes, L., Schmidtko, S., Garabato, A. N., Sutherland, P. & Kuusela, M. (2021). Summertime increases in upper-ocean stratification and mixed-layer depth. *Nature,* 591, 592–598. https://doi.org/10.1038/s41586-021-03303-x

Schindelegger, M., Green, J. A. M., Wilmes, S.-B., & Haigh, I.D. (2018). Can we model the effect of observed sea level rise on tides?. *Journal of Geophysical Research: Oceans*, 123, 4593-4609. https://doi.org/10.1029/2018JC013959

Schönfeld, W., & Jensen, J. (1991). Anwendung der Hauptkomponentenanalyse auf Wasserstandszeitreihen von deutschen Nordseepegeln. *Die Küste*, 52, 212–75

Schrottke, K., & Heyer, H. (2013). Aufbau von integrierten Modellsystemen zur Analyse der langfristigen Morphodynamik in der Deutschen Bucht: AufMod. *Bundesamt für Seeschifffahrt und Hydrographie.* https://doi.org/10.2314/GBV:780783271

Schwanghart, W. (2020). Ordinary Kriging, MATLAB Central File Exchange. Retrieved February 25, 2020. https://www.mathworks.com/matlabcentral/fileexchange/29025-ordinary-kriging, accessed on 15/04/2021

Segar, A. S. (2018). Introduction to Ocean Science, Fourth Edition, Second digital edition version 4.13, ISBN 978-0-9857859-1-8 4

Shalowitz, A. L. (1962). Shore and sea boundaries: With special reference to the interpretation and use of coast and geodetic survey data (Vol. 1). Washington, DC: Government Printing Office

Shalowitz, A. L. (1964). Shore and sea boundaries: With special reference to the interpretation and use of coast and geodetic survey data (Vol. 2). Washington, DC: Government Printing Office

Siefert, W. & Lassen, H. (1985). Gesamtdarstellung der Wasserstandsverhältnisse im Küstenvorfeld der Deutschen Bucht nach neuen Pegelauswertungen. *Die Küste*, 42, 1–77

Sievers, J., Milbradt, P., Ihde, R., Valerius, J., Hagen, R., & Plüß, A. (in review). An Integrated Marine Data Collection for the German Bight – Part I: Subaqueous Geomorphology and Surface Sedimentology. Submitted to: *Journal of Earth System Science Data*. https://doi.org/10.5194/essd-13-2573-2021

Simpson, J. H. (1981). The shelf-sea fronts: implications of their existence and behavior. *Philosophical Transactions of the Royal Society*, 302, 521–546. https://doi.org/10.1098/rsta.1981.0181

Stewart, R. H. (2008). Introduction To Physical Oceanography. Prentice Hall: Texas. http://dx.doi.org/10.1119/1.18716

St-Laurent, P., Saucier, F. J., & Dumais, J. F. (2008). On the modification of tides in a seasonally ice-covered sea. *Journal of Geophysical Research*, 113(C11014). https://doi.org/10.1029/2007JC004614

Sündermann, J. & Pohlmann, T. (2011). A brief analysis of North Sea physics. *Oceanologia*, 53(3), 663–689. https://doi.org/10.5697/oc.53-3.663

Sumich, J.L. 1996. An Introduction to the Biology of Marine Life, sixth edition. Dubuque, IA: Wm. C. Brown., 30–35

Talke, S. A., Horner-Devine, A. R., Chickadel, C. C., & Jessup, A. T. (2013). Turbulent kinetic energy and coherent structures in a tidal river. *Journal of Geophysical Research: Oceans*, 118, 6965–6981. https://doi.org/10.1002/2012JC008103

Talke, S. A., & Jay, D. A. (2017). Archival Water-Level Measurements: Recovering Historical Data to Help Design for the Future, *US Army Corps of Engineers: Civil Works Technical Series*, 412, Report CWTS-02

Talke, S. A. & Jay D. A. (2020). Changing Tides: The Role of Natural and Anthropogenic Factors, *Annual Review of Marine Science*, 12:121–151. https://doi.org/10.1146/annurev-marine-010419-010727

Taylor, G. I. (1922): Tidal Oscillations in Gulfs and Rectangular Basins. *Proceedings of the London Mathematical Society*, s2-20(1), 148–181. https://doi.org/10.1112/plms/s2-20.1.148

Tobler, W. R. (1970). A Computer Movie Simulating Urban Growth in the Detroit Region. *Economic Geography,* 46, 234. https://doi.org/10.2307/143141

Tornevik, H. (1977). Application of EOF to sea level forecasting. European Centre for Medium-Range Weather Forecasts (ECMWF), Workshop on the use of Empirical Orthogonal functions in Meteorology

Trupin, A., & Wahr, J. (1990). Spectroscopic analysis of global tide gauge sea level data. *Geophysical Journal International*, 100 (3), 441–453. https://doi.org/10.1111/j.1365-246X.1990.tb00697.x

Überla, K. (1968) Faktorenanalyse. Springer-Verlag, Berlin, ISBN 978-3-642-53343-3

Van Haren, H., Maas, L., Zimmerman, J. T. F., Ridderinkhof, H., & Malschaert, H. (1999). Strong inertial currents and marginal internal wave stability in the central North Sea, *Geophysical Research Letters*, 26(19), 2993–2996. https://doi.org/10.1029/1999GL002352

Van Leeuwen, S., Tett, P., Mills, D., & van der Molen, J. (2015). Stratified and nonstratified areas in the North Sea: Long-term variability and biological and policy implications. *Journal of Geophysical Research: Oceans*, 120(7). https://doi.org/10.1002/2014JC010485

Van Loon, H., & Rogers, J. C. (1978) The Seesaw in Winter Temperatures between Greenland and Northern Europe. Part I: General Description. *Monthly Weather Review*, 106, 296–310. https://doi.org/10.1175/1520-0493(1978)106<0296:TSIWTB>2.0.CO;2

Wahl, T., Haigh, I. D., Woodworth, P. L., Albrecht, F., Dillingh, D., Jensen, J., Nicholls, R. J., Weisse, R., & Wöppelmann, G. (2013). Observed mean sea level changes around the North Sea coastline from 1800 to present. *Earth-Science Reviews,* 124, 51–67. https://doi.org/10.1016/j.earscirev.2013.05.003

Wahl, T., Jensen, J., & Frank, T. (2010). On analysing sea level rise in the German Bight since 1844. *Natural Hazards and Earth System Sciences*, 10, 171–179. https://doi.org/10.5194/nhess-10-171-2010

Wahl, T., Jensen, J., Haigh, I., D., & Frank, T. (2011). Improved estimates of mean sea level changes in the German Bight over the past 166 years. *Ocean Dynamics*, 61 (5), 701–715. https://doi.org/10.1007/s10236-011-0383-x

Walker, T., & Bliss, E. W. (1932). World Weather V. *Memoirs of the Royal Meteorological Society*, 4(36), 53–84

Wallace, J. M., & Gutzler, D. S. (1981). Teleconnections in the Geopotential Height Field during the Northern Hemisphere Winter. *Monthly Weather Review,* 109 (4): 784. https://doi.org/10.1175/1520-0493(1981)109<0784:TITGHF>2.0.CO;2

Wang, Z. B., Elias, E. P., van der Spek, A. J., & Lodder, Q. J.: Sediment budget and morphological development of the 450 Dutch Wadden Sea: impact of accelerated sea-level rise and subsidence until 2100. *Netherlands Journal of Geosciences*, 97(3), 183-214. https://doi.org/10.1017/njg.2018.8

Willmott, C. J. (1984): On the Evaluation of Model Performance in Physical Geography. In: Gary L. Gaile und Cort J. Willmott (Hg.): Spatial Statistics and Models. Dordrecht, s.l.: Springer Netherlands, *An International Series in the Philosophy and Methodology of the Social and Behavioral Sciences*, 40, 443–460. https://doi.org/10.1007/978-94-017-3048-8_23

Wölfl, A.-C., Snaith, H., Amirebrahimi, S., Devey, C.W., Dorschel, B., Ferrini, V., Huvenne, V. A. I., Jakobsson, M., Jencks, J., Johnston, G., Lamarche, G., Mayer, L., Millar, D., Pedersen T. H., Picard, K., Reitz, A., Schmitt, T., Visbeck, M., Weatherall, P., & Wigley, R. (2019). Seafloor Mapping – The Challenge of a Truly Global Ocean Bathymetry. *Frontiers in Marine Science*, 6(283). https://doi.org/10.3389/fmars.2019.00283

Woodworth, P. L., Shaw, S. M., & Blackman, D. L. (1991). Secular trends in mean tidal range around the British Isles and along the adjacent European coastline. *Geophysical Journal International*, 104(3), 593–609. https://doi.org/10.1111/j.1365-246X.1991.tb05704.x

Woodworth, P. (2010). A survey of recent changes in the main components of the ocean tides. *Continental Shelf Research*, 30, 1680–1691. https://doi.org/10.1016/j.csr.2010.07.002

Woodworth, P., Hunter, J. R., Marcos, M., Caldwell, P., Menedez, M., & Haigh, I. D. (2017). Towards a global higher-frequency sea level data set. *Geoscience Data Journal*, 3(2), 50–59. https://doi.org/10.1002/gdj3.42

WSV (2020). Wasser- und Schifffahrtsverwaltung des Bundes, portal of the associated Central Data Management ZDM. https://www.portalnsk.de/, accessed on 29/10/2020

Zijl, F., Verlaan, M., & Gerritsen, H. (2013). Improved water-level forecasting for the Northwest European Shelf and North Sea through direct modelling of tide, surge and non-linear interaction. *Ocean Dynamics*, 63(7), 823-847. https://doi.org/10.1007/s10236-013-0624-2

Appendix

Annual time series and trends (T.-) of MSL according to Niehüser et al. (in prep.), reconstructed tidal high water of PC1 (Rec) and measured tidal high water (Mea).

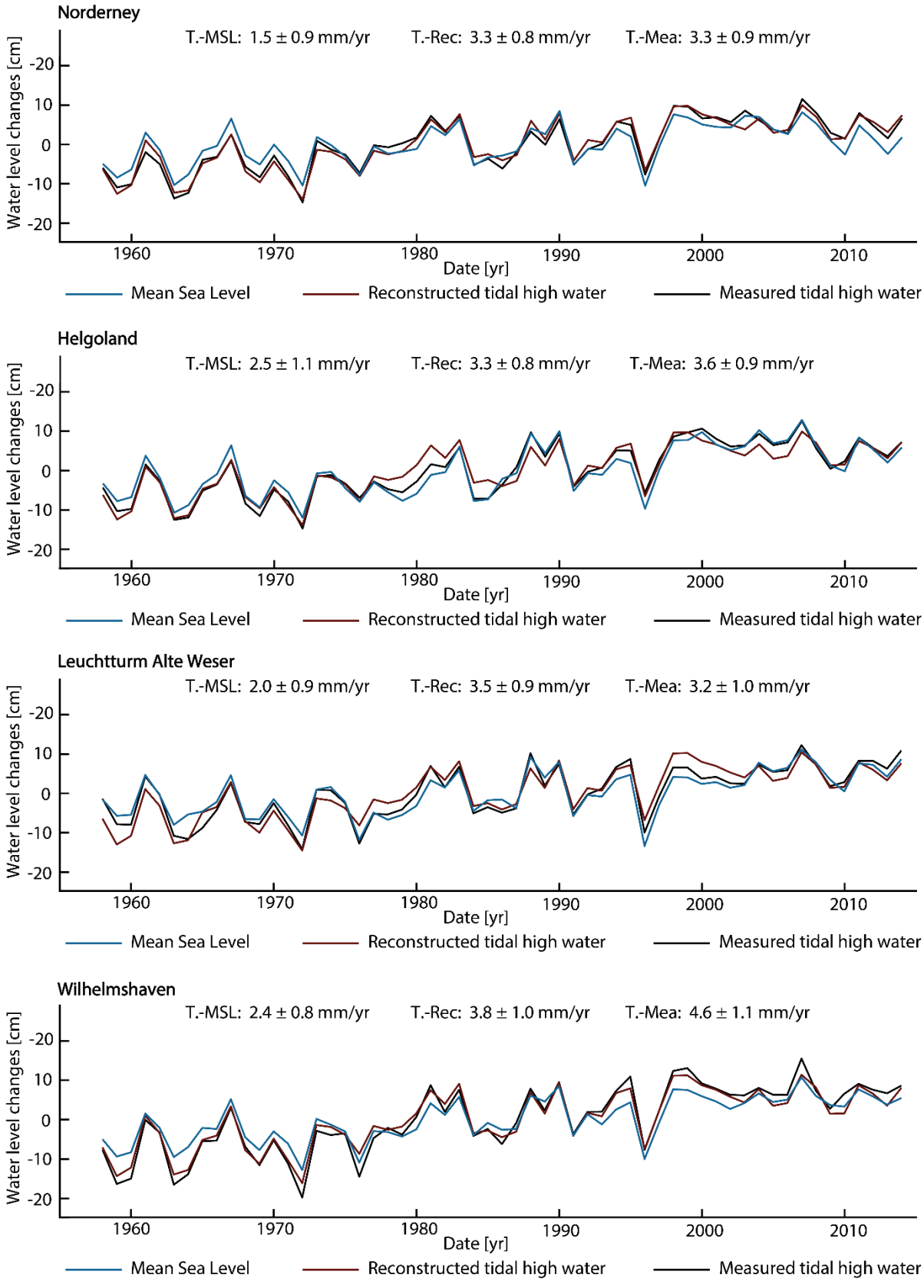

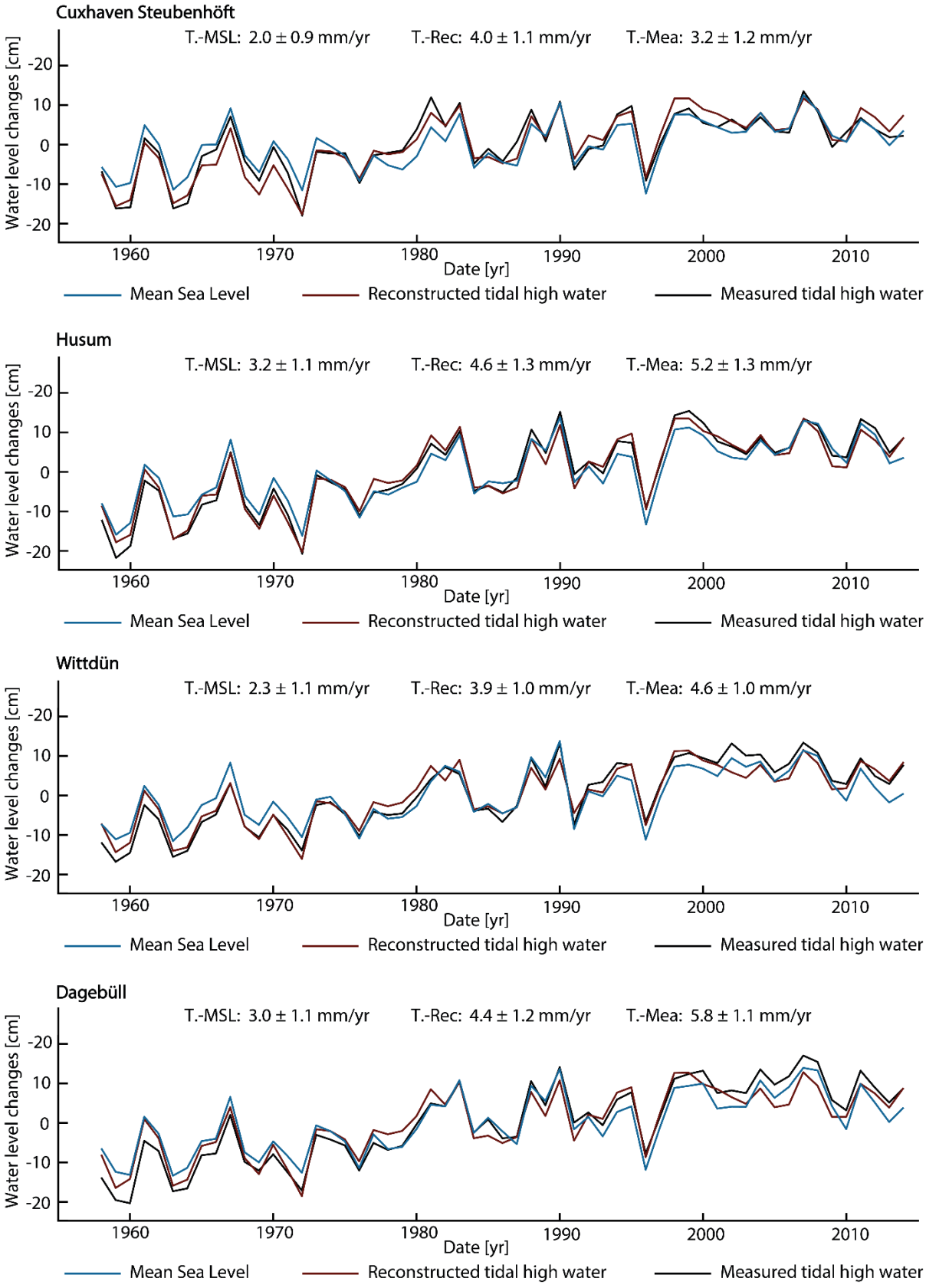
Cuxhaven Steubenhöft
T.-MSL: 2.0 ± 0.9 mm/yr
T.-Rec: 4.0 ± 1.1 mm/yr
T.-Mea: 3.2 ± 1.2 mm/yr
Husum
T.-MSL: 3.2 ± 1.1 mm/yr
T.-Rec: 4.6 ± 1.3 mm/yr
T.-Mea: 5.2 ± 1.3 mm/yr
Wittdün
T.-MSL: 2.3 ± 1.1 mm/yr
T.-Rec: 3.9 ± 1.0 mm/yr
T.-Mea: 4.6 ± 1.0 mm/yr
Dagebüll
T.-MSL: 3.0 ± 1.1 mm/yr
T.-Rec: 4.4 ± 1.2 mm/yr
T.-Mea: 5.8 ± 1.1 mm/yr
Water level changes [cm]
-20
10
0
-10
-20
1960
1970
1980
1990
2000
2010
Date [yr]
Mean Sea Level
Reconstructed tidal high water
Measured tidal high water

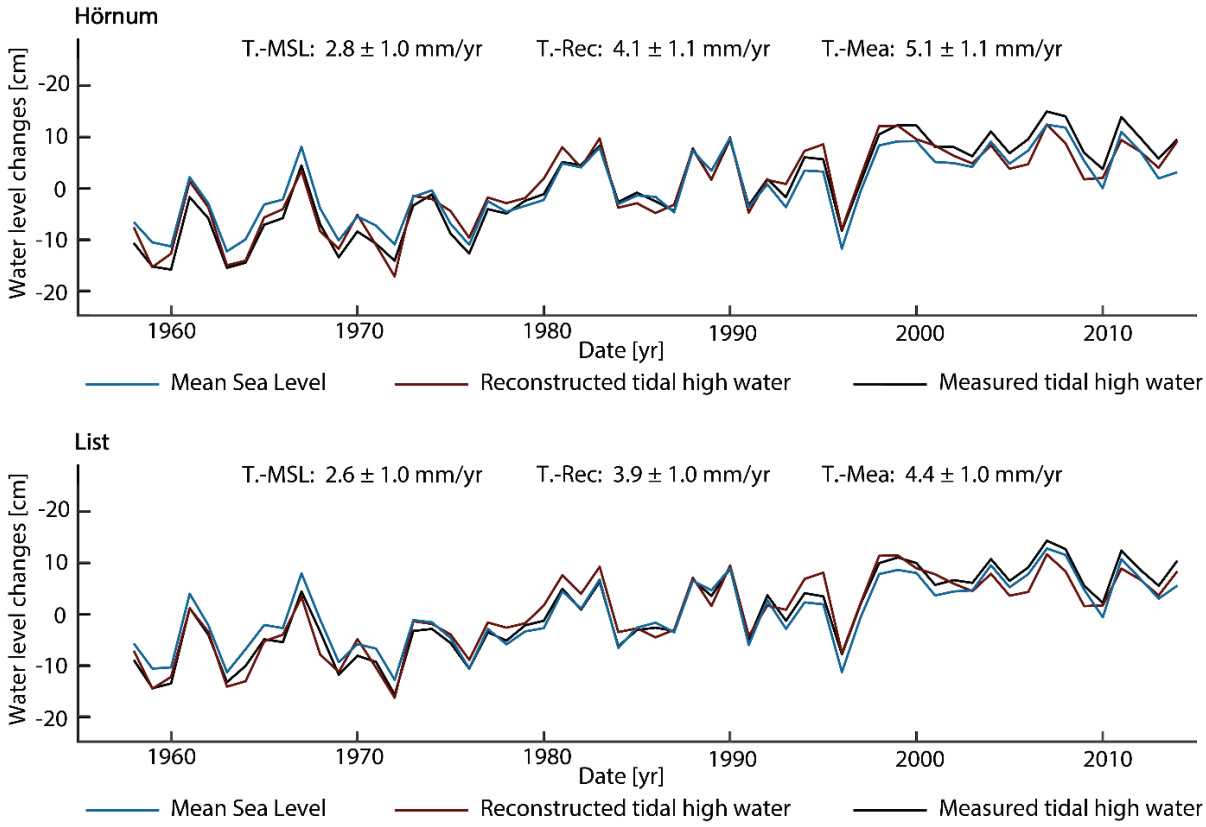
Hörnum
T.-MSL: 2.8 ± 1.0 mm/yr
T.-Rec: 4.1 ± 1.1 mm/yr
T.-Mea: 5.1 ± 1.1 mm/yr
Water level changes [cm]
-20
10
0
-10
-20
1960
1970
1980
1990
2000
2010
Date [yr]
Mean Sea Level
Reconstructed tidal high water
Measured tidal high water
List
T.-MSL: 2.6 ± 1.0 mm/yr
T.-Rec: 3.9 ± 1.0 mm/yr
T.-Mea: 4.4 ± 1.0 mm/yr
Water level changes [cm]
-20
10
0
-10
-20
1960
1970
1980
1990
2000
2010
Date [yr]
Mean Sea Level
Reconstructed tidal high water
Measured tidal high water

Herausgeber:
Forschungsinstitut Wasser und
Umwelt (fwu) der Universität Siegen
Paul-Bonatz-Straße 9-11
57076 Siegen